In vitro dynamics of Kode FSL construct modification of cell membranes

Bhawana Prakash

2024

Kode Technology Innovation Laboratory

School of Engineering, Mathematical and Computer Sciences

Faculty of Design and Creative Technologies

Auckland University of Technology

A thesis submitted to Auckland University of Technology
in fulfilment of the requirements for the degree of Doctor of Philosophy

Abstract

The biological membrane molecular landscape manages almost all interactions of the cell with its environment. Thus, manipulating biological membranes has the potential to improve our understanding of how cells interact with one another and provide new avenues for diagnosis and treatment.

Kode technology is a passive modification technology which uses function, spacer, lipid constructs (FSL) to modify biological membranes. Despite various FSL constructs being known for many years for effective cell modification many aspects of their dynamics of cell modification, cytotoxicity profile, and subsequent fate are not known. Additionally, FSL construct retention behaviour on kodecytes has not been explored. If the dynamics of FSL cellular labelling are better understood, improved methods of Kode transformation may be possible, or at least the impact of variables in koding experiments will be better understood and controlled.

Three FSL constructs, FSL-FLRO4, FSL-BODIPY (different fluorophore as functional group), and FSL-biotin (biotin as functional group) were chosen for this study as they could be identified by flow cytometry, fluorescence spectroscopy, fluorescence microscopy methodologies. This research initially explored the dynamics of FSL uptake by red blood cells and Jurkat cells, and considered factors like concentration, temperature, time, protein/serum presence, and the glycocalyx. The impact of each of these variables around the micellar concentration of FSL constructs during FSL uptake was also analysed.

Retention studies showed that at 37°C, kodecytes lose FSLs when stored in protein or BSA-supplemented media. Extended experiments found that the FSLs lost to the media were not able to efficiently re-label fresh RBC and appeared to have been inactivated. It was found that the storage medium in which koding reaction takes place actually acquires proteins and lipids shed from 37°C incubated cells and this capture released FSLs and prevent them from relabelling cells. Additionally, media supplemented with protein/plasma-lipid although not necessarily causing the loss of FSL from kodecytes, do instead interfere with the ability to relabel.

Thus, one of the important observations was that the act of incubation at 37°C leads to the formation of RBC-derived membranous entities released to the media (e.g. proteins, lipids, and microvesicles), which then interfere with the uptake of FSL. Hence, it could be said that the act of koding inhibits the uptake of the FSL construct, and thus changes the dynamics of FSL uptake over time.

Scanning Electron Microscopy (SEM) studies of visible characteristics of kodecytes did not identify any specific consequence due to the FSL, but rather the observed changes are due to the methodology - primarily 37°C incubation.

The conclusions from this research are that although many stages of the koding process are predictable, some of the underlying mechanisms are complex, and influenced by multiple external factors. Overall, this research has led to a greater depth in understanding of the koding process, and new observation will inform future experiments.

Lists of Figures

List of Tables

Attestation of Authorship

I hereby declare that this submission is my own work and that, to the best of my knowledge and belief, it contains no material previously published or written by another person (except where explicitly defined in the acknowledgements), nor material which to a substantial extent has been submitted for the award of any other degree or diploma of a university or other institution of higher learning.

11/11/2024

Signature Date

Bhawana Prakash

11th November 2024

Acknowledgements

I express my gratitude to my supervisors, Professor Steve Henry and Dr. Eleanor Williams, for their invaluable assistance and support. I would especially like to thank Professor Steve Henry for all his valuable and helpful advice and inspiration during my doctoral studies.

To my unofficial supervisor, Professor Nicolai Bovin, I also offer heartfelt thanks. Nicolai's willingness to share his experience in chemistry, biophysics is invaluable.

I express my gratitude to my peers at the AUT Centre for Kode Technology for their camaraderie, encouragement, and guidance. I am appreciative that I had the chance to collaborate with such an amazing team of individuals.

Lastly, I want to express my gratitude to my family for their belief in me and support.

Statutory declaration:

The donor gave verbal consent for blood to be used to create reagents.

Chapter 1 Introduction

Cells are fundamental to modern biochemical research and are irreplaceable tools for a myriad of laboratory and therapeutic applications. Moreover, there has been a marked transition in cell biology, immunology, and neuroscience research from structural characteristics of cells to understanding of their dynamics processes.[1] To study the dynamics of cells' behaviours and their associated interactions, it is imperative to artificially modify (label or functionalize) them. Unfortunately, modifying what a cell does is not easy, as small manipulations in the cell's environment can have a detrimental effect on the cell's viability and function.[2] Additionally, considering the complexity and dynamic nature of the cell membrane, it is challenging to bioengineer the cellular landscape without being cytotoxic or potentially interfering with the cell's functionality.[2,3]

Kode technology offers passive modification of cells by means of the incorporation of desired functional components with biocompatibility and functionality.[4] For many years, several FSL constructions have been used to effectively modify cells.[5-7] Despite the fact that FSL constructs have been used *in vitro* and *in vivo*, many aspects of their dynamics of cell transformation, cytotoxic profile, and subsequent fate remain unknown. Additionally, FSL construct uptake during the koding process and their retention behaviour after koding have yet to be explored. Thus, this study was designed to explore the dynamics and mechanisms of uptake, retention, fluorescence performance characteristics, and release/loss of FSL constructs from cell membrane.

1.1 Structure and Composition of Biological Membrane

Cellular membranes are essentially a cooperative assembly of lipids, proteins, and carbohydrates. All cell membranes consist of a lipid bilayer. However, the membranes of different cell types have different lipid profiles.[8] The bilayer structure and fluidity of the membrane are largely the responsibility of lipids. Membrane lipids are amphipathic molecules, comprising two main parts: the hydrophilic head group (higher affinity to polar solvents) and hydrophobic tails (higher affinity to nonpolar solvents).[9,10]

As the technology used in this thesis is a lipid-based construct and is relevant to modification of the cell membrane lipid largely, this aspect (lipid) of the cell will be

explored in detail with a focus on the red blood cell (RBC) membrane which is the primary cell used in this research.[11] The major lipid classes present in the cell membrane are: glycerophospholipids, sphingophospholipids, phosphosphingolipids, and glycolipids. Within the context of this thesis, key membrane lipids that have been associated with the labelling and functionalization processes have been reviewed.

1.1.1 Glycerophospholipids

Glycerophospholipids are the most abundant lipids in the cell membrane, making up the background or matrix of the bilayer.[12] It consists of polar phosphate containing a hydrophilic head group and two hydrophobic acyl chains joined by a glycerol backbone, as depicted in Figure 1. Their hydrophobic portion contains saturated or *cis*-unsaturated fatty acyl chains of varying lengths. Based on head group modification, the most common glycerophospholipids found in biological membranes are phosphatidylcholine (PC), phosphatidylethanolamine (PE), phosphatidylserine (PS), phosphatidylinositol (PI), and phosphatidic acid (PA).[12] The structure of the most common glycerophospholipids is shown in Figure 1. Almost 70% of the total lipid content in eukaryotic membranes is composed of glycerophospholipids, with PC and PE being the most dominant glycerophospholipids, accounting for nearly 40–50% and 20–45%, respectively, while PS, PA, and PI make up around 10%.[13]

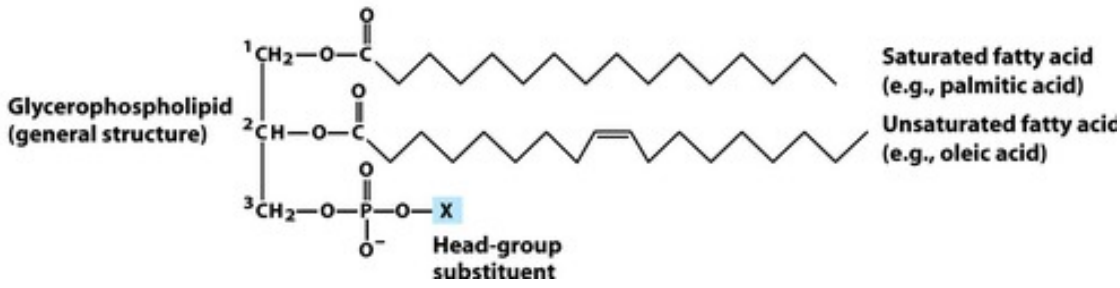

Figure 1: Schematic chemical structure of Glycerophospholipid. Adapted from Chattopadhyay, A, 2017.[14]

1.1.2 Sphingophospholipids

Sphingophospholipids are active participants in maintaining signal transduction and cellular regulation.[15] Sphingophospholipids are phosphorous-containing lipids that contain an unsaturated amino alcohol sphingosine as its backbone (rather than glycerol in glycerophospholipids), and here, a fatty acid is joined to sphingosine via an amide linkage (rather than ester linkage in glycerophospholipids).[16] Sphingomyelins are the

simplest of all sphingophospholipids and are the most crucial component of the myelin sheath surrounding the axon of a nerve cell.

1.1.3 Glycolipids

Glycolipids are crucial to the growth and differentiation of cells[17], cell-cell recognition and attachment[18-20], immune responses[21] and host cell recognition by bacteria and viruses.[22] These sugar-containing lipids are found exclusively in the nocytosolic monolayer of the membrane, partitioning preferentially into lipid rafts and generally constituting 5% of the lipid molecules in the outer membrane. The variability in characteristics such as sugar type, linkage type, branch positioning, shape, charge, ring size, and epimeric and anomeric configuration results in more than 1×10^{12} possible structural combinations from a six-sugar glycan.[23] This confirms the fact that sugars, owing to their distinct branching structure, contain several orders of magnitude more information in a short sequence than any other biological oligomers.

The most relevant glycolipids, with respect to blood group antigens, are glycosphingolipids. Here, oligosaccharide chains are conjugated to a sphingolipid, also known as ceramide. Ceramides are *N*-acyl derivatives of sphingosine, an amino alcohol containing a long unsaturated carbon chain. The fatty acids linked to the amino group of the sphingosine residue are either saturated or unsaturated molecules containing 16 to 26 carbon atoms. The oligosaccharide unit is linked covalently to the hydroxyl group on carbon-1 of the sphingosine residue. Glycosphingolipids comprise about 10.5% of the RBC membrane [24] and hence are its integral part. In addition to ABO blood group determinants, it also carries contributing factors for Lewis, H, I, P1PK, GLOB, and FORS. The glycolipid molecule (Figure 2) is anchored to the external lipid membrane of the RBC by its bilipid tail. The glycolipid antigens are acquired from the plasma, in contrast to glycoprotein-based ABO antigens.

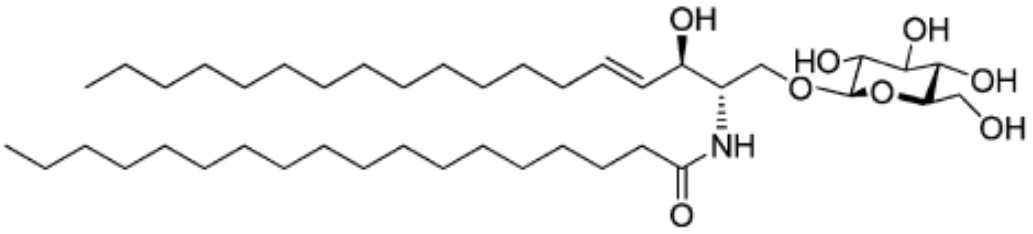

Figure 2: Schematic chemical structure of glycolipid (glycosphingolipid).Adapted from Xia Y, Peng L, 2018. [25]

1.2 Membrane Fluidity

Membrane fluidity is a complex feature of the cell membrane that reflects the main membrane characteristic organisation (gel or liquid crystal structure).[26] Basically, it determines the ease of diffusion and mobility of lipids and proteins in the plane of the membrane.[27] Different combinations of movement that lead to membrane fluidity are lateral diffusion of molecules in the plane of the membrane, transverse diffusion of molecules from one monolayer to the other, and the phase transition leading to lateral phase separation.[28] As the membrane is a heterogeneous structure, it comprises several coexisting domains with different fluidity characteristics.[29]

Lipid and protein composition regulate membrane fluidity.[30] It is affected by biochemical factors (degree of fatty acid unsaturation, protein/phospholipid ratio, phospholipids/cholesterol ratio) and some biophysical factors (pH, temperature, electric charges).[26] Saturated lipid acyl chains tend to form non-fluid, tightly packed gel phases at physiological temperatures, whereas unsaturated lipid acyl chains fluidize the bilayer. It is important to mention that cholesterol aids in maintaining membrane fluidity as well. Cholesterol mitigates the effect of temperature on membranes and acts as a buffer. It keeps lower temperatures from hindering fluidity and higher temperatures from excessively enhancing fluidity.

Maintenance of membrane fluidity is essential for cell function, viability, growth, and reproduction. Additionally, it also plays a crucial role in the efficiency of ligand binding, in the outcome of direct cell-to-cell contacts, and in the modulation of the activity of membrane enzymes.[31]

1.3 Membrane Lipid Asymmetry

Membranes allow cellular compartmentalization by facilitating interfaces to coordinate cellular interaction; hence, they are integral to how a cell functions. The compositional differences between the inner and outer leaflets of the plasma membrane have been well studied.[9] The asymmetric lipid distribution across the membrane is also well defined.[10] The outer monolayer has predominantly choline-containing glycerophospholipids PC and SM, while the inner monolayer consists of considerable amounts of amine- containing glycerophospholipids PE and all PS, together with the minor PI components as shown in Figure 3.

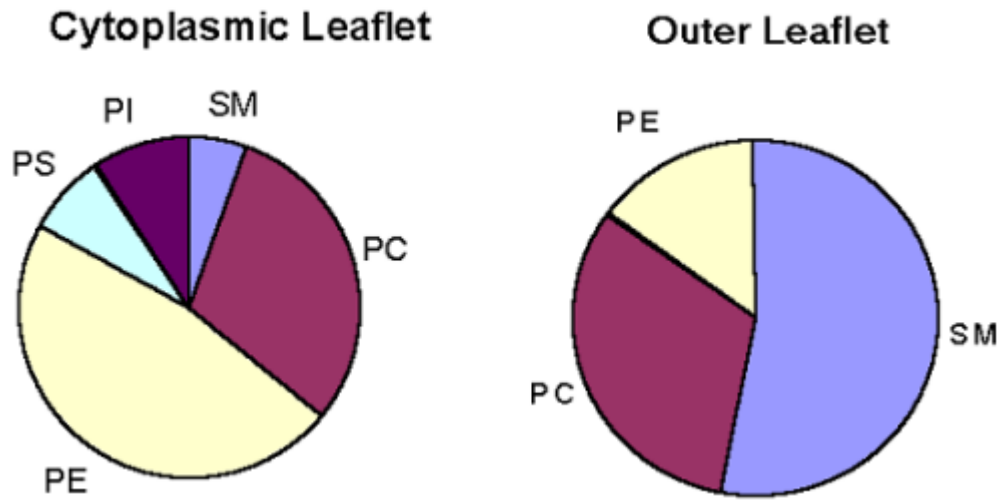

Figure 3: Major phospholipids distribution between the RBC membrane. Phospholipid distribution is shown in the human RBC cytoplasmic and outer leaflet: sphingomyelin (SM), phosphatidylcholine (PC), phosphatidylethanolamine (PE); phosphatidylserine (PS) and phosphatidylinositol (PI). Adapted from Filipe HAL, 2014.[32]

Additionally, it is important to note that lipid head groups are not the only limiting factor for lipid asymmetry, but also lipid saturation and chain length.[10] RBC exhibits similar lipid localization in each leaflet of the membrane bilayer, along with an equal distribution of cholesterol between the two leaflets.[11] Moreover, the higher abundance of unsaturation in the fatty acyl chains of RBC inner leaflet [33] facilitates the enhanced fluidity and low viscosity of its membrane. [34]

This asymmetric lipid distribution, or lipid gradient, is generated and maintained by a combination of protein-lipid interaction, slow trans-bilayer diffusion, and different types of energy-dependent and energy-independent lipid transport proteins/lipid

translocators.[35,36] The lipid translocators can be divided into three classes: i) cytofacially-directed, ATP-dependent transporters, aminophospholipids translocases also known as flippases; ii) exofacially-directed, ATP-dependent transporters, translocases also known as flippases; and iii) bidirectional, ATP-independent transporters known as scramblases.[37] Flippases, being the most selective, catalyse the movement of lipids from the outer to the inner monolayer, while flippases do the opposite against a concentration gradient in an energy-dependent manner. On the contrary, scramblases facilitate the bidirectional transfer of lipids in an energy-independent manner.[11]

Although the RBC membrane skeleton is primarily responsible for maintaining its discoid shape, the role of glycerophospholipid asymmetry across the membrane cannot be undervalued.[38] Transmembrane asymmetry of glycerophospholipid, in particular the exclusive localization of PS to the inner monolayer, has several functional implications in erythrocytes. RBC with exposed PS at their outer surface (thalassaemic and sickle red cells) are recognised and phagocytosed by macrophages[39] (reticuloendothelial system, especially spleen) and monocytes [40] hence, the localization of PS in the inner monolayer is critical to RBC survival. Furthermore, the conservation of PS to the inner monolayer ensures the unrestricted passage of normal red cells through the microvasculature by preventing its adhesion to vascular endothelial cells.[11,41]

1.4 Lipid Microdomain

The Singer-Nicholson fluid mosaic model predicted the random distribution of lipid and protein owing to their free rotational and lateral diffusion within the plane of the membrane.[42] Hence, it implies homogeneous organisation of membrane material. But numerous lines of evidence suggest that within the membrane, movement of most of the protein is partially restricted, and the membrane is highly asymmetric (heterogeneous), with differences in the lipid and protein composition between the inner and outer layers of the membrane. Protein-protein, protein-lipid, and lipid-lipid interactions are responsible for this lateral heterogeneity and compartmentalization in membrane organisation [43].

Compartmentalization of the cell membrane into functional microdomains plays a key role in facilitating processes like cell signalling, cell adhesion, and membrane trafficking. There are different types of membrane microdomains depending on size, composition,

and dynamics. Within the context of this thesis, the lipid based microdomain would be discussed. Lipid rafts (membrane microdomains, Figures 4A and 4B) are proposed to be highly ordered, specific subdomains enriched in cholesterol and saturated lipids such as sphingolipids, discrete from the surrounding sea of disordered, primarily unsaturated lipid species.[43] These subdomains arise due to interactions of cholesterol with saturated acyl chains, resulting in tight packing of these lipids in comparison to phospholipids, which are rich in kinked, unsaturated acyl chains. A liquid-ordered (lo) phase and a more loosely packed liquid-disordered (ld) phase arise due to this differential lipid packing. Cholesterol, along with the intermolecular hydrogen bonds present in sphingolipids, plays a crucial role in regulating phase behaviour.[44] The sorting of lipid and proteins is facilitated by the ability of lipids and protein to intercalate into this closed packed highly ordered subdomain. Additionally, lipid raft seems to be capable of regulating (either facilitating or inhibiting) neurotransmitter signalling or transport by guiding the clustering and trafficking of receptors and transporters. Lipid rafts can be planar (flat, Figure 4A) or non-planar (invaginated, Figure 4B).[45]

Caveolae (Figure 4B), a non-planar sub-type of lipid raft, which has biochemical similarity to lipid rafts, was identified 70 years ago. Their presence on the membrane is cell-type dependent (absent in most neurons and lymphocytes but in abundance in endothelial and adipocytes). Most caveolae are simple vesicular invaginations but can have branching networks in some cell types. Moreover, the other defining feature of caveolae is the presence of the cholesterol-binding protein caveolin. This protein is suggested to play an indirect role in various cellular processes by regulating plasma membrane organization and in particular, the distribution of both caveolae and lipid rafts (thus regulating cholesterol-dependent microdomains).[43]

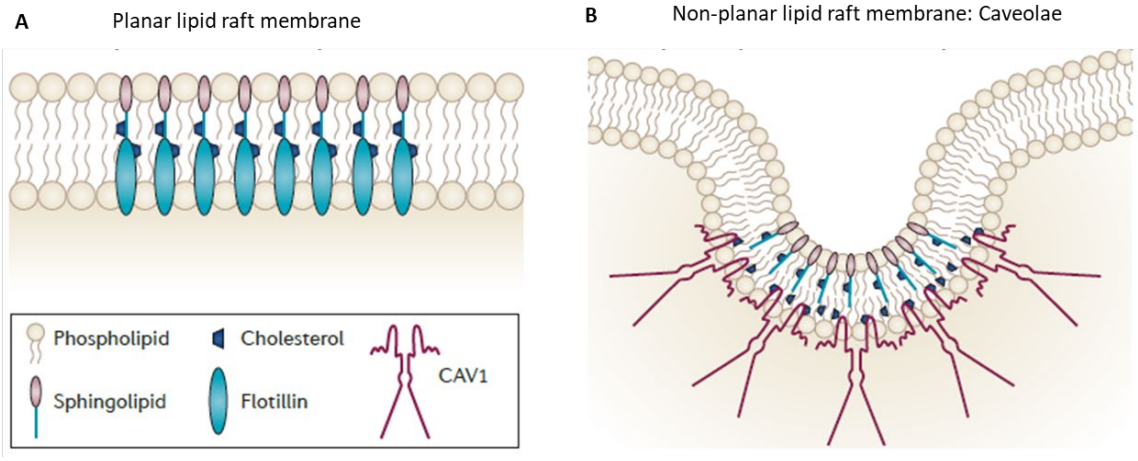

Figure 4: Schematic representation of membrane microdomains. The plasma membrane is composed of lipid rafts and non-lipid raft microdomains. Lipid rafts can be planar (flat) or non-planar (invaginated). A) Planar lipid raft microdomain. Planar lipid rafts derive their name because these microdomains are in the same plane as the non-raft membrane. B) Non-planar lipid raft microdomains. Non-planar lipid rafts, also known as invaginated lipid rafts or caveolae, are not situated in the same plane as the rest of the plasma membrane. Caveolae require caveolin proteins for their formation. Caveolin1 (CAV1) molecules in (B) are shown as hairpin-shaped structures in the inner leaflet. Adapted from Lisanti MP et al, 2015.

1.5 Membrane proteins

Protein molecules can be bound to, or associated with, the cell membrane in a variety of ways. Based on how the protein is associated with the membrane, it can be categorised into two general groups.

a. Peripheral membrane proteins
b. Integral membrane proteins

Peripheral membrane proteins require mild treatment for their dissociation from the membrane, forming lipid-free entities; hence, this suggests that they are loosely held to the membrane by weak non-covalent interactions, mainly electrostatic interactions.[42] On the contrary, integral membrane proteins require drastic treatment with reagents for their dissociation from the membrane. This leads to the formation of lipid-associated entities, hence suggesting that they are permanently embedded within the membrane.[42] Depending upon the relationship of integral membrane proteins with the bilayer, they can be further classified into transmembrane proteins and integral monotopic proteins.

Transmembrane proteins span the entire plasma membrane and are amphipathic in nature. Their hydrophobic region interacts with the hydrophobic tails of the lipid

molecules in the interior of the bilayer. Additionally, their hydrophilic regions are exposed on either side of the membrane. Integral monotopic proteins can be found attached to either side of the membrane (the cytosolic monolayer or the external surface cell). The type and amount of protein in a membrane are highly flexible and depend on the function of the cells. More than 50 transmembrane proteins of various abundances ranging from a few hundred to a million copies per red cell have been well characterized.[11] Different membrane proteins aid in transportation and adhesion; hence, they regulate the interactions of red cells with other blood cells and endothelial cells as signalling receptors.[11]

Most RBC-associated proteins are peripheral membrane proteins bound to the cytosolic side of the lipid bilayer. Spectrin is the most abundant of these proteins and is the main component of the cytoskeleton, which in turn maintains the structural integrity and biconcave shape of the membrane.[11]

Various blood group antigens are defined by a large fraction of transmembrane proteins. With respect to AB0 (H) blood group, glycophorin is an important single-pass transmembrane glycoprotein. The external part of this protein carries all the carbohydrates, accounting for 60% of the molecular mass. Around 40% of glycosylation and 90% of the negative charge of RBC membranes (conferred by the saccharide sialic acid) are associated with glycophorin.[24]

Band 3 protein is another transmembrane protein exposed to the RBC. It is a multipass membrane protein that regulates blood CO_2/HCO_3 exchange and is often known as an anion transporter.[46,47] Additionally, owing to the architecture of the Band 3 transmembrane protein, it aids in the selective transport of hydrophobic molecules across the membrane.

1.6 Critical role of membrane dynamics

The fluid-mosaic model of biomembranes establishes the importance of lipid dynamics for membrane function. The liquid-crystalline nature of the lipid bilayer was brought to the forefront and was recognised as the matrix of biological membranes, which is a stable bilayer of mostly phospholipids that maintain liquid-like properties in their molecular motions. All membrane components, including proteins, can have various

forms of motion (conformational, translational, and rotational movements) with different time scales, as shown in Figure 4. Regarding speed of movement, individual bonds are fastest in movement, followed by motions of lipid segments. The time scale of motion covers over 15 orders of magnitude, from femtoseconds to hours.[14]

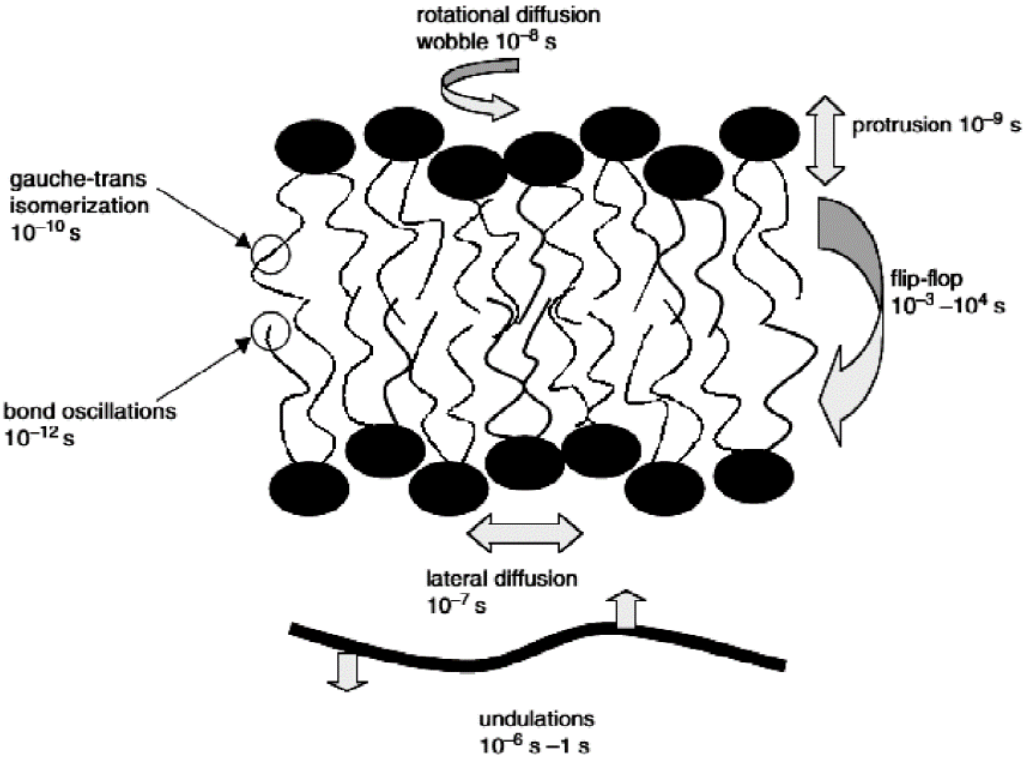

Figure 4: Lipid motion in biological membrane and their respective characteristic times. Adapted from Filipe HAL, 2014.[32]

Fluid character influences the working of the biological membrane immensely and is imperative to its functionality. It facilitates the distribution of membrane lipids and proteins from the insertion site to other regions of the cell, allows membranes to fuse and mix molecules, and ensures the even distribution of membrane molecules. Furthermore, the spontaneous desorption and insertion of lipids, which is another critical movement or motion, is significant for the interaction of other molecules with biomembranes.[14,32,48]

Membrane order and dynamics can be influenced by biochemical factors (degree of fatty acid unsaturation, protein/phospholipid ratio, phospholipid/cholesterol ratio) and some biophysical factors (pH, temperature, electric charges, and interaction with

solvents and solutes).[26] Saturated lipid acyl chains tend to form non-fluid, tightly packed gel phases at physiological temperatures, whereas unsaturated lipid acyl chains fluidize the bilayer. It is important to mention that cholesterol aids in maintaining membrane fluidity as well. Cholesterol mitigates the effect of temperature on membranes and acts as a buffer. It prevents lower temperatures from inhibiting fluidity and higher temperatures from increasing fluidity too much. Membrane fluidity and order have a considerable impact on solute permeation and uptake and release processes.

1.7 Cell surface modification techniques

Cell surface composition mediates all interactions of the cell with its environment, along with cell function and cell-cell interaction. Hence, cells have the potential to serve as therapeutic and delivery agents, making them an invaluable biomedical tool. Cells are also very essential for various laboratory-based diagnostic applications.[49] This rich repertoire of molecules (lipids, proteins, and carbohydrates) offers an excellent opportunity to engineer the cell membrane and is a powerful tool to manipulate interactions between cells and the surrounding environment.

Cell surface engineering, functionalization, or modification can be defined as a technique through which the cell surface is modified by means of the localization of biofunctional moieties or endogenous labels, conferring new characteristics and functions to cells. However, cell surface engineering is particularly challenging owing to the highly dynamic and complex nature of the cell membrane. Here, both lipid and protein components of the membrane are continuously internalised, displaced, degraded, and replaced by de novo synthesis.[50] Additionally, a small change to the biological environment of cells, like temperature, osmolarity, ionic strength, and pH, induced by surface modification is highly detrimental to the cell's viability and/or function.[51]

The starting point of any cell modification strategy involves looking into how to interface the cell with the desired exogeneous material of interest. Over the years, a variety of chemical and material science strategies have been developed to synthetically impart cells (surfaces) with new properties and functions by redefining the molecular landscape of the plasma membrane (Figure 5).

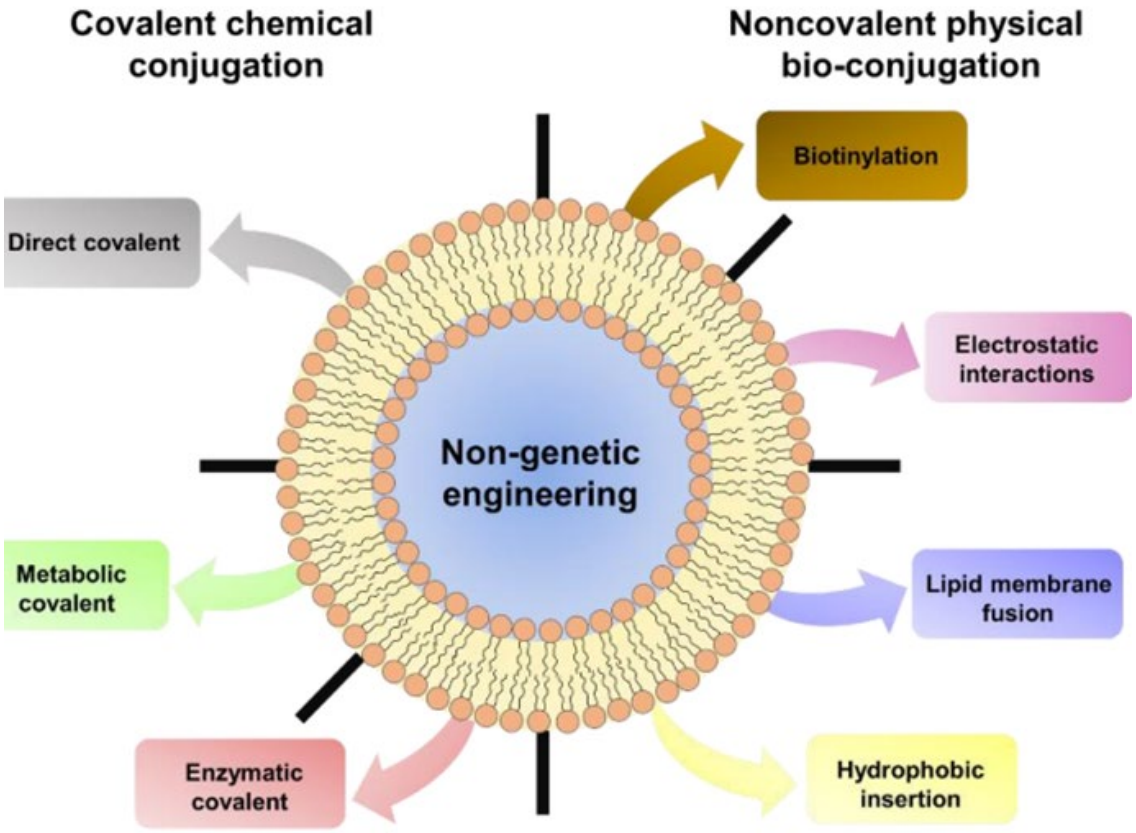

Figure 5: An overview of present research in non-genetic cell surface engineering. Chemical and material science strategies developed to synthetically impart cells (surfaces) with new properties and functions by redefining the molecular landscape of the plasma membrane. Adapted from Lui et al, 2019. [52]

As reviewed by various authors [51,53], cell surface modification has commonly been achieved by two major methods: Genetic engineering and non-genetic engineering. Genetic engineering works by means of the incorporation of exogenous genetic material into cells, which in turn codes for an artificial cell surface receptor to modulate its functionality.[54] Although robust and versatile in its methodology, genetic modification is reported to include a complex and poorly controllable, time-consuming modification process. Moreover, it is limited to single allele modification and does not modify all types of cells, especially stem cells and slowly dividing cells.[55]

The non-genetic cell surface modification process is further broadly divided into two categories:

a) Covalent conjugation

b) Non-covalent bioconjugation

Figure 6 represents the schematics of the mode of non-genetic cell surface modification interactions.

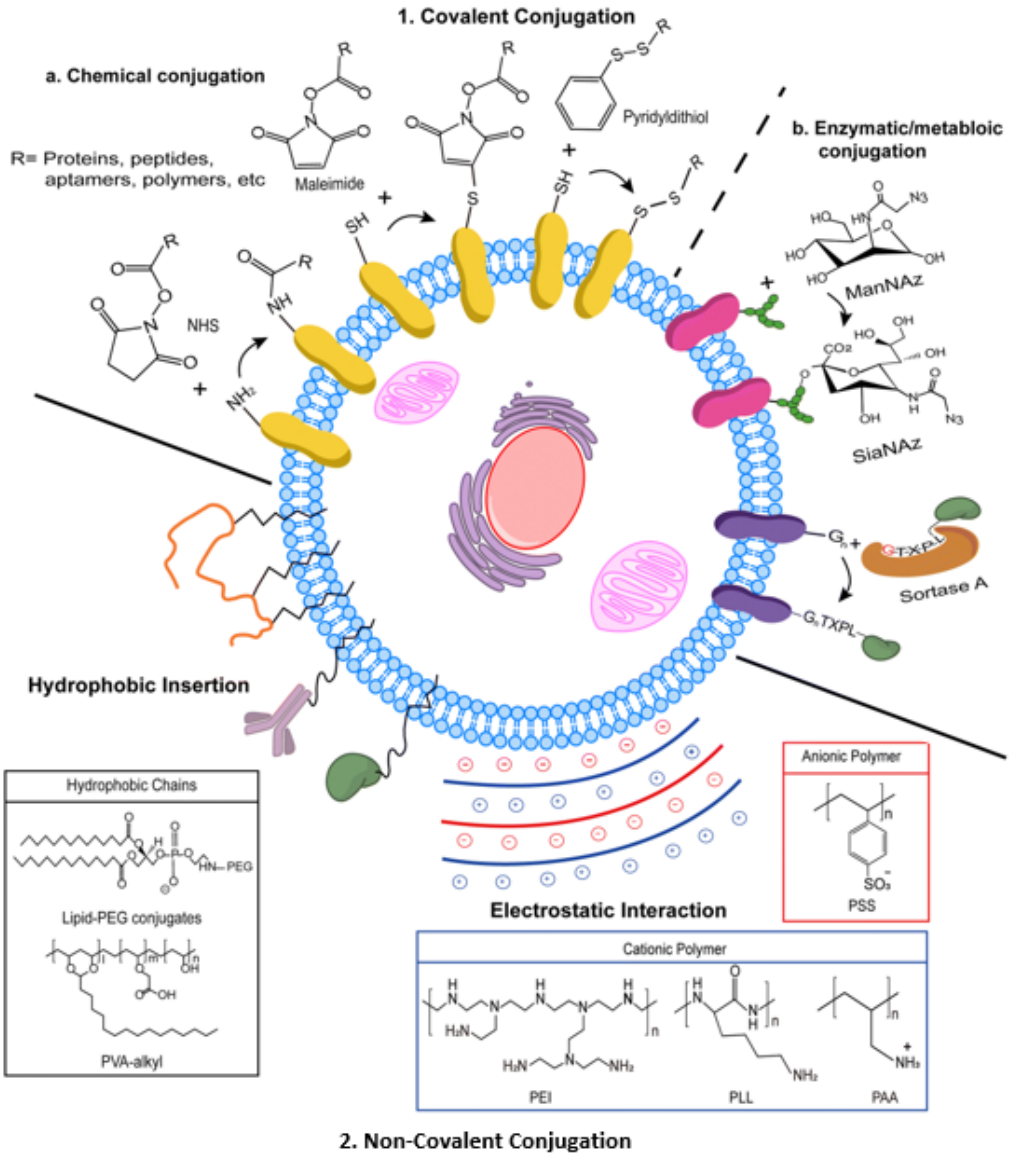

Figure 6: Schematics of the mode of non-genetic cell surface modification interactions (in detail). Adapted from Lee et al, 2018. [55]

1.7.1 Covalent conjugation

Covalent conjugation is achieved by pairing the desired exogeneous material with the cell surface through the formation of a strong molecular bond made by the sharing of electrons in the atoms. Here, the pre-existing (direct) or introduced (indirect) functional

group on the cell surface protein, lipids, or polysaccharides chemically ligates with targeting ligands. Direct covalent modification is the most straightforward cell remodelling strategy. It takes advantage of naturally present, surface-exposed functional groups (parts of proteins or carbohydrates) as grafting points.[55] The most straightforward approach involves the direct chemical reaction of an amino (lysine—NH_2) or thiol (cysteine—SH) group presented on a cell membrane protein with a compatible reactive group or functionalized cross-linkers on exogeneous material. For example, *N*-hydroxysuccinimidyl ester (NHS) groups, maleimides, and pyridyl dithiol-conjugated material selectively attaches to surface-exposed amine groups and thiol groups[52] (Figure 6).

Indirect covalent modifications mostly include metabolic-mediated and enzymatic-mediated modifications. Both modification strategies require multiple steps to achieve the desired cross-linking. For metabolic-mediated modifications, a chemically reactive functional group (which is absent from the native plasma membrane) is first introduced into target biomolecules via metabolic pathways. These metabolically introduced functional groups are known as “chemical reporters” by the endogenous machinery of the cell. In the second step, the reporter group covalently reacts with the target functional molecules through bio-orthogonal ligation (or click chemistry). Azides and ketones are the most common chemical reporters metabolically incorporated into the cells by unnatural sialic acid biosynthesis. The corresponding biorthogonal ligations of azide are aryl phosphine, alkyne, and cycloalkyne, while the reaction of ketone requires hydrazide [52,56] (Figure 6).

For enzymatic-mediated modifications, the reactive functional group is generated or made available through enzymatic treatment of the originally existing cell surface molecules. Here, the limited presence of aldehydes and ketones containing surface functional groups is enhanced through enzymatic treatment (galactose oxidase) to successfully attach complementary surface-modifying exogeneous molecules (Figure 6).

Direct covalent conjugation strategies have broad applicability; however, they provide the least control over cell surface modification as the degree of modification is difficult to regulate. The drawbacks associated with the indirect covalent conjugation approach are mainly that the reactive groups are only generated through chemical and enzymatic

treatment of existing cell surface molecules. Both approaches introduce significant physiological alterations, mostly leading to damage to existing functional components of the cell.[2]

1.7.2 Non-covalent conjugation

Non-covalent conjugation is possibly a passive modification strategy where exogeneous molecules spontaneously modify or functionalize cell surfaces via either the spontaneous insertion of hydrophobic anchors or electrostatic interaction or adsorption. Different mechanisms of non-covalent modification are listed below.

Electrostatic interaction

The outer surface of mammalian cells is reported to carry a net negative charge owing to the presence of sialic acid residues on glycoproteins, phosphate groups of phospholipids, and carboxylate groups on proteins. Electrostatic interaction modifies the cell surface by utilising the opposite charge interaction between the negatively charged cell membrane and the positively charged modifying materials (cationic polymers). Cells initially modified with cationic polymers can be engineered again via a layer-by-layer technique by sequentially applying anionic and cationic polymers, forming modified cells with multi-layered structural assembly and a defined microenvironment. [57,58] This non-invasive encapsulation confers a reduced molecular recognition of the modified cells, hence making it a prominent functionalizing agent for cell transplantation research.[58] However, the biocompatibility of cationic polymers is a major issue of concern with electrostatic interaction.

Hydrophobic interaction

Hydrophobic residues in the transmembrane helices region of the integral membrane proteins facilitate or enable their complementary interaction with the hydrophobic lipid bilayer, hence anchoring the membrane protein into the cell membrane.[2] This hydrophobic effect, which regulates the incorporation and orientation of transmembrane proteins, has been utilised for cell surface modification. Thus, hydrophobic interaction can be understood as a complementary interaction between the hydrophobic zones in the cell membrane and the hydrophobic residues in the modifying exogeneous labels. When biofunctional moieties (like fluorophores, peptides,

chelators, etc.) coupled with an appropriate hydrophobic anchor are admixed with cells, the hydrophobic component can spontaneously insert into the lipid bilayer, anchoring the conjugated cargo on the surface.[59] The hydrophobic anchors coupled to the functional moieties could either be lipophilic (non-lipid)[49] or lipid-based analogous.[55]

Surface modification with hydrophobic insertion allows membrane-anchored bioactive molecules to participate in the dynamic movement of the cell membrane, unlike covalent conjugation and electrostatic interaction. Most importantly, cells modified with lipid-conjugated biomaterials have been documented to resume normal cellular activities with negligible toxicity.[60,61] Although molecules of interest must be hydrophobized (by lipid analogous or lipophilic alkyl chain conjugation), conferring variable retention time, it could be summed up that hydrophobic insertion techniques offer rapid and nontoxic modification to a wide range of cells. Within the context of this thesis, non-covalent conjugation-based labels are of interest and are discussed.

1.8 Non-covalent Cell surface labelling agents

Over the years, the most widely used cell-modifying agents have included labels like radionuclides or fluorescent-based labels. Some commonly used modifying agents are discussed below.

1.8.1 Radiolabels/Radionuclides based labels

All elements can exist as two or more isotopes, some being stable indefinitely while others are unstable (radionuclides). Radionuclide decays mainly through emitting α particles, β particles, and γ radiation, which is detected and visualised by scintillation systems, positron emission tomography (PET), single photon emission computed tomography (SPECT), or gamma cameras. The quick detection of even minimally emitted radiation underlies the utility and high sensitivity of the radioactive label.

Radionuclide-based membrane anchoring agents (like lipophilic long alkyl chains or hydrophobic groups) have been evaluated as cell membrane labelling agents, owing to their property of anchoring into the lipid bilayer of the cell membrane. Radionuclides lipophilic agents, like Hexadecyl-4-^{124}I-iodobenzoate (^{124}I-HIB) [62] (Figure 7A), ^{64}Cu- labeled hexadecyl-1,4,7,10-tetraazacyclododecane-tetraacetic acid-benzoate (^{64}Cu-DOTA-HB) [63] (Figure 7B) and ^{18}F-HFGhexadecyl-4-^{18}F-fluorobenzoate (^{18}F-HFB) [64]

(Figure 7C), anchors to the cell membrane by simply incubating with it. ^{124}I-HIB and ^{18}F-HFB are radiotracer synthesized from a lipophilic long-chain ester and have been shown to label adipose-derived stem cells (ADSCs) and mesenchymal stem cells (MSCs), respectively. In the case of ^{64}Cu-DOTA-HB, hexadecyl benzoate (HB) has lipophilic property; hence, it mediates an easy and tight anchorage of the radionuclide onto rat ADSCs.

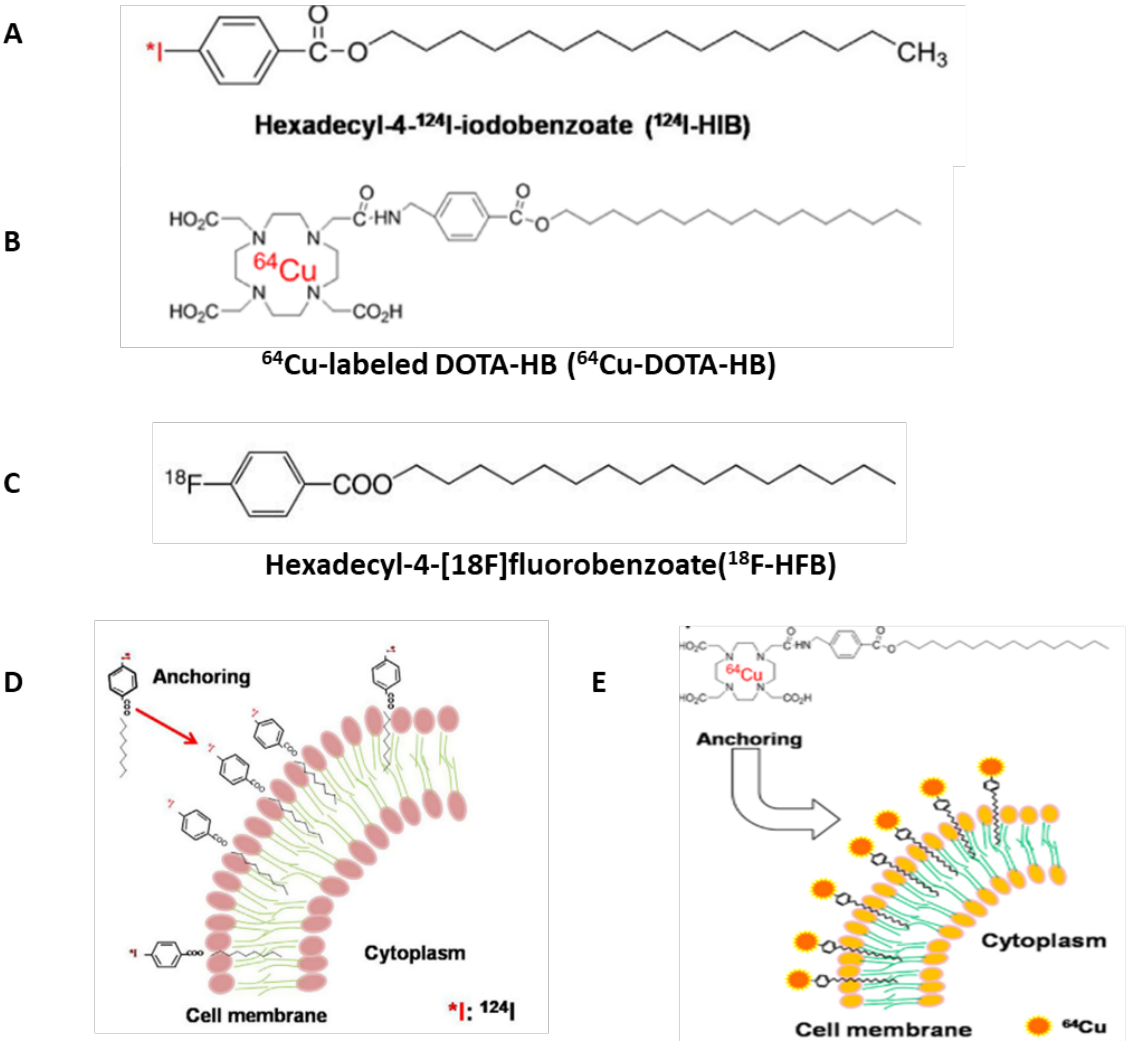

Figure 7: Chemical structures of radionucleotide based lipophilic labeling probes. **A**) ^{124}I-HIB, **B**) ^{64}Cu-DOTA and **C**) ^{18}F-HFB. Schematic diagram of a **D**) ^{124}I- HIB and **E**) ^{64}Cu-DOTA-HB labeled cell. Adapted from Kim et al, 2015, and Ma et al, 2005. [62,63,65]

Although labelling cells with radionuclide labels via non-covalent conjugation is promising, there are still many challenges to overcome. Due to the short half-life of ^{18}F radionuclide (109.7 min), it has a detection limit of 5-6h; hence, tracking of labelled cells

is limited by the radionuclide label half-life. This has also impacted the evaluation of its cytotoxic effect on labelled cells. Additionally, the label uptake into cells was only found to be 25%, and it showed significant leakage into the supernatant, inferring low retention and stability.[65,66] ^{64}Cu and ^{124}I based radionuclides have a comparatively longer half-life, but even after 2 hours of incubation with cells, their cell labeling efficiency is only around 50% with ≥ 80% viability.[62,65]

It could be summarised that although labelling cells with radionuclide labels allows for sensitive detection of a very small number of cells, issues regarding cellular and systemic toxicity still need to be evaluated. Moreover, lower uptake rates by cells, probe leakage, and/or relative rapid loss of signals have limited its further application.

1.8.2 Fluorescence based labels

Fluorescence based labelling technology has grown over last few years as exogeneous fluorophores are known to be particularly suitable for probing biological structure and function.[67] It is important to understand why fluorescence-based labelling techniques are so often chosen and why fluorescence detection is the key in a multi-billion-dollar detection industry? The answer is complex, and factors vary for different applications. But generally, fast signal acquisition, sensitivity, simultaneous use of multicoloured dyes for multiplex assays, small label size and localized signals characteristics of fluorescence detection drive the decision.

Fluorescence based membrane labels/probes which label cell membrane via possibly passive modification with hydrophobic anchors can be categorised into

a. Lipophilic fluorescent probes/non-lipid membrane probes
b. Fluorescent analogous of natural lipids/Lipid conjugates

1.8.2.1 Lipophilic fluorescent probes/non-lipid membrane probes:

Lipophilic fluorescent probes have little structural resemblance to natural lipid biomolecules, hence, are nonlipid in nature. It can be broadly divided into two groups. First category comprises of long-chain hydrocarbons (carbocyanine) lipophilic probes (Figure 8A): molecules which bears a charged fluorophore that localize the probe at the membrane's surface and lipophilic aliphatic "tails" that insert into the membrane and

thus anchor the probe to the membrane. Most widely used carbocyanines membrane probes have been the PKH, DiI, and DiO.[68] PKH lipophilic probes such as PKH2, PKH67 (green), PKH3 and PKH26 (red) have been used for labelling and tracking lymphocytes. DiI, and DiO series of lipophilic dyes are comparatively recent and is often used as a long-term tracer for neuronal cells.[68] Although, carbocyanine dyes appear in to broadly cover the visible spectral range, they exhibit irregular and inefficient labeling.[69] They have limited water and physiological buffer solubility, as the probes have a requirement of organic solvent to disperse in. Moreover, PKH dyes require osmolarity-regulating agent as diluent for labelling cells and have been reported to micro environmental contamination.[70]

Second category comprises of polycyclic aromatic hydrocarbons like classic membrane probes (Figure 8B). Particularly notable members of this group are DPH, pyrenes, NBD, prodan, laurdan. These probes tend to localize within or at cell membrane. They are used for studying structural, biophysical (viscosity, polarity, lipid order) and membrane dynamic (fluidity, membrane fusion/budding) properties of biological membranes.[71] Membrane probes limitations are quite like carbocyanine based dyes. They are insoluble in water and aggregate strongly, thus possess variable non-uniform dye-dependent characteristics. Incorporation of membrane probes like DPH increases the bilayer thickness leading to local ordering effect.[71]

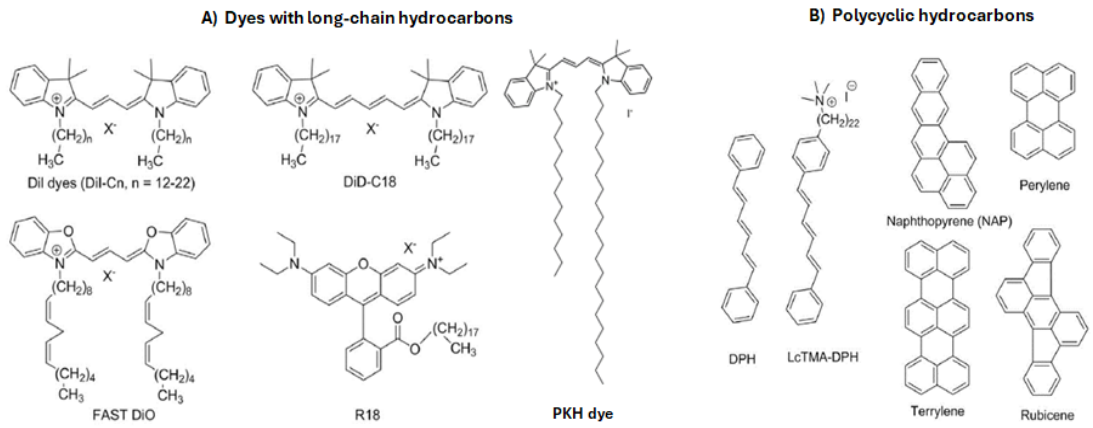

Figure 8: Chemical structure of lipophilic fluorescent probes.**A**) Dyes with long-chain hydrocarbons: Dialkylcarbocyanine dye, Octadecyl Rhodamine B Chloride (R18), PHK26 red dye. **B**) Dyes with polycyclic hydrocarbons: DPH (1,6-Diphenyl-1,3,5-hexatriene), 22-(diphenylhexatrienyl)-docosyltrimethylammonium (LcTMA-DPH), Naphthopyrene (NAP), Perylene, Terrylene, Rubicene.

1.8.2.2 Fluorescent analogous of natural lipids/Lipid conjugates:

Owing to the complexity of plasma membrane, observing, and understanding specific interactions within the membrane is a challenging endeavour. Lipid bilayer being a heterogeneous collection of lipid molecules, creates an inner and outer leaflet and it is the primary structure of the membrane. Because the vast majority of naturally occurring membrane lipids are non-fluorescent, extrinsic fluorescence-based membrane probes have a particular advantage. Hence, it would enable researchers to study complex biological with exquisite sensitivity in applications ranging from imaging to flow cytometry.

As previously discussed in section 1.1, membrane lipids can broadly be defined as hydrophobic or amphiphilic small molecules which consist of a hydrophobic chain and a hydrophilic head group region. Accordingly, there are in principle two regions within the molecule to which fluorescent dyes can be coupled. Fluorescent analogs of naturally occurring lipid classes are briefly described below.

In the fluorescent phospholipid analogs, the fluorophore can be attached to one (or both) of the fatty acyl chains or to the polar head group. The attachment position of the fluorophore determines whether it is in the nonpolar interior or at the water/lipid interface when the phospholipid analog is incorporated into a lipid bilayer membrane.

Several glycerophospholipid analogs with fluorescent dye (Pyrene, DPH, NBD) labelled acyl chain and fluorescent head group are available. Phospholipids based probes are useful probe of lipid–water interfaces and for monitoring membrane fusion. Fluorescent Sphingolipid analogs like NBD C6-Ceramide have been extensively used for understanding sphingolipid metabolism in cells. Additionally, fluorescent fatty acids and steroids-based analogues are also available as derivatives based on NBD, pyrene and dansyl -fluorophores.

Fluorescent lipid analogues probes are structurally like natural lipids; hence they are proposed to remain buried in hydrophobic interior of lipid membranes and emits fluorescence by mimicking their natural counterpart. Several methods have been proposed for labelling cells using lipid analogues. One of the easiest procedures involves simple incubation of cells with fluorescent lipids. This has been reported to be least effective as rapid internalization enables very small amount to be retained on membrane.[72] For example, fluorescent derivative of ceramide is incorporated into cells by simple incubation step, but it mostly accumulates in the Golgi apparatus followed by endoplasmic reticulum and membrane retention is minimal.[72]

Another widely used procedure involves incubation of cells with BSA-fluorescent lipid analogue complex. This protocol involves multiple temperature incubation setup. Temperature variation causes activation of stress responses. Moreover, it also enhances internalization of probes leading to low fluorescent signal intensities rendering fluorescence detection difficult.[73,74] Additionally, presently available fluorescent lipid analogues require organic solvent (chloroform or mixtures of benzene or toluene) for solubility and are also limited in application as there is a need of carrier (liposomes) for gentler and more reproducible labelling of cells.[75,76]

Given the differing, and often complementary, advantages and limitations for fluorescence based described, there is need to develop better non-cytotoxic, stable, uniform, intense, and reproducible fluorescent labeling agents of cells.

1.9 Dynamics of uptake of glycolipids in cell membrane

The concept of “spontaneous uptake” of hydrophobic anchors/antigen to modify the RBC membrane has long been studied and documented.[48] Different uptake mechanisms

(for natural and exogenous lipid-based entities) via non-covalent modification are discussed here.

1.9.1 Uptake of natural glycolipids

Glycolipids, by nature of their lipid tail, are proposed to spontaneously self-acquire from the surrounding milieu into the RBC membranes (and other cells). Additionally, modification of the membrane was also suggested to be aided by unique properties of the plasma membrane, like the capability of membrane lipids to rearrange themselves (Section 1.3). The following sections detail the dynamics of the uptake of various glycolipid-based antigens.

1.9.1.1 J and R antigen uptake

Stormont in 1949, reported that when bovine's J-negative RBC was incubated with J- positive plasma, J-negative RBC transformed to J-positive. It was inferred that this *in vitro* transformation of RBC was acquired on contact with plasma.[77] Stormont findings was further supported by work undertaken in sheep, wherein the R-negative RBC transformed to R-positive after sufficient incubation with plasma from R-positive sheep.[78]

1.9.1.2 Lewis antigen uptake

The transformation of human RBCs with Lewis antigen was first studied by Sneath and Sneath in 1955.[79] Initial studies explored whether the Lewis RBC antigens in a patient could be transformed after transfusion of different Lewis groups.[79,80] During the course of the study, a recipient of Le(a-b+) received a transfusion of Le(a+b-) blood. After post-transfusion separation of samples from patients, the donor RBCs were found to have transformed from Le(a-b+) to Le(a+b+). Hence, it was inferred that the donor RBC had acquired Le^a Lewis antigen from the recipient's plasma.

Sneath and Sneath reproduced the above finding of Lewis antigen transformation *in vitro* as well. [79] During this study, one part of packed RBC was co-incubated and continuously shaken with ten parts of plasma at 35°C for at least three days, with plasma replacement every 24 hours. The results indicated that within 24 hours, Le(a+b-) RBCs acquired Le^b from Le(a-b+) plasma and transformed to Le(a+b+); Le(a-b+) RBCs acquired

Le^a from Le(a+b-) plasma and transformed to Le(a+b+). These results hold true when cells are either A_2 or O cells. Moreover, Le(a+b-) and Le(a-b+) RBC, when incubated with Le(a-b-) plasma, gradually lose their antigens, while Le(a-b-) RBC acquires either antigen.[79] Hence, in summary, red cells lacking Lewis antigens would acquire them from plasma containing them. Likewise, red cells expressing Lewis's antigens would lose them to plasma lacking them, particularly inferring the soluble nature of Lewis antigens.

Although the methodology involved in the *in vitro* work of Sneath and Sneath established plasma as a carrier medium for most upcoming insertion experiments, the structural nature of the acquired Lewis antigen from plasma was still undiscovered and it was largely believed to have a glycoprotein based nature. [81]

In 1969, Marcus and Cass reported that Lewis blood group antigens are not intrinsic to red cells, i.e., the Lewis antigens are acquired on red cells from plasma and are not synthesised in situ. [79,82] This study also put an end to previous assumptions about the glycoprotein nature of Lewis antigens in plasma and reported that they are glycosphingolipids. [82]

1.9.1.3 ABH Antigen uptake

The ABH antigen uptake phenomenon was first observed and reported by Renton and Hancock in 1962. [83] From the Renton and Hancock study (in an *in vivo* setting), it could be summarised that when O cells were transfused to group A and B patients, circulating O cells acquired A and B antigens present in the plasma. [83] These observations compelled Renton and Hancock to further study the phenomenon in *in vitro* settings. In the planned experiments, O red cells were incubated at 37°C with A_1 blood and A_1 plasma. Results obtained from an *in vitro* study showed that the O red cells could not acquire A antigen. This result was not found to be surprising, as it agreed with the slowness of antigen uptake in *in vivo* settings, along with additional factors interfering with the uptake (induced hemolysis due to prolonged incubation at 37°C). [83]

In 1974, Garretta reported the acquisition of A and B antigen by O red cells in an *in vitro* setting.[84] Here, the O red cells were incubated with five times more volumes of A and B serums at 37°C with frequent resuspension.[84] Additionally, in 1975, Tilley and co- workers also showed that A, B, and A_1Le^b antigens were acquired by red cells that

had been incubated with glycosphingolipid fractions generated by the serum of donors from groups A, B, and A_1, Le(a^-b^+).[85] This study also reported some important observations, like: when a time-dependent uptake study was performed at 37°C, uptake of antigen was found to be better at 2 than 1 h, and the uptake did not increase post-3 h of incubation; Uptake of antigen by red cells was inhibited when the lipid fraction had serum added to it.[85] In summary, these studies implied that various parameters, like duration of incubation, temperature of incubation, and concentration of the antigen fraction, regulate the amount of antigen uptake by red cells.

1.9.2 Uptake of exogenous glycolipids

Studies on exogenous glycosphingolipids, especially gangliosides (charged glycolipids) uptake from the culture medium has been documented by a wide range of cells *in vitro.* Preliminary study on kinetics of uptake of different exogeneous ganglioside by cells was carried forward by Callies and co-workers in 1975.[86] Herein, murine CI-1-D fibroblast, chicken embryo fibroblasts and chicken erythrocytes were utilized to estimate the accumulation of exogeneous gangliosides at 37°C and 2- 4°C, over the period of 2 h. It was concluded that gangliosides uptake at 37°C was biphasic in nature i.e., uptake occurred (in two phases) with intermediate plateau of saturation: initially gangliosides incorporated with time and attained plateau within 15 minutes, henceforth, after 10 minutes uptake gained momentum again to attain a final stage approximately after 2 h. Additionally, at 2-4°C, uptake of gangliosides was lower compared to 37°C but was still quite detectable. Out of all the cells used in this study, chicken erythrocytes accounted for the least amount of uptake at both 37°C and 2-4°C.[86]

Study on the mechanism of ganglioside uptake projected that the exogeneous ganglioside could be present in the solution as either monomers, oligomers, or micelles. There are three possible modes by which gangliosides can incorporate into the membrane: serum sensitive loosely associated micelles; serum resistance, trypsin releasable forms, consists of more firmly held monomers or micelles (interact via attachment to proteins exposed on cell membrane/ protein-bound); trypsin stable (impervious to proteolytic enzyme's attach) mainly monomers acquired into the hydrophobic regions of the membrane.[87,88] Physical properties of gangliosides regulate the three abovementioned modes of incorporation as due to the amphiphilic properties of gangliosides, the aggregates i.e., micelles of different shapes are formed in the

suspension solution when concentration reaches above its critical micellar concentration. Chemical composition of its hydrophobic and hydrophilic regions regulates the shapes of these aggregates. Various factors are predicted which could regulate the net uptake of ganglioside onto the cell membrane, like, ganglioside concentration, temperature and length of incubation process, serum, cell shape and electric charges, cell age and washing techniques. Fluorescent analogues of gangliosides have been utilized to study the localization process after its uptake. These studies gave inadequate insight into ganglioside localization because of limited resolution of light microscope.[88]

Exogenous lipid-based probes have been demonstrated to interact with RBC largely by adsorption. Uptake via endocytosis is unlikely to occur because mature RBC do not carry out endocytosis, yet some investigations have shown endocytosis in adult RBC. The interaction of lipid-based probes with RBC is affected by their composition, charge and concentration, as well as the temperature and time of incubation. Increasing these settings can promote interaction but also RBC damage.[48]

Exogeneous lipid-based probes have been demonstrated to adsorb both loosely (removed by washing) and tightly (removed by enzyme treatment) to the RBC surface.[88] Negative charge, extended incubation time, higher incubation temperatures, and increased probe concentration all improve RBC-lipid-based probe interaction.[48,89] Damage to the RBC membrane was also shown to increase as incubation duration and temperature were increased.[90] Increased temperature would enhance the collision rate between RBC and lipid-based probes as well as the fluidity of membranes, thereby creating more favourable conditions for lipid-based probe transmission.[13,91]

1.10 Cellular uptake of lipid-analogous probes or lipid conjugates

Lipid-analogous probes, upon contact with the cell's outer membrane, may interact with the extracellular matrix or plasma membrane components and then potentially penetrate the cell. This interaction is hypothesised to mainly happen through adsorption, fusion, and lipid exchange. The interaction between cells and probe may involve a combination of these interactions. Identifying the specific mechanisms involved might be challenging, particularly when multiple pathways of uptake may operate concurrently under particular circumstances. Additionally, these interactions

will depend on both the characteristics/surface activity of the probe and the physical properties of the host membrane.[92,93] Potential factors affecting these interactions are discussed in detail in section.

1.10.1 Adsorption

Adsorption occurs when lipid-analogous probes become stably associated with the cell surface or glycocalyx without becoming incorporated into the cell membrane or internalised within the cell. This type of association is non-specific and occurs due to electrostatic, van der Waals, and hydrophobic forces.[94,95] The probes may be loosely adsorbed to the cell membrane, in which case they can be removed by washing, or may be tightly adsorbed to the cell surface.[96,97] Following adsorption lipid exchange and/or fusion may occur, but usually the probe remains intact and distributed onto/into the lipid membrane.[94] However, the nature of the interactions between probe and lipid bilayers is complex and involves different steps (insertion/uptake, translocation and desorption).[14,93]

There is limited information available on mechanism of lipid-analogous probe interactions with biological membranes which is surprising considering their biological significance. Filipe HAL. (2014) proposed different models to explain the interaction of lipid- analogous probe with biological or lipid membranes. These models were based on the solubility of the probe (molecule of interest) in the aqueous medium and the lipid bilayer.[14,92] The three different models based on the solubility of the molecules of interest (probe) are

- Probes with high solubility in the aqueous media and insoluble in the lipid bilayer
- Probes with very low solubility in the aqueous media and a high partition into the lipid bilayer
- Probes with a moderate solubility in the aqueous media and lipid bilayer

The first model deals mostly with the target molecule (probe), which is completely soluble in the aqueous medium and does not associate significantly with the lipid bilayer. Thus, the probe molecules in the vicinity of the lipid bilayer on one side will permeate directly into the other side of the bilayer with a given rate constant.[14] Additionally, the second model deals mostly with the probe, which is highly soluble in

the lipid bilayer with minimum or no solubility in aqueous media. The third model requires the target molecule to be moderately soluble in aqueous media as well as in the lipid bilayer. According to the third model, it is hypothesised that the target probe is unrecognisable by transporters in the membrane, and the amphiphilic molecules cross the membrane barrier by probably passive mechanisms. The target molecule binds with the lipid bilayer moderately, i.e., by the partition-diffusion mechanism, and the target molecule gradually equilibrates between the distinct compartments.[14]

1.10.2 Endocytosis

Lipid-analogous probes can be taken up into cells via endocytosis. The cell membrane engulfs lipid-based probes, forming an endocytic vesicle.[98] The probe is normally sent to lysosomes for destruction, although it may occasionally escape into the cytoplasm. Endocytosis can be divided into two main uptake pathways: phagocytosis (immune-regulated uptake of large particles) and pinocytosis. The mechanism is comparable to the absorption of small molecules and fluids from the surrounding environment. It is found in nearly every cell and is necessary for food intake.[99] It can occur through both specific (mediated by receptor-ligand binding processes) and non-specific mechanisms.[100,101] Uptake via endocytosis is unlikely to occur as mature RBC do not carry out endocytosis, although some studies have reported the detection of endocytosis in adult RBC.[102]

1.10.3 Factors influencing interaction between lipids-analogue and cells

The interaction between lipid analogous probes and cells is dependent on many factors. For example, on the cell type, probe composition and conformation in the solution phase, and environmental conditions.[87]

The uptake of lipid conjugates or lipid analogue probes by biological membranes has been shown to be affected by their conformation in the solution phase. In particular, they could be present in aqueous solution as either monomers, micelles (mixtures of monomers and micelles), or aggregates.[87,88] The nature of their conformation is determined by the structure of the compound. Thus, understanding the conformation (free or micelle) of probes in the solution phase (i.e., characterisation) is important to understanding their interaction with cells.[103,104] According to Schwarzmann G., the critical micelle concentration (CMC) regulates the uptake of lipid conjugates into the

biological membrane.[99] The CMC is defined as the concentration above which micelles form in a dispersion of amphipathic molecules. The amphipathic molecules are found in the aqueous phase as monomers below the CMC, but above the CMC, the monomers group together to form micelles.[105] Monomers and micelles are in a dynamic equilibrium above CMC. Both the molecule's characteristics and the external environment have an impact on CMC.[106-109] With regard to phospholipids, this includes their charge, temperature, pH, ambient electrolytes, and structure (including the size and structure of the head group and the length and saturation of hydrophobic lipid chains). Surface tension (Wilhelmy Plate, Du Nouy ring, and Pendant drop methods), electrical conductivity, calorimetry, static and dynamic light scattering, and fluorescence (quenching) spectroscopy are some of the techniques used for determining CMC.[109] The technique and data interpretation have a significant impact on the measured CMC outcome. There is no one gold standard approach to assess CMC, and there isn't always a consensus on how to interpret experimental results to find the CMC point. Techniques are chosen according to the specifications and properties of the molecule that has to be measured. Lipid conjugates at or above CMC have shown to reduce their uptake compared to when present in the monomer form. [87,88]

Additionally, various other factors which affects the net uptake of lipid conjugates are:

- The cell type, cell shape, cell age, membrane fluidics and cellular activity (dormant of actively dividing cells).[87,88]
- Concentration[79,86,88]
- Physical and chemical characteristics (size, the phospholipid composition, charge)[103]
- Environmental factors

Temperature: The interaction between lipid conjugates and cells is temperature- and time-dependent. At 37°C, lipid conjugate uptake is significantly higher than at 4°C. The kind of interaction that takes place can also be influenced by temperature. At 37°C, for instance, endocytosis is more likely to occur in actively dividing cells, but at 4°C, the primary mechanism is probably lipid exchange and adsorption. Additionally, at low temperature, lipid conjugate incorporation is shown to markedly decreased probably by lowering the fluidity of the membrane.[48,86] Serum plays a significant role in a variety of

culture media. Apart from its many physiologic impacts on cells, it inhibits the uptake of lipid conjugates into cells.[48,110] The presence of serum lipids and proteins e.g. HDL and albumin have been shown to reduce lipid conjugate cell interaction.[48] Change in pH and presence of salt in the transformation media can affect the uptake adversely.[48,94]

1.11 Kode™ Technology

Kode technology is a surface modification technology that enables the uptake or attachment of chemically synthesised functional components to biological and non-biological surfaces. The modification is attained by amphipathic Function-Spacer-Lipid (FSL) constructs or Kode constructs in a very easy and harmless manner. Currently, over 60 FSLs are available, with more in the development phase. Each FSL is based on a common design consisting of three units: a functional head group, a spacer, and a lipid tail.[111]

1.11.1 FSL constructs

FSL constructs are made up of three parts: a functional head group (F), a linker or spacer molecule (S), and a hydrophobic lipid tail (L). Because FSL molecules are configurable, each component (lipid tail, spacer, and head group) can be adjusted and optimised for a specific function.[112,113]

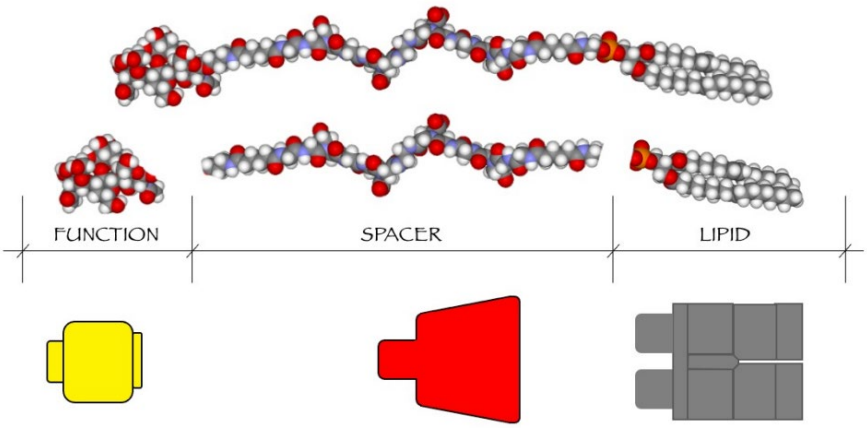

Figure 9**:** Schematic representation of a Kode FSL construct. The upper image shows a generic Kode construct based on a carboxymethylglycine (CMG) spacer linked to a DOPE lipid tail. The 'building block toy figure' representations beneath show a yellow head representative of a single type of functional head, the red body represents a spacer, and the grey legs represent a lipid tail.[3,111]

Functional head group

The functional head group is the bioactive component of the FSL construct, and it can be nearly anything, such as fluorescent markers, glycans, peptides, antimicrobial agents, or other small molecules (Table 1). This capacity to carefully choose a specific and desirable functional molecule enables FSL-based diagnostics to achieve a high level of specificity and sensitivity. To summarise, the functional head group is (typically) small, very specific, and well defined. Additionally, it is mostly hydrophilic in nature.[114]

Table 1: Families of bioactive functional heads used for FSL constructs.

FSL Construct Functional Head groups	**Selected examples**	**References**
Glycans	ABO, Lewis, H, P1PK, GLOB, FORS, hyaluronic acids, sialic acids	[3,4,115]
Peptides	Miltenberger, syphilis, chagas, leptospira, CMV	[6,116]
Fluorophores	FITC, BODIPY	[5,7]
Anti-microbial	Selenium, spermine	[117,118]
Reactive groups	Maleimide, succinimide, click-coupling	unpublished
Enzyme substrates	Sortase	unpublished
Oligonucleotides	Various	unpublished
Charges	Polycations	unpublished

Spacer

The spacer is a biologically inert core component of the FSL construct. It facilitates the chemical conjugation of the functional head with the lipid tail. This linker unit presents the FSL construct with very important novel features. Primarily, spacers enable a high degree of dispersibility in water. Water dispersibility adds an attractive feature to the FSL constructs as it simplifies its applicability and renders the technology suitable for use with cells, unlike organic solvents required to dissolve some lipid and non-lipid membrane-based probes (discussed in Section 1.8.2). Spacer also increases the distance of the functional group from the membrane, thereby reducing steric hindrance and, in turn, enhancing both sensitivity and specificity.[3,112]

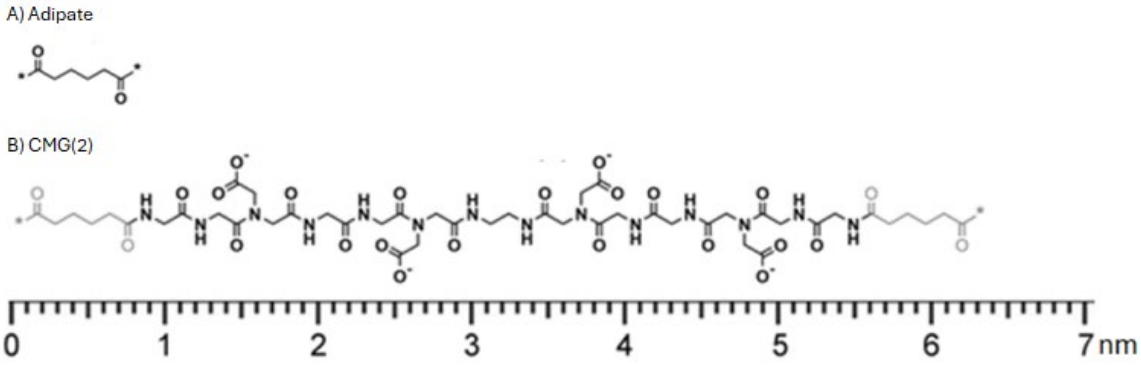

Figure 10: Chemical structural of most common spacers used to make FSLs.[111,119] **A**) the adipate, **B**) CMG (2) spacers.

A variety of spacers are available (Table 2), and they can be further tailored to optimise bioactivity; the short adipate linker (1 nm) and longer carboxymethylglycine (CMG) motif (7 nm) are the most common ones in use (Figure 10).[119] The 'flexible-rigid' structure of the CMG spacer is unique in that it is somewhat rigid, but at a central hinge region, it has a significant degree of flexibility that permits the two parts to spin with relative freedom.[111]

Table 2: Diagrammatic representation showing several FSL spacer configurations. **A**) natural glycolipid, **B**) adipate spacer **C**) CMG(2) spacer **D**) CMG(4) **E**) β-DD spacer and **F**) branched TCMG spacer.[111]

	Different spacer configurations	Schematic diagram
A	Natural glycolipid	
B	Adipate spacer	
C	CMG (2) spacer	
D	CMG (4)	
E	β-DD spacer	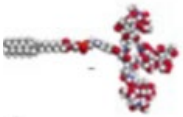
F	Branched TCMG spacer	

Lipid Tail

The lipid tail, being hydrophobic, conveys an amphiphilic property to the FSL construct. The hydrophilic head group, along with the spacer, facilitates dispersion of the FSL construct in water, and the lipid tail enables spontaneous self-assembly and spontaneous membrane uptake. Dioleoylphosphatidylethanolamine (DOPE) is one of the most commonly used lipids for FSL construct formation.[112] Being a membrane phospholipid, it works very efficiently with biological assays. Moreover, a variety of other lipids, like cholesterol and ceramide, are also available (Figure 11). Functional heads, spacers, and lipid tails can be interchanged to make a variable Kode construct with optimised bioactivity. Figure 11 shows the possible multiple configurations of the FSL construct that can be synthesised.[3]

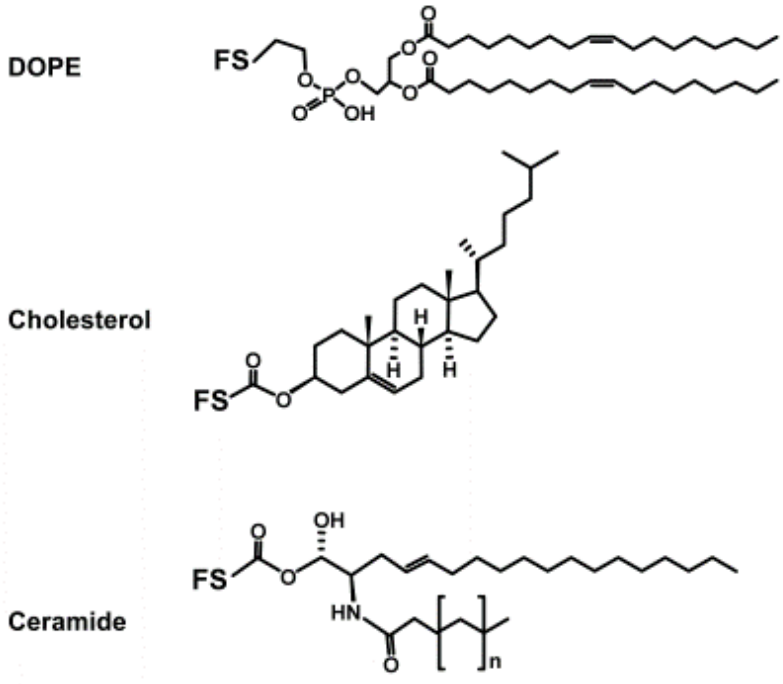

Figure 11: Structural variation of lipids commonly used as tail in FSL constructs.[119]

1.11.2 Summary of uptake of FSL constructs by cells

Owing to the lipid tail of natural glycolipid, its suggestive passive membrane uptake has long been known and has been used to modify the surface of RBC since 1955.[112] However, various associated drawbacks of these natural glycolipids, like nonhomogeneous insertion due to poor solubility and multistep, tedious purification methods from natural sources, have limited their application.[3] Kode or FSL constructs were originally designed to be synthetic analogues of natural glycolipids. However, it was soon realised that the technology had the potential to attach almost any bioactive compound to a cell membrane with possibly minimal side effects.[111]

Blood group antigen-related structures make up a significant component of the 60 FSL. and RBC koding with blood group based FSLs (FSL-A, FSL-B) have been widely studied.[4,115] Additionally, the Lewis blood group system which is highly complex, with a wide spectrum of phenotypic and antigenic variations [3] have also been extensively analysed by Kode technology. [120,121]

Transformation of RBC is a simple method that involves incubation of RBC with a solution of FSL constructs. During the incubation duration possibly the lipid tail of FSL

embeds itself in the glycocalyx of the RBC, leaving the antigenic functional head group exposed (schematic representation in Figure 12) and therefore in an ideal position to interact with antibodies, enabling antigen-antibody interactions (Figure 12). Transformed RBCs thus display normal functionality in *in vitro* assays.[122]

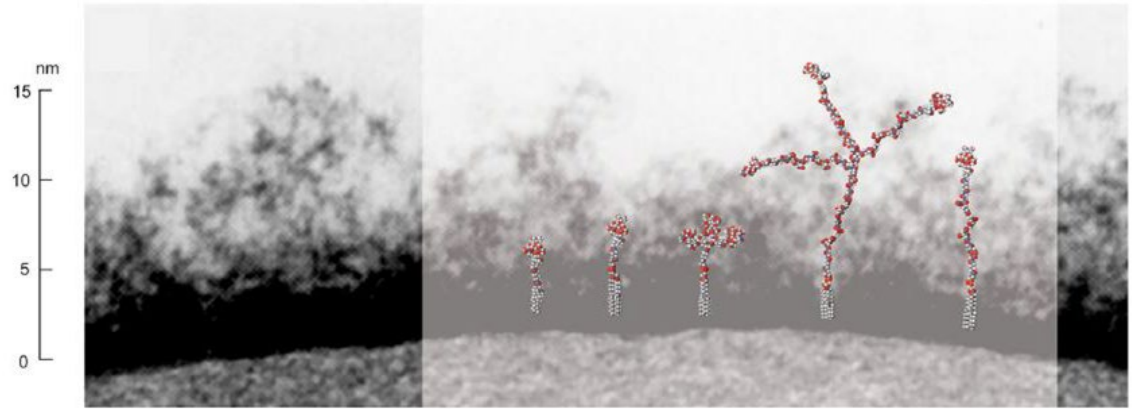

Figure 12: Schematic location of FSLs of different design in RBC of glycocalyx. Adapted from Henry and Bovin, 2018 [4] who reproduced and modified from Dane et al, 2015,[123] and Voet and Voet, 2011. [124]

Kode technology was initially developed to attach blood group glycans to red blood cells for use as quality control.[3] However, Kode technology application in immunohematology has increased and includes quality control kits, competency training panels, diagnostic reagents using artificial rare blood group antigens, and infectious disease markers.[3,122] In research and diagnostic assays, kodecytes outperform normal human red blood cells for a number of reasons.[3,122] Kode technology is a method of altering surfaces, such as those of human red blood cells, such that the cells can express blood group antigens, even ones that are physiologically unfamiliar to them. This makes it possible to create cell-based reagents that are completely standardised in terms of the antigen they express and the amount of it they express.[3,112] Therefore, batch-to-batch variance that is associated with assays that use natural RBC as antigen targets is eliminated by this aspect of Kode technology. Kode technology helped assess xeno-antigens and antibodies in human plasma and offered modern instruments to examine the subject of complement stability using kodecytes rather than animal cells.[120,121]

Since then, it has been used to modify any kind of cell (RBC, white blood cells, platelets, tissue cells, cell lines), enveloped viruses, liposomes, and nonbiological surfaces (such as plastics, metals, and glass).[4,5,7,115] FSL constructions can be used to modify organisms and multicellular entities in addition to individual cells. Additionally, an organism's compartments can be labelled. Additionally, cells and particles can be captured and rendered immobile on solid surfaces using FSL constructions.[112,125]

Microorganisms can be labelled and attached to surfaces using Kode technology. It can also be applied as a surface coating with antibacterial properties. FSL constructions have a strong track record in virology research, and they can be used in a variety of ways to either build diagnostic surrogates or label viruses and virus-like particles. Additionally, FSL can serve as a toolkit for lectin research. Cell adhesion and other processes, many of which are mediated by lectins, including selectins, siglecs, and galectins, can be studied using living cells, cell vesicles, and liposomes koded with a specific FSL glycan that binds with lectins.[115,125,126]

Presently, Kode technology and the resulting kodecytes are being utilised as potent research instruments in a variety of cell-based diagnostics; most recently, FSL-Gala, AGI-134 is being assessed as potential immuno-oncotherapeutic agent.[111] Owing to the presence of a wide range of R&D FSL constructs, Kode technology remains the most comprehensive and user-friendly cell modification methodology for transforming the surfaces of cells with bioactive material for research and diagnostics.[125-127]

Since 2001, when the first Kode construct was synthesised, various FSL constructs have been utilised in modifying RBC. Although various parameters that regulate FSL construct (especially glycolipid based FSL construct) modification in RBC have been studied, the mechanisms underlying this process, and its limitations are not well understood. This thesis sets out to address various questions that will help explore the dynamics and mechanisms of uptake, retention, release, and loss of FSL constructs. Here, FSL fluorophore constructs are being used to explore the above-mentioned issues as fluorescence-based detection technology is simple and superior (discussed in Section 1.8.2).

1.12 Rationale of the study

To be of translational relevance for diagnostic and therapeutic applications, ideally, cells must be improved or changed by artificially modifying them. Unfortunately, very small changes in the cell's environment (e.g., exposure of cells to organic solvent, heat, agitation, change in pH, or osmolarity) have been documented to have adverse effects on cell viability and/or differentiated functions. Hence, bioconjugation/bioengineering protocols and the presence of biofunctional moieties should not impair the viability, growth, or receptor expression of the modified cells. Moreover, a well-engineered cell surface modification agent should allow for optimizing desired functionality and minimum compromise of the cell's antigenicity.[128] Owing to the complexity and dynamic nature of the cell surface, internalization and degradation of surface modification are major challenges.[129,130] Therefore, prolonging the retention of engineered membrane components on the surfaces of cells should be a desired target. In addition, the synthetically modified cells should be biocompatible, as they would be exposed to a complex mechanical and biochemical environment *in vivo.*[131,132]

Kode or FSL constructs were originally designed to be synthetic analogues of natural glycolipids. However, it was soon realised that the technology had the potential to attach almost any bioactive compound to a cell membrane with minimal side effects. Kode Technology aims to eliminate most of the difficulties associated with the other technology as it offers modification of cells by means of the incorporation of desired functional components with biocompatibility and functionality. Despite the *in vitro* and *in vivo* use of FSLs, many aspects of their dynamics of cell modification and subsequent fate are still poorly understood. In this regard, this study explored the dynamics and mechanisms of uptake, retention, fluorescence performance characteristics, and release/loss of FSL constructs.

1.13 Research aims

The aim of this research was to:

- Determine the dynamics of the koding process.
- Establish the consequences of koding on the morphology of RBC kodecytes and further establish the viability and metabolic status of kodecytes prepared from actively dividing cells.
- Determine the impact of media and temperature variations on the retention of FSL constructs in kodecytes.
- Establish the consequences of kodecytes interaction with unkoded cells.

Chapter 2 Base Methods

2.1 Methods and Chapters overview

Chapter two describes the base methodology used in this research. Chapter three explores the impact of RBC storage age on FSL construct uptake, examining if storage age influences forming of kodecytes. Chapter three also investigates the dynamics of FSL uptake into inactive (RBCs) and dividing cells, considering factors like concentrations, temperature, time, protein/serum presence, and the glycocalyx. Chapter four explores the mechanism of FSL uptake, i.e., how FSL constructs label the cell membrane. Chapter five explores the FSL-FLRO4 signal loss observed during the koding process. Chapter six investigates whether the uptake of FSL constructs under different koding conditions (i.e., temperature, duration, concentration, cell types) impacts the integrity of the membrane and the long-term survivability of the kodecytes. Finally, chapter seven examines the retention of FSL constructs in kodecytes under different conditions of temperature, time, concentrations, and storage medium with protein and serum.

2.2 Reasons for using RBCs as model membrane in this study

The cell membrane is paramount for cell surface modification techniques, and the RBC membrane is crucial for its proper functioning, integrity, and survival. Additional unique merits associated with RBCs, like a stable membrane, the lack of internal organelles and associated membranes, higher biocompatibility, abundance (the most abundant type of blood cells in the body), biodegradability (aged or damaged RBC being completely biodegradable in the reticuloendothelial system without the generation of toxic by-products [52,133]), uniformity in shape and size, and their potential use as an autonomous delivery carrier for bioactive substances, make them a preferred model membrane for studying exogenous labelling agents. Hence, in this study, FSL construct labelling characteristics were primarily analysed on RBCs. Additionally, FSLs were also evaluated for their labelling, cytotoxic, and retention characteristics in actively dividing cells like Jurkat cells and PC-3 cells.

2.3 Materials and Sample preparation

2.3.1 Overview of FSL constructs used in this study

Primarily, three FSL constructs were selected to be studied (Figure 13). They differed in two basic aspects: different functional head groups, fluorophores (FSL-FLRO4 and FSL- BODIPY) and a vitamin (FSL-biotin and FSL-BODIPY), and spacer moieties, one short adipate (FSL-FLRO4) and one long CMG2. Using different head groups and spacers potentially allows for detecting any difference in the interaction of FSL constructs and cells owing to the variation in the structure of FSL (Table 3). FSL-FLRO4 and FSL-biotin are commercially available (GlycoNZ, NZ). Additionally, two more FSL constructs (FSL- GB3 and FSL-Zero) were used in this study when either a structural analogue of FSL-FLRO4 was required or a lack of (significant) functional head group was a requirement.

FSL-FLRO4

FSL-FLRO4 is a fluorophore-based FSL construct where the functional moiety is a fluorescein residue, conjugated via an adipate spacer to the DOPE lipid tail (Figure 13A). FSL-FLRO4 is an important fluorescence-based FSL construct as it has an excitation maximum wavelength of 494 nm, which closely matches the 488 nm wavelength of the spectral line of the argon-ion laser, making it a useful label for flow cytometry and confocal laser-scanning microscopy applications. Although fluorescein residue is one of the most commonly used fluorescent reagents due to its high absorptivity and fluorescence quantum yield, it is limited by its photobleaching properties and broad emission spectrum.

FSL-BODIPY

FSL-BODIPY is another green, fluorescent FSL construct, where the functional moiety is a BODIPY residue, conjugated via a hydrophilic CMG2 spacer to the DOPE lipid tail (Figure 13B). FSL-BODIPY is spectrally similar to FSL-FLRO4, but owing to the presence of BODIPY residue, it is relatively insensitive to changes in pH, displays little or no spectral overlap, has a narrow emission bandwidth (resulting in high peak intensity), and has greater photostability. However, the low polarity of BODIPY residue makes FSL-

BODIPY interact with the lipid membranes and thus does not behave like most other FSL constructs, which have hydrophilic head groups.

FSL-biotin

FSL-biotin is comprised of a monomer of biotin (vitamin B7) conjugated to a CMG2 based spacer, which in turn is conjugated to a DOPE lipid tail (Figure 13C). In this study, biotinylated kodecytes are secondarily modified non-covalently with streptavidin conjugated with green fluorophore (Alexa Fluor 488) for detection. FSL-biotin detection with streptavidin conjugated with Alexa Fluor 488 is compatible with flow cytometry. Additionally, due to the high affinity and specificity of the biotin residue with streptavidin, this probe can be used to amplify signals even in the presence of minimally kodecytes.

FSL-GB3

FSL-GB3 has the blood group GB3 trisaccharide (also known as Pk) as its functional head group, conjugated via an adipate-based spacer to the DOPE lipid tail (Figure 13D). Both FSL-GB3 and FSL-FLRO4 have an adipate-based spacer with nearly identical molecular weights. In order to counteract the confounding effects of structural dissimilarities and discover any differences in interaction with FSL-FLRO4 resulting from structural variation, FSL-GB3 has been used in a few experiments that were set up as analogues of FSL-FLRO4.

FSL-Zero

Since FSL-Zero lacks a large functional head group and is hence essentially benign or inert, it was selected for use in specific experimental settings. This allows it to mimic the spacer and lipid components of the FSL construct, also known as the "spacer-lipid" reaction control 110. It transforms cells like any other FSL and has a negative charge to it. FSL-Zero is available in three forms: FSL-Zero (amine), FSL-Zero (acetamide), and FSL- Zero (succinate), two of which were used in this study. FSL-Zero structures are shown in Figures 13E and 13F.

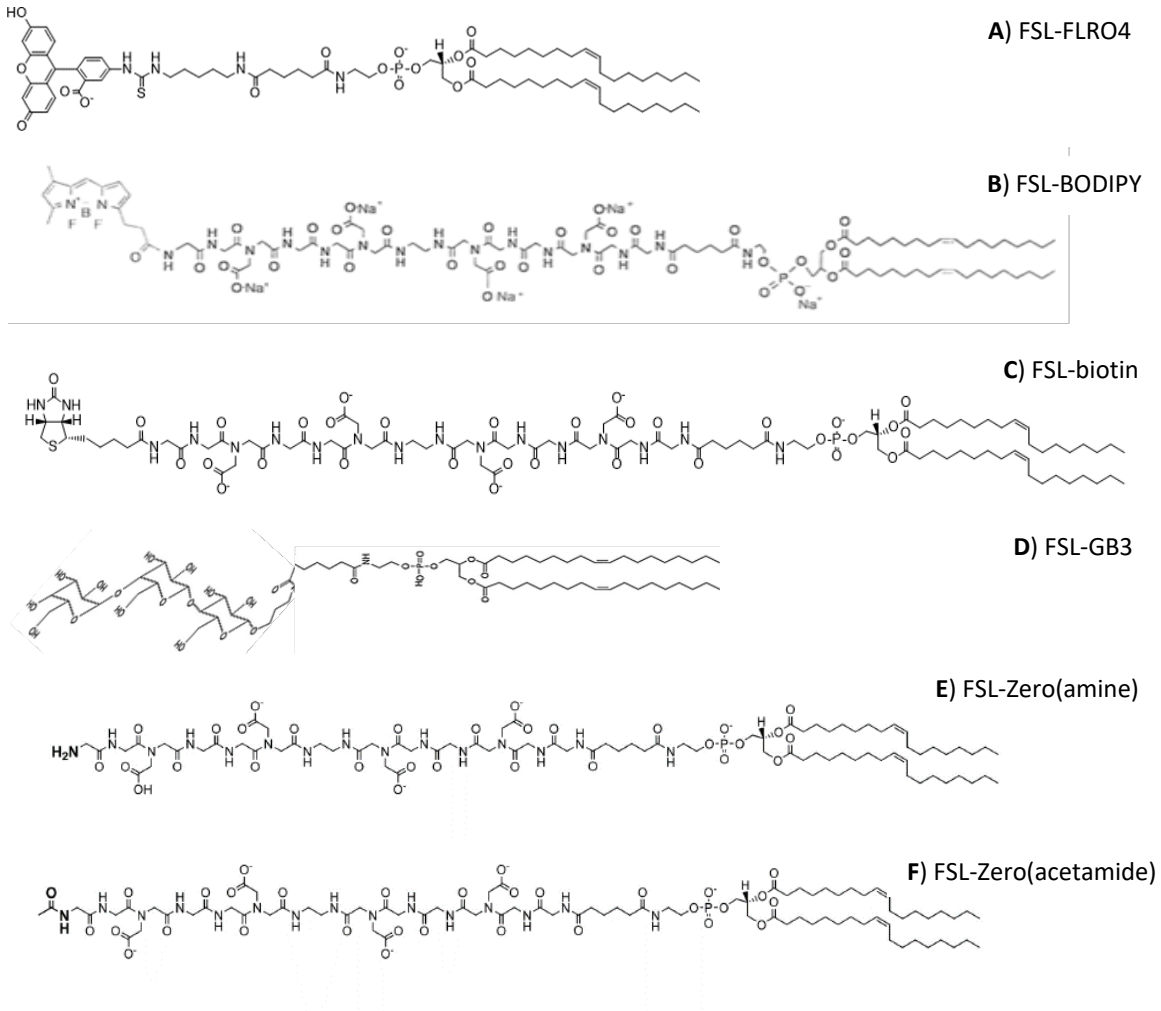

Figure 13: Chemical structure of the FSL constructs examined in this study. **A**)FSL-FLRO4 has a fluorescein head group, attached to an adipate spacer **B**)FSL-BODIPY has a BODIPY head group with CMG2 spacer **C**) FSL-biotin has a biotin head group with CMG2 spacer **D**) FSL-GB3 has a blood group GB3 trisaccharide head group with adipate spacer B) FSL-Zero (amine) has amine residue, conjugated via a CMG2 spacer **E**) FSL-Zero (acetamide) has an acetamide residue attached to CMG2 spacer. All these FSL constructs have a common DOPE phospholipid tail.

Table 3: Summary of FSL constructs used in this research. CMG2 = Carboxymethylglycine, Ad = adipate, DOPE = 1,2-di-O-oleoyl-sn-glycero-3-phosphoethanolamine.

FSL	F	S	L	kodecytes
FSL-FLRO4	Fluorescein	Ad	DOPE	FLRO4-kodecytes
FSL-BODIPY	BODIPY	CMG2	DOPE	BODIPY-kodecytes
FSL-biotin	Biotin	CMG2	DOPE	biotin-kodecytes
FSL-GB3	Glycan	Ad	DOPE	GB3-kodecytes
FSL-Zero (amine)	NH_2	CMG2	DOPE	Zero (NH_2)-kodecytes
FSL-Zero (acetamide)	$CH3CONH_2$	CMG2	DOPE	Zero ($CONH_2$)-kodecytes

FSL constructs reconstitutionAll FSL constructs (GlycoNZ, NZ) were obtained in powdered form. FSL constructs were reconstituted at a concentration of 2 mg/mL in either RBC preservation solution, CellStab (BIO-RAD, New Zealand), or serum-free cell culture media to make the stock solution. The stock solution was aliquoted for later use and stored at -85°C. Immediately before use, the FSL stock solution was thawed at RT and briefly vortexed before use. Desired working concentrations were prepared by diluting the stock solution in either CellStab or serum-free cell culture media, depending on the cells to be koded.

2.3.2 Kode terminology

The following terminology, published previously, has been adopted [4,134,135] in this thesis, with modifications.

- Koding is the process of cell or surface modification with FSL constructs.
- Kodecytes are cells transformed with the FSL construct.
- The working solution of the FSL construct used to modify cells is described as “µM concentration-FSL-name". For example, the solution of FSL-FLRO4 at 50 µM is termed 50 µM FSL-FLRO4.
- For this research project to distinguish if kodecytes were prepared from inactive cells (RBCs) or active cells (Jurkat cells, PC-3 cells), an additional modification has been incorporated into the kodecyte terminology, wherein the type of cell transformed is preceded by the FSL construct used for modifying those cells.
- RBC koded with FSL at a given concentration is known as “cell µM concentration FSL-kodecytes”. For example, RBC koded with 50 µM FSL-FLRO4 is termed RBC 50 µM FLRO4-kodecytes.
- Jurkat cells koded with FSL at a given concentration are known as “cell µM concentration FSL-kodecytes.” For example, Jurkat cells koded with 50 µM FSL-FLRO4 are termed Jurkat 50 µM FLRO4-kodecytes.

2.3.3 Overview of cells used in koding process

Two distinct cell types were chosen to examine FSLs for their dynamics of uptake, performance characteristics, stability, and cytotoxicity profile:

- RBC, which have a stable or inactive membrane and are very robust and non-proliferating
- Cell lines that have an active membrane with proliferating and actively dividing cells

RBC preparation

The blood donor gave verbal consent for blood to be used to create reagents. Blood samples were drawn in ethylenediamine tetracetic acid (EDTA) tubes and centrifuged at 3500 rpm for 5 minutes at 4°C. The supernatant was removed, and RBC was washed three times with working strength (1×) PBS (pH 7.4) to remove plasma and buffy coat (platelets and white blood cells). Isolated RBC was resuspended in CellStab (10%), stored at 4°C, and used within 10 days of collection. Prior research has demonstrated that the outcomes derived from various donors vary only slightly. FSL-fluorphore constructs from three distinct donors were compared in my earlier work. The variation in results from various donors was negligible. Since I didn't want to add any more variables and make the data more reliable, I just utilised the results from one donor in my thesis.

Jurkat cells

Jurkat cells were a generous gift from Dr. Hilary, Sheppard Lab, University of Auckland. Jurkat cells (ATCC TIB-152) are suspension or non-adherent T lymphoblasts established from the peripheral blood of an acute T-cell leukaemia patient.

Overview of Jurkat cells maintenance: Jurkat cells were routinely cultured in T25 tissue culture flasks (Nunc; cat# 156367) using Roswell Park Memorial Institute-1640 medium (RPMI 1640, Life Technologies, cat# 11875), which was supplemented with 10% (v/v) Newborn Calf Serum (NBCS, Life Technologies, cat# 16016-159), 1 × GlutaMax (Life Technologies, cat# 35050061), and 1% penicillin/streptomycin (Life Technologies, cat# 51401220). Actively growing cells were maintained between 1-2 × 10^6 cells per mL at 37°C in a 5% CO_2/95% air-humidified atmosphere in a CO_2 incubator. Regular

observation of growing cultures was important to avoid 90–100% cell confluency and media pH changes as they affect cell health adversely. Growing cells were subcultured at regular intervals to facilitate their exponential growth phase. Around 70–80% cell confluency is considered to be near the end of the exponential phase and ready to be subcultured. As Jurkat cells are suspension cell lines, they do not require any dissociation agent and were subcultured by centrifuging down the cultures at 130 × g for 5 min to pellet cells. The spent medium or supernatant was removed, and the pellet was washed using the working strength of PBS. Finally, the pellet was resuspended in fresh complete medium and reseeded into fresh T25 flasks.

PC-3 cells

PC-3 cells were a generous gift from the School of Science at Auckland University of Technology. PC-3 cells (ATCC CRL-1435) are adherent epithelial cells established from a human prostatic adenocarcinoma.

Overview of PC-3 cells maintenance: PC-3 cells were routinely cultured in T75 tissue culture flasks using a complete growth medium comprising RPMI 1640 medium supplemented with 10% (v/v) NBCS, 1 × GlutaMax, and 1% penicillin/streptomycin. Actively growing cells were maintained between 1-2 × 10^6 cells per mL at 37°C in a 5% CO_2 95% air-humidified atmosphere in a CO_2 incubator. The subculturing procedure involved a brief rise of growing cells with the serum-free medium, followed by the addition of the cell dissociation agent TrypLE™ Express. Once cells were detached, complete growth medium was added, and the content was collected and spun at 130 × g for 5 minutes to pellet cells. The spent medium/supernatant was removed, and finally, the pellet was resuspended in fresh complete growth medium and reseeded into fresh T25 flasks.

Jurkat cells and PC-3 cells were frozen on a regular basis and maintained in liquid nitrogen to avoid extended passage culture. Extensive research suggests that passage number impacts the cell line's characteristics over a period of time [136-138]. Compared to cells at lower passages, cells at higher passage experience modifications in morphology and growth rate [136-138]. Thus, for experimental reproducibility and reliability, the use of overpassed cells in experiments was avoided.

2.4 Standard protocol for the koding process

Regardless of what type of cells were used, the koding process was essentially the same. The schematic overview of the methodology is shown in Figure 14, followed by a detailed explanation of the standard procedure for preparing RBC, Jurkat, and PC-3 kodecytes.

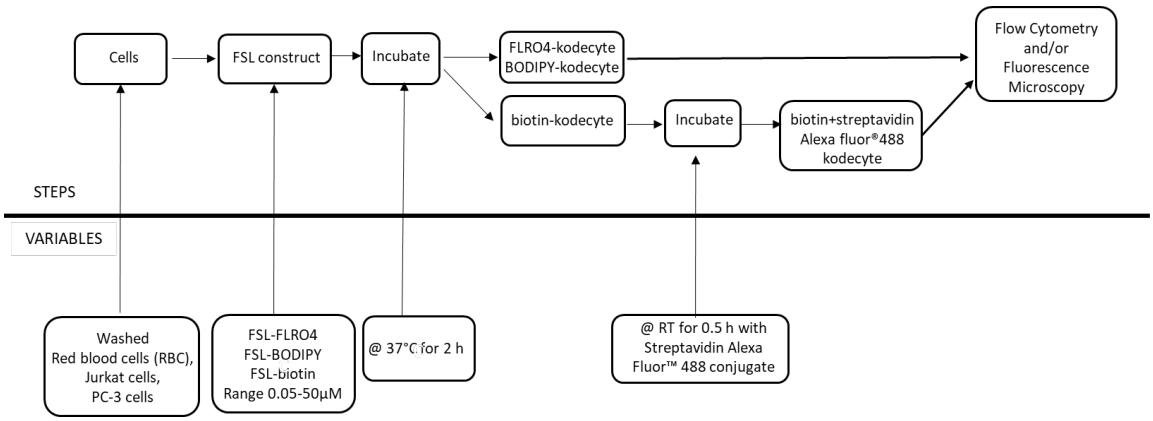

Figure 14: Schematic overview of the standard koding procedure for preparing kodecytes.

2.4.1.1 Flow Cytometry analysis

Flow cytometry has been utilised in routine laboratory and research facilities in many different settings. It is a laser-based technique applied to detect and quantify the physical, chemical, and fluorescent characteristics of cells or particles.[139] Flow cytometry is a versatile and extremely powerful technology, because it is rapid (measures thousands of particles per second) and quantitative. It also offers multiparametric measurements of a large number of cells, which allows for a robust statistical analysis.[139-141]

The universal components of a flow cytometer are fluidics, optics, and electronics. To summarise what a flow cytometer does, fluorescently labelled cells in suspension are

focused for interrogation by the lasers. The resulting fluorescence and scatter signals (forward and side scatter) are collected, filtered, and converted into electronic signals. These electronic signals are finally converted into digital data that is acquired and recorded for analysis. With respect to forward scatter (FSC) and side scatter (SSC) signal detection, FSC conveys information about cell size and membrane integrity, while SSC provides information about cell complexity, granularity, and membrane roughness. Information generated from FSC and SSC is unique to cells and is key to distinguishing them from debris and noise.[139]

Flow cytometry can be used to test a vast range of materials, for example, DNA and microparticles.[142,143] It has been primarily useful for studying white blood cells (WBC) but has found extensive use in examining RBCs in different immunohematology settings.[144] When studying RBCs by flow cytometry, there are a few methodological considerations, for example, avoiding agglutination and gating regions on the FSC and SSC plots (linear or log).[145]

With respect to RBC staining, literatures have suggested the use of logarithmic settings for FSC and SSC.[145,146] Logarithmic amplification of the forward and side scatter causes clustering of most of the events as a discrete group. Gating around a discrete group leads to the minimum exclusion of events with increased forward or side scatter.[145,146] Additionally, to assess the fluorescence intensity of single cells exclusively, doublets were gated out using the doublet exclusion method.[147] Hence, for this study, kodecytes and unkoded cells were gated on a log scale, and mean fluorescence was measured for the cell population and shown as Mean Fluorescence Intensity (MFI).

2.4.2 RBC kodecytes

A detailed explanation of the standard procedure for the preparation of RBC kodecytes is as follows:

- FSL constructs stock solution was diluted to the desired concentration with CellStab to obtain working stock.
- RBC were washed twice with 1× PBS and once with CellStab by centrifugation in an Immufuge on high for 1 minute.

- One volume of FSL (typically 100-500µL) at a given working stock was incubated with one volume of packed RBC at 37°C for two hours, with gentle mixing after 1 hour. Control or unkoded cells were prepared simultaneously by incubating one volume of CellStab with one volume of RBC at 37°C for two hours.
- After incubation, kodecytes and unkoded cells were washed twice with 1 × PBS and once with CellStab by centrifugation, as mentioned above. The last wash is always the solution used for analysis.
- After incubation kodecytes and unkoded cells were washed twice with 1× PBS and once with CellStab by centrifugation as mentioned above. Last wash is always the solution used for analysis.
- For flow cytometry analysis (see section 2.4.1.1), kodecytes were acquired and examined using Cytek Northern Lights™ flow cytometry instrument. At a flow rate of 15µL/minute, 10,000 events were collected, and data obtained from flow cytometer is shown as Mean Fluorescence Intensity (MFI). Data were analysed using Kaluza® Flow Cytometry Analysis Software (version 3.1).
- For fluorescence microscopy analysis, after incubation and washing, koded cells were diluted to give a 5% suspension. Cell suspension (~6µL) was placed on microscope slides, and the cover slipped. Kodecytes and unkoded cells were observed for fluorescence using an Olympus BX51 microscope at 10× magnification.
- Cells were excited at 488 nm, and emissions were recorded at 1.9 s exposure time using a WIB filter (with an emission wavelength of 550nm). To track cells that did not fluoresce, subsequent Differential Interference Contrast (DIC) images were also recorded.

RBC biotin-kodecytes conjugation with Streptavidin, Alexa Fluor™ 488 conjugate.

- Streptavidin, Alexa Fluor™ 488 conjugate, was diluted in 1× PBS to obtain a concentration of 2 mg/mL (stock solution). Diluted to 1 mg/mL in CellStab for further use.
- A 5% suspension of biotin-kodecytes and unkoded cells (section 2.3.1) was prepared.

- An equal volume of 5% biotin-kodecytes was incubated with 1 mg/mL (of Streptavidin, Alexa Fluor™ 488 conjugate, for 30 minutes at RT in the dark, wrapped in tin foil to protect from light, to form biotin+streptavidin Alexa Fluor™ 488 kodecytes (biotin+SAF488 kodecytes).
- An additional control was prepared for establishing secondary labelling with streptavidin Alexa Fluor™ 488. It was prepared by incubating unkoded cells with 1 mg/mL of streptavidin Alexa Fluor™ 488 conjugate for 30 minutes at RT in the dark. This control estimates the autofluorescence produced by streptavidin Alexa Fluor™ 488 and also indicates if the streptavidin, Alexa Fluor™ 488 conjugate binding to biotin kodecytes is specific (typically, these are negative controls).
- Biotin-kodecytes were also measured as a control to detect any background signals.
- After incubation, kodecytes and various controls were washed twice with 1 × PBS and once with CellStab by centrifugation to remove unbound streptavidin, Alexa Fluor™ 488 conjugate, and suspended in CellStab.
- Samples were prepared and analysed by flow cytometry and fluorescence microscopy.

2.4.3 Jurkat kodecytes

The standard procedure for the preparation of Jurkat kodecytes is as follows:

- FSL construct stock solution was diluted with medium (RPMI serum-free) to obtain the desired working stock, transformation, or koding solution.
- Jurkat cells were spun down at 130 x g for 5 minutes, and the pellet was resuspended to estimate cell density.
- An equal volume of Jurkat cell suspension (approximately 1 × 10^6 cells/mL; suspended in RPMI serum-free medium) was added to an equal volume of FSL working stock or RPMI serum-free (negative control) and incubated for 2 h at 5% CO_2 at 37°C.
- Kodecytes were washed twice by centrifuging the cell suspension at 130 × g for 5 minutes after the incubation step.
- Pelleted kodecytes were finally resuspended in 500 µL of RPMI serum-free and serum-supplemented medium and analysed by flow cytometry.

- For fluorescence microscopic analysis, 6 µL of washed kodecyte was dispensed on a glass slide. Kodecytes and unkoded cells were observed for fluorescence using an Olympus BX51 microscope at 100 × and 200 × magnification with a WIB filter at 550nm emission wavelength for a 1.9-second exposure time. To track cells that did not fluoresce, matching DIC images were also recorded for every fluorescent image.

2.4.4 PC-3 kodecytes

PC-3 kodecytes were only prepared for fluorescence microscopy analysis. Standard procedures for the preparation of PC-3 kodecytes are outlined below.

- PC-3 monolayers were prepared by diluting the cell suspension in pre-warmed serum-containing media to the required concentration, typically 4×10^5 to 1×10^6 cells/mL. Nearly 25 µL of cell suspension were seeded into the required wells in a Terasaki tray so that each treatment was performed in duplicate.
- The Terasaki tray was incubated overnight in 5% CO_2, at 37°C until the monolayer was ~60% confluent.
- The following day, an FSL transformation solution was prepared in serum-free media.
- PC-3 monolayers were washed 2 × with serum-free media by removing the supernatant with a pipette and adding media with a dropper.
- The following steps were performed in the dark as much as possible. FSL transformation solution was added into the respective wells and incubated at 37°C with 5% CO_2 for 2 h.
- After incubation, the cell monolayer was washed 3 × with PBS.
- Finally, for imaging, 10 µL of 1 × PBS was added to each well, and the Terasaki plate was covered and inverted. Cells were excited at 488 nm, and emission was recorded at 1.9-second exposure time using the WIB filter (with an emission wavelength of 550nm) of the fluorescence microscope (Olympus BX-51 microscope). To track cells that did not fluoresce, matching DIC images were also recorded for every fluorescent image.

Chapter 3 Results – Dynamics of FSL uptake

3.1 Overview

Various FSL constructs have been known for many years for effective modification of cells. Despite *in vitro* and *in vivo* use of several FSL constructs, many aspects of their dynamics of cell modification, cytotoxicity profile and subsequent fate are not well understood. Although previous work based on agglutination using serology has established a few parameters for labelling of Red Blood Cells (RBC) with blood group based FSL constructs, the serology-based technique has restricted applicability to blood group FSL constructs. Thus, it is critical to use other sensitive technologies to understand the mechanism (and associated limitations) underlying FSL construct cell modification processes.

Flow cytometry, being a rapid and very sensitive technology, has a wider range of detection, and the data generated by flow cytometry can help quantify the result in detail. Additionally, it is an exceedingly versatile and effective method for single-cell quantitative and qualitative research. Hence, for this study, flow cytometry was utilised as the main instrument to establish parameters for the optimum understanding of FSL construct dynamics and mechanisms of uptake, loss, and retention. Additionally, other instruments like fluorescence spectrophotometer, fluorescence microscopy, scanning electron microscopy, and Muse cell analyser were also used to either cross-check results obtained from flow cytometry or as a tool to further process information generated by flow cytometry.

3.2 RBC storage-age and its effect on the uptake of FSL constructs

Overview: RBC concentrates intended for transfusion are generally stored for up to 42 days at 4°C in appropriate additive solutions [148]. During the course of the storage, many changes, commonly known as ‘‘RBC storage lesions’’, are known to occur. These changes could be biochemical, biomechanical (e.g., deformability), or immunologic in nature, and prolonged storage of RBC can impact laboratory measurements of RBC parameters [149]. It was, therefore, of concern that extended *in vitro* storage of RBC at 4°C and, in turn, usage of relatively older RBC for the koding process could impact uptake of FSL constructs. Experiments were designed to investigate the effect of storage-age of

RBC on uptake of FSL constructs in order to establish if selection of RBC to make kodecytes and results were RBC storage-age dependent.

Methodology: The methodology was designed to test the hypothesis that the RBC's storage age influences the uptake of the FSL construct. The schematic overview of the method is presented in Figure 15, followed by a detailed explanation of the experimental protocol.

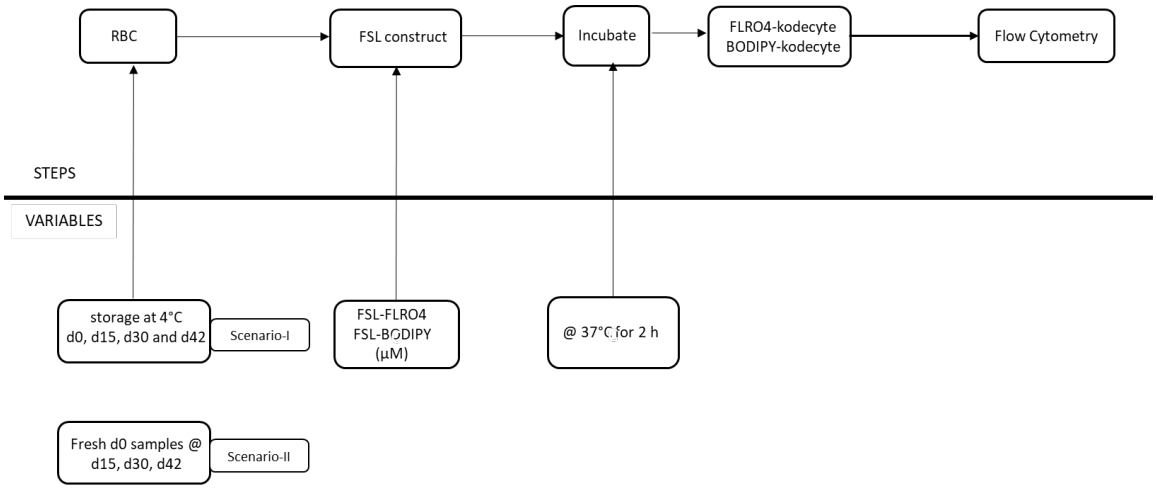

Figure 15: Schematic overview of methodology testing RBC storage age and its effect on the uptake of the FSLs.

3.2.1 FLRO4-kodecytes

Two scenarios were analysed to study the effect of the storage-age of RBC on the uptake of FSL-FLRO4. In the first scenario, RBCs were stored at 4°C over a period of 42 days in CellStab, and RBCs were aliquoted (from the storage lot) at predetermined times and evaluated for their ability to label with FSL constructs. Kodecytes were prepared using various concentrations of FSL constructs at d0 (the day on which blood was collected and processed), d15, d30, and d42 and compared to d0.

In the second scenario, d0 RBCs (from different batches) and aged RBCs of different durations were tested for their insertion effectiveness on the same day, i.e., freshly processed RBCs were compared with stored RBCs. For this experiment, fresh blood was collected and processed into kodecytes on the days when the stored RBCs turned 15, 30, and 42 days old. For both scenarios, unwashed and washed post-preparation kodecytes were analysed.

Figure 16A shows the impact of the storage age of RBC on FSL-FLRO4 uptake across the tested concentrations of 3-50 µM for the first scenario. Kodecytes made from d0 RBCs (Figure 16A) gave the highest mean fluorescence intensity (MFI, fluorescence signal), which increased with increasing FSL concentration. This was seen regardless of the storage age of RBCs. It could be seen that after d0, older RBCs gave lower MFI's, which correlated with age (i.e., the older the RBC, the lower the MFI). However, the changes in MFI were much less at 30-42 days compared to day 15, suggesting stabilisation of uptake of FSL after 30 days. Statistical analysis of change in MFI was carried out using PRISM GraphPad. To determine if MFI changed significantly over storage age of RBC, mean MFI of d15, d30 and d42 were compared to the MFI result from d0. Two-way ANOVA and Dunnett's multiple tests were used to test the statistical significance. Decrease in fluorescent intensity is significant for $p<0.05$ (*) and statistically highly significant for $p<0.001$(***) and $p<0.0001$ (****). The statistical study demonstrated that kodecytes prepared from older RBC generated lower MFI than fresh (d0) RBC, and this difference in MFI was statistically significant. This observation was true across all tested concentrations. Additionally, the statistical analysis also revealed that for 3 and 6 µM kodecytes the difference in the MFI of kodecytes prepared from d15 stored RBC compared to d30 and d30 to d42 was statistically non-significant. For 13, 25, and 50 kodecytes, the difference was found to be statistically significant ($p<0.05$ *) between d15 and d30. However, irrespective of the concentration of kodecytes, the difference in the MFI was statistically non-significant between d15 and d30.

In Figure 16B, the same data (as in Figure 16A) was normalized against d0 to allow a more direct comparison of MFI change (i.e., MFI obtained from kodecytes made from d15, 30, and 42 old RBCs normalized against d0, then indicated in % change). This result highlights that irrespective of FSL concentration (3-50 µM) with respect to d0 RBC kodecytes, the fluorescence signal reduced at approximately the same rate, which is about 30% at d15, moving to 45-50% for days 30-42. From these results, it could be concluded that FSL-FLRO4 uptake was greater for RBCs stored for a shorter time compared to RBCs stored for a longer time.

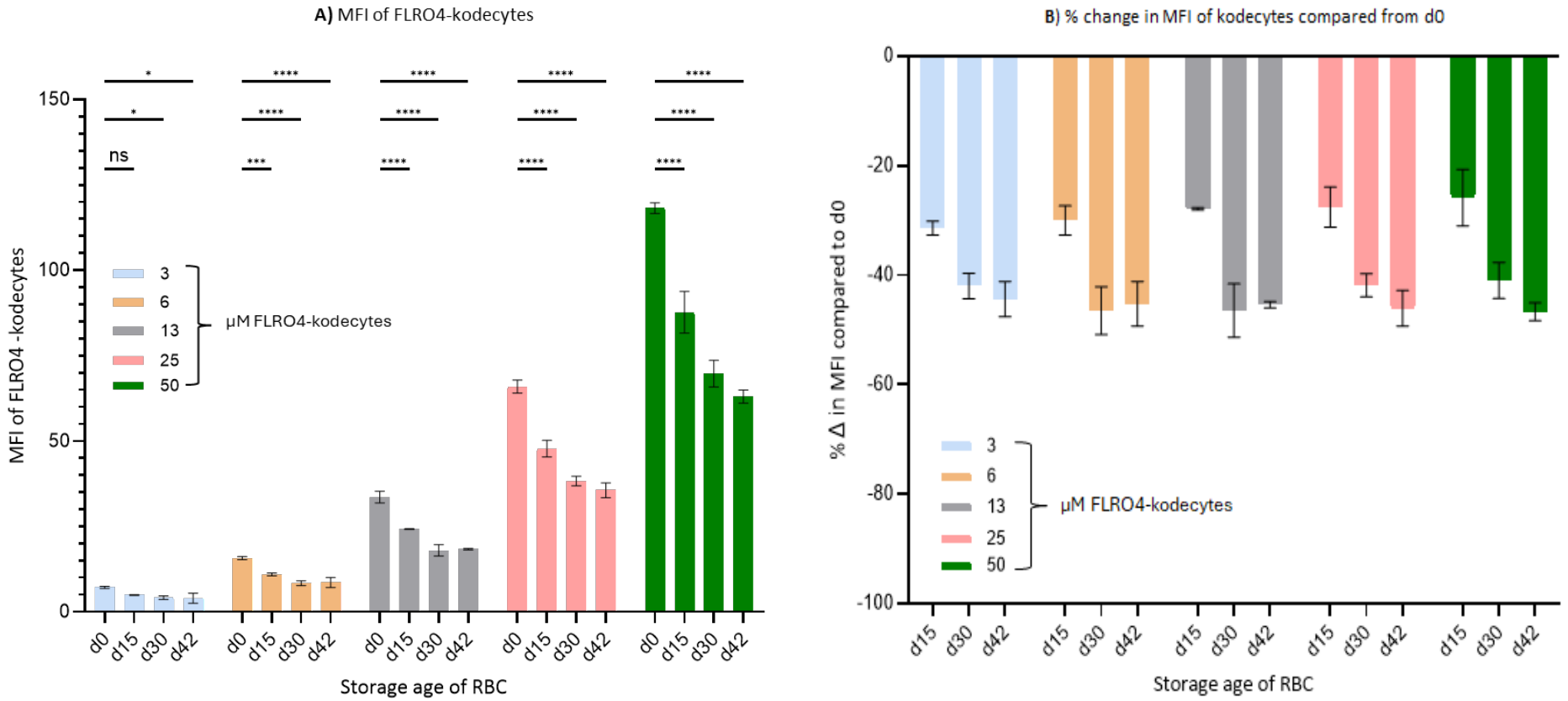

Figure 16: RBC storage age and its effect on uptake of FSL-FLR04 (first scenario). **A**) MFI of RBC FLRO4-kodecytes, at two-week intervals on d0, 15, 30, and 42. **B**) The % change was determined as a change in MFI of kodecytes compared to d0. Results shown are mean ± standard deviation, n=7. ANOVA with Dunnett's multiple comparison test is carried out to test the statistical significance. *P<0.05, ***P<0.001, ****P<0.0001.

To verify the previous results, experiments were repeated (testing the second scenario); however, this time, d0 RBCs and aged RBC of different durations (i.e., from different collection or batch of RBCs) were tested for their uptake effectiveness of FSL-FLRO4 constructs on the same day (second scenario). By making d0 cells fresh each time, the MFI generated from the baseline could be assured to be stable with respect to the experiment, i.e., d0 and d15 RBC sets were tested for their labelling effectiveness at the same time from two different lots of RBCs (unpaired samples) compared to, d0, d15, d30, and d42 RBCs tested for labelling efficiency over a period of time against d0 prepared on one occasion (paired samples). This whole experiment set-up (performed with two conditions) increases the ability (and the robustness) to measure the effect of the storage age of RBCs on the labelling effectiveness with FSL-FLRO4.

MFI obtained from the confirmatory experiments (second scenario) revealed comparable results (raw data not shown). Figure 17 accounts for a baseline difference from d0 RBC (MFI obtained from kodecytes made from different storage ages normalized against d0, indicated in % change). Results obtained from the first scenario tie in well with the second scenario studies (Figures 16 and 17) as there was no apparent difference in the uptake of FSL-FLRO4 between the two scenarios depending on the storage-age of RBCs.

Overall, these results show that older RBCs are less efficient than younger RBCs in labelling with FSL-FLRO4. Therefore, it was suggested that RBCs for making kodecytes should be less than 15 days old or younger, preferably only a few days old.

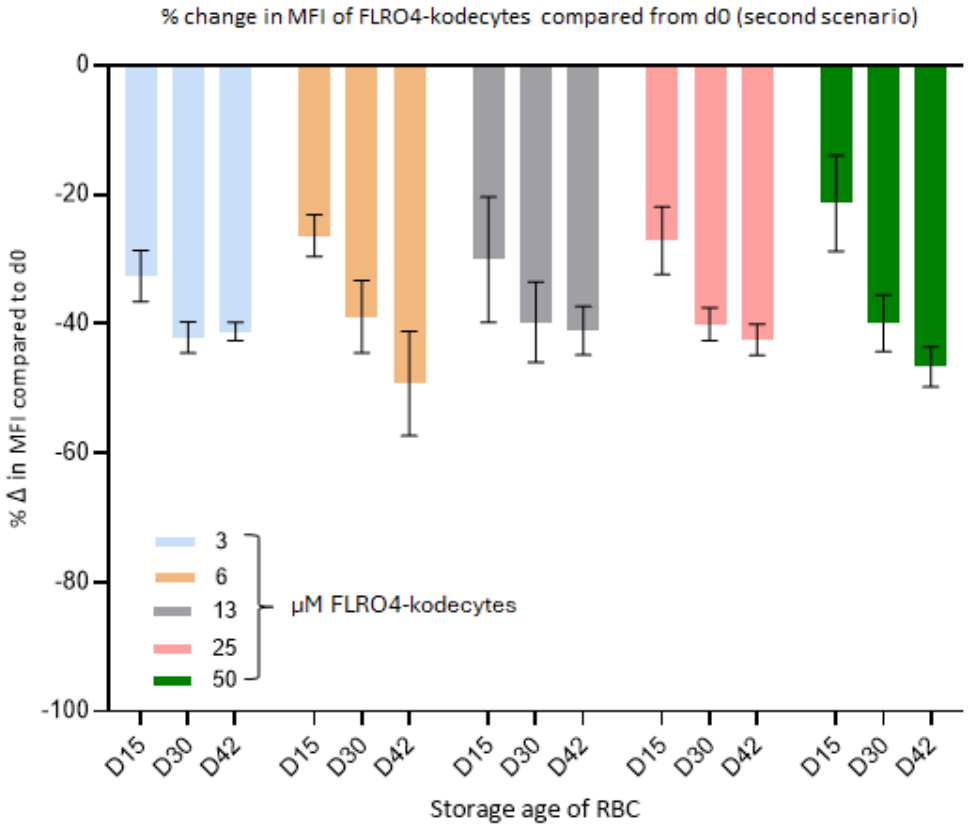

Figure 17: MFI from the confirmatory experiments (second scenario). d0 RBC and aged RBC of different durations were assessed for their koding effectiveness on the same day. The % change was determined as a change in MFI of kodecytes compared to d0. Results shown are mean ± standard deviation, n=4.

3.2.2 BODIPY-kodecytes

In order to evaluate the FSL-FLRO4 labelling results, FSL-BODIPY, a different fluorophore with different characteristics (see Section 2.3.1), was also measured for its labelling effectiveness at different storage ages of RBC. Because FSL-FLRO4 uptake based on RBC storage age from two different scenarios showed comparable results (Figures 16 and 17), only the first scenario was tested with FSL- BODIPY. In comparison to FSL-FLRO4, a more comprehensive concentration range of FSL-BODIPY from 0.4 to 50 µM was evaluated. From Figure 18A, it could be seen that at tested concentration, when RBCs were labelled with FSL-BODIPY at two-week intervals (d0, 15, and 30), FSL-BODIPY uptake was similar for different storage ages of RBC, and unlike FSL-FLRO4, the difference in the MFI generated from BODIPY-kodecytes prepared from different storage age RBC was not statistically significant (statistical significance was determined by two-way ANOVA, $p<0.05$).

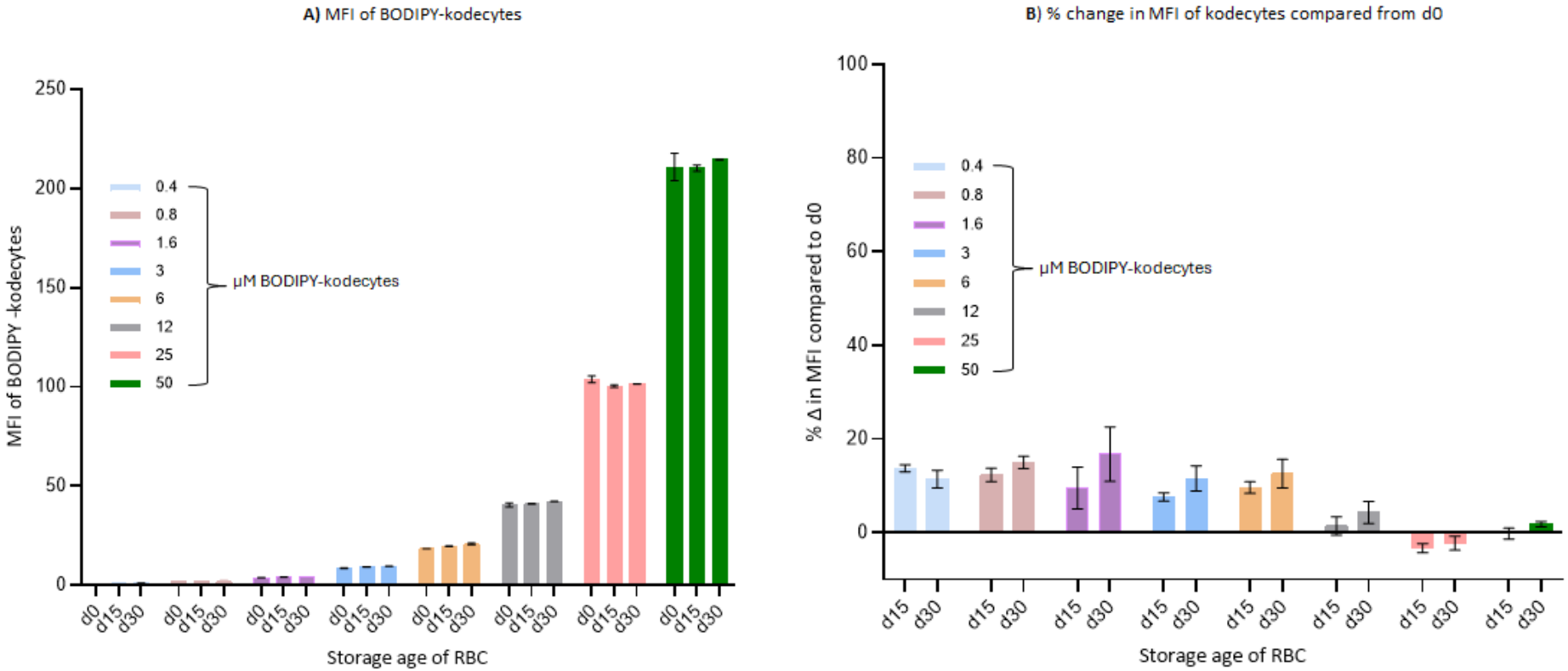

Figure 18: RBC storage age and its effect on uptake of FSL-BODIPY.A) MFI of RBC BODIPY-kodecytes, labelled at two-week intervals, starting from d0, 15, and 30. **B**) Change in BODIPY-kodecytes MFI compared to d0 (indicated as %). Results shown are mean ± standard deviation, n=2.

For direct comparison, the raw data shown in Figure 18A was normalised against d0 RBC kodecytes. Figure 18B outlines the change in FSL-BODIPY MFI at d15 and 30 (standardised against d0, indicated in %). This result highlights that except for 25µM FSL- BODIPY, fluorescence signals increased by approximately 10% and 15% when kodecytes were prepared from RBC stored for a duration of 15 and 30 days, respectively. However, for 25 µM FSL-BODIPY, the fluorescence signal decreased by approximately 3% for d15 and 30 stored RBC. It was speculated that the difference in the uptake trend for 25 µM FSL-BODIPY was possibly due to a concentration-related aggregation factor or some other factor (an experimental error). Statistical significance was tested using two-way ANOVA, $p<0.05$. The analysis showed no interaction. Overall, the results indicate that although, in the case of lower concentrations, there was an increase in MFI when kodecytes were made from older RBC, the fluorescence signal levelled off for higher concentrations. In summary, unlike FSL-FLRO4, the storage age of RBC does not impact the uptake of FSL- BODIPY (into the RBC membrane).

The RBC storage age-based uptake study highlighted the following aspects:

- Results suggest that FSL-FLRO4 has concentration-independent, RBC storage-age-dependent labelling. Most changes in labelling are apparent on day 15, and the changes are much less for 30–42-day old RBCs compared to day 15.
- Unlike FSL-FLRO4, the storage-age of RBC does not impact the labelling of FSL- BODIPY, as there was no significant difference in the uptake of FSL-BODIPY when different-aged RBCs were used.
- Based on the results obtained from the RBC storage age-based uptake study, it was decided to use RBC no older than 15 days of storage at 4°C for making kodecytes. This would help maintain consistency in the usage of stored RBC (by minimising experimental variables) and ensure reliable and reproducible results.
- Although there was a significant difference between the results of the two different FSLs, the phenomenon observed with FSL-BODIPY may not be consistent with most other FSL constructs.

The differences between FSL-FLRO4 and FSL-BODIPY were unexpected; however, this could be possibly attributed to the fact that FSL-BODIPY has a highly lipophilic functional group, which has been reported to change polarity with high retainability [150,151]. As a result of the relative high lipophilicity of BODIPY dye, it tends to bind and localise onto the cellular membrane [150-153]. Hence, it could be suggested that prolonged storage of RBC at 4°C did not impact the uptake of FSL-BODIPY because it has a slightly different mechanism of labelling from the other FSLs. Most often FSL constructs (except FSL-biotin and FSL-BODIPY) have a hydrophilic head; thus, experiment results from FSL-FLRO4 are probably more applicable to generic FSL.

3.3 Factors impacting the uptake of FSL constructs in RBC and Jurkat cells

RBCs are atypical cells in that they are relatively inactive, and their membrane is very stable. Therefore, to extend the RBC observations, the cell membrane of active cells (i.e., Jurkat cells) was also included. In this section, the dynamics of cellular uptake of FSL-FLRO4, FSL-BODIPY, and FSL-biotin into the RBC and Jurkat culture cell lines were investigated using flow cytometry.

3.3.1 Effect of FSL constructs concentration

Methodology: Experiments were performed to establish the relationship between FSL construct concentration and transformation effectiveness. For the concentration-dependent uptake study of FSL constructs, kodecytes and unkoded cells (as controls) were prepared at 37°C after 2 h of incubation of RBC/Jurkat cells with respective FSL constructs (detailed protocol in Section 2.4). RBCs and Jurkat cell kodecytes were prepared with FSL-FLRO4, FSL-BODIPY, and FSL-biotin at increasing concentrations of 0.05–50 µM and 0.1–25 µM, respectively (Table 4). After completion of the incubation step, both unwashed and washed kodecytes were analysed by flow cytometry. The data presented below was obtained from washed kodecytes, as MFI generated from either unwashed or washed kodecytes was not significantly different. The schematic overview of the method is presented in Figure 19.

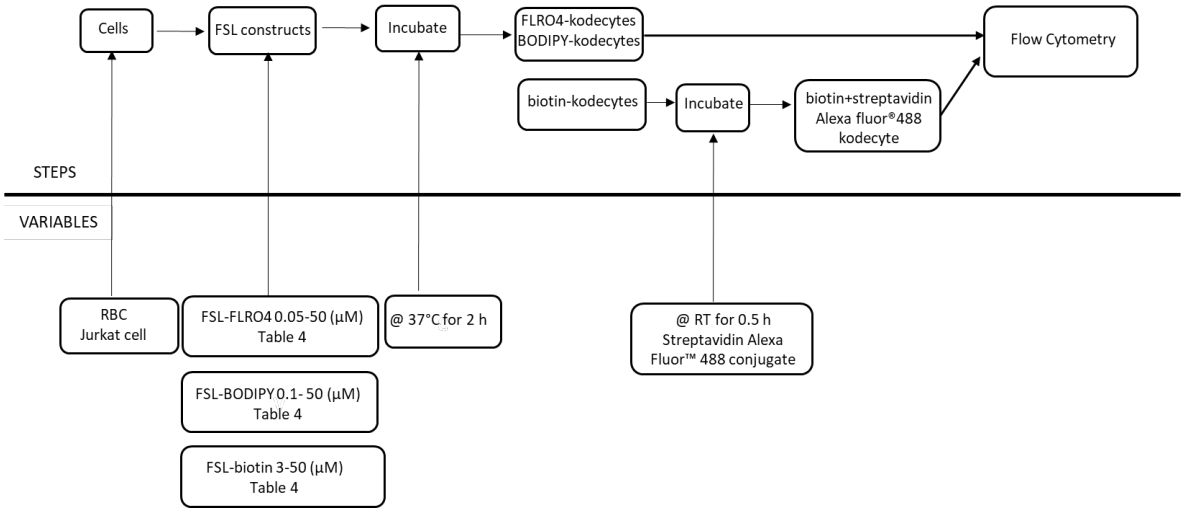

Figure 19: Schematic overview of method testing concentration-dependent uptake of FSL constructs in RBC and Jurkat cells.

Table 4: A detailed account of the FSL construct concentrations used in this section. RBC and Jurkat kodecytes were examined to study concentration-dependent uptake at 37°C after 2 h of incubation.

Cell types	FSL constructs	**Concentration (µM)**										
		0.05	**0.1**	**0.2**	**0.4**	**1**	**2**	**3**	**6**	**13**	**25**	**50**
RBC	FSL-FLRO4	×	×	×	×	×	×	×	×	×	×	×
	FSL-BODIPY		×	×	×	×	×	×	×	×	×	×
	FSL-biotin							×	×	×	×	×
		0.05	**0.1**	**0.2**	**0.5**	**1**	**3**	**5**	**10**	**15**	**20**	**25**
Jurkat	FSL-FLRO4		×	×	×	×	×	×	×	×	×	×
	FSL-BODIPY							×		×		×
	FSL-biotin						×	×		×		×

Results:

RBC kodecytes

Figure 20A shows that, as expected, as the concentration of FSL constructs increased, the RBC kodecytes fluorescent signal (MFI) also increased. Additionally, uptake was linear for all tested FSL constructs, and saturation in MFI was not observed. Hence, FSL-FLRO4, FSL-BODIPY, and FSL-biotin all showed an expected dose-dependent cellular uptake. Unkoded or control cells (0 µM) generated negligible fluorescence signals (data not shown). For FSL-biotin, an additional control with only Streptavidin Alexa Fluor™ 488

was prepared from unkoded cells (and no fluorescence was observed). This indicates that the Streptavidin Alexa Fluor™ 488 binding to biotin-kodecytes is specific.

These results also allow for comparisons of the relative fluorescence of different FSL constructs. It is important to note that, unlike FLRO4 and BODIPY-kodecytes, which are directly analysed, biotin-kodecytes require the secondary addition of Streptavidin Alexa Fluor™ 488 (biotin+SAF488 kodecytes) for detection by flow cytometry. Thus, this experiment's results helped compare the fluorescent signal obtained from direct or primary labelling (FLRO4 and BODIPY-kodecytes) to indirect or secondary Streptavidin Alexa Fluor™ 488 fluorophore labelling analysis of biotin kodecytes.

In Figure 20B, the MFI generated by BODIPY and FLRO4-kodecytes (the same data from Figure 20A) was normalised against the biotin+SAF488-kodecytes MFI to allow a more direct comparison of MFI change (indicated in %). To do that, the obtained MFI intensity from the BODIPY and FLRO4 kodecytes was normalised by dividing all the obtained MFI by the maximum brightness of the biotin+SAF488 kodecytes. The maximum fluorescence signal was set to 100% in all measured data (biotin+SAF488 kodecytes). This result highlights that, irrespective of FSL-FLRO4 concentrations, with respect to biotin+SAF488 kodecytes, FLRO4 kodecytes produce approximately 80% less fluorescence signal. Additionally, compared to biotin+SAF488 kodecytes, BODIPY-kodecytes generate around 50% less fluorescent signal at lower concentrations (3 to 13µM), whereas at higher concentrations (25 to 50µM), it changes to nearly 30%. Similarly, in Figure 21C, the MFI of FLRO4-kodecytes was normalised against BODIPY-kodecytes (100%) to allow for comparison between FLRO4 and BODIPY-kodecytes (direct or primary labelling technique). It was observed that (Figure 20C) in comparison to BODIPY-kodecytes, FLRO4-kodecytes generate approximately 50% less fluorescence signal at lower concentrations (0.1 to 2µM), which decreases to nearly 65% for higher concentrations (3 to 50µM). From these results (Figures 20A, B, and C), it could be implied that at comparable concentrations, biotin+SAF488 kodecytes are most fluorescent, followed by BODIPY and FLRO4-kodecytes.

RBC kodecytes

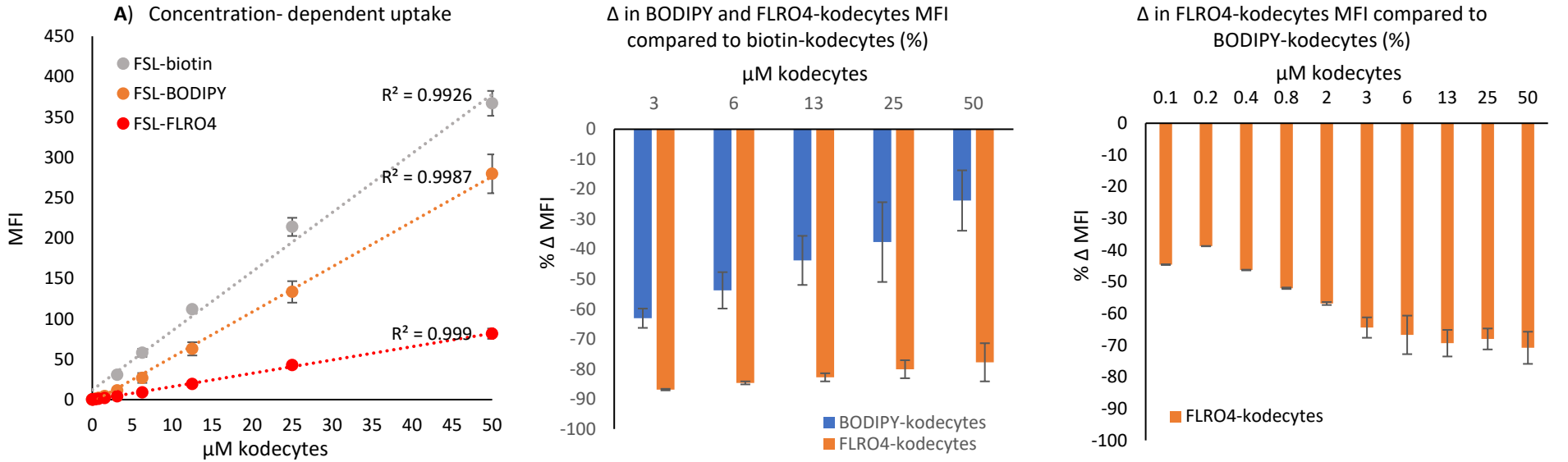

Figure 20: The concentration-dependent uptake of FSLs by RBC. kodecytes were prepared with FSL-FLRO4, FSL-BODIPY, and FSL-biotin at a range of concentrations (representing a molarity range of 0 to 50 µM). **A)** MFI of FLRO4, BODIPY, and biotin+SAF488 kodecytes. **B)** The change in MFI of BODIPY and FLRO4-kodecytes compared to biotin+SAF488 kodecytes (%). **C)** The change in MFI of FLRO4-kodecytes compared to BODIPY-kodecytes (%). Experiments were performed three times, and the data (obtained from washed kodecytes) is expressed as the mean ± SD.

Jurkat kodecytes

As seen previously (Figure 20A) with RBC kodecytes, the data in Figure 21A shows that the MFI generated by Jurkat kodecytes increases with concentration, i.e., all examined FSL constructs demonstrated a concentration-dependent cellular uptake. Additionally, the results shown in Figures 21B and 21C were also in agreement with the previously seen results with RBC kodecytes (Figures 20B and 20C). Jurkat FLRO4 and BODIPY- kodecytes produce approximately 65% and 20% less fluorescence signals compared to biotin+SAF488 kodecytes (100%) (Figure 21B). Additionally, compared with Jurkat BODIPY-kodecytes (100%, Figure 21C), FLRO4-kodecytes generated nearly 50% and 30% less fluorescence signals at 5 and 25 µM concentrations. Finally, it could be shown that the Jurkat biotin+SAF488-kodecytes are the most fluorescent, followed by BODIPY and FLRO4-kodecytes.

Flow cytometry data are presented as dot plots and histograms, where each dot in a forward scatter versus side scatter plot represents a single cell. These are helpful in revealing information regarding the homogeneity or uniformity of the labelled population[154] i.e., the labelled cells can be differentiated based on their uptake behaviour, which hence enables the identification of subpopulations of cells with different intensities. For example, a two-peak histogram means there are dim and bright cells in the main population of labelled cells.

FSL concentrations at 25 µM have been chosen as a representative concentration to show flow cytometric dot plots and histogram data below (Figures 22 and 23), as this concentration was analysed for a concentration-based uptake study for both RBCs and Jurkat cells. From the flow cytometric dot plots and histograms (shown in Figures 22 and 23), it was seen that RBC and Jurkat cells kodecytes responded as one homogenous population, and discrete subpopulations of kodecytes with different intensities were not detected, i.e., cells taking up much more or much less FSL constructs than the main population were not found.

Jurkat kodecytes

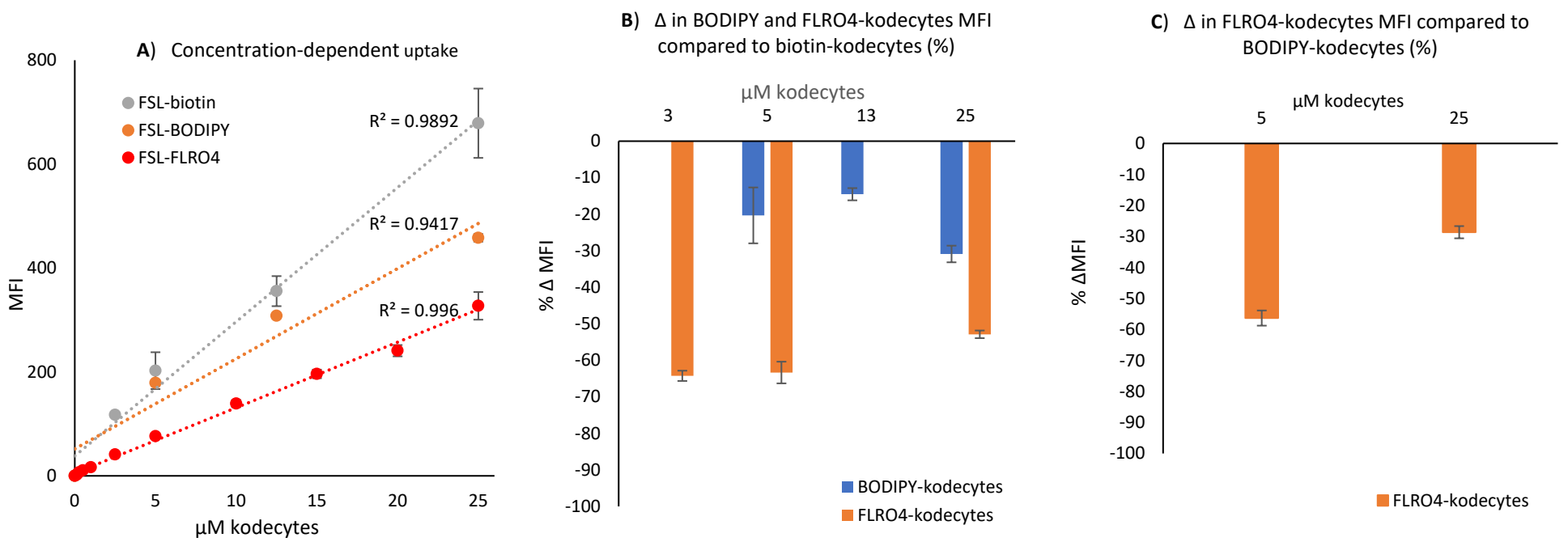

Figure 21: The concentration-dependent uptake of the FSLs by Jurkat cells. Jurkat kodecytes were prepared with FSL-FLRO4, FSL-BODIPY, and FSL-biotin at a range of concentrations (representing molarity ranges from 0 to 25 µM). **A)** MFI of FLRO4, BODIPY, and biotin+SAF488 kodecytes. **B)** The change in MFI of BODIPY and FLRO4-kodecytes compared to biotin+SAF488 kodecytes (%). **C)** The change in MFI of FLRO4-kodecytes compared to BODIPY-kodecytes (%). Experiments were performed twice, mean ± SD.

RBC			
Control/unkoded	FLRO4 kodecytes	BODIPY-kodecytes	biotin+SAF488 kodecytes
0 µM	25 µM	25 µM	25 µM

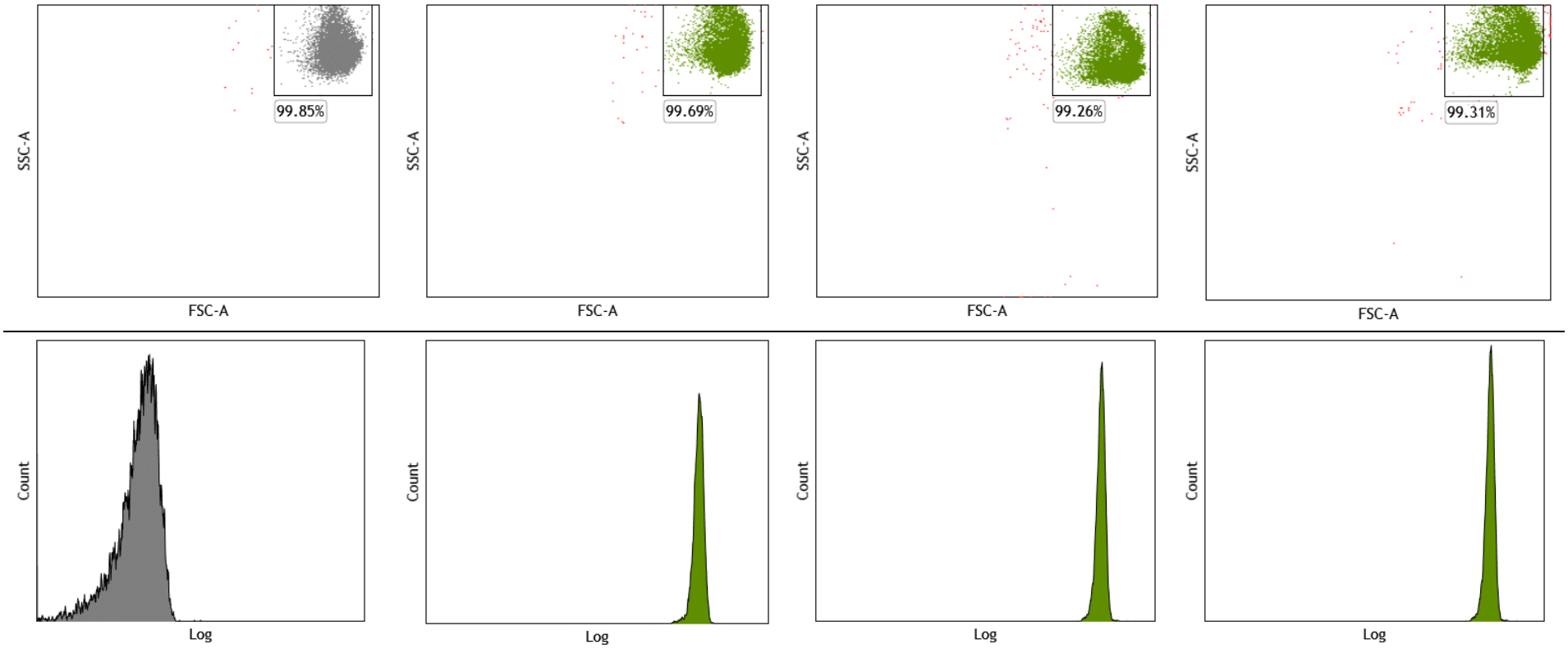

Figure 22: Dot plot and histograms of unkoded RBCs and RBC kodecytes. The dot plot and respective histogram obtained from unkoded RBCs and 25 µM FLRO4, BODIPY, and biotin+SAF488-kodecytes shows one homogenous population.

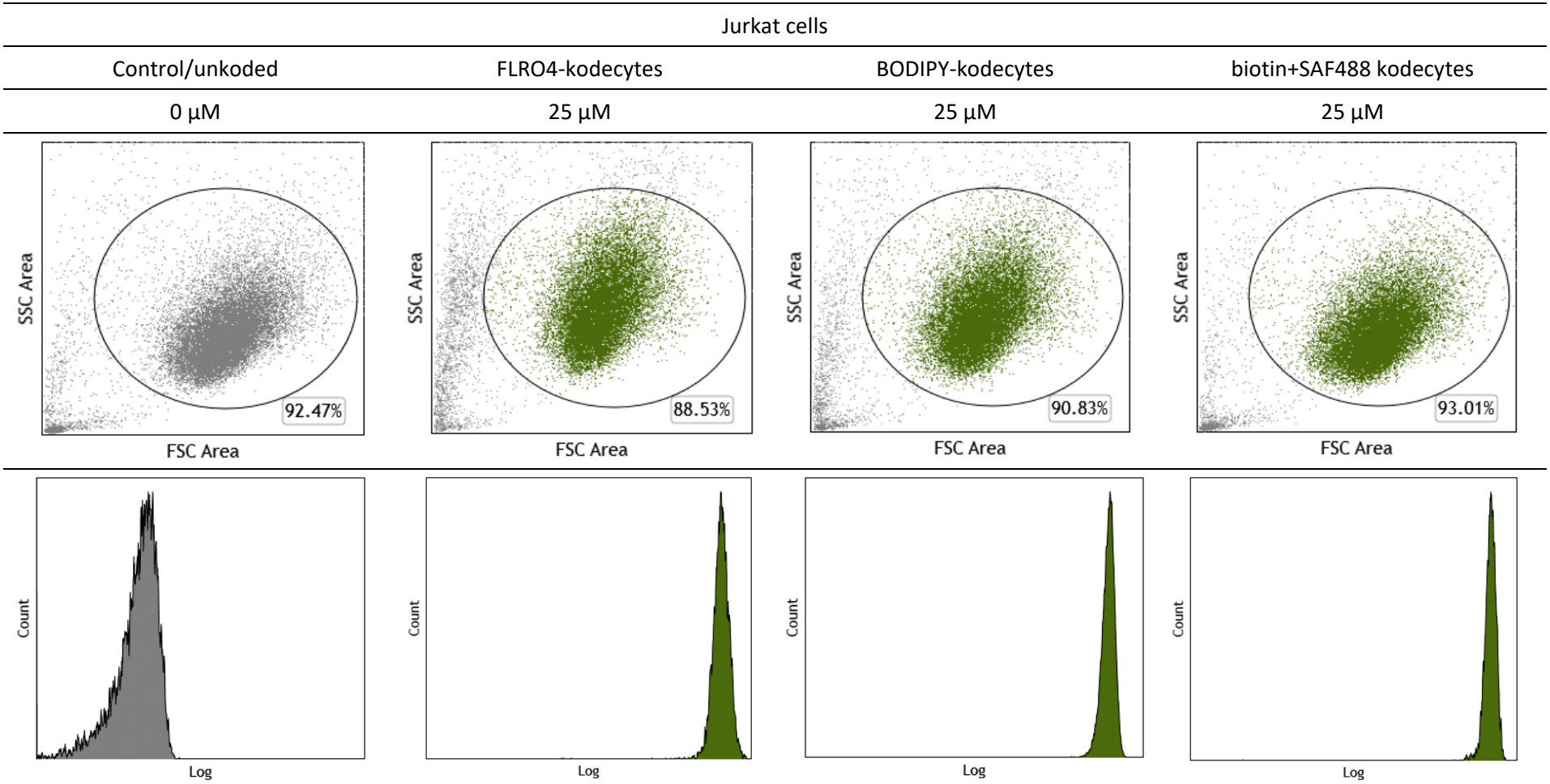

Figure 23: Dot plot and histograms of unkoded Jurkat cells and Jurkat-kodecytes. The dot plot and respective histogram obtained from unkoded Jurkat cells and 25 µM FLRO4, BODIPY, and biotin+SAF488-kodecytes shows one homogenous population.

Summary: The findings show that all examined FSL constructs exhibited concentration-dependent cellular uptake, and Jurkat and RBC kodecytes stained as a single, homogeneous population (regardless of the concentration of the FSL constructs). Finally, it could be shown that the biotin+SAF488 kodecytes are the most fluorescent, followed by BODIPY and FLRO4 kodecytes. RBC and Jurkat kodecytes both showed comparable trends.

3.3.2 Effect of temperature on FSL uptake

Overview: Previous work on blood group based FSL constructs used for red cell modification was predominantly carried out at 37°C, and uptake was measured indirectly by agglutination. The use of agglutination to measure FSL uptake has its limitations and can be influenced by several factors, including RBC shape. In contrast, flow cytometry enables a more direct measurement of modification. Hence, to learn more about the effect of temperature on FSL construct uptake *in vitro*, temperature-dependent uptake of FSL was measured using flow cytometry. Additionally, temperature-dependent uptake of FSL-FLRO4, FSL-BODIPY, and FSL-biotin has not been analysed before, and in this section, different koding temperatures were examined for their koding effectiveness at a comprehensive range of concentrations.

The recommended storage temperature for RBC is 2–8°C (refrigeration temperatures), as, at this temperature range, cellular metabolism is slower and bacterial growth is suppressed. Therefore, if RBCs are at their optimum storage condition at 2–8°C, studying the uptake of FSL constructs within this temperature range would be useful. Additionally, room temperature (RT) was an obvious choice for the simplicity of large-scale manufacturing (rather than 37°C). Hence, experiments were carried out to estimate and compare the uptake of FSL-FLRO4, FSL-BODIPY, and FSL-biotin at 2–8 °C, RT, and 37°C.

Temperature-dependent uptake studies were not performed at lower temperatures for Jurkat cells, as 37°C is considered the optimum temperature for growing and maintaining culture cells and incubating culture cells at 4°C and RT is detrimental to their viability and optimum performance.

Methodology: The methodology was designed to test the temperature-dependent uptake of FSL constructs by RBC. The schematic overview of the method is presented in Figure 24, followed by a detailed explanation of the experimental protocol.

- One volume of working concentrations of FSL constructs was added to one volume of packed RBCs. The contents were mixed to ensure even suspension. Control or unkoded cells were also prepared simultaneously by incubating one volume of CellStab with one volume of RBCs.
- For 0-time point analysis (0 h), samples were aliquoted from the mixture and assessed in both unwashed and washed states by flow cytometry. RBC and FSL mixtures were divided into three sets, with each set maintained at 37°C, RT, and 4°C.
- For 37°C and RT mixtures, samples were aliquoted at predetermined time intervals for up to 24 h and assessed by flow cytometry.
- For FSL-FLRO4 and FSL-BODIPY, 4°C incubation was also extended to a 240 h (d10) testing period, with regular testing at 1, 2, 4, 6, 24, 48 (d-2), 72 (d3), 192 (d8), and 240 h (d10) in both unwashed and washed states. For FSL-biotin, incubation at 4°C was extended to a 120-h (d5) testing period, with regular testing at 1, 2, 6, 24, 48 (d2), and 120 h (d5).

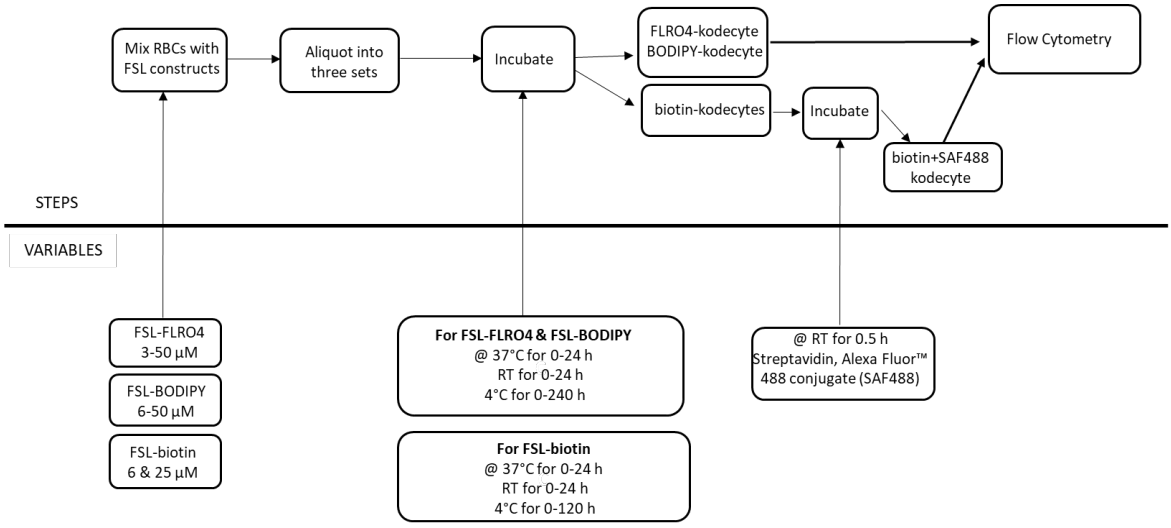

Figure 24: Schematic overview of method testing temperature-dependent uptake of FSL constructs in RBC.

FSL-FLRO4

In Figure 25, three different koding temperatures (37°C, RT, and 4°C) were tested and compared for their effectiveness to make FLRO4-RBC kodecytes at low, medium, and high concentrations of FSL (6, 25, and 50µM), respectively. In Figure 25, it could be shown that, at specific a time, MFI increases with increasing temperature. This trend was observed for all tested concentrations (6, 25, and 50 µM). Interval testing also confirms that 4 h at 37°C and 6 h at RT are the optimum incubation times, as MFI was at its maximum at these time points. Thereafter, MFI declined following 4 h at 37°C and between 6 and 24 h of incubation at RT. The result also confirms that FSL-FLRO4 can be taken up by RBCs at refrigeration temperature (4°C; Figure 25). However, at 4°C, it does not show the same progression or rate in labelling (effectiveness) as seen with 37°C and RT methods, i.e., at the same point in time, FSLs were taken up fastest by RBCs at 37°C, followed by RT and 4°C. FSL-FLRO4 uptake increased over time at 4°C, and it seems to keep on labelling and not attain a plateau or the same uptake as 37°C even after 240 h/d10 (the last time point of analysis for 4°C).

Statistical analysis of change in MFI with respect to change in temperature, time, and concentration of FLRO4-kodecytes was determined using PRISM GraphPad. Two-way ANOVA and Tukey's multiple tests were used to test the statistical significance. Decrease/change in fluorescent intensity is significant for $p<0.05$ (*), $p<0.003$(**) and statistically highly significant for $p<0.001$(***) and $p<0.0001$ (****). It was seen that irrespective of the concentration of FLRO4-kodecytes made at 37°C after 4 h and 6 h of koding, the decrease in MFI (compared to 24 h) was found to be highly significant $p<0.0001$ (****). The decrease in MFI at RT after 4 h of koding was also found to be significant. Additionally, at 4 °C, after 4 h and 6 h of koding (compared to 0, 1 and 2 h), the increase in MFI was also found to be significant for 6 µM FLRO4-kodecytes and highly significant for 25 and 50 µM FLRO4-kodecytes. There was also a significant increase in the MFI (compared to 2 h) after 24 h of koding at 4 °C.

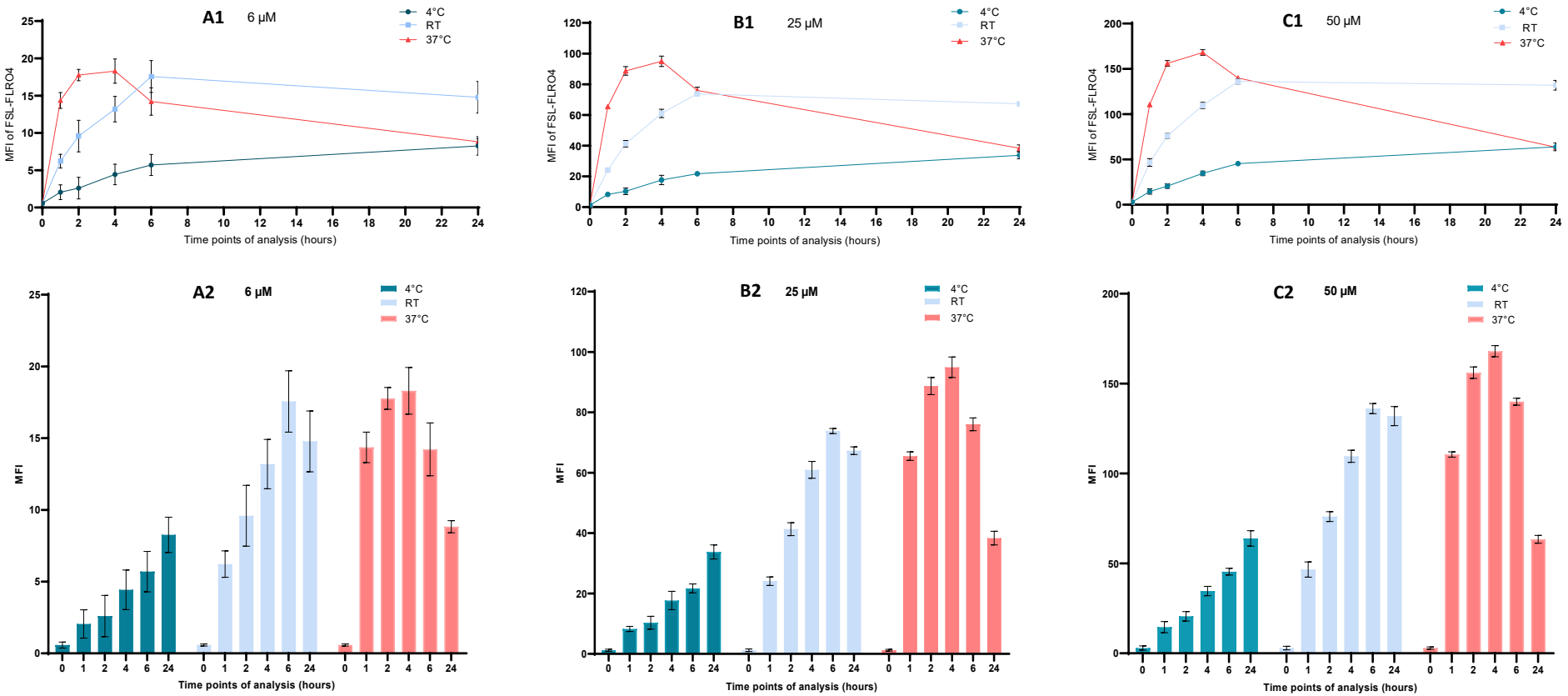

Figure 25: Temperature-dependent uptake of FSL-FLRO4 in RBC. Data obtained by flow cytometry. Uptake of 6 (**A1** and **A2**), 25 (**B1** and **B2**), and 50 µM (**C1** and **C2**) of FSL-FLRO4 was measured at 37°C, RT, and 4°C over a period of 24 h. Experiments were performed thrice, and the data is expressed as the mean ± SD. Note that the Y axis is different between data sets and the data in Figures **A1, B1,** and **C1** corresponds to Figures **A2, B2,** and **C2** in scatter and column format; see Figure 26 for the data presentation at the same scale.

For direct comparative purposes of the relative levels of uptake (same scale for the Y axis), the data in Figure 25 is reproduced in a single graph (Figure 26). Additionally, it also shows the prolonged uptake of FSL-FLRO4 at 4°C over a period of 240 h (d10). Overall, it could be seen that, with respect to 37°C, after 2-4 h of incubation at RT, nearly 50% to 60% of available FSL-FLRO4 was taken up by RBC (Figure 26). Whereas at 4°C, labelling efficiency accounted for approximately 14% to 20%. This trend was observed for all tested concentrations.

Table 5 summarises the interval testing comparison at different temperatures and indicates equivalence points of FSL-FLRO4 uptake at RT and 4°C with respect to 37°C (after 1 h). It could be suggested that across the concentration range, RBC transformed at 37°C for 1 h and RT for 4 h generate comparable MFI. Additionally, for the lower concentrations, uptake at 4°C essentially reached the same level as the 37°C/1 h transformation after 48 h and at higher concentrations after 192 h. It should be noted that no flow cytometric analysis was performed between 72 and 192 h, and the 37°C (1 h) MFI could have been observed prior to 192 h.

Table 5: Equivalence points of FSL-FLRO4 uptake at RT and 4°C compared to 37°C (after 1 h), non-key data points are represented in light grey.

Temperature	Time (h)	Mean Fluorescence Intensity (MFI)		
		µM FLRO4-kodecytes		
		6	25	50
37°C	1	14 ± 1	66 ± 1	111 ± 1
RT	4	13 ± 2	61 ± 3	110 ± 3
4°C	48	14 ± 2	50 ± 1	84 ± 4
4°C	192	20 ± 1	65 ± 2	113 ± 1

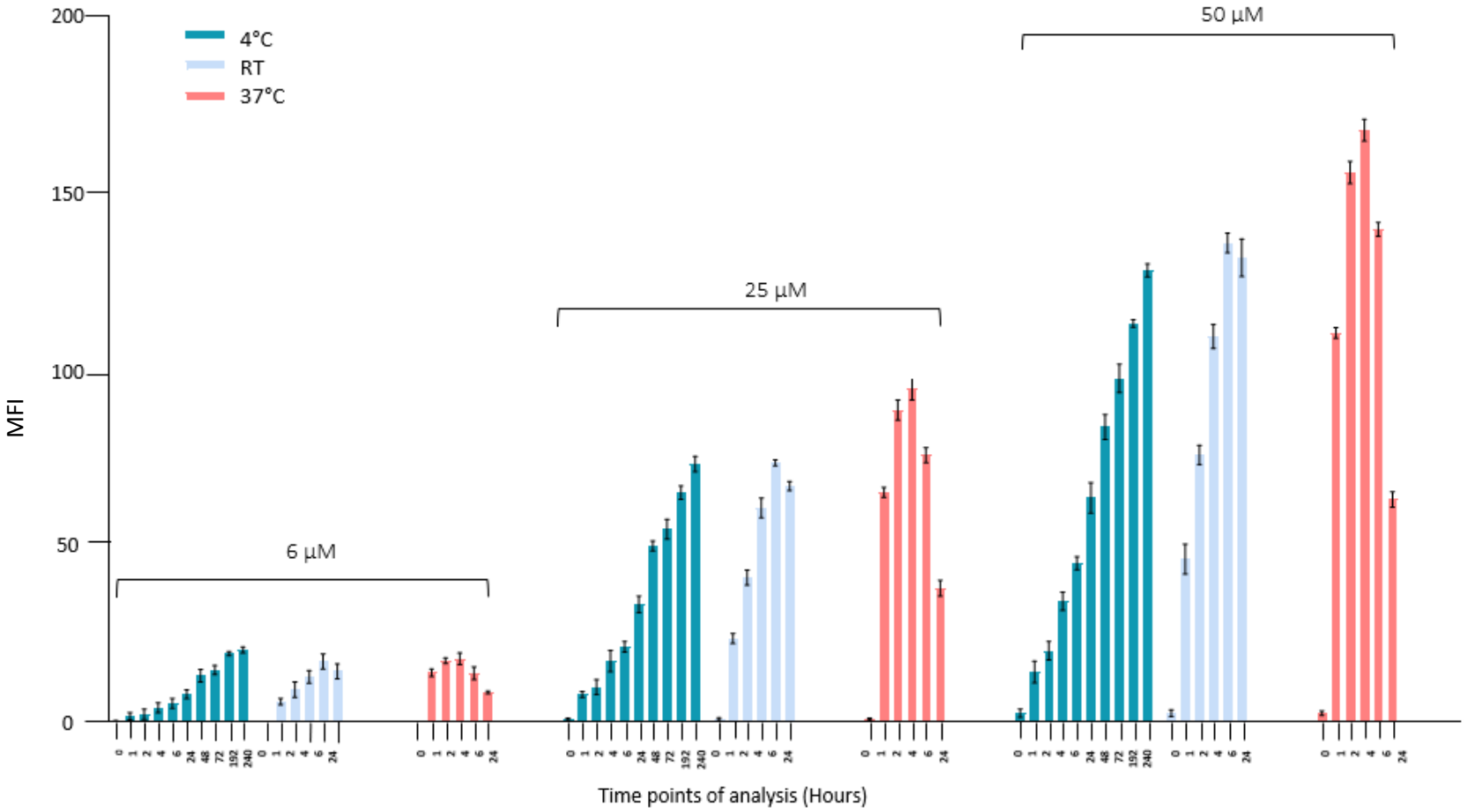

Figure 26: Overall comparative temperature-dependent uptake of FSL-FLRO4. Uptake of FSL-FLRO4 is shown at 37°C and RT over 24 h and 4°C over 240 h (d10).

FSL-BODIPY

In Figure 27, it could be seen that for tested concentrations, when RBC were labelled with FSL-BODIPY at different temperatures for the same point in time, MFI increased with increasing temperatures. Although for 37°C and RT, at the 24 h incubation time interval, the MFI was at its highest, there appears to be a minimal improvement in MFI after 2 and 6 h time points, respectively. Hence, it could be proposed that after 2 h at 37°C and 6 h at RT, MFI seems to approach a plateau. Like FSL-FLRO4, FSL-BODIPY can label RBC at 4°C (Figures 25 and 26), although the uptake of FSL constructs at 4°C is slower compared to 37°C and the RT method. Additionally, as expected, at 4°C, uptake plateaued after day 8 as MFI changed minimally.

Statistical analysis of change in MFI with respect to change in temperature, time, and concentration of BODIPY-kodecytes was determined using PRISM GraphPad. Two-way ANOVA and Tukey's multiple tests were used to test the statistical significance. Change in fluorescent intensity is significant for $p<0.05$ (*), $p<0.003$(**) and statistically highly significant for $p<0.001$(***) and $p<0.0001$ (****). From the statistical analysis, it can be seen that, irrespective of concentration of BODIPY-kodecytes at 37°C after 4 h of koding, the change in MFI (compared to 24 h) is not significant. However, there was a significant increase in the MFI (compared to 2 h) after 24 h of koding at 4 °C.

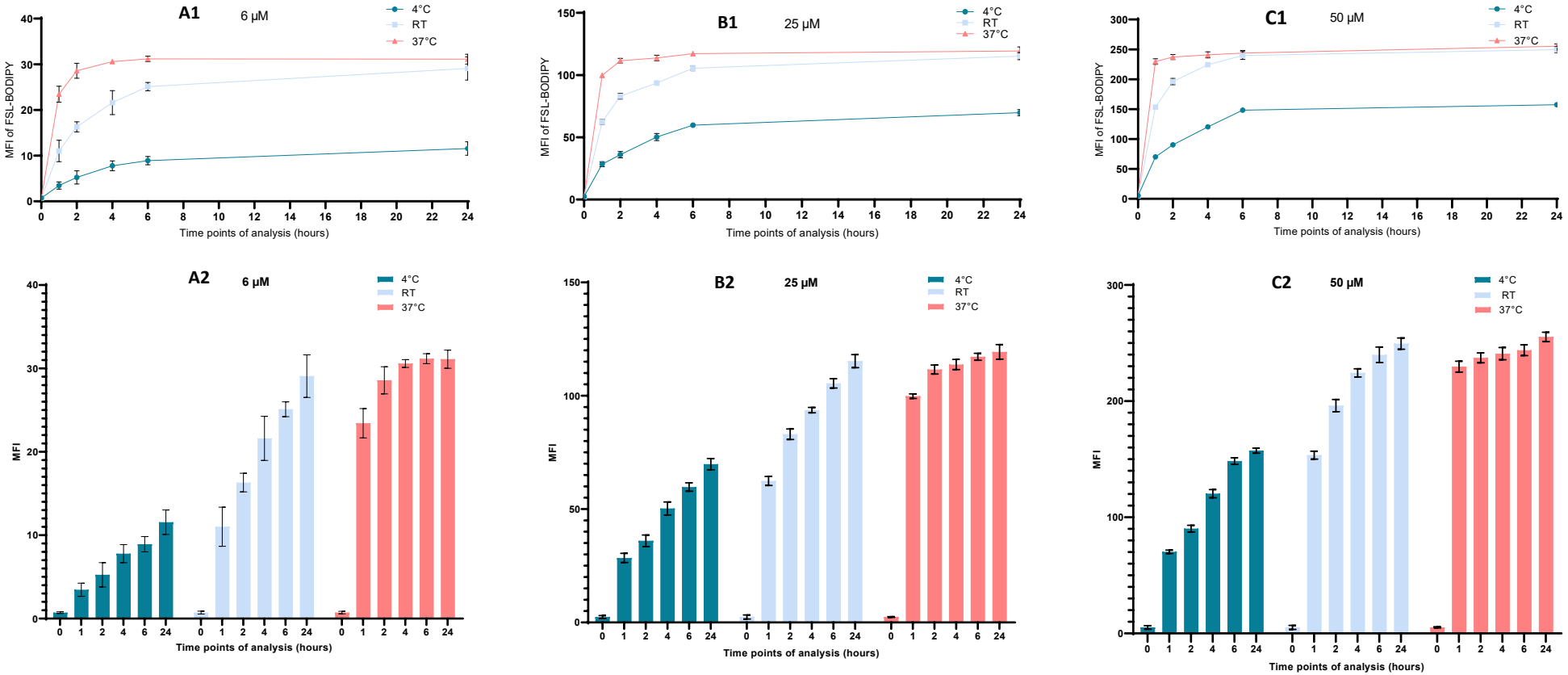

Figure 27: Temperature-dependent uptake of FSL-BODIPY in RBC. Data obtained by flow cytometry. Uptake of 6 (**A1** and **A2**), 25 (**B1** and **B2**), and 50 (**C1** and **C2**) µM of FSL-BODIPY was measured at 37°C, RT, and 4°C over a period of 24 h. Experiments were performed thrice, and the data is expressed as the mean ± SD. Note that the Y axis is different between data sets and the data in Figures **A1, B1,** and **C1** corresponds to Figures **A2, B2,** and **C2** in scatter and column format; see Figure 28 for the data presentation presented at the same scale.

For direct comparative purposes of the relative levels of uptake (same scale for Y axis), the same data is reproduced in a single graph (Figure 28) with additional time points at 4°C up to 240 h (d10). Overall, the labelling effectiveness of FSL-BODIPY varied within concentration ranges, with slower uptake at lower concentrations (by nearly 15%). Additionally, with respect to 37°C, within 2 h of incubation at RT, nearly 80% of FSL- BODIPY was taken up by RBC, and it improved to 90% within 4 h. Whereas at 4°C, it was nearly 30% and 50%, respectively.

Table 6 indicates equivalence points of FSL-BODIPY uptake at RT and 4°C with respect to 37°C (after 1 h). RBC transformed at 37°C for 1 h and RT for 4–6 h generated nearly similar fluorescence signals. As there was no testing between 4 and 6 h, chances are that the MFI obtained at 6 h could have been observed prior to the 6 h testing point. Additionally, uptake at 4°C essentially seems to reach a plateau after 192 h. From Table 6 (and Figure 28), it could be suggested that for 6 and 25 µM FSL-BODIPY, uptake at 4°C essentially reached the same level as the 37°C/1 h transformation after 240 h. However, a comparable MFI of 50 µM was not achieved even after 240 h of koding (it was about 10% lower).

Table 6: Equivalence points of FSL-BODIPY uptake at RT and 4°C compared to 37°C (after 1 h).

Temperature	Time (h)	Mean Fluorescence Intensity (MFI)		
		µM BODIPY-kodecytes		
		6	25	50
37°C	1	23 ± 1	100 ± 1	230 ± 5
RT	4	22 ± 3	94 ± 2	224 ± 4
4°C	192	20 ± 1	92 ± 2	191 ± 3
4°C	240	22 ± 1	94 ± 3	202 ± 5

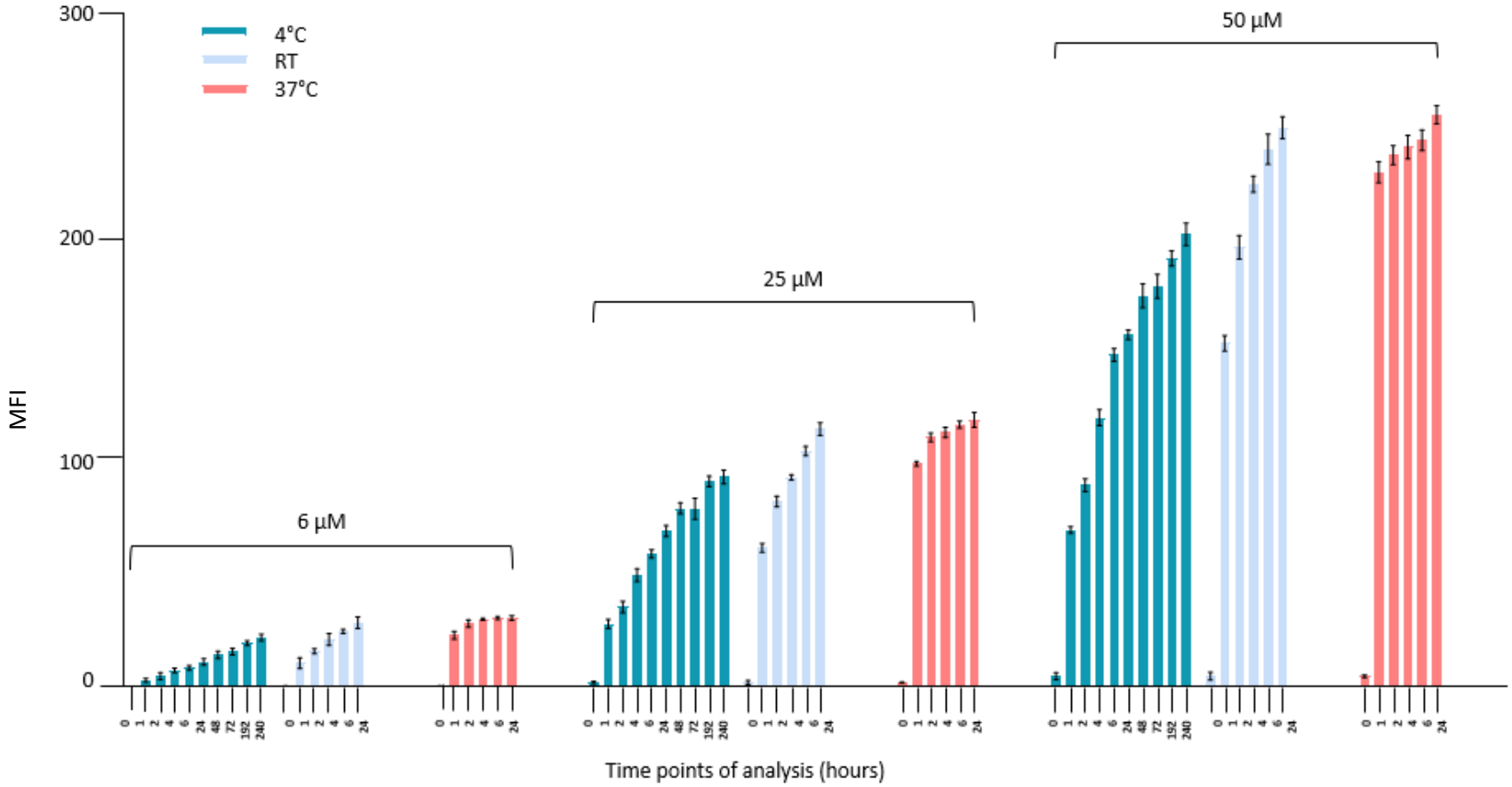

Figure 28: Overall comparative temperature-dependent uptake of FSL-BODIPY. Uptake of FSL-BODIPY is shown at 37°C and RT over 24 h and 4°C over 240 h (d10).

FSL-biotin

The uptake of FSL-biotin is temperature-dependent, and as expected was fastest at 37°C. Transformation of RBC at RT closely follows this uptake, (Figure 29). Interval testing revealed that the uptake was maximum after 24 h of incubation at 37°C or RT, but biotin+SAF488 kodecytes reached their plateau within an hour of incubation at either temperature. For both 37°C and RT, lower concentrations appeared to approach the plateau within 1 h of incubation. For the higher concentration range, it took longer. Like FSL-FLRO4 and FSL-BODIPY, FSL-biotin can transform RBC at 4°C (Figures 25, 27, and 39). On of the most important observation is that, although the overall rate of uptake of FSL-biotin at 4°C was slower compared to 37°C and RT incubation, at 0 h it was much quicker and efficient. For example, within seconds of mixing RBC with FSL-biotin, biotin+SAF488 kodecytes accounted for nearly 35% of the uptake.

Statistical analysis of change in MFI with respect to change in temperature, time, and temperature of biotin+SAF488 kodecytes was determined using PRISM GraphPad. Two-way ANOVA and Tukey's multiple tests were used to test the statistical significance. Change in fluorescent intensity is significant for $p<0.05$ (*), $p<0.003$(**) and statistically highly significant for $p<0.001$(***) and $p<0.0001$ (****). From the statistical analysis, it can be seen that, for 6 and 25 µM biotin+SAF488 kodecytes at 37°C after 2 h of koding, the change in MFI is not significant. However, there was a significant increase in the MFI for 50 µM biotin+SAF488 kodecytes. Irrespective of concentration of FSL-biotin, at 4°C, after 24 h of koding (compared to 2 h), increase in MFI is highly significant.

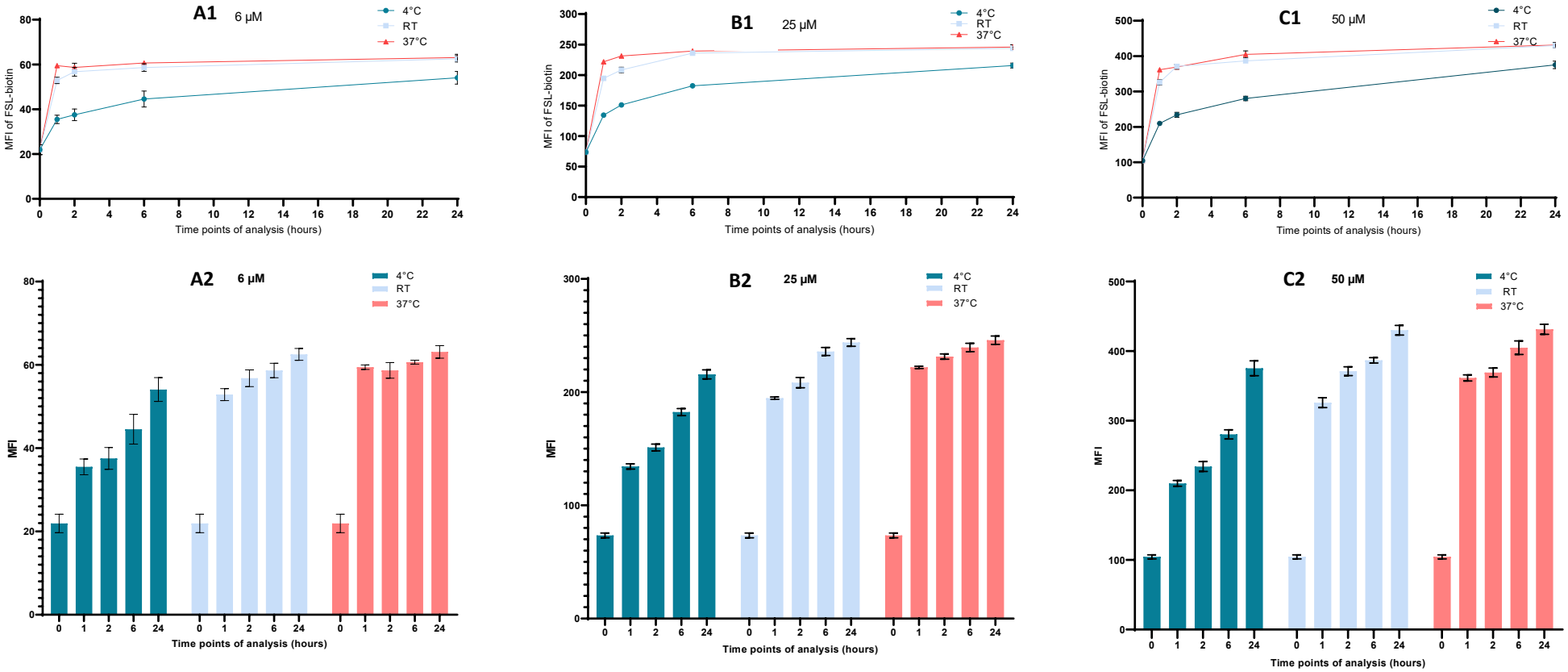

Figure 29: Temperature-dependent uptake of FSL-biotin in RBC. biotin-kodecytes were detected with Streptavidin, Alexa Fluor™ 488 conjugate. Data obtained by flow cytometry. Uptake of 6 (**A1** and **A2**), 25 (**B1** and **B2**), and 50 (**C1** and **C2**) µM of FSL-BODIPY was measured at 37°C, RT, and 4°C over a period of 24 h. Experiments were performed thrice, and the data is expressed as the mean ± SD. Note that the Y axis is different between data sets and the data in Figures **A1, B1,** and **C1** corresponds to Figures **A2, B2**, and **C2** in scatter and column format; see Figure 30 for the data presentation at the same scale.

For direct comparative purposes of the relative levels of uptake (same scale for Y axis), the same data is reproduced in a single graph (Figure 30) with additional time points at 4°C up to 140 h (d5).

Table 7 below summarises interval testing comparisons of FSL-biotin uptake at 37°C, RT, and 4°C over a period of 24 h and 120 h (5 days), respectively. For both lower and higher concentrations, RBC transformed at 37°C/1 h and RT/1 h generated comparable MFI. Insertion at 4°C essentially reached the same level as the 37°C/1 h transformation after 24 h. It should be noted here that there was no testing between 6 and 24 h; chances are that biotin+SAF488 kodecytes MFI (attained at 24 h) could have been observed prior to the 24 h testing point.

Table 7: Equivalence points of FSL-biotin uptake at RT and 4°C compared to 37°C (after 1 h).

Temperature	Time (h)	Mean Fluorescence Intensity (MFI)		
		µM biotin-kodecytes		
		6	25	50
37°C	1	59 ± 1	222 ± 1	361 ± 4
RT	2	57 ± 2	208 ± 4	371 ± 6
4°C	24	54 ± 3	216 ± 4	375 ± 11

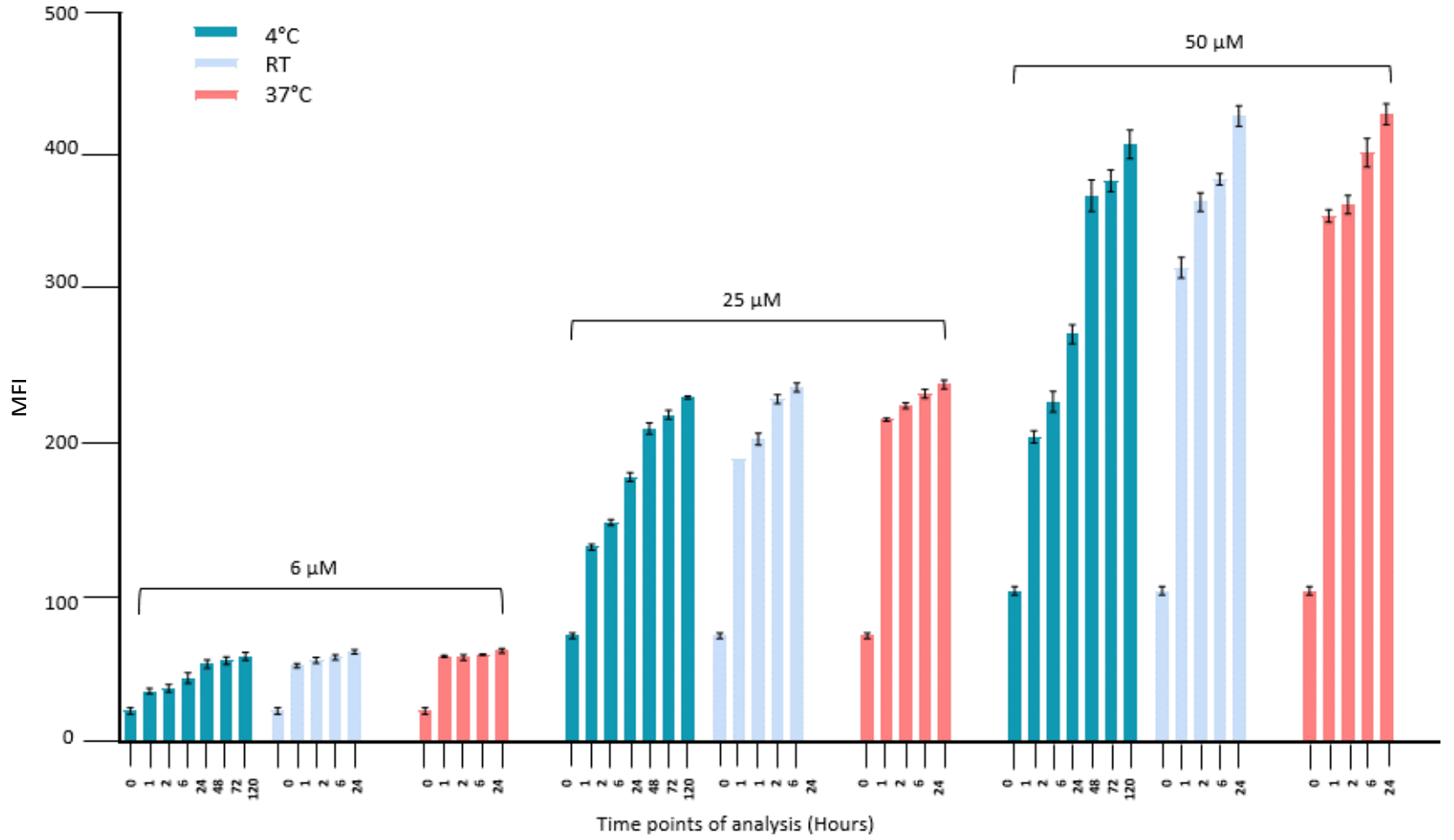

Figure 30: Overall comparative temperature-dependent uptake of FSL-biotin. Uptake of FSL-biotin is shown at 37°C and RT over 24 h and 4°C over 120 h (d5).

Comparative evaluation of FSL constructs koding efficiency

In marked contrast to FSL-FLRO4 and FSL-BODIPY, the labelling efficiency of FSL-biotin at 4°C (and RT) was much higher. For example, within seconds of mixing RBC with FSL-biotin (0 h), biotin+SAF488 kodecytes accounted for nearly 35% of the uptake. This finding was different from what was shown with FSL-FLRO4 and FSL-BODIPY, where the kodecytes took up less than 1% of the FSLs at 0 h. Additionally irrespective of the tested concentration of FSL-biotin, it demonstrated better koding efficiency.

In order to examine the notable difference in labelling efficiency of FSL-biotin and other FSL constructions in more detail, MFI data obtained from 25µM FLRO4, BODIPY, and biotin-kodecytes at 37°C and RT was replotted (Figure 31A and 31B). Additionally, for direct comparative purposes (of the relative levels of uptake after 0 and 1 h), the data shown in Figures 25, 27, and 29 are reproduced in Figure 31. For this, the MFI obtained from respective kodecytes at 0 and 1 h was standardised against a 2 h time point, i.e., the MFI at 0 h and 1 h was calculated as a percentage of the 2 h (maximum).

Figure 31 confirms the marked contrast in the labelling efficiency of FSL-biotin with respect to FSL-FLRO4 and FSL-BODIPY at the 0 h time point. So, it would be appropriate to analyse whether this increase in labelling efficiency of the FSL-biotin at 0 h is a consequence of the detection methodology of biotin-kodecytes using Streptavidin, Alexa Fluor™ 488 conjugate. As mentioned in Section 2.4.1, to detect biotin-kodecytes, there is an additional step wherein the biotin-kodecytes are incubated with Streptavidin, Alexa Fluor™ 488 conjugate, for 30 minutes at RT. Hence, with respect to FLRO4 and BODIPY kodecytes, biotin-kodecytes get an extra 30 minutes of incubation at RT (because of the consequence of their detection methodology). This incubation time frame could be proposed to aid in the uptake and rearrangement of the possibly trapped FSL-biotin construct in glycocalyx, hence enhancing the availability of biotin-kodecytes for detection.

Relative uptake of FSL constructs at 37°C and RT (compared from 2 h)

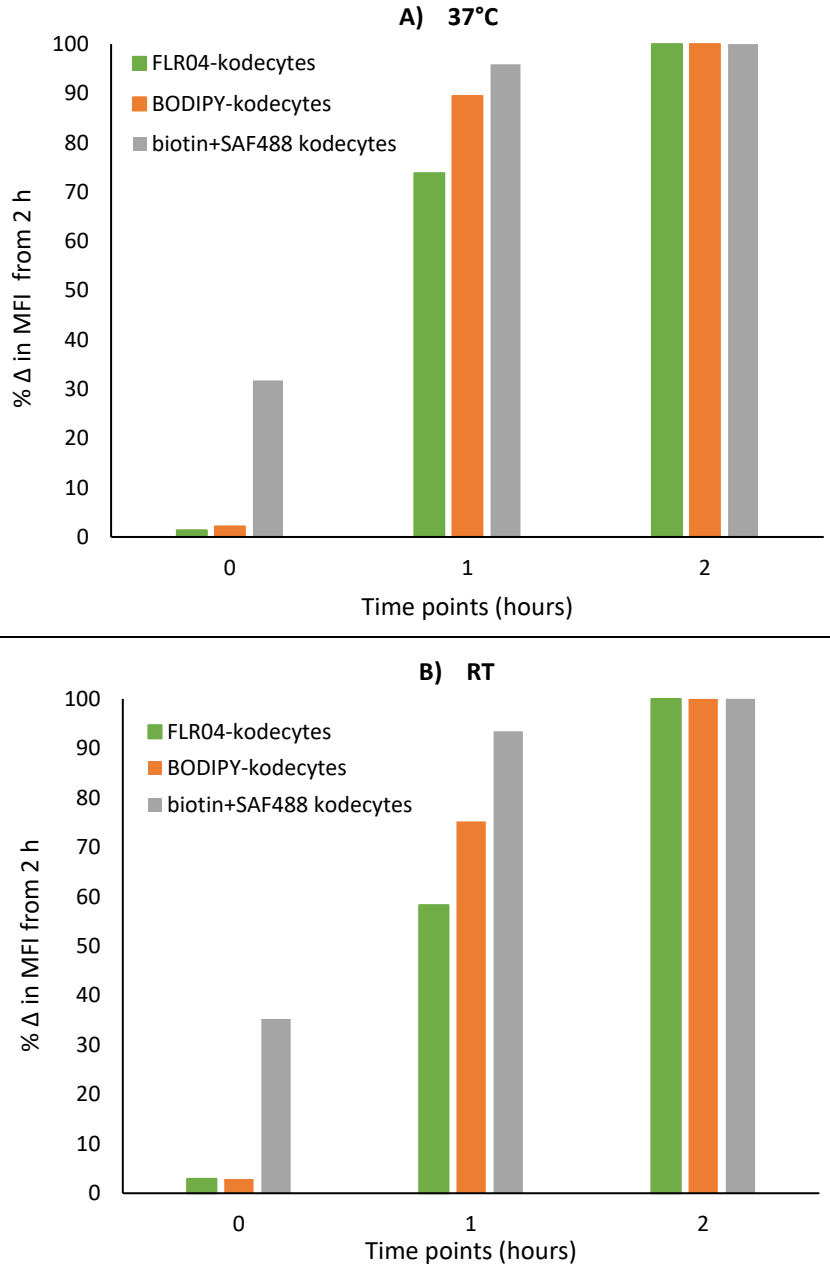

Figure 31: Relative uptake of different FSLs at 37°C and RT. Relative MFI of BODIPY, FLRO4, and biotin+SAF488-kodecytes at **A**) 37°C and **B**) RT at 0 and 1 h. The change in MFI at 0 h and 1 h was calculated as a percentage of the 2 h (maximum, 100%).

To cross-check this scenario and remove the variability of an extra half-hour incubation used for detection of biotin-kodecytes, further experiment was planned, wherein FLRO4-kodecytes and BODIPY-kodecytes were treated similar to biotin+SAF488 - kodecytes. For this, RBC was incubated with 25µM of different FSL constructs at 37°C. Then samples were aliquoted at 0, 0.5, 1, and 2 h of incubation and washed. The 0 h time point time frame was maintained strictly. After specific time,

samples were washed using working strength PBS thrice. FLRO4 and BODIPY- kodecytes were incubated with CellStab and biotin-kodecytes with Streptavidin, Alexa Fluor™ 488 conjugate for half an hour at RT. Finally, kodecytes were washed and analysed by flow cytometry. Figure 32 represents the % change in MFI compared from 2 h time point (MFI at 2 h is considered to be 100%).

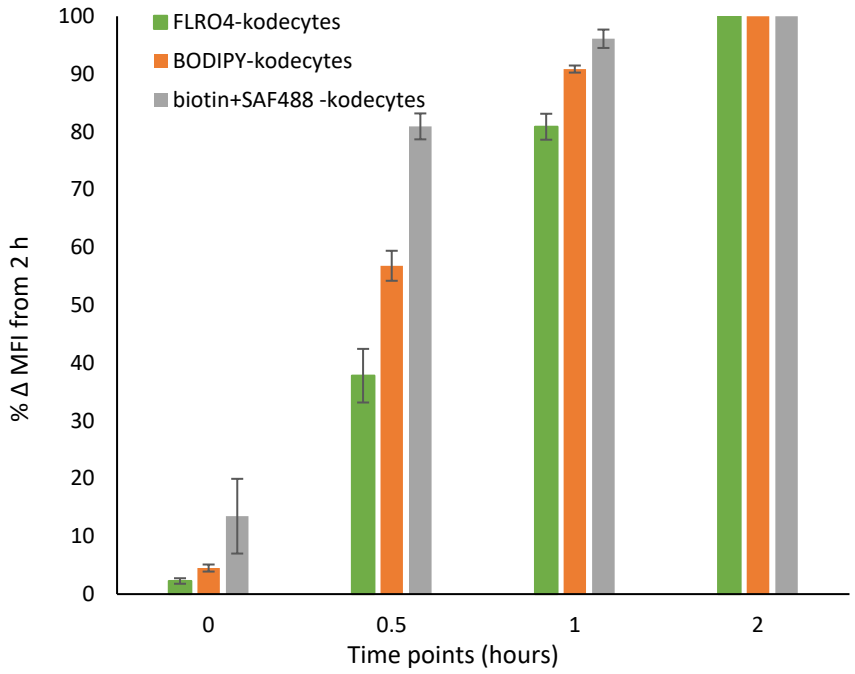

Figure 32: Analysing the enhanced koding efficiency of biotin-kodecytes. For this, the consequence of the detection methodology of biotin-kodecytes using Streptavidin, Alexa Fluor™ 488 conjugate was examined. Relative MFI of 25 µM FLRO4, BODIPY, and biotin+SAF488 kodecytes at 0, 0.5, and 1 h. The MFI at 0, 0.5, and 1 h was calculated as a percentage of the 2 h (maximum 100%).

Figures 31 and 32 show that, compared to FSL-FLRO4 and FSL-BODIPY, FSL-biotin labelling efficiency was quicker and more efficient. In Figure 31, the difference in labelling efficiency among different kodecytes was more, and when it was retested to remove the variability of an extra half-hour incubation used for the detection of biotin-kodecytes, it decreased. However, regardless of koding temperatures, FSL-biotin uptake efficiency was superior to that of FSL-FLRO4 and FSL-BODIPY.

A larger koding difference (Figure 31) is possibly due to extensive sample handling, as three concentrations were tested for transformation efficiency at three different temperatures. Thus the 0 h time point analysis could have extended from 0 h to minutes.

When 0 h time point uptake was re-analysed with strict time frame maintenance (Figure 31) at a single concentration, the uptake rate for biotin+SAF488-kodecytes decreased compared to the results interpreted in Figure 31. However, from the overall data, it could be proposed that FSL-biotin was capable of faster transformation compared to FSL-FLRO4 and FSL-BODIPY.

As within 1 h of koding (37°C), nearly 95% of FSL-biotin and 91% of FSL-BODIPY were taken up by RBCs, it is important to analyse the uptake efficiency of FSL constructs at closer time. The comparison of closer uptake time points (5, 15 minutes) against the maximum transformation time point (100%) would provide a more precise koding efficiency of FSLs.

There could be multiple factors that might impact the temperature-dependent uptake of FSL constructs. Temperature is known to impact the lipid bilayer's fluid state. At 37°C, the membrane is more fluid than at RT and 4°C, making the uptake of the FSL construct more rapid. Hence, it could be suggested that the smaller degree of FSL construct incorporation at a lower temperature of 4°C was due to a decrease in membrane fluidity. Additionally, temperatures might also regulate the availability of FSL constructs to incorporate into the RBC membrane.

Temperature-based uptake study highlighted following aspects of the study along with relevant outline for further investigations.

- The uptake of FSL constructs increases with temperature, with koding at 37°C demonstrating the fastest uptake of FSLs, regardless of the different FSL-construct.
- To better comprehend the kinetics of cellular uptake at 37°C, a shorter interval of time points within the first hour of transformation needs to be carried out. This aspect of the study would also negate the possibility that the kodecyte fluorescence signal observed after 1 h of koding was not generated prior to 1 h of testing.

- With respect to RBCs, prolonged undesirable incubation at 37°C could be substituted with an alternative combination of incubation times at RT and 4°C. Thus, it is important to estimate and compare the transformation efficiency of FSL constructs using a combination of different temperatures and incubation times.
- It is important to highlight that, with FSL-BODIPY and FSL-biotin, there was no fluorescence signal loss during extended incubation at 37°C; however, there was a loss with FSL-FLRO4. Hence, the reasons behind FSL-FLRO4 signal loss during 24 h incubations at 37°C need to be investigated.
- For a better understanding of the FSL transformation/uptake phenomenon, post-transformation solutions from different time intervals should be evaluated for the presence of any residual FSL constructs. Therefore, it was planned that the post-transformation solution would be recovered as a supernatant and assessed for the presence of residual FSL constructs by analysing their possibility to transform fresh RBC.

3.3.3 Effect of time on FSL uptake

Overview: The previous temperature-based uptake study highlighted the importance of evaluating shorter koding duration for uptake of the FSL construct (within the first hour of incubation at 37°C). Additionally, it was also considered that, for a better understanding of the mechanism of uptake of FSLs by RBCs, after completion of the respective koding duration, the post-transformation solution could be evaluated for the presence of any residual FSL constructs. Hence, to determine the dynamics of cellular uptake of FSL-constructs at 37°C in greater detail, a time-course uptake study was set up.

Methodology: The following methodology was designed to test the time-dependent uptake of FSL constructs in RBC over a period of 24 h. The schematic overview of the method is presented in Figure 33, followed by a detailed explanation of the experimental protocol.

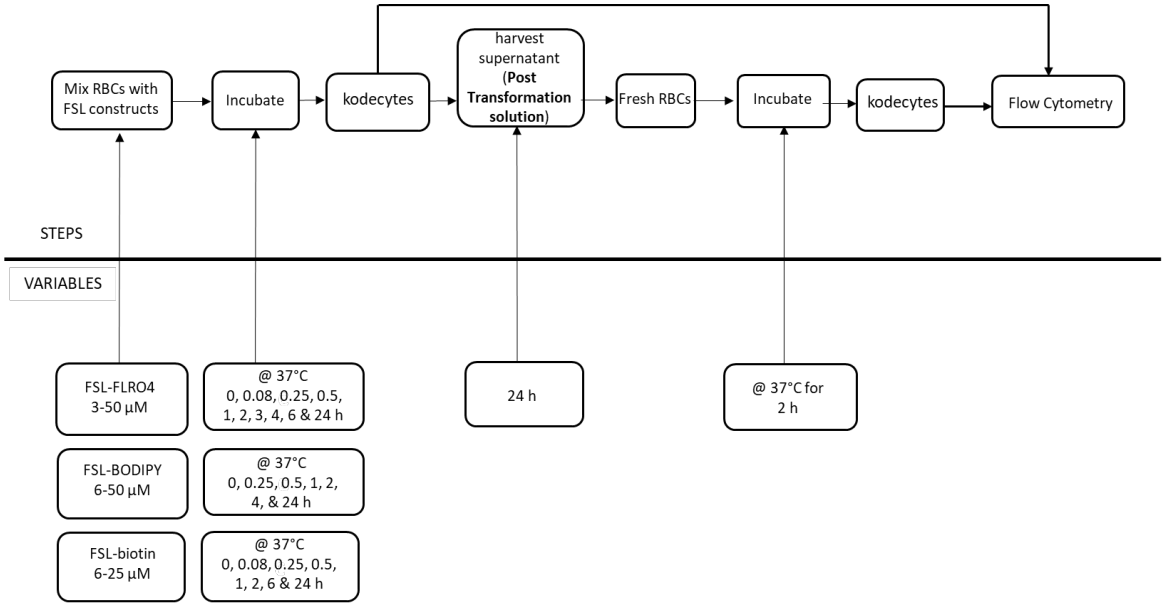

Figure 33: Schematic overview of method testing time-dependent uptake of FSLs at 37°C in RBC over a period of 24 h.

The following protocol outlines the steps.

- RBCs were incubated with FSL constructs at 37°C for up to 24 h. Samples were aliquoted at predetermined intervals (Table 8), and MFI was estimated by flow cytometry.
- After 24 h of incubation, RBC and FSL mixture content was centrifuged in an Immufuge on high for 3 minutes to separate supernatant, i.e., post transformation solution (PTS). It was further centrifuged at 130×g for 5 minutes to ensure removal of any residual kodecytes.
- The post-transformation solution was evaluated for the presence of residual FSL constructs by analysing its possibility to transform fresh RBCs. To achieve this, an equal volume of post-transformation solution was incubated with an equal volume of packed RBCs for 2 h at 37°C.
- MFI obtained from kodecytes after 4 h for FSL-FLRO4 and 24 h for FSL-BODIPY and FSL-biotin was combined with MFI obtained from respective post-transformation solution kodecytes to obtain maximum MFI, which would be used as a reference point for 100% uptake (maximum MFI). Henceforth, the koding efficiency of the FSL construct at a predetermined time was calculated as the percentage of the reference point of 100% uptake (maximum MFI).

- Flow cytometry analysis of unwashed and washed samples of FSL-FLRO4 and FSL-BODIPY kodecytes revealed minimal differences in MFI values. Therefore, to ensure reliable and reproducible results, MFI obtained from washed samples was only analysed. It is important to mention that in the case of FSL-biotin kodecytes, only washed samples should be analysed, as it is important to remove any outliers in the data generated from non-specific bindings of Streptavidin, Alexa Fluor™ 488 conjugate. For all tested FSL constructs, only washed samples were analysed.

Table 8: Time-dependent uptake of FSLs in RBC at 37°C over a period of 24 h. The Table also shows the time point at which post-transformation solution (PTS) was evaluated for the presence of residual FSL construct.

FSL constructs	Concentration (μM)	Kodecytes obtained at time points (h)	PTS kodecytes obtained after time point (h)
FSL-FLRO4	3, 6, 12, 25, 50	0, 0.08, 0.25, 0.5, 1, 2, 3, 4, 6, 24	24
FSL-BODIPY	3, 6, 12, 25, 50	0, 0.25, 0.5, 1, 2, 4, 24	24
FSL-biotin	6, 25	0, 0.08, 0.25, 0.5, 1, 2, 6, 24	24

FSL-FLRO4

FSL-FLRO4 constructs showed a time-dependent uptake at 37°C in RBC as MFI increased with an increase in incubation time. It could be seen from Figure 34 that FSL-FLRO4 uptake gradually increased past 5 minutes of incubation, and MFI attained at 1 h was not observed prior to the 1 h testing point. Additionally, FSL-FLRO4 uptake was fastest in the first hour, with a slower increase in MFI thereafter. At the 4 h time point of analysis, the fluorescence signal (MFI) was highest, and past this time point of incubation, MFI started decreasing. It was expected that the post-transformation solution (obtained at 24 h) would account for the loss of the FSL-FLRO4 signal; hence, after completion of the 24-hour incubation, the supernatant was separated and incubated with fresh RBC. It was observed that MFI obtained from kodecytes prepared from 24 h of supernatant did not match up to the level of fluorescence lost from kodecytes obtained at the 24 h incubation time point. Chapter 5 discusses the experimental setup and results obtained to understand the unaccounted signal loss for FSL-FLRO4.

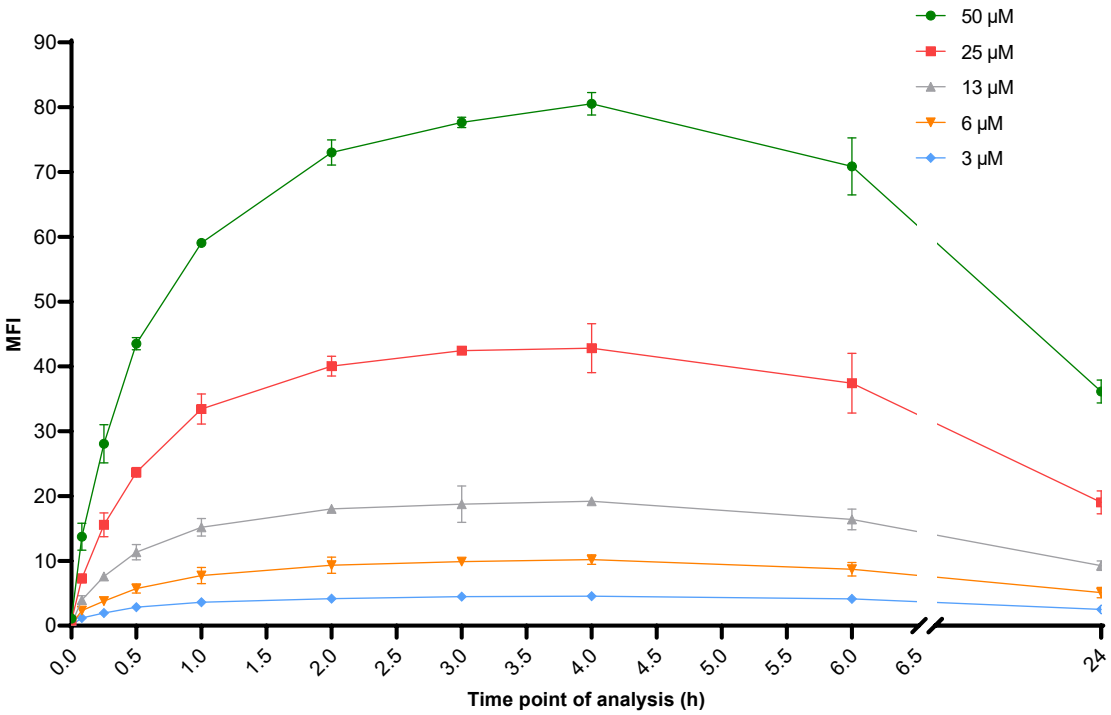

Figure 34: Time-dependent uptake of FSL-FLRO4 in RBC at 37°C over 24 h. Data obtained by flow cytometry. Experiments were performed thrice, and the data is expressed as the mean ± SD.

Koding efficiency of FSL-FLRO4 at specific time period was calculated as the percentage of maximum MFI (reference point of 100% uptake) which is sum of MFI obtained from FLRO4-kodecytes at 4 h time point and kodecytes prepared from post transformation solution (24 h). Figure 35 summaries the kinetic of uptake of FSL-FLRO4 across the tested concentrations. Within just 5, 15 and 30 minutes of incubation/koding, FSL accounted for approximately 31%, 48%, 65% and 17%, 32%, 55% uptake, respectively. Across the tested concentration range the most rapid uptake was observed in the first hour of incubation, accounting for approximately 80% of maximum signal obtained. Fluorescence signal increased only minimally afterwards.

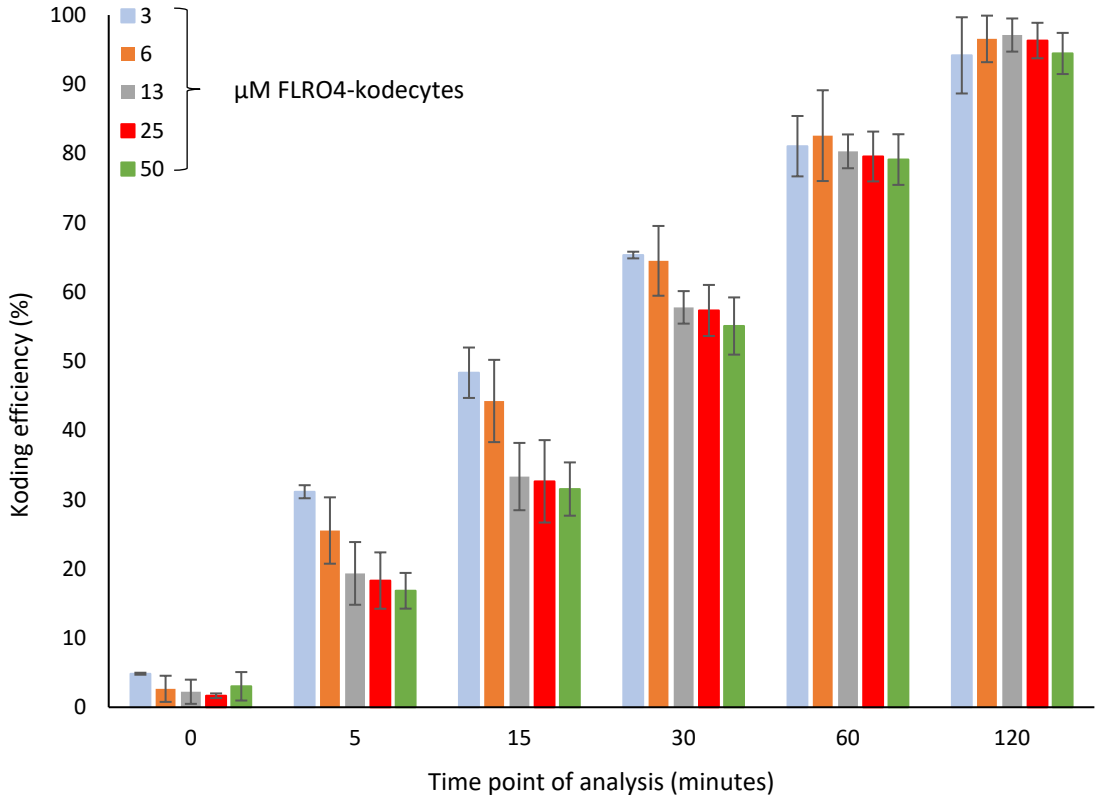

Figure 35: Dynamics of uptake of FSL-FLRO4 in RBC, flow cytometry data. The koding efficiency was calculated as percentage of the maximum uptake and is plotted against time in minutes. Koding efficiency at 0 h corresponds to MFI of RBC and FSL-FLRO4 mixture aliquoted immediately after incubation with FSL-FLRO4, while the maximum MFI (4 h MFI +PTS MFI; not shown) is 100%.

The statistical significance of finding that lower concentrations of FSL-FLRO4 (3 and 6 µM) had better koding efficiency than higher concentrations (13 µM and above) during 5, 15, and 30 minutes of koding period was examined using a two-way ANOVA with Tukey's multiple comparison test. Significant changes in koding efficiency are defined as *P<0.05, **P<0.005, ***P<0.0005, and ****P<0.0001. The koding efficiency of 3 and 6 µM FSL-FLRO4 was examined at all koding durations and compared to all other tested concentrations. The results of the statistical analysis showed that up to 30 minutes of koding duration, 3 and 6 µM FSL-FLRO4 had significantly higher koding efficiency (although with a different P value) than all other concentrations. However, after 60 and 120 minutes of koding, this change is not significant.

Due to the nature of FSL constructs, in koding solution (depending on their concentration), they would probably exist as either free monomers (below CMC) or micelles (at and above CMC). Based on earlier studies, FSL-FLRO4 and FSL-biotin in

aqueous solution (dispersed in PBS pH 7.4) have been shown to form micelles at 14–30 µM and 5-130 µM concentrations, respectively.[111] The analysis of the FSL-BODIPY micelle and its respective CMC had not been reported previously. Possibly the uptake of FSL constructs below CMC is because free FSLs are acquired by the cell membrane spontaneously. Additionally, depending on the nature of micelle [89], there are a few different possibilities for the uptake of FSL above CMC, like whether FSL monomers dissociate from micelles and are then acquired by the cell membrane or whether FSL micelles do not dissociate and are acquired by the cell membrane as a whole FSL micellar unit. The following results would be discussed with respect to micellar FSL possibilities.

From Figure 36, it could be seen that lower concentrations (free FSLs), especially 3 and 6 µM, seem to be taken up faster within the initial incubation period than higher concentrations (CMC), and as the incubation period progresses, the rate of uptake becomes more uniform across the concentration range. This phenomenon of a slower uptake rate for higher concentrations (CMC) during preliminary incubation time points could be attributed to the nature of micelles. It could be proposed that during the initial phase of incubation, FSL-FLRO4 at higher concentrations are in micellar form (or transitioning) with a low off-rate, owing to which they are more stable and do not allow exchange or dissociation of their monomers readily in the solution phase. As the incubation time progresses, micelles will have more time to incorporate into the membrane's surface, levelling off the uptake efficiency of lower concentrations.

Methodology for exploring micelle concept

To investigate the micelle phenomenon, an experiment was set up wherein a non-fluorescent FSL construct, FSL-GB3 (Figure 13D), was used along with FSL-FLRO4 (in two different ratios) to attain a strength of 50 µM (representing micelle form of FSLs). FSL- GB3 was chosen for this study as it has an adipate-based spacer (like FSL-FLRO4); hence, confounding effects generated because of structural dissimilarities could be avoided. Table 9 summarises the various individual and combinations of FSL constructs (in different ratios) used in this experiment to examine the micelle hypothesis. FSL-GB3 being non-fluorescent only represents the concentration part and highlights the effect of the micelle on the fluorescence signal. In this experimental set-up, RBC was incubated with individual FSL (FSL-FLRO4, FSL-GB3) and grouped FSL constructs representing

micelles (FSL-FLRO4+FSL-GB3) at 37°C for 5 and 60 minutes. The respective kodecytes were washed and analysed by flow cytometry.

Table 9: Exploring the micelle concept of FSL-FLRO4. To examine the micelle hypothesis, various individual and grouped combinations of FSL-FLRO4 and FSL-GB3 were tested.

FSL constructs	Concentration (µM)	Time points of analysis (minutes)
FSL-FLRO4	6	5, 60
FSL-GB3	44	5, 60
FSL-FLR04 + FSL-GB3*	6 + 44	5, 60
FSL-FLRO4	13	5, 60
FSL-GB3	37	5, 60
FSL-FLR04 + FSL-GB3*	13 + 37	5, 60

* *Probably exists as micelles because above or near CMC*

Results

Figure 36A shows that, when RBC FLRO4-kodecytes were made in the presence (of different ratios) of FSL-GB3 representing micellar concentration, the fluorescence signal decreased. This trend was observed at both 5 and 60 minutes of testing. Figure 36B represents the percentage change in MFI, showing the effectiveness of labelling after 5 and 60 minutes of incubation in the presence of different ratios of FSL-GB3. Uptake decreased by 60% ± 4 and 47% ± 1 after 5 minutes and 36% ± 4 and 32% ± 2 after 60 minutes of incubation in the presence of two tested ratio combinations of FSL-GB3. It could be hypothesised that the presence of FSL-GB3 is affecting the availability of FSL- FLRO4 for koding RBC, i.e., FSL-GB3 at tested concentrations may be affecting the concurrent uptake of FSL-FLRO4 by retaining the FSL-FLRO4 in a micellar form and reducing its interaction with RBC. Additionally, the abovementioned results also help conclude that during preliminary incubation, higher concentrations contribute to relatively slower uptake owing to micelle formation, and as the time of incubation progresses, it levels out the uptake efficiency.

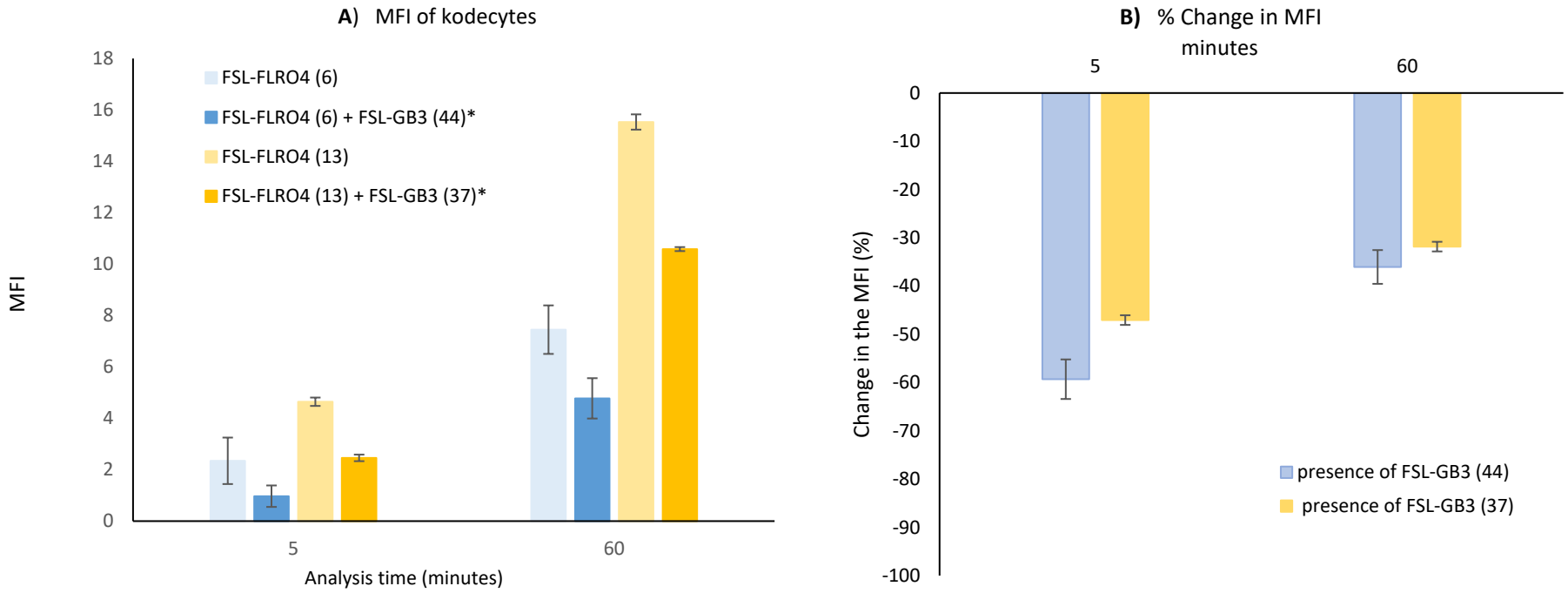

Figure 36: Exploring the micelle concept of FSL-FLRO4. Micelle hypothesis examined by analysing uptake of FSL-FLRO4 in the concomitant presence of FSL-GB3 by flow cytometry **A)** MFI obtained after 5 and 60 minutes of incubation at 37°C, when RBC FLRO4-kodecytes were made in the presence (of different ratios) of FSL-GB3. **B)** % change in MFI, depicting the effectiveness of labelling after 5 and 60 minutes of incubation in the presence of different ratios of FSL-GB3.

FSL-BODIPY

Figure 37 shows that FSL-BODIPY has time-dependent uptake, and within 15 minutes of incubation with RBCs, MFI increases rapidly. Although MFI attained at 60 minutes was not observed prior to the 60 minutes testing point, FSL-BODIPY showed an extremely fast uptake within 15 to 30 minutes of incubation, as MFI increased considerably. Furthermore, unlike FSL-FLRO4, FSL-BODIPY uptake approaches a plateau after 2 h of incubation.

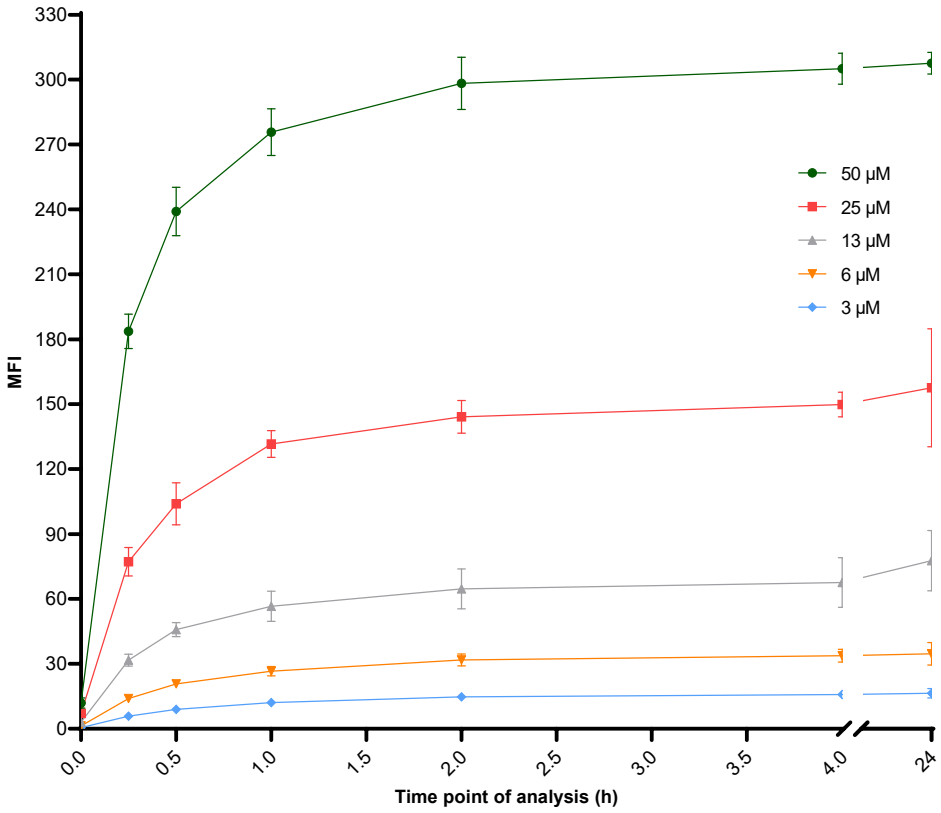

Figure 37: Time dependent uptake of FSL-BODIPY in RBC at 37°C over 24 h. Data obtained by flow cytometry. Experiments were performed thrice, and data is expressed as mean ± SD.

The koding efficiency of FSL-BODIPY at a specific time was calculated as the percentage of maximum MFI (reference point of 100% uptake), which is the sum of MFI obtained from kodecytes at the 24 h time point and kodecytes prepared from the post-transformation solution (24 h). The dynamics of uptake of FSL-BODIPY across the tested concentrations are shown in Figure 38. The rate of uptake was different across the tested concentrations (possibly due to CMC). For example, within 15 minutes of

incubation, FSL tested at a lower concentration (free FSLs) accounted for 35% efficiency, whereas it was nearly 60% at a higher concentration of FSL (above CMC). Furthermore, in the first 60 minutes of incubation, approximately 80% of FSL-BODIPY was taken up by the RBCs, and thereafter, only a minimal change occurred.

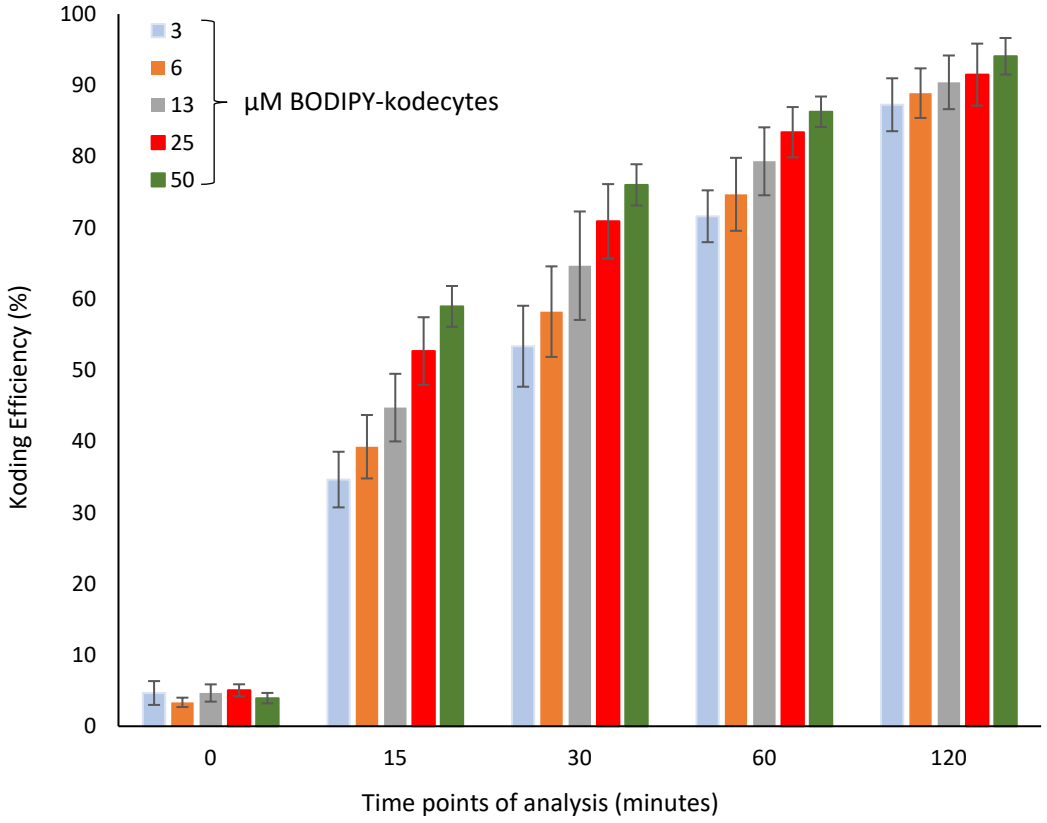

Figure 38: Dynamics of the uptake of FSL-BODIPY in RBC, flow cytometry data. The koding efficiency was calculated as a percentage of the maximum uptake and plotted against time in hours. Koding efficiency at 0 h corresponds to the MFI of RBC and FSL-BODIPY admixture aliquoted immediately after incubation with FSL-BODIPY, while the maximum MFI (24 h MFI +PTS MFI; not shown) is 100%.

Figure 38 shows that FSL-BODIPY uptake looks like reaching its optimum faster for higher concentrations range (50, 25 and 12 µM) than lower concentrations range (6 and 3 µM). A two-way ANOVA with Tukey's multiple comparison test was used to examine the statistical significance of the observation of the effect of concentration of FSL-BODIPY on its koding efficiency (i.e., that lower concentration FSL-BODIPY (3 and 6 µM) had reduced koding efficiency than higher concertation (13 µM and above) during 15 and 30 minutes of koding period). A change in koding efficiency is considered significant at

*P<0.05, **P<0.005, ***P<0.0005, ****P<0.0001. For this, koding efficiency of 3 and 6 µM FSL-BODIPY was compared to all other tested concentrations at all tested koding durations. The statistical analysis revealed that 3 and 6 µM BODIPY had significantly lesser koding efficiency (although with a different P value) than tested higher concentrations up to 30 minutes of koding duration. However, this difference is not significant at 60 and 120 minutes of koding. The observation of concentration-dependent uptake of FSL-BODIPY suggests that the concentration of FSL regulates the rate of cellular uptake by determining the amount of FSL that would be available for acquisition into the RBC cell membrane. As shown in Figure 36, possibly the difference in koding efficiency may be due to the nature of FSL- BODIPY CMC.

The CMC of FSL-biotin and FSL-FLRO4 has been examined and reported previously; however, the analysis of the FSL-BODIPY micelle and its respective CMC has not been studied. During this study, a fluorescent plate reader-based experiment was set up to possibly propose the CMC of FSL-BODIPY. However, this way of examining the CMC is an indirect method, as other, more sophisticated methods are available. When the fluorescence of FSL-BODIPY dispersions at increasing concentrations was analysed, it was shown that at increasing concentrations, FSL-BODIPY dispersions showed increased fluorescence until ≈13 µM (results not shown); above this concentration, the change in fluorescence signal was not significant. This result possibly suggests that the CMC of FSL-BODIPY could be around 13 µM, and above this concentration, all additional FSL constructs form micelles (which are quenched and hence contribute no fluorescence). Thus, in the case of FSL-BODIPY, it could be hypothesised that the apparent faster uptake for higher concentrations could be due to the relatively less stable micelle form, wherein, owing to its higher off-rate, micelles (which function as reservoirs of monomers) would dissociate faster, releasing monomers that would be acquired at a quicker rate. Furthermore, at lower concentrations (below CMC), there would be fewer monomers available, leading to restrained uptake and a slower uptake rate.

In contrast to FSL-FLRO4 uptake (Figure 36), Figure 38 shows that FSL-BODIPY uptake looks like reaching its optimum faster for higher concentrations range (50, 25, and 12 µM) than lower concentrations range (6 and 3 µM). The observed results could possibly be due to the difference in nature of CMC (stability, conformation), which in turn is influenced in part by the combination of functional group, spacer, and lipid together

with concentration, temperature, size, and hydrophobicity/hydrophilicity. Additionally, irrespective of koding duration, more FSL-BODIPY is acquired by the RBC membrane than FSL-FLRO4. This could be possibly due to the BODIPY hydrophobic functional group.

FSL-biotin

Figure 39 shows that FSL-biotin has an extremely fast uptake in the first 5 minutes of incubation, as there is a sharp rise in MFI. Uptake continues past 30 minutes with a slower increase of the MFI over time, and it approaches a plateau after 120 minutes. From the results obtained, it can be concluded that the FSL labelling trend was similar across the tested concentrations.

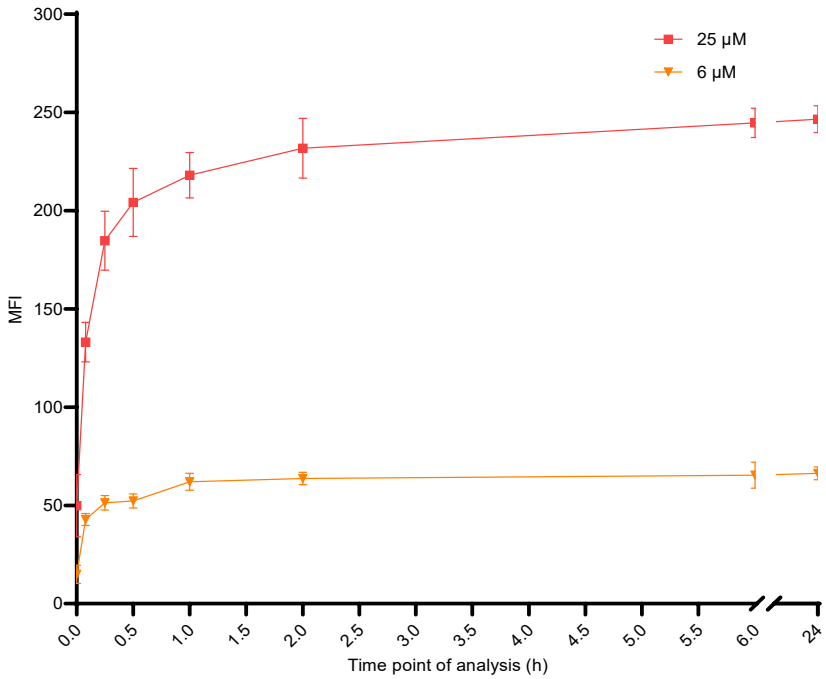

Figure 39: Time-dependent uptake of FSL-biotin in RBC at 37°C over 24 h. Experiments were performed twice, and the data is expressed as mean ±SD.

The koding efficiency of FSL-biotin at different time periods was calculated as the percentage of maximum MFI (reference point of 100% uptake), which is the sum of MFI obtained from kodecytes at the 24 h time point and kodecytes prepared from the post-transformation solution (24 h). Figure 40 summarises the dynamics of uptake of FSL- biotin, and it could be seen that it varied marginally across the tested concentrations of FSL-biotin. The increase in the uptake efficiency of FSL-biotin was

substantial at the 0 h time point. Within just seconds of mixing RBC with FSL-biotin, biotin-kodecytes accounted for approximately 23% ±7 and 20% ±6 uptake for 6, and 25 µM, respectively. This is in marked contrast to the results seen with FLRO4 constructs. The proposed explanation for this scenario has been discussed in Section 3.3.2 wherein an experiment was set up to analyse whether this was a consequence of the detection methodology of biotin-kodecytes using Streptavidin, Alexa Fluor™ 488 conjugate. Respective experiments revealed that biotin+SAF488 kodecytes labelled RBCs faster than FLRO4 and BODIPY kodecytes at the 0 h time point, but the difference was not as much as seen in Figures 33 and 34. Partly the difference in uptake effectiveness was attributed to extensive handling of samples, as three different concentrations were tested for their labelling efficiency at three different temperatures (37°C, RT, and 4°C). Hence, the 0 h time point analysis could have been extended to 0–5 minutes.

As mentioned earlier, the FSL-biotin labelling efficiency study became more well-defined when closer time points of uptake (5, 15 minutes) were compared against the maximum uptake time point (reference point of 100% uptake), which was performed through a time point dependence study. Within 5 minutes of incubation, FSL-biotin accounted for approximately more than 50% of uptake, and thereafter, it increased to approximately 85% within an hour of incubation. It could be seen from Figure 40 that, although FSL- biotin uptake at 1 h was not observed prior to the 1 h testing point, koding efficiency increased sharply past 5 minutes of incubation, and the fluorescence signal started to plateau after 15 minutes of incubation. This experiment confirms that irrespective of concentration used, after 0, 5, and 15 minutes of koding duration, compared to FSL- FLRO4 and BODIPY, FSL-biotin labels the RBCs at a faster rate. The statistical significance of the observation that (6 and 25µM) FSL-biotin was most effective (compared to FSL-FLRO4 and BODIPY) in koding at 0, 5, and 15 minutes of the koding period was examined using a two-way ANOVA with Tukey's multiple comparison test. The statistical analysis revealed that after 0 and 15 minutes of koding, compared to FSL-FLRO4 and BODIPY, the koding efficiency of FSL-biotin was statistically different and significant at both 6 and 25µM (and better), with **P<0.001 and ***P<0.0003.

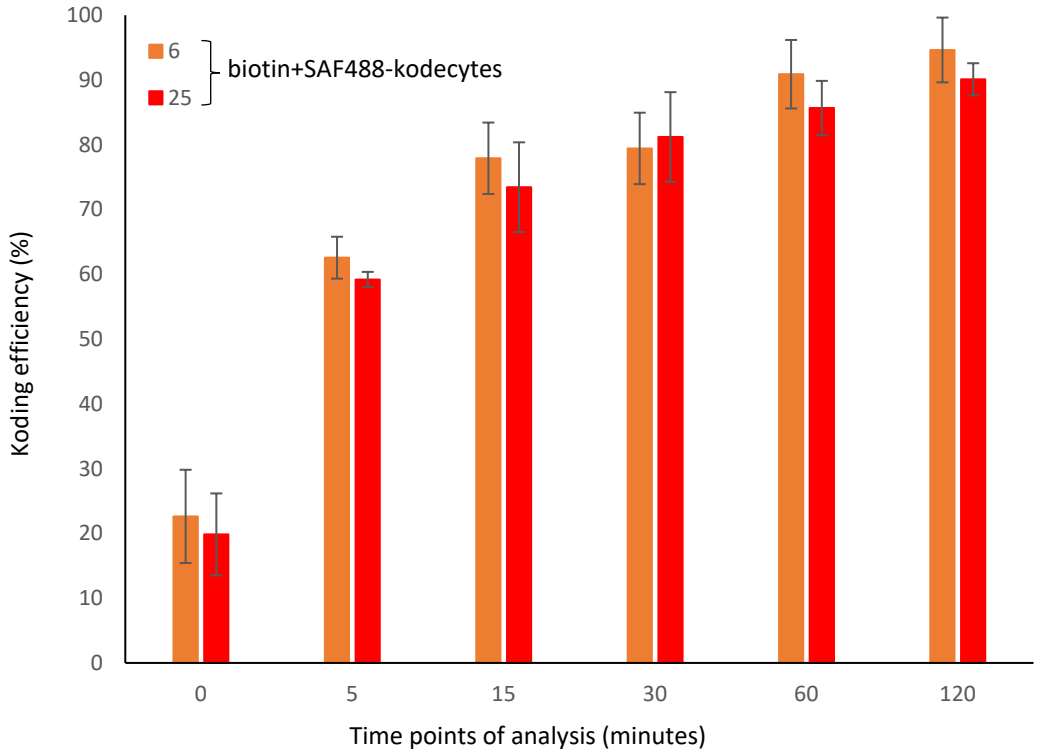

Figure 40: Dynamics of uptake of FSL-biotin in RBC, flow cytometry data. The koding efficiency was calculated as a percentage of the maximum uptake and plotted against time in hours. Koding efficiency at 0 h corresponds to the MFI of RBC and FSL-biotin mixed and aliquoted immediately after incubation with FSL-biotin, while the maximum MFI (24 h MFI +PTS MFI; not shown) is 100%.

In the case of FSL-biotin, results showed (Figure 40) that irrespective of different concentrations, FSL-biotin uptake at different koding durations was very similar. This possibly indicates that unlike FSL-FLRO4 and FSL-BODIPY, the formation of micelles does not impact the rate of FSL-biotin, as the CMC of FSL-biotin has been reported to be between 14 and 30 µM. Possibly, either the micellar form of FSL-biotin is very unstable, aiding in faster dissociation (into free FSL) and fast uptake by the membrane, or FSL-biotin forms micelles at different concentrations than reported by the CMC study. This probability could be true as the CMC value reported in the respective study was measured in 1 × PBS, and hence it does not provide a true representation of the medium (and behaviour of FSL-biotin) used in this study, which is CellStab.

Jurkat kodecytes

Experiments were also conducted to analyse the time-dependent uptake of 13 µM FSL-FLRO4 and FSL-BODIPY by Jurkat cells at 37°C. Labelling effectiveness was estimated

with regular testing at 5, 30, 60 and 120 minutes. Prolonged incubation of Jurkat cells with FSL beyond 120 minutes was not continued (as in case with RBCs) because serum deprivation for longer can cause harm to cell health and ultimately affect cell viability. This would result in confounding results [155].

As shown in Figure 41, for FSL-FLRO4 and FSL-BODIPY, MFI increases with time, with faster uptake within the first 30 minutes of incubation. FSL-FLRO4 uptake seems to have reached a plateau after 120 minutes of incubation, as there was a minimal increase in MFI between time points 60 and 120 minutes. FSL-BODIPY saturation of uptake was not observed as MFI maintained an increasing trend and kept increasing past 1 h of incubation, and a plateau in uptake needed to be attained.

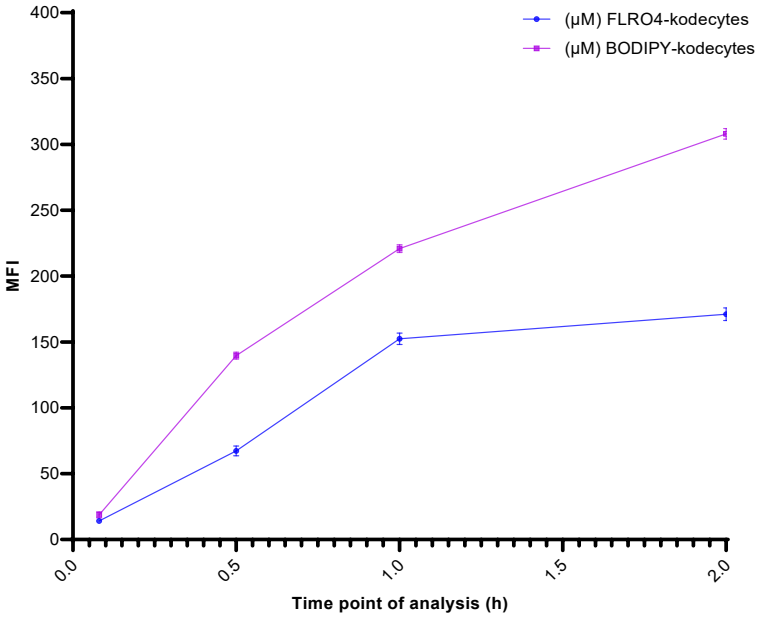

Figure 41: Time-dependent uptake of FSLs in Jurkat cells at 37°C over 2 h. 13 μM of FSL-FLRO4 and FSL-BODIPY was used for preparing Jurkat Kodecytes. Data obtained by flow cytometry. Experiments were performed in triplicate, and the data is expressed as mean ± SD.

Figure 42 summarises the dynamics of uptake of 13 μM FSL-FLRO4 and FSL-BODIPY in Jurkat cells. Here, MFI obtained after 2 h of incubation (the highest MFI) was used as a reference point for 100% insertion. The koding efficiency of FSL-FLRO4 and FSL-BODIPY at different time intervals was calculated as the percentage of maximum MFI and considered as the reference point of 100% uptake (2 h). It could be inferred from Figure 42 that for FSL-FLRO4 and FSL-BODIPY, within 30 minutes of incubation, approximately 40% uptake was achieved. Thereafter, within an hour of incubation, it

increased to about 89% and 72% for FSL-FLRO4 and FSL-BODIPY, respectively, suggesting the fluorescence signal has plateaued for FSL-FLRO4.

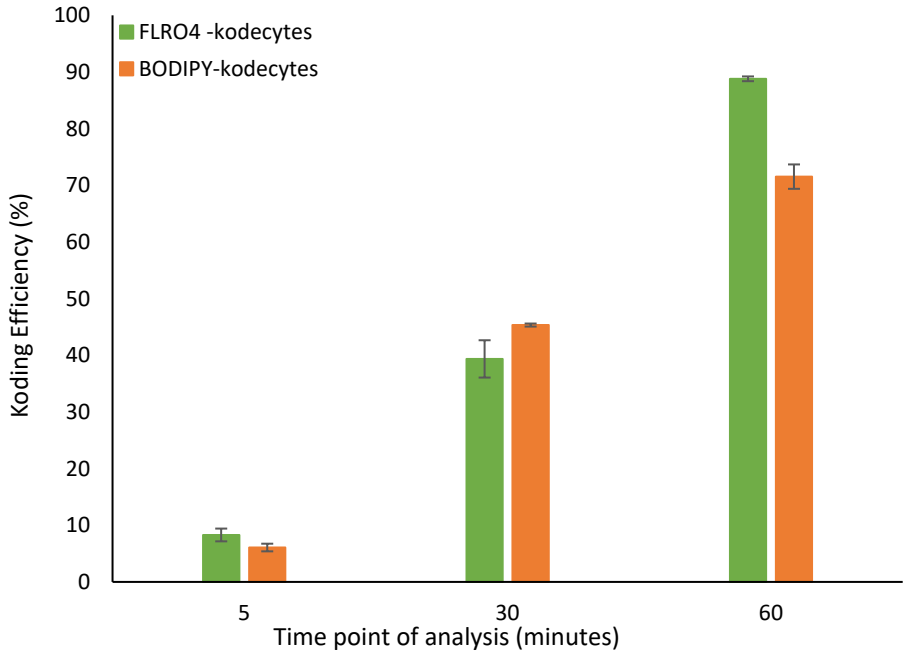

Figure 42: Dynamics of uptake of FSL-FLRO4 and FSL-BODIPY in Jurkat cells. Koding efficiency at 2 h (not shown) corresponds to 100% uptake. The koding efficiency after 5, 30, and 60 minutes time interval was calculated as a percentage of the maximum insertion (2 hours) and plotted against time in hours.

3.3.4 Effect of Protein on FSL uptake

Overview: Experiments were performed to study the effect of BSA (protein) on FSL transformation effectiveness, i.e., how the absence or presence of different levels of BSA in the transformation medium could regulates the uptake of FSL constructs by the RBCs.

Methodology overview: The following methodology was proposed to test the uptake of FSL constructs from BSA- free and BSA-supplemented transformation solutions into RBC. The schematic overview of the methodology is presented in Figure 43, followed by an overview of the experimental protocol.

- The FSL-FLRO4 and FSL-BODIPY working stock or transformation solution were made with different amounts of BSA (CellStab as a diluent).

- 6 and 50 µM RBC FLRO4 and BODIPY-kodecytes were prepared by incubating RBC with FSL transformation medium (with and without BSA) for 2 h at 37°C.
- Respective kodecytes were analysed to measure and compare the uptake of FSL construct in the presences of BSA by flow cytometry.

Table 10: The uptake of FSLs by RBCs in the presence of BSA. Data generated by flow cytometry. Table shows different concentrations (µM) of BSA and its approximate representation in %. FSL uptake was tested at 37°C after 2 h of koding.

FSL constructs	BSA concentration (µM)	BSA concentration (%)
FSL-FLRO4	6 - 1200	0.03- 10
FSL-BODIPY	50 - 1200	0.2 - 10

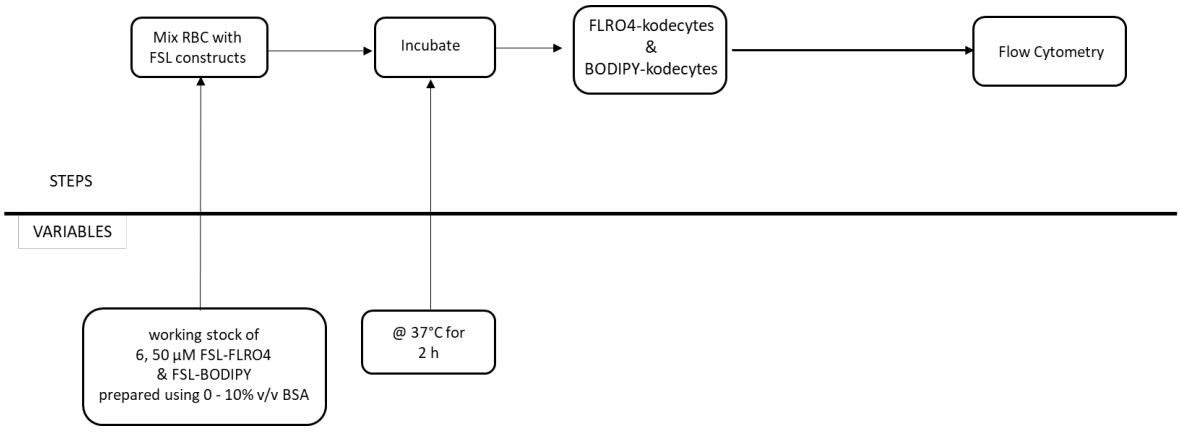

Figure 43: Schematic overview of method testing the effect of BSA on koding process.

Results

FSL-FLRO4

The result in Figure 44A shows the effects of BSA on FSL-FLRO4 uptake efficiency by RBC at the tested concentrations of 6 and 50 µM. Here, results are interpreted compared to FLRO4-kodecytes prepared in the absence of BSA (0%). From the figure, it could be seen that as the concentration of BSA in the FSL transformation medium increased, its labelling effectiveness (of FSL-FLRO4 in RBC) decreased, i.e., the FLRO4-kodecytes were most fluorescent and generated the maximum signal when the FSL-FLRO4 transformation medium was devoid of BSA (0%). This was more apparent for 50 µM than 6 µM FLRO4-kodecytes. For 6 µM FLRO4-kodecytes, 0.03 to 0.1% BSA in the

transformation medium could not impact FSL-FLRO4 uptake notably as the MFI was very similar. Significant changes in the MFI were observed from 0.2% BSA onwards. For 50 µM FLRO4-kodecytes, differences in the MFI were very apparent at 0.03% BSA. Two-way Anova with Šídák's multiple comparison test is carried out to test the statistical significance of difference in the MFI of 6 and 50 µM FLRO4-kodecytes in the presence of different gradients of BSA. Change in fluorescent intensity is considered highly significant for $p<0.0001$ (****). From the analysis, it was established that the mean difference of FI between 50 and 6 µM FSL-FLRO4 was highly significant with increasing concentration of BSA from 0.03 to 3%. However, the difference in MFI of 50 and 6 µM FLRO4-kodecytes was insignificant when BSA concentration in the koding media was in the range of 6 to 10% BSA.

In Figure 44B, the same data (as in Figure 44A) was normalised against FLRO4-kodecytes prepared in the absence of BSA (0%), to allow a more direct comparison of MFI change (indicated in % change). This result highlights that with respect to 0% BSA, the fluorescence signal reduced to approximately about 30% for 0.1% BSA, moved to 45– 80% for 0.4–2% BSA, and finally stabilised at 6% BSA onwards.

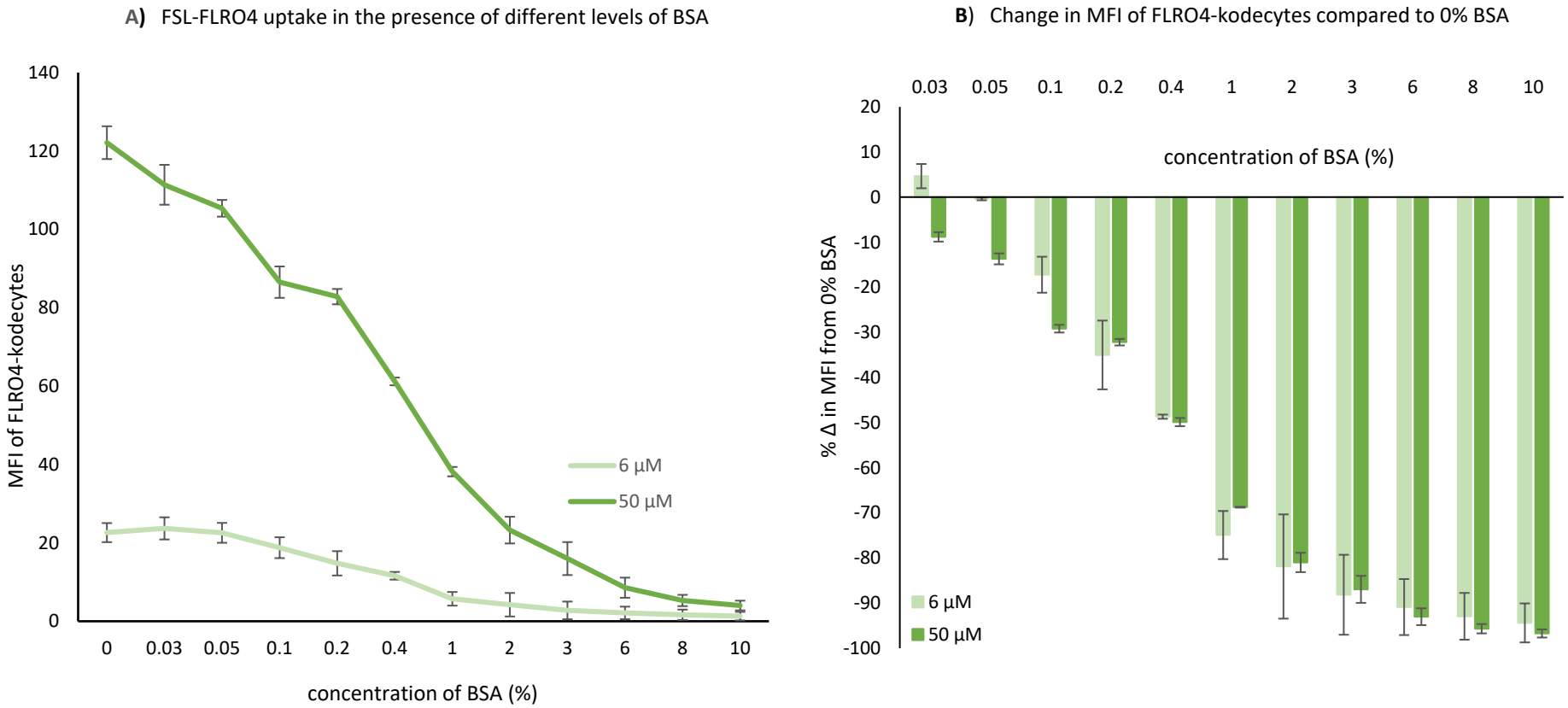

Figure 44: FSL-FLRO4 uptake in RBCs in the presence of different levels of BSA. **A**) MFI of kodecytes was measured by flow cytometry when RBCs were incubated in BSA-free and BSA-supplemented FSL-FLRO4 transformation solutions. **B**) Change in FLRO4-kodecytes MFI compared to 0% BSA (indicated as %). FSL-FLRO4 transformation medium was prepared in the presence of 0-10% BSA. Results shown are mean ± standard deviation, n=2.

FSL-BODIPY

In order to validate the FSL-FLRO4 labelling results, FSL-BODIPY, a different fluorophore, was also measured for its labelling effectiveness in the presence of different concentrations of BSA in the FSL-BODIPY transformation medium. From Figure 45A, it could be seen that, when RBC was labelled with FSL-BODIPY in the presence of different percentages of BSA, FSL-BODIPY uptake was impacted considerably, i.e., compared to 0% BSA. At the lowest tested concentration of 0.2% BSA, FSL-BODIPY uptake decreased substantially, and unlike FSL-FLRO4, there was a sizable difference in the MFI even at the presence of 0.2% BSA (in the koding media).

Two-way Anova with Šídák's multiple comparison test is carried out to test the statistical significance of difference in the MFI of 6 and 50 µM BODIPY-kodecytes in the presence of different gradients of BSA. Change in fluorescent intensity is considered highly significant for $p<0.0001$ (****). From the analysis, it was established that the mean difference of FI between 50 and 6 µM FSL-BODIPY was highly significant with increasing concentration of BSA from 0.2 to 2%. However, the difference in MFI of 50 and 6 µM BODIPY-kodecytes was insignificant when BSA concentration in the koding media was in the range of 3 to 10% BSA.

In Figure 45B, the same data (as in Figure 45A) was normalised against BODIPY-kodecytes prepared in the absence of BSA (0%), to allow a more direct comparison of MFI change (indicated in % change). Figure 45B outlines the change in FSL-BODIPY MFI standardised against 0% BSA. This result highlights that in the presence of 0.2% BSA, fluorescence signals decreased by approximately 60%, and in the presence of 1% BSA, MFI decreased to approximately 85%. From 3% BSA onwards, MFI seems to have attained stabilization. This trend was maintained across the tested concentrations of 6 and 50 µM FSL-BODIPY.

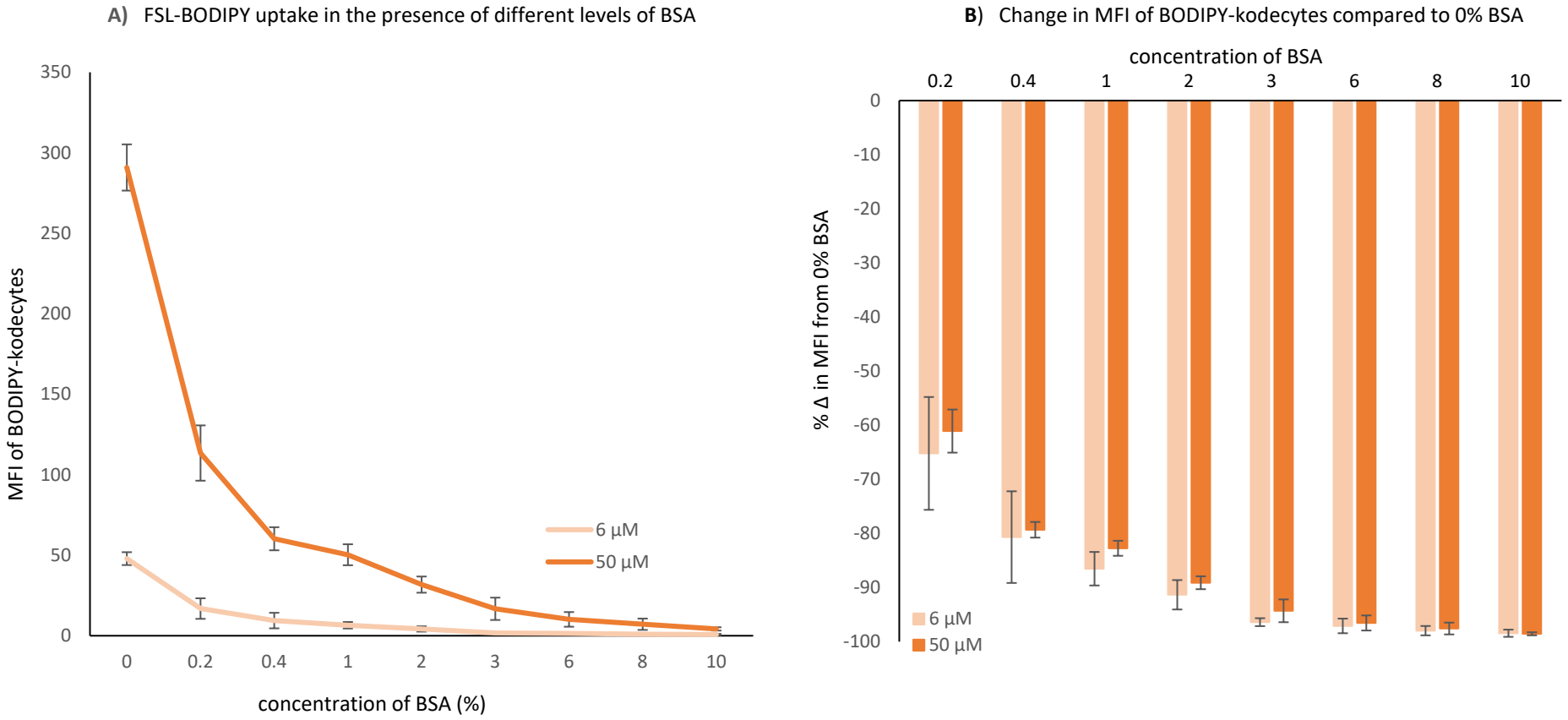

Figure 45: FSL-BODIPY uptake in RBCs in the presence of different levels of BSA. **A**) MFI of kodecytes was measured by flow cytometry when RBCs were incubated in BSA-free and BSA-supplemented FSL-FLRO4 transformation solution. **B**) Change in BODIPY-kodecytes MFI compared to 0% BSA (indicated as %). FSL-BODIPY transformation medium was prepared in the presence of 0-10% BSA. Results shown are mean ± standard deviation, n=2

Overall, the results in Figures 44 and 45 indicate that when RBC were transformed with respective FSL constructs in the presence of BSA, the uptake efficiency of FSL-FLRO4 and FSL-BODIPY were both adversely affected. However, at comparable BSA concentrations (essentially between 0.2-2%), FSL-FLRO4 koding efficiency was impacted to a lesser extent compared to FSL-BODIPY constructs (Figure 46). For a clearer picture, MFI of 6µM FLRO4 and BODIPY-kodecytes obtained at similar conditions have been compared. The result shown in Figure 46 represents 6µM FLRO4 and BODIPY-kodecytes MFI data obtained from respective transformation mediums having 0.2–10% BSA after being standardised against 0% BSA. This represents a more efficient transformation/koding by FSL-FLRO4 than FSL-BODIPY, as FSL-FLRO4 uptake was impacted to a lesser extent (in the presence of BSA/protein). At 0.2 and 0.4 % BSA, this difference in koding was found to be highly statistically significant (***P<0.0001).

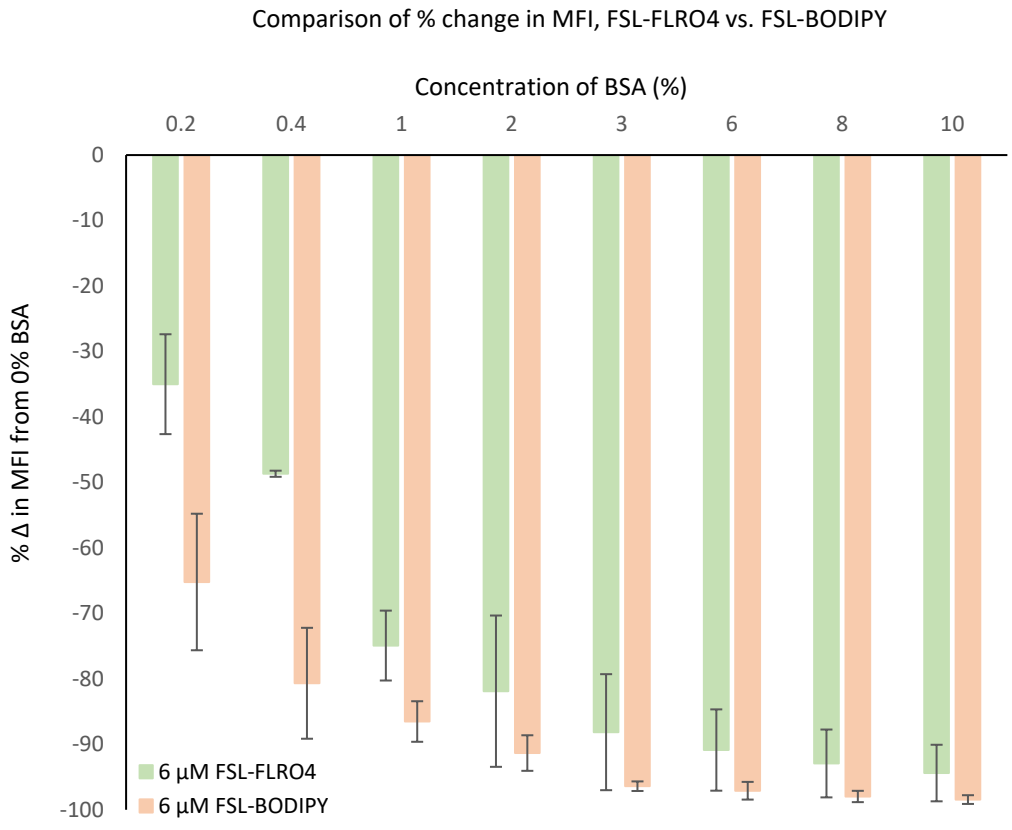

Figure 46: Relative MFI of FLRO4 and BODIPY-kodecytes obtained from the respective transformation media in the presence of 0.2–10% BSA. The % change in MFI of RBC kodecytes is compared to 0% BSA. Data are represented from 6µM FLRO4 and BODIPY-kodecytes.

From the results, the following conclusions can be drawn: Firstly, uptake of FSL by RBCs decreases in BSA-supplemented FSL working stock/transformation solution, and the degree of decrease depends on the concentration of BSA in the solution. This implies

that BSA is potentially interacting with FSL and interfering with its labelling of RBCs. Secondly, the uptake of FSL by RBCs decreases significantly even in the presence of 0.2% BSA, and the effect of the amount of BSA on the uptake of FSL plateaus around 6% BSA. This implies that at higher concentrations of BSA, a saturation effect is coming into play. Finally, the BSA-supplemented transformation solution significantly reduced the koding efficiency of the two tested FSLs, with FSL-BODIPY showing a more significant decrease of over 30%. The phenomenon observed with FSL-BODIPY could be attributed to the fact that FSL-BODIPY has a highly lipophilic functional group. Thus, it could be proposed that in the presence of BSA (in the transformation medium), FSL-BODIPY constructs were more likely to be interacting with BSA, resulting in an FSL complex, and as the FSL units were held up in the complex, they were not available for labelling of RBCs.

3.3.5 Effect of Serum on FSL uptake

Overview: Serum is vital for the proper functioning and maintenance of actively dividing cells [156,157]. Lipophilic substances like serum have been proposed to affect the optimal uptake of FSL (i.e., if transformation medium is supplemented with serum) [112]. Hence, it was essential to establish if the presence of serum in the transformation medium would affect the uptake of FSL adversely using flow cytometry. For this aspect of the study Newborn Calf Serum, (used as supplement to basal growth medium in cell culture applications) was used. For this, serum-free and serum-supplemented FSL-FLRO4 transformation mediums were tested for their koding effectiveness. Two cell lines, PC-3 cells, an adherent cell line, and Jurkat cells, a suspension cell line, were tested for their transformation into kodecytes in the presence of serum. For Jurkat cells, uptake effectiveness was tested using two methodologies, flow cytometry and fluorescence microscopy, whereas for PC-3 cells, it was tested using fluorescence microscopy only. For fluorescence microscopy, the effectiveness of transformation was based on low background and better fluorescent cells, and for flow cytometry, results were compared based on the MFI generated by incubation of cells in serum-free and serum-supplemented FSL-FLOR4 transformation medium.

Methodology overview: Setting up the PC-3 monolayer for fluorescence microscope imaging:

- The PC-3 monolayer was set up by diluting the cell suspension in pre-warmed serum-containing media to the required concentration, e.g., 4×10^5 cells/mL. 25 µL of cell suspension were seeded into the required wells in the Terasaki tray so that each treatment was performed in duplicate.
- The Terasaki tray was incubated overnight in 5% CO_2 at 37°C until the monolayer was ~60% confluent.
- The following day, FSL-FLRO4 working stock (25, 50 µM) was prepared in serum-free and serum-supplemented media.
- Before incubation/koding of the PC-3 monolayer with FSL-FLRO4 in serum-free or serum-supplemented media, cells were washed twice with serum free media or serum-supplemented media by removing the supernatant with a pipette and adding media with a dropper.
- The following steps should be performed in the dark as much as possible. 12 µL of the FSL-FLRO4 serum-free or serum-containing media at concentrations 6, 25, and 50 µM was added into the respective wells and incubated at 37°C with 5% CO_2 for 2 h.
- After completion of the 2 h incubation, the kodecytes and unkoded cells monolayer was imaged. For this, cells were excited at 488 nm and emission recorded at 1.9 s exposure time using the WIB filter (with an emission wavelength of 550nm) of the fluorescence microscope (Olympus BX-51 microscope). To track cells that did not fluoresce, subsequent DIC images were also recorded for every fluorescent image.

Setting up Jurkat cells for fluorescence microscope imaging:

- Actively growing Jurkat cells were harvested at the required concentration of 1×10^6 cells/mL. FSL-constructs were prepared at 6, 25, and 50 µM in CellStab.
- One part of cell suspension was added to one part of freshly prepared FSL-FLRO4 in serum-free or serum-supplemented media and incubated for 2 h at 5% CO2 and 37°C.
- After the incubation step, kodecytes were washed twice by adding respective media and spinning at 130 x g for 5 minutes.

- Kodecytes were finally resuspended in the respective media, and approximately 6µL was placed on the microscope slide and the cover slipped. Cells were observed for fluorescence using an Olympus BX51 microscope at 10× magnification with a WIB filter at 550nm emission wavelength for a 1.9s exposure time.

Setting up Jurkat cells for flow cytometry analysis:

- Steps were the same until incubation/koding and washing. After the incubation step, kodecytes were washed twice by adding the respective media and spinning at 130 × g for 5 minutes.
- Pelleted kodecytes were finally resuspended in 500 µL of serum-free and serum- supplemented medium and analysed by flow cytometry to establish the MFI.

Fluorescence microscopy results

PC-3 kodecytes

The results shown in Figures 47 and 48 compare the koding effectiveness of serum-free and serum-supplemented FSL-FLRO4 transformation media with respect to the fluorescent images taken in different scenarios. From the fluorescence image, it could be seen that when koding was done in serum-free media (25, 50 µM), FLRO4-PC-3 kodecytes had a homogenous intense fluorescent signal (compared to serum-supplemented negligible background fluorescence), and the staining appears to intensify with increasing concentrations of FSL-FLRO4 (Figure 47). However, serum-supplemented media showed strongly fluorescent foci-like artefacts and had prominent background signals. Since the kodecytes were not washed after the completion of 2 hours of koding, the FSLs that were not acquired by the cells remained in the transformation medium and perhaps could also add to the intense background. Additionally, the results shown in Section 2.6.3 infer the fact that approximately 80% of FSL-FLRO4 was acquired by the Jurkat FLRO4-kodecytes, so not much residual FSLs would have remained in the post-transformation solution. Overall, based on the results shown in Figure 47, it could be suggested that optimal uptake requires serum-free media.

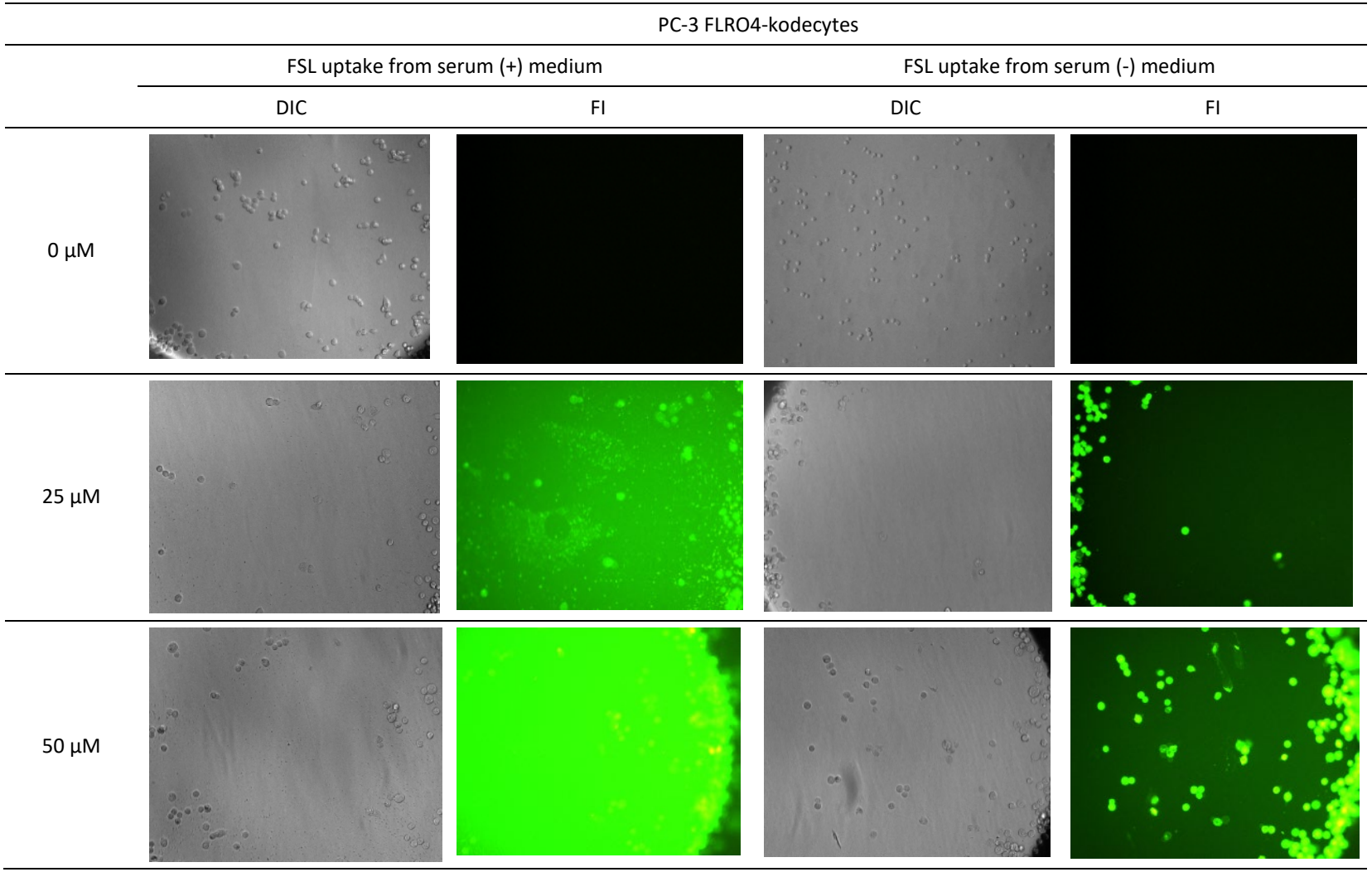

Figure 47: Effect of serum in the koding of PC-3 cells examined by fluorescence microscopy. PC-3 monolayers transformed with 25 and 50 µM FSL-FLRO4 in serum-free and serum-supplemented transformation solution. Fluorescent images with their respective DIC are displayed at 10 × magnification at 1.9 s exposure time.

Jurkat-kodecytes

From Figure 48, it could be seen that Jurkat cells transformed far more effectively in serum-free transformation media with brighter cell membrane staining and no background interference. However, it needs to be mentioned that after koding Jurkat cells with FSL-FLRO4, the kodecytes were washed and then examined by fluorescence microscopy. Hence, the FSLs that remained in the post-transformation media were washed off, and images would account for a negligible background.

Kodecytes transformed in serum-supplemented media were comparatively less fluorescent. Hence, it could be concluded that the presence of serum in the koding or transformation solution slows down the uptake of FSL by the cells. Results shown in Figures 47 and 48 suggest that serum (basically serum lipids and proteins) is potentially interacting with FSL and interfering with its labelling of Jurkat cells. To establish more clearly whether serum affects the koding process, it is important that data be generated quantitatively, and results analysed.

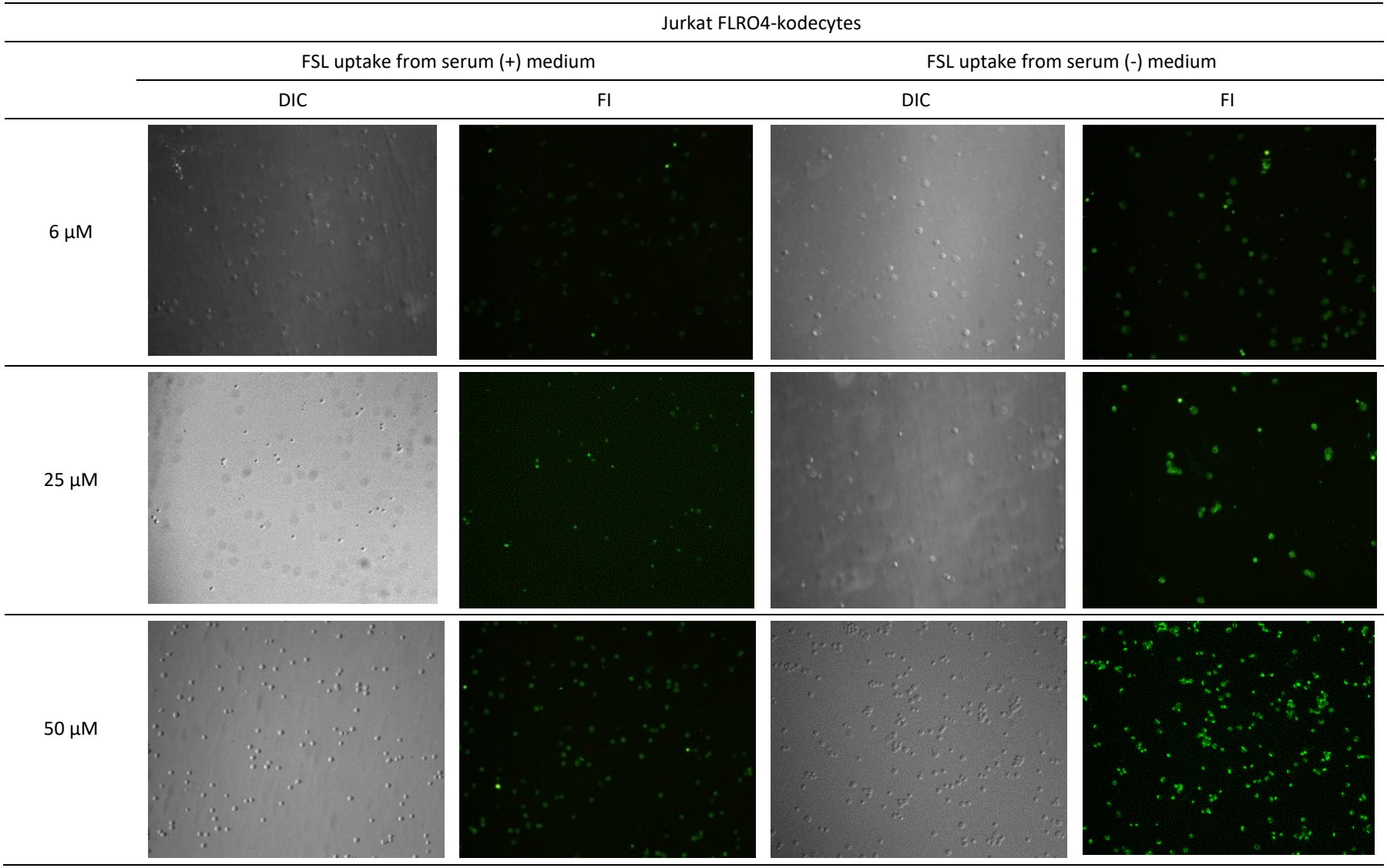

Figure 48: Effect of serum in the koding of Jurkat cells examined by fluorescence microscopy. Jurkat suspension cells transformed with 6, 25 and 50 µM FSL-FLRO4 in serum-free and serum-supplemented transformation solution. DIC and fluorescent images displayed at 10 × magnification at 1.9 s exposure time.

Flow cytometry results

The result presented in Figure 49 shows the impact of serum on FSL-FLRO4 uptake by Jurkat cells at the tested concentrations of 6 and 50 µM. From the flow cytometry data, it could be seen that the presence of serum in the FSL transformation medium (koding medium) generally, adversely affected the koding effectiveness of FSL-FLRO4, i.e., the FLRO4- kodecytes were most fluorescent and generated the maximum signal when the FSL- FLRO4 transformation medium was devoid of serum (0%).

A two-way ANOVA with Tukey's multiple comparison test is used to determine whether the addition of serum in koding media affects the fluorescence signal generated by kodecytes at the tested concentrations. A change in fluorescence intensity is considered significant at $p<0.004$ (**). Figure 49 indicates the presence of serum in koding media does not significantly affect the koding efficiency of 6 and 13 µM FLRO4-kodecytes. However, at 25 and 50 µM FLRO4-kodecytes, the presence of serum in koding media has a substantial effect on their koding efficacy.

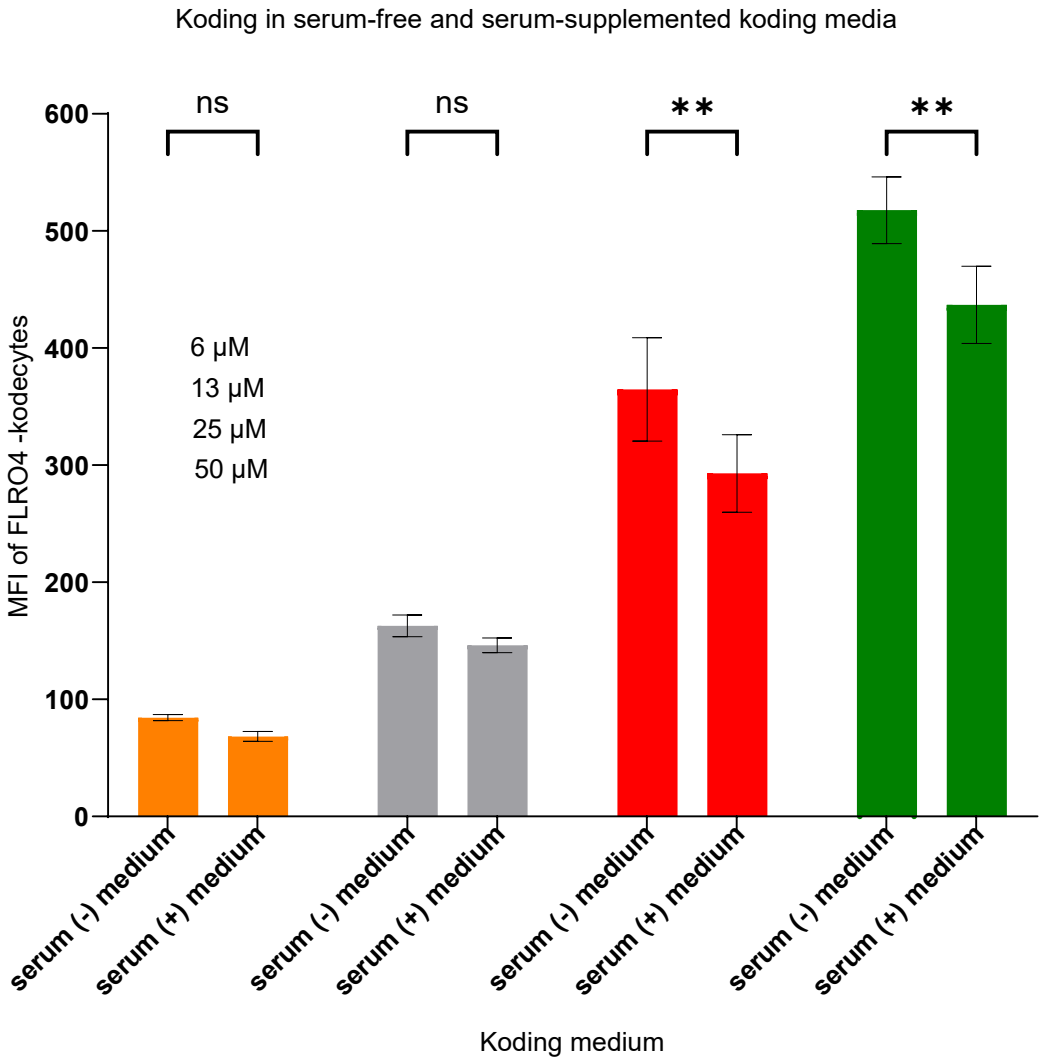

Figure 49: Flow cytometry analysis of the effect of serum on koding of Jurkat cells. Comparison of MFI of Jurkat FLRO4-kodecytes transformed in serum-free and serum-supplemented transformation media (koding media). Results shown are mean ± standard deviation, n=3, $p<0.004$(**).

3.4 Chapter summary:

The following conclusion could be deduced from the cellular uptake of FSL constructs studied in different scenarios.

- The uptake of FSL constructs by RBCs and culture cells is a function of the time and temperature of incubation (or koding duration).
- The temperature and time-based uptake study shows that FSL-biotin was acquired most efficiently, followed by FSL-BODIPY and FSL-FLRO4.

- The uptake efficiency of FSL-FLRO4 and FSL-BODIPY was adversely affected when RBCs were transformed in the presence of BSA. However, at comparable BSA concentrations (essentially between 0.2 and 2%), FSL-FLRO4 was capable of faster transformation compared to FSL-BODIPY constructs (statistically significant). The fact that uptake of FSL- BODIPY significantly decreased in the presence of BSA could be attributed to the highly lipophilic functional group of FSL-BODIPY, which, in the presence of BSA, was more likely to interact with BSA, interfering with its labelling of RBCs.
- Cellular uptake of the FSL construct decreased when proliferating cells like Jurkat cells (non-adherent cells) and PC-3 (adherent cells) were transformed in serum- supplemented FSL transformation medium.
- This study shows that lipophilic substances like serum and BSA affect the optimal uptake of FSL in non-proliferating red cells and proliferating, actively dividing Jurkat cells and PC-3 cells, indicating that lipids and proteins are potentially interacting with FSL and interfering with its labelling of cells.
- Overall, the rate of uptake of FSLs is determined by the escape of monomers from micelles, which in turn is temperature- and time-dependent, irrespective of the nature of the membrane.

Chapter 4 Interaction of FSL constructs with biological membrane

This aspect of the study aimed to answer the question: Firstly, how does the cell membrane acquire FSL constructs? Secondly, during the process of labelling, does FSL construct de-label or/and relabel kodecytes, and thus, does FSL uptake (during the koding process) involve an equilibrium state between the FSLs in the transformation solution and the biological membrane? If, during koding, an equilibrium state exists, when does the equilibrium start to set in? To answer these questions, the interrelationship between FSL constructs in the transformation solution pre- and post-koding were explored.

Under ideal experimental conditions, dissociated free FSLs would be acquired by the cell membrane via their lipid tails. However, FSL micelles or free molecules may also become entrapped within the glycocalyx. Therefore, it needs to be examined whether and how much the glycocalyx influences the uptake of FSL. This would further inform where FSL predominantly accumulates in/on the cell membrane. Hence, experiments were also designed to test whether the presence (or absence) of glycocalyx corelate effect the rate of the FSL transformation process.

4.1 Stabilization of uptake of FSL constructs

Overview: The time-course-dependent uptake study in RBC helped establish the rate of cellular uptake (and koding efficiency) of FSL constructs at 37°C. The methodology used in the time-course-dependent study involved prolonged incubation of FSL constructs with RBC at 37°C (discussed in Section 3.3.3). Here, (an improved) second methodology is presented. It is based on the understanding gained from the temperature-based uptake study of the FSL construct that an improved temperature and incubation could be used. In this improved approach, prolonged (undesirable) incubation at 37°C was replaced with a more favourable combination of RT and 4°C incubation. The koding efficiency of FSL constructs in this new scenario and, in turn, the maximum uptake of FSL were determined by flow cytometry.

Methodology: This alternative methodology was used to test the stabilisation of the uptake of FSL- FLRO4 in RBCs using a combination of different incubation durations and temperatures. The schematic overview of the method is presented in Figure 50. The following protocol outlines the experimental protocol:

Initially, for FSL-FLRO4, two scenarios were tested, the first being a more elaborate combination of incubation duration at different temperatures. Based on the insight gained from analysing two setups for the maximum uptake of FSL-FLRO4, a more concise combination of incubation durations and temperatures was used for FSL-BODIPY and FSL-biotin.

- Scenario-I: In this scenario, the RBCs were transformed with FSL-FLRO4 at 37°C for 1 h, maintained at RT for 4 h, and then at 4°C for one week. MFI of kodecytes was analysed over a week at respective time points using flow cytometry, i.e., kodecytes were analysed after 1 h incubation at 37°C, 4 h at RT, and on d3 and d7 at 4°C incubation.
- Scenario-II: In this scenario, the RBCs were transformed with FSL-FLRO4 at 37°C for 1 h, maintained at RT for 6 h, and then at 4°C up to 24 h. MFI of kodecytes was analysed after 1 h of incubation at 37°C, hourly at 6 h of incubation duration at RT, and 24 h at 4 °C.
- Optimized: For FSL-BODIPY and FSL-biotin, RBCs were transformed with FSL at 37°C for 1 h, maintained at RT for 4 h, and then at 4°C up to 24 h. MFI of kodecytes was analysed after 1 h of incubation at 37°C, 4 h at RT, and 24 h at 4°C.

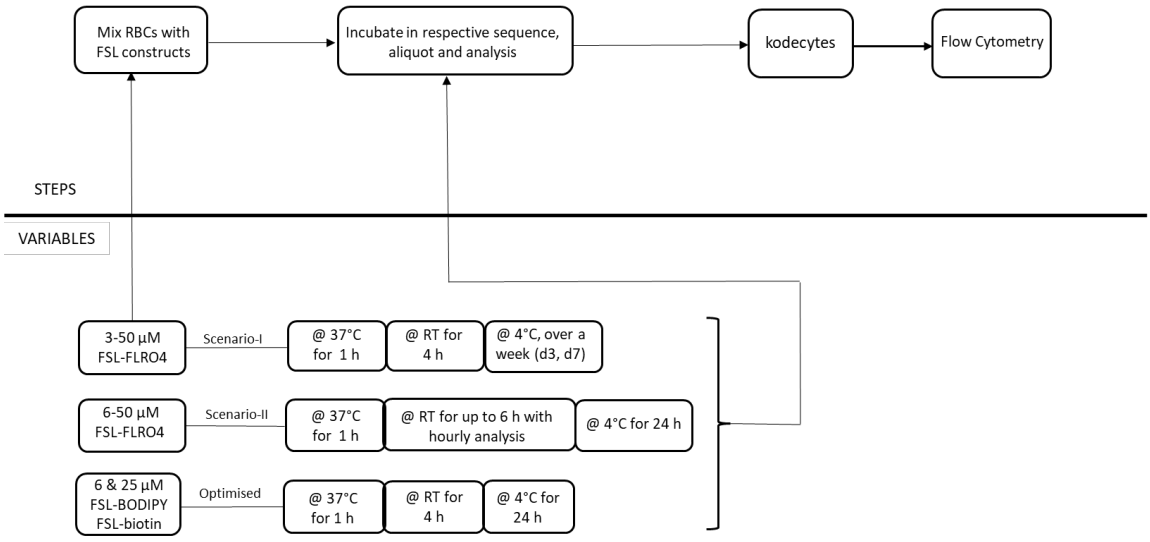

Figure 50: Schematic overview of method testing stabilisation of the FSLs uptake in RBCs. This alternative methodology test combination of different koding durations and temperatures.

FSL-FLRO4

Figure 51 shows that the MFI obtained from FLRO4-kodecytes at different incubation temperatures and analysis time points across the tested concentration of 3–50µM (scenario-I). MFI were attained from samples analysed after 1 h of incubation of RBCs with FSL-FLRO4 at 37°C (indicated by the red dot), 4 h at RT (dark blue), and 7 days at 4°C (light blue). Samples maintained at 4°C were analysed on d3 and d7 to observe any noteworthy difference in MFI due to the increased duration of incubation (from d3 to d7). In Figure 51, MFI obtained during 37°C, RT, and 4°C incubation is plotted against a concentration range of 3 µM–50 µM.

From Figure 51, it could be proposed that across all tested concentrations, MFI increased noticeably when incubation was prolonged from 1 h 37°C to 4 h RT. After this time point, MFI plateaued, i.e., there was minimal change in MFI when incubation increased from RT to d3 at 4°C. MFI remained approximately unchanged when incubation increased from d3 to d7 for 3 and 6 µM FSL-FLRO4. In contrast, for 13, 25, and 50 µM, MFI decreased but not drastically.

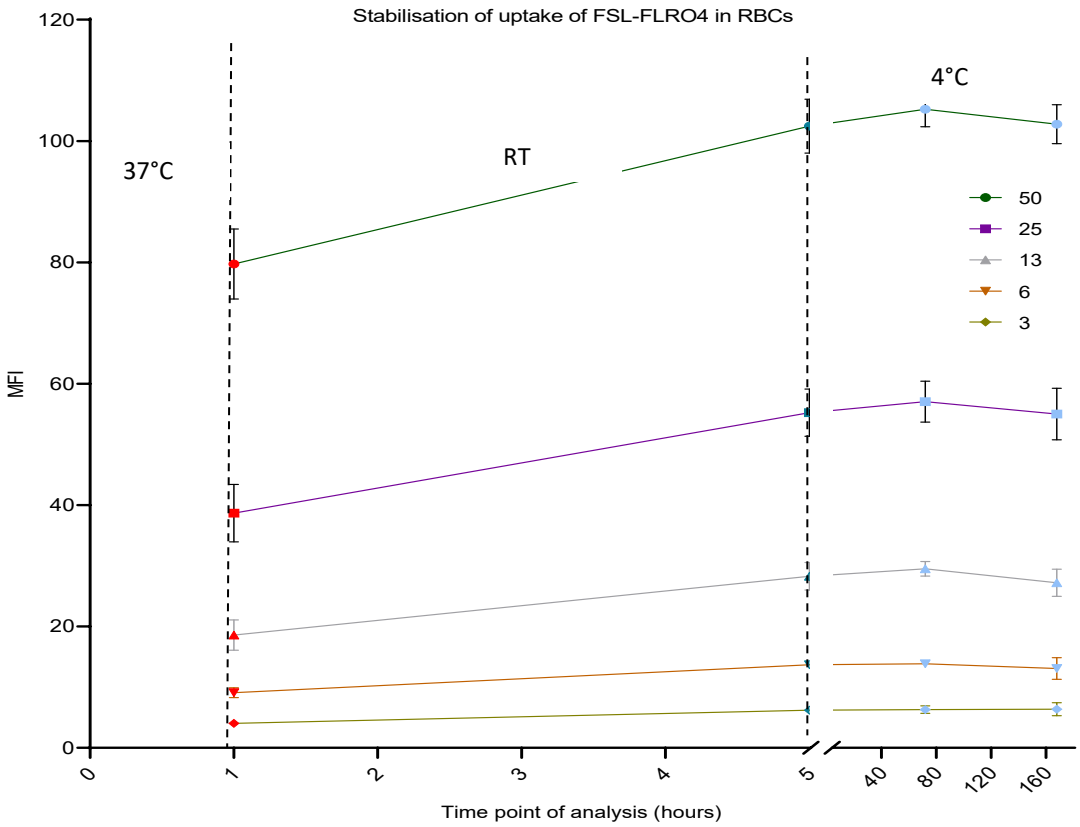

Figure 51: Stabilisation of uptake of FSL-FLRO4 in RBCs (scenario-I). MFI of FLRO4-kodecytes obtained after 1 h incubation at 37°C as red dot, 4 h at RT as dark blue dot, and on d3 and d7 at 4°C as light blue dots. Experiments were performed three times, and the data is expressed as mean ± SD.

Based on the results shown in Figure 51, a time frame can be proposed for when the maximum uptake of FSL-FLRO4 in RBCs approaches. It is important to note that it is not a single time point but a time period. This can be suggested to be after 1 h of incubation at 37°C until 4 h at RT. Although maximum uptake appears to approach earlier for higher concentrations (50, 25 µM) of FSL-FLRO4, it is not much different from lower concentrations.

Since MFI shifted the most during 4 h of incubation at RT, it was decided that shorter time points would be tested on d0 (after 1 h of incubation at 37°C) at RT incubation. This would establish a well-defined time point for maximum uptake of FSL-FLRO4 in RBCs (indicating clearer stabilisation of uptake and loss from the membrane). To analyse this, RBCs and the FSL-FLRO4 mixture were analysed at closer intervals at RT and 4°C (scenario-II). Thus, MFI was determined at 37°C (after 1 h of incubation), at RT (hourly testing for 6 h), and at 4°C (subsequent 24 h of incubation).

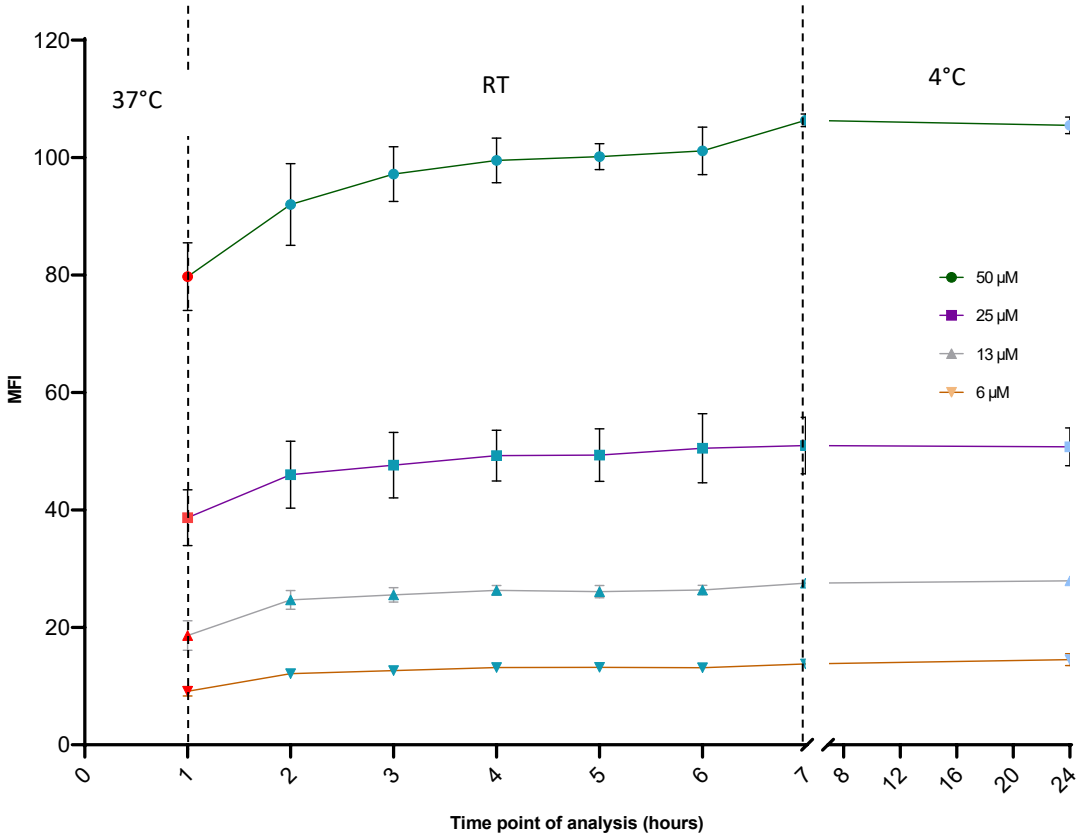

Figure 52: Stabilisation of uptake of FSL-FLRO4 in RBCs (scenario-II) MFI of FLRO4-kodecytes obtained after 1 h incubation at 37°C (red dot), with hourly testing at RT (dark blue) and successive 24 h at 4°C (light blue). Experiments were performed three times, and the data is expressed as the mean ± SD.

Figure 52 supports the result shown in Figure 51. The main observations that can be made from Figure 52 is that some FSL uptake still occurred during RT incubation (after the initial 1 h of incubation at 37°C). However minimum uptake happened during 4°C incubation. This was found to be true across the tested concentrations. During the RT incubation period, the majority of uptake of FSLs occurs within 3 h, and beyond that, uptake increases gradually but not substantially. Hence, it could be suggested that a plateau in uptake (in turn, maximum uptake or stabilisation of FSL uptake) seems to approach during RT incubation afterwards (after 3 h). It was also apparent from Figure 52 that there was a slight dip in MFI for concentrations 13 and 6 during the latter half of RT incubation, and for concentrations 25 and 50, MFI decreased when incubation was continued from RT to 4°C. These changes or differences are marginal with respect to all other shifts in MFI. The minor change in MFI could be attributed to experimental errors.

It could be concluded that the steadiness in uptake appeared to reach approximately after 1 h of incubation at 37 °C, followed by 3 h of incubation at RT. Hence, this result aids in understanding the rate of uptake of FSL-FLRO4, i.e., how readily the FSL construct is taken up and retained and when stabilisation of uptake approaches.

FSL-BODIPY

In order to have an insight into the maximum uptake of other FSL constructs at different incubation temperatures, FSL-BODIPY, a different fluorophore, and FSL-biotin were also analysed for their labelling efficiency at different temperature combinations and incubation periods. Based on the FSL-FLRO4 maximum uptake study (Figure 52), a more precise time frame under which maximum uptake of the FSL construct could be studied was proposed. Hence, only the second setup (of 1 hour 37°C, 4 hours RT, and 4 hours RT) was tested for FSL-BODIPY and FSL-biotin. Compared to FSL-FLRO4, a lower concentration range of FSL-BODIPY and FSL-biotin (from 6 to 25 µM) was evaluated. These concentrations are still relevant, representing lower and higher concentrations from the earlier study.

Figure 53 shows the MFI of BODIPY-kodecytes obtained after respective incubation durations: 1 h at 37°C, 4 h RT, and 24 h at 4°C. Of all three different incubation temperatures, MFI increased the most within 1 h of incubation at 37°C. Thus, it could be proposed that for FSL-BODIPY, uptake was fastest within the first incubation duration of 1 h at 37°C, followed by slower uptake in the later half at RT and 4°C. The maximum transformation appeared to have been reached during 37°C incubation, as MFI did not change drastically during the transition to RT and 4°C incubation. The change in BODIPY-kodecytes MFI at different incubation temperatures can be better understood in terms of percentage change. From Figure 53, it could be seen that for 6 and 25µM BODIPY-kodecytes, the fluorescence signal increased by approximately 10% and 4% when incubation continued from 37°C to RT and RT to 4°C, respectively. Overall, the results indicate that although there was an increase in MFI when BODIPY-kodecytes were incubated for an increased duration at RT and 4°C, and was not substantial. Based on the result shown in Figure 53, it is proposed that for FSL-BODIPY, maximum uptake reaches within 1 h of incubation at 37 °C. In summary, in comparison to FSL-FLRO4, FSL-

BODIPY is taken up faster by the RBC membrane and thus attains maximum uptake faster.

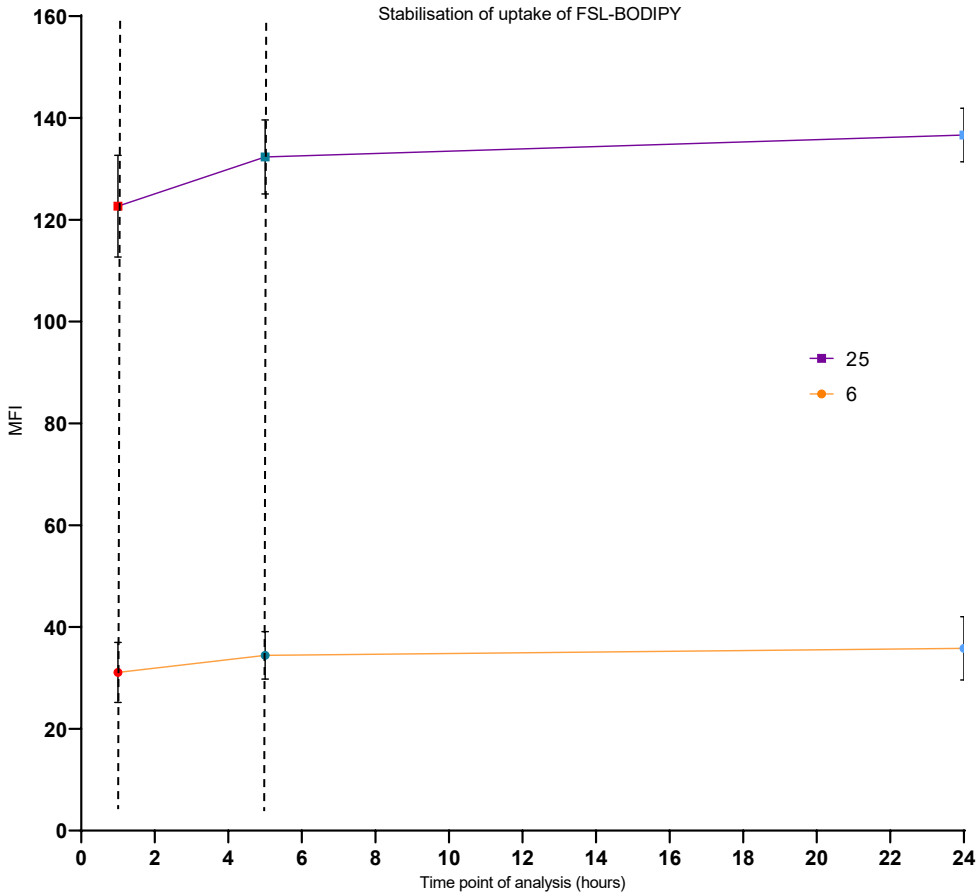

Figure 53: Stabilisation of uptake of FSL-BODIPY in RBCs. MFI of BODIPY-kodecytes after 1 h incubation at 37°C (red dot), 4 h RT (dark blue), and 24 h at 4°C (light blue). Experiments were performed twice, and the data is expressed as mean ± SD.

FSL-biotin

Figure 54 shows the MFI obtained from biotin+SAF488 kodecytes after 1 h of incubation at 37°C (red dot), 4 h of RT (dark blue), and 24 h at 4°C (light blue). MFI reached its highest for both tested concentrations at 37°C, with a minimum increase during RT and 4°C incubation. The change in biotin+SAF488 kodecytes MFI at different incubation temperatures, when indicated in %, highlights that for 6 and 25µM FSL-BODIPY, the fluorescence signal increased by approximately 2% and 5% when incubation continued from 37°C to RT and 4°C, respectively. Based on this result, it could be proposed that

biotin+SAF488 kodecytes attain maximum labelling at 37°C and approach maximum uptake at 37°C.

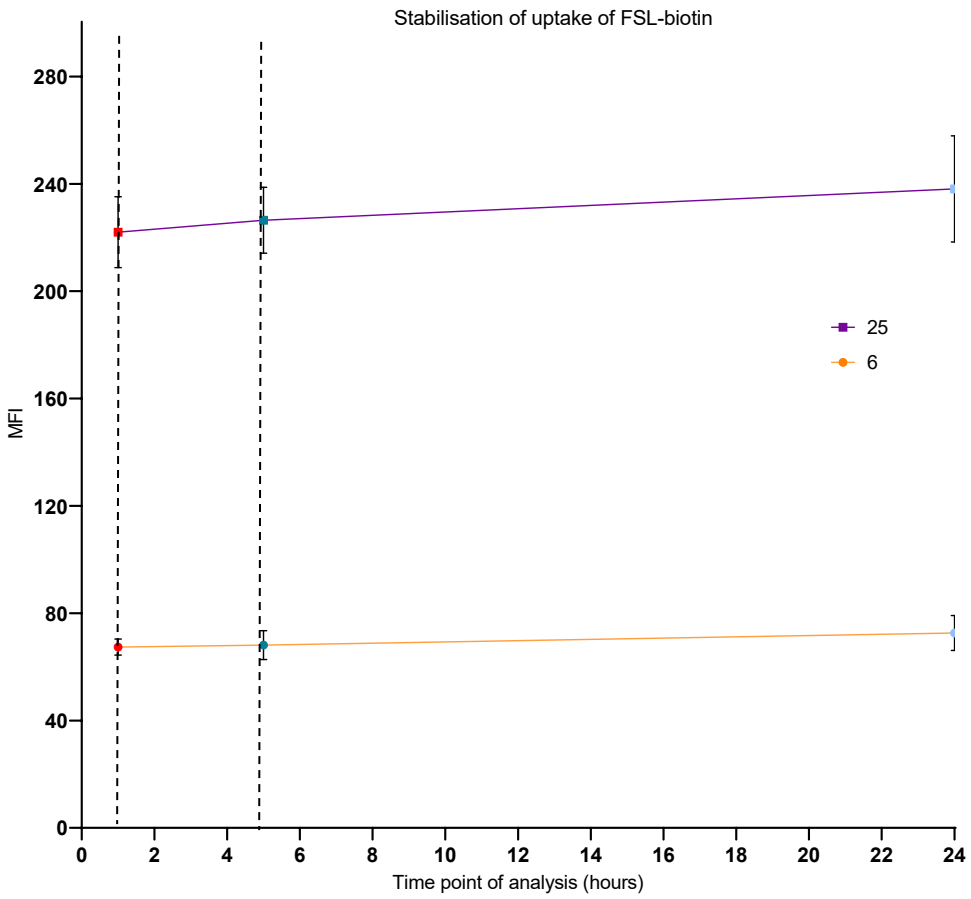

Figure 54: Stabilisation of uptake of FSL-biotin in RBCs. MFI of biotin+SAF488 kodecytes obtained after 1 h incubation at 37°C (red dot), 4 h RT (blue line), and after 24 h at 4°C. Experiments were performed twice, and the data is expressed as mean ± SD.

The maximum/stabilisation of uptake of FSL constructs study highlighted the following aspects:

- For FSL-FLRO4, the maximum uptake (thus stabilisation in FSLs acquisition) seems to approach and set in after 1 h of incubation at 37°C and 3 h of incubation at RT.
- Unlike FSL-FLRO4, FSL-BODIPY, and FSL-biotin, maximum uptake approaches faster and within 1 h of incubation at 37°. Hence, it could be proposed that FSL- BODIPY and FSL-biotin are acquired and attain stabilisation (proposed) onto the RBC membrane at a much faster rate than FSL-FLRO4, with FSL-biotin being the fastest.

- This study possibly confirms the finding cited in sections 3.3.2 and 3.3.3 that, compared to FSL-FLRO4 and FSL-BODIPY, FSL-biotin are acquired in the RBCs at a faster rate.

4.2 Evaluation of residual FSL construct in the post transformation solution

Overview: Understanding the interrelationship between FSL constructs in the transformation solution pre- and post-koding would aid in informing FSL uptake dynamics, i.e., if the koding process, involve an equilibrium state between the FSLs in the transformation solution and the biological membrane? In order to evaluate this, the post transformation solution (obtained after koding from various duration) was examined for its ability to kode fresh RBCs, thus exploring the koding efficiency (and mechanism) of the post transformation solutions. Flow cytometry and fluorescent plate reader-based detection methodologies were used to (indirectly) detect and quantify any residual FSL construct in the post-transformation solution.

Methodology: Currently, the standard maximum koding time is 2 h at 37°C. To understand the koding process more comprehensively, kodecytes (of different concentrations) were prepared using different incubation durations (up to 2 h), and respective post- transformation solutions were evaluated for residual FSL (that was able to modify cells). The data obtained from the transformation solution and post-transformation solution (supernatant) was compared to establish the trend of FSL construct uptake. To summarise, this alternative methodology was designed to test the residual FSL construct in the post-transformation solution. The schematic overview of the method is presented in Figure 55, followed by the experimental protocol.

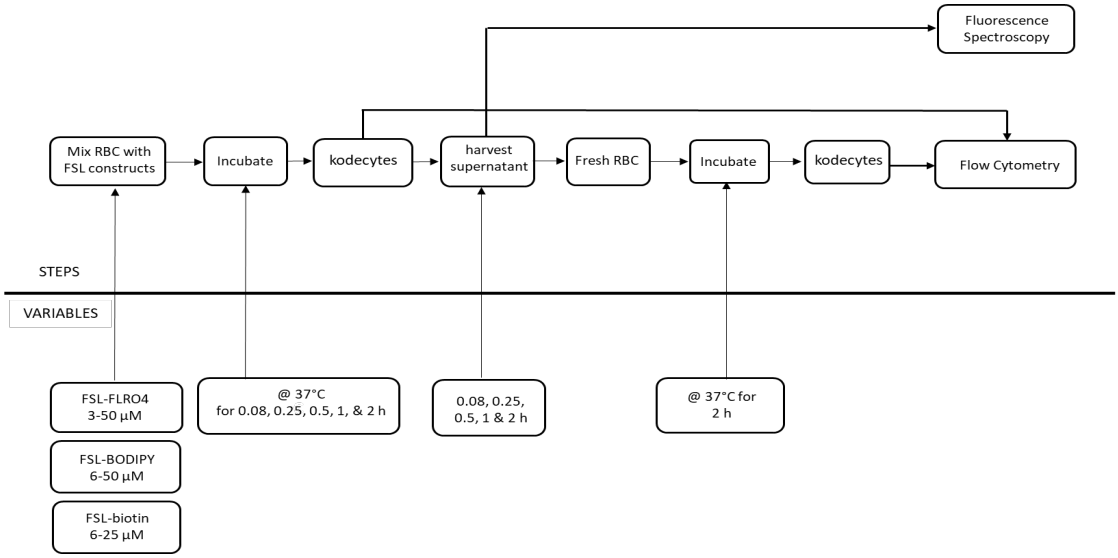

Figure 55: Schematic overview of method testing the residual FSLs in the post-transformation solution.

Preparation of kodecytes and recovery of the supernatant

- RBC kodecytes were prepared at increasing concentrations of FSL constructs for time periods of 5, 15, 30, 60, and 120 minutes. A fresh aliquot of RBC and FSLs was used for each time point.
- Post-transformation (after 5, 15, 30, 60, and 120 minutes of incubation), the solution used for transformation was recovered as a supernatant.
- Respective supernatant or post-transformation solution was examined for the lost FSL-FLRO4 signal by two methodologies: flow cytometry and fluorescence spectrophotometer (fluorescence plate reader).

Detection and quantitation of FSL in recovered post-transformation solutions

- For the flow cytometry analysis, the post-transformation solution was analysed for the presence of residual FSL-FLRO4 by measuring its ability to transform fresh RBCs into kodecytes using flow cytometry. The MFI of kodecytes prepared from different transformation mediums and the supernatant were compared at the respective time points.

- For fluorescence spectrophotometer analysis, the supernatant recovered from respective time points was measured for fluorescence signal readouts by fluorescence spectrophotometer (microplate-based assays). Sample preparation for fluorescence spectrophotometer analysis is laid out in detail in Section 4.2.2.

Table 11: Determination of residual FSL construct in post-transformation solution. Table contain the different concentrations, time periods for kodecyte preparation, and time points at which the supernatant was harvested and evaluated for residual FSL construct.

FSL constructs	Concentration (µM)	Koding duration (minutes)	Quantification of residual FSL (minutes)
FSL-FLRO4	3, 6, 13, 25, 50	5, 15, 30, 60, 120	5, 15, 30, 60, 120
FSL-BODIPY	6, 13, 25, 50	15, 30, 60, 120	15, 30, 60, 120
FSL-biotin	6, 25	15, 30, 60, 120	15, 30, 60, 120

4.2.1 Flow Cytometry

Flow cytometry-based detection of residual FSL in kodecyte supernatant (after labelling) was an obvious choice because of its highly sensitive detection system. Essentially, this analysis is based on the principle of evaluating the post-transformation solution for the presence of residual constructs by analysing its ability to transform fresh RBCs. Subsequently, the fluorescence signals obtained from kodecytes prepared from post-transformation solutions and kodecytes prepared from actual transformation solutions were compared to determine the labelling efficiency.

The standard protocol for kodecyte formation utilises packed RBCs, but there is always a small amount of dilution as packed cells are approximately 85% packed. It should be noted that at each sampling post kodecytes, due to the fact that the PCV of the kodecytes is such, there would be nearly 10% dilution of the solution going forward. The numbers have not been corrected to reflect this, but a comment would be made where necessary.

FSL-FLRO4

Figure 56 shows the MFI of FLRO4-kodecytes prepared from fresh transformation solution (dark green) and post-transformation solution (light green) at respective koding times. MFI of kodecytes (prepared from fresh transformation solution) increases with increasing koding duration. In contrast, the MFI of kodecytes prepared from the post-transformation solution showed an opposite trend. Kodecytes prepared from a shorter koding duration post-transformation solution (5, 15, 30 minutes) generated more fluorescence signal than kodecytes prepared from a longer koding duration (60 and 120 minutes) post-transformation solution. This result was expected as the shorter the incubation time (in the working stock), the more residual FSL-FLRO4 constructs would be expected to remain in the post- transformation solution (and hence more intensity from the respective post-transformation kodecytes). However, kodecytes prepared with post-transformation solution did not show a direct correlation in amount of MFI increase with respect to kodecytes prepared with working stock, as approximately 45% of the fluorescence signal was unaccounted for. For example, collective MFI generated from 5 minutes of working stock and post-transformation solution kodecytes did not equate to MFI generated from 2 hours of working stock kodecytes.

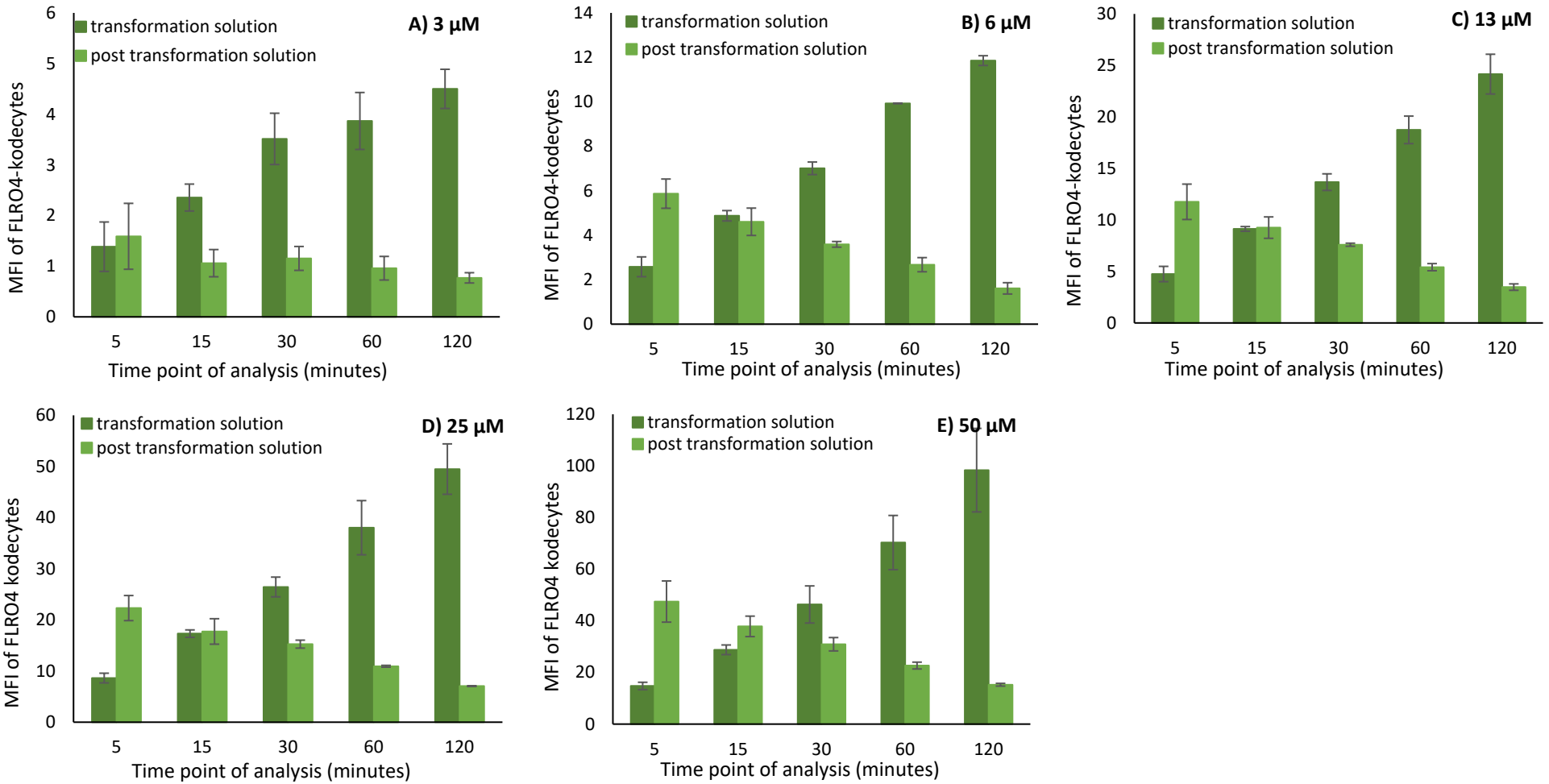

Figure 56: Detection of residual FSL-FLRO4 in the post-transformation solution (capable of making kodecytes) obtained from different koding times (5, 15, 30, 60, 120 minutes). MFI of kodecytes obtained from transformation (dark green) and post-transformation solutions (light green). FSL-FLRO4 was tested at concentrations ranging from **A**) 3 µM, **B**) 6 µM, **C**) 13 µM, **D**) 25 µM, and **E**) 50 µM. Experiments were performed three times, and the data is expressed as the mean ± SD.

The unaccounted signal loss could be due to various reasons. Additional experiments were performed to evaluate this. After kodecytes were prepared from the post-transformation solution, a second batch of post-transformation supernatant was harvested from this lot of kodecytes and further tested for any residual FSL by incubating them with fresh RBCs. The result obtained from this study are shown in Figure 57.

Figure 57 shows that the second lot of post-transformation solution could kode fresh RBCs (and generate time-dependent fluorescence signals), indicating that some FSL constructs remained in the second lot of post-transformation solutions. However, the MFI of kodecytes prepared from the second lot of post-transformation solution (obtained from different time points) did not differ substantially enough.

The results shown in Figures 56 and 57 suggest that, irrespective of incubation or koding duration, residual FSL remains in the post-transformation solution. However, the amount of residual FSL constructs in the post-transformation solution differs, as the post-transformation solution obtained from a shorter koding duration has more residual FSL constructs than a longer koding duration. Based on the finding, it could be suggested that the koding process could be occurring via equilibrium binding, i.e., FSL uptake into the membrane continues till some kind of stabilisation is attained between the FSL construct present on the membrane and the transformation solution. Additionally, equilibrium seems to be approaching between 60 and 120 minutes of koding, as the acquisition of FSLs in RBCs plateaus within this time period. Moreover, the koding capability of residual FSLs obtained from 60 and 120 minutes post-koding was very comparable.

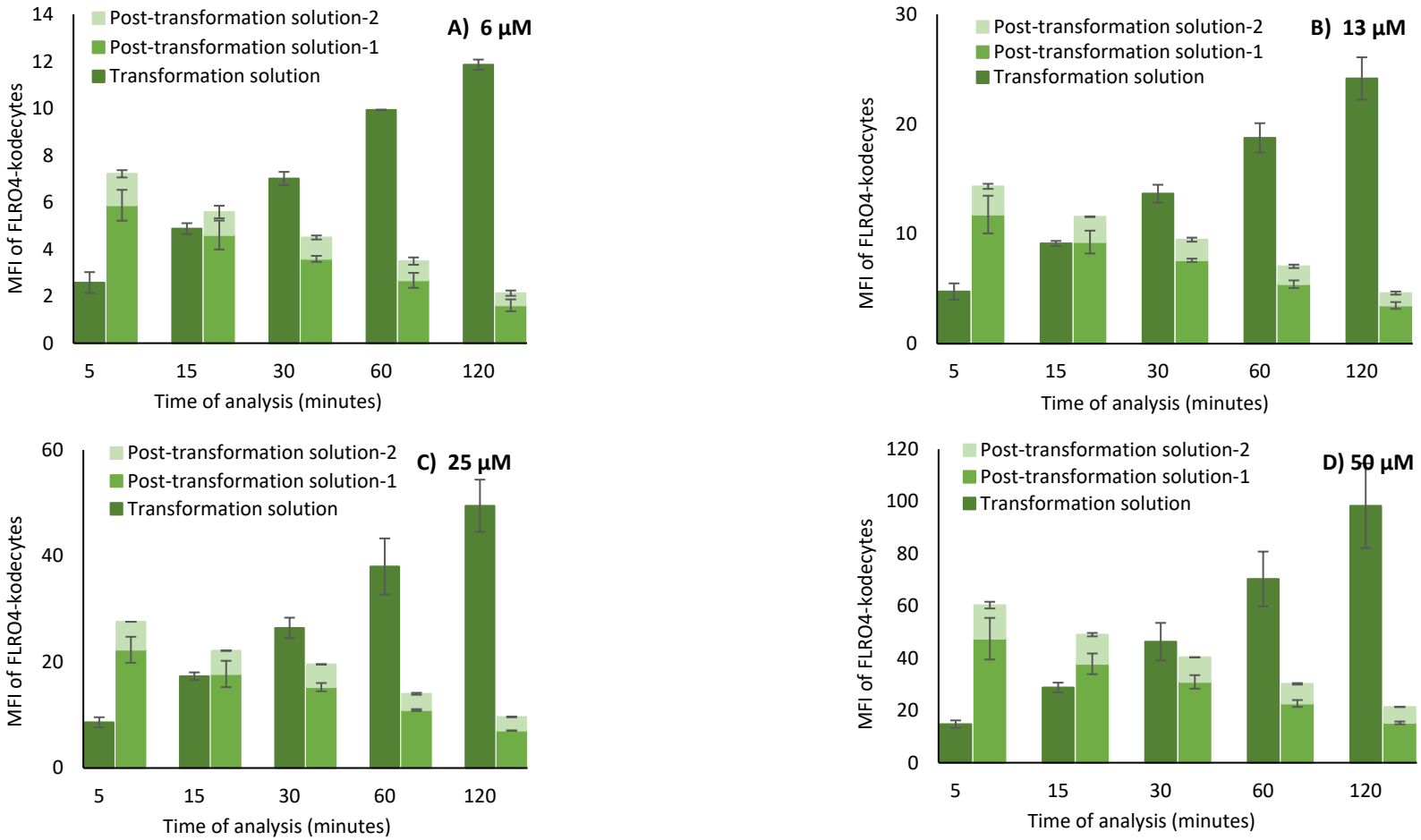

Figure 57: Detection of residual FSLs in two consecutive supernatants (post-transformation solutions) obtained from respective koding times (5, 15, 30, 60, 120 minutes). MFI of FLRO4 kodecytes was obtained from transformation solution (dark green), post-transformation solution-1 (medium green), and post-transformation solution-2 (light green). FSL-FLRO4 was tested at concentrations ranging from **A**) 6 µM **B**) 13 µM **C**) 25 µM and **D**) 50 µM. Experiments were performed three times, and the data is expressed as the mean ± SD.

FSL-BODIPY

Figure 58 shows that the FSL-BODIPY post-transformation solution could kode fresh RBCs and generate time-dependent fluorescence signals, i.e., a shorter contact period with the FSL-construct, more residual FSLs remaining uninserted in the supernatant, and hence more capacity to generate fluorescence signals. For example, kodecytes prepared from a 15-minute post-transformation solution generated the most signals. Additionally, Figure 58 shows that some fluorescence signal was unaccounted for, as observed in the case of FSL-FLRO4. In the case of FSL-FLRO4, approximately 45% of the fluorescence signal was unaccounted for, whereas it was only 15% for FSL-BODIPY. This loss in fluorescence signal could be partly attributed to the dilution effect, as packed cells are approximately 85% packed, and MFI obtained from kodecytes prepared from working solution and post-transformation solution should be discounted. However, there was activity in the post transformation solution. It is important to note that the results shown in Figure 58 could not be performed again because of COVID lockdown and the unavailability of flow cytometry.

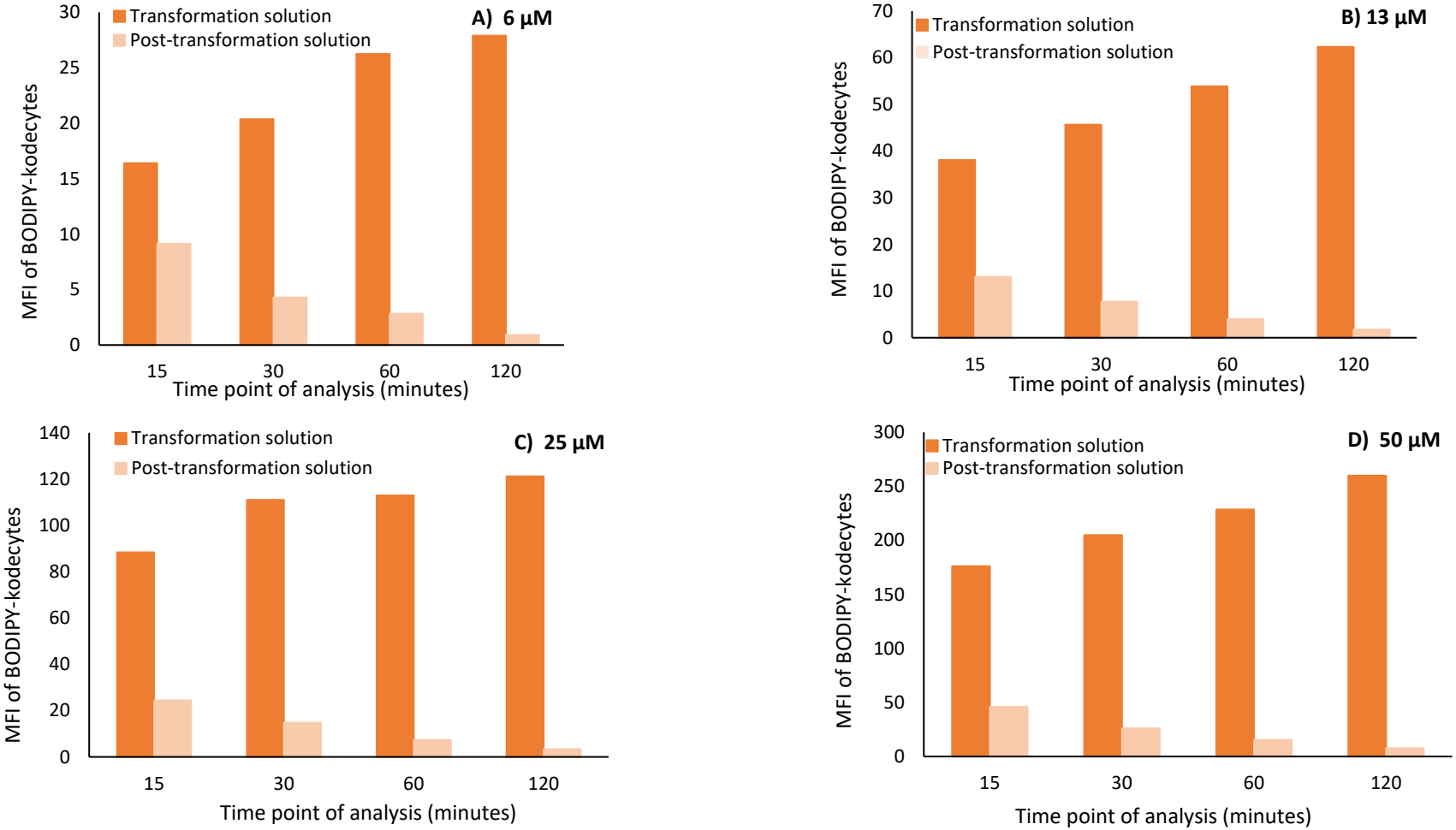

Figure 58: Detection of residual FSL-BODIPY in post-transformation solution (capable of making kodecytes) obtained from different koding times (15, 30, 60, and 120 minutes). MFI of BODIPY kodecytes was obtained from transformation solutions (dark orange) and post-transformation solutions (light orange). FSL-BODIPY was tested at concentrations ranging from **A**) 6 µM **B**) 13 µM **C**) 25 µM and **D**) 50 µM.

FSL-biotin

Similar to FSL-FLRO4 and FSL-BODIPY, the FSL-biotin post-transformation solution contained residual constructs and could kode fresh RBCs. It generated time-dependent fluorescence signals. From Figure 59, it could be proposed that only a 5% fluorescence FSL-biotin signal was unaccounted for. This contrasts with the FSL-FLRO4 results, where the signal loss was almost 45%, and the FSL-BODIPY results, which were 15%. It is important to note that the results shown in Figure 59 could not be performed another time because of COVID lockdown and the unavailability of flow cytometry.

The detection of residual FSL constructs (capable of making kodecytes) in the post-transformation solution study highlighted the following aspects:

- This study indicates that RBCs do not take up all available FSL constructs, and residual FSL constructs capable of making kodecytes are available post-koding in the transformation solution. This was irrespective of the harvesting time of the post-transformation solution.
- Residual FSL constructs were found to be present in the post-transformational solution obtained for all three FSL constructs analysed in this study.
- Kodecytes prepared from post-transformational solution (during 5 to 60 minutes time points) never accounted for the total fluorescence signal with respect to the 2 h time point koding duration. This difference in fluorescence signal was highest for FSL-FLRO4 and negligible for FSL-biotin.
- Based on overall findings it could be said that irrespective of the duration of incubation of RBC with FSL, (varying degree of) residual FSL remains in the post-transformation solution/supernatant and possibly koding process could be occurring via equilibrium binding.
- Therefore, it could be said that when FSL constructs in the immediate vicinity of the bilayer are in equilibrium with the FSL constructs in the transformation solution, a state of balance or saturation is achieved. In this study, this is achieved about 1 h for the tested FSL constructs.

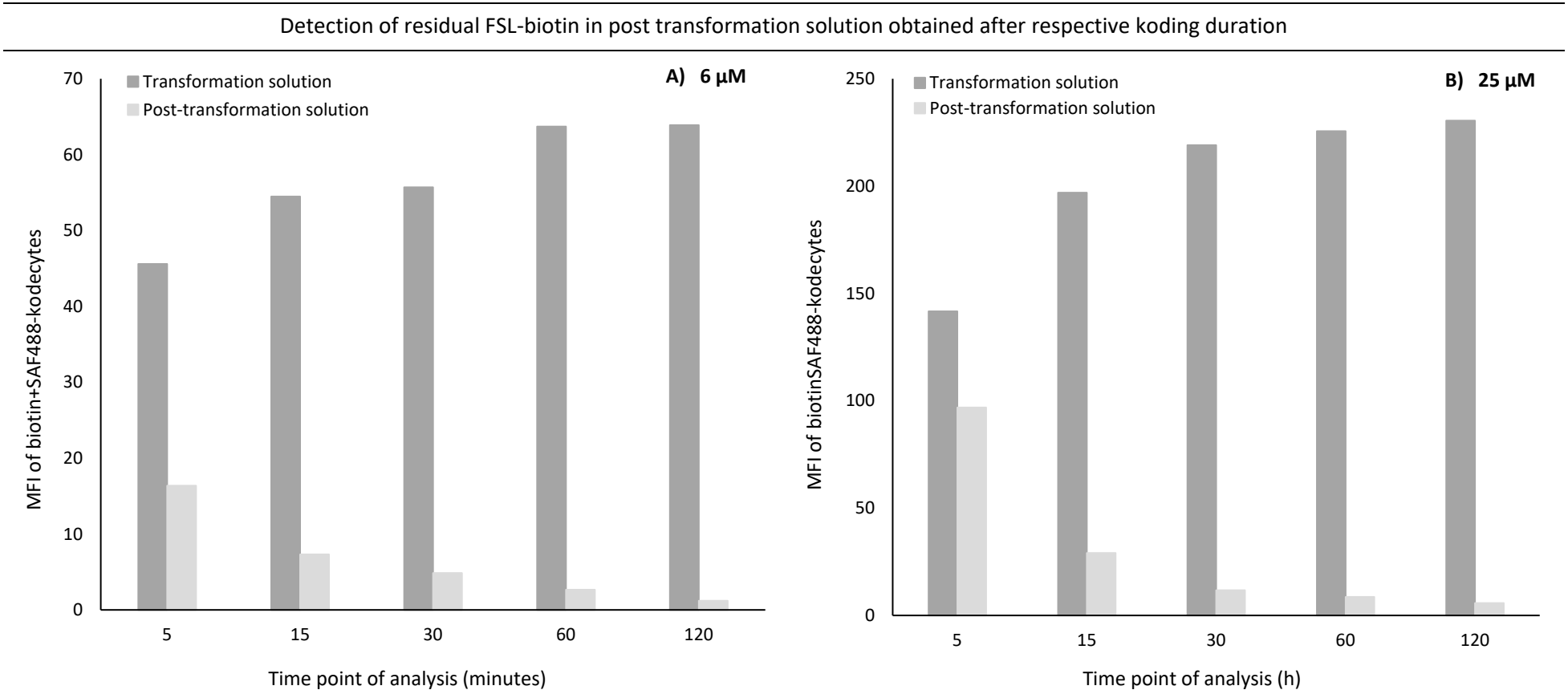

Figure 59: Detection of residual FSL-biotin in post-transformation solutions (capable of making kodecytes) obtained from different koding times (5, 15, 30, 60 and 120 minutes). MFI of biotin+SAF488 kodecytes obtained from transformation (dark grey) and post-transformation solution (light grey) FSL-biotin was tested at concentrations of **A**) 6 µM and **B**) 25 µM.

4.2.2 Fluorescence spectrophotometer

Overview: The uptake of FSL-FLRO4 and FSL-BODIPY have been studied in detail using flow cytometry (Section 2). In this section, an alternative methodology based on a fluorescence spectrophotometer (96 well microplate) assay was tested for examining the effectiveness of koding of FSL-FLRO4 and FSL-BODIPY by measuring the (unknown) concentration of FSL remaining in the kodecyte supernatant (i.e., post-transformation solution) after transformation. Potentially, this methodology would help in the indirect detection and quantification of any residual FSL construct in the post-transformation solution and aid in further understanding the rate of interaction of FSLs construct with biological membrane. Possibly, FSL constructs first diffuse into the region near the bilayer, and afterwards will equilibrate within the membrane.

Fluorescence spectrophotometer-based assays have been extensively used to determine the amount or concentration of fluorescent analytes in unknown fluorescent samples because the technique is non-laborious, easily accessible, and quantitative [158,159]. These assays are based on the basic concept that the fluorescence intensity is linearly proportional to the concentration of the fluorescent molecule. This linear proportionality with concentration applies to optically dilute samples, e.g., solutions with an absorbance of less than 0.05 [159-161].

Methodology: This methodology was designed to test the concentration of residual FSL construct in the post-transformation solution using fluorescence spectrophotometer. In this study, the standard or calibration curve was derived from a set of solutions obtained by serial dilution of fluorescent FSL constructs. The fluorescence intensities generated from known FSL concentrations (covering a desirable concentration range) were plotted versus concentration. The resulting calibration curve was used to determine the concentration of FSL (unknown samples) in the post-transformation solutions harvested after different time durations of incubation of RBCs with FSL. In the fluorescence plate reader set up, the fluorescence intensity of a given sample is measured using Tecan Spark® 10M in triplicate. Excitation and emission wavelengths were set at 495 nm and 520 nm, respectively, and the fluorescence signal was acquired in relative fluorescence units (RFU), which accounts for the amount of fluorescence light signal emitted by the sample.

The schematic overview of the method (testing the residual FSLs by fluorescence spectrophotometer) is presented in Figure 60, followed by the detailed experimental protocol.

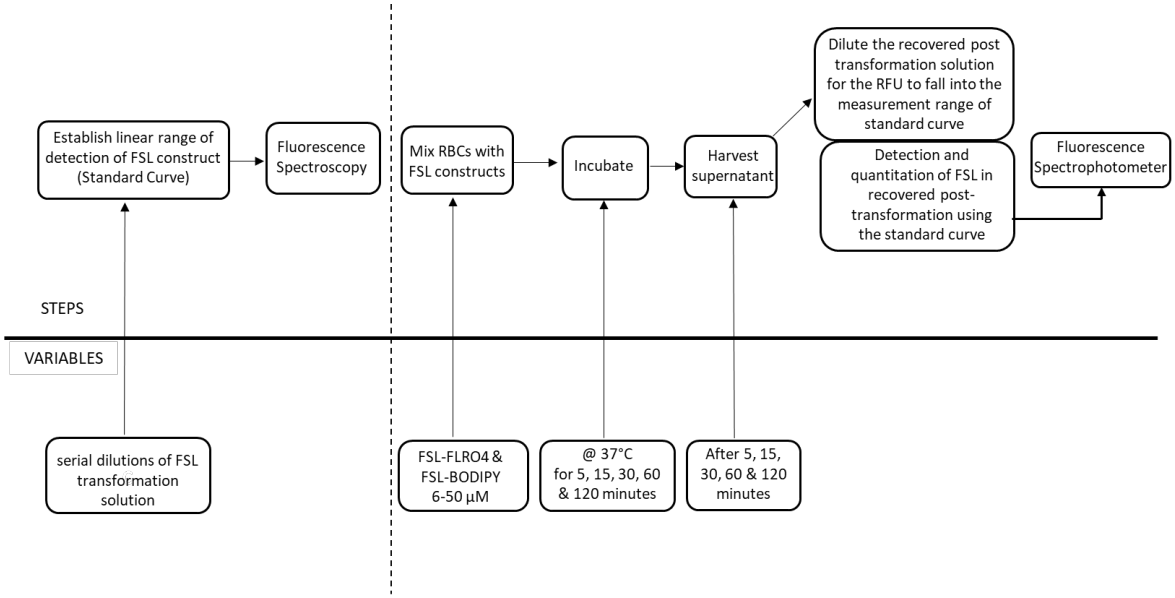

Figure 60: Schematic overview of method testing the residual FSLs by fluorescence spectrophotometer. The concentration of residual FSL construct in the post-transformation solution was quantified using fluorescence spectrophotometer.

The methodology involves working in three major stages, as mentioned below.

- Establishing linear range of detection to prepare a standard curve.
- Preparation of kodecytes and recovery of supernatant (post transformation solution).
- Detection and quantitation of FSL in recovered post-transformation solution by fluorescence spectrophotometer.

Linear range of detection

In order to maintain the linear proportionality between fluorescence signal/intensity and (tested) concentration, it is important to first establish the linear signal range of the fluorescence detection system. For fluorescence-based detection systems, the linear range is proposed to be a range from its limit of quantification up to a threshold intensity, above which the responsivity becomes increasingly non-linear with increasing intensity. This decrease in the fluorescence intensity is observed at higher

concentrations because too high a concentration will saturate the detector or cause the instrument to use a very low gain (an insensitive setting).

To obtain a linear range of detection for FSL construction, a standard or calibration curve was prepared. A few important factors that were important when planning the preparation of the standard curve for FSL constructs are mentioned below.

- Firstly, standard concentrations should cover the range of concentrations that were expected from samples, i.e., the harvested post-transformation solution.
- Secondly, fluorescence signals generated by FSL constructs should be reproducible, and they should not decrease over the time period of being measured.
- Finally, the linearity between fluorescence signals and concentration should not break down at the tested dilution range.

To prepare the standard curve of FSL working stock, serial dilutions covering a 1024-fold range and including zero were made. After testing various concentration ranges, a concentration range of 0.002 to 1.56 µM was finalised for FSL-FLRO4 and FSL-BODIPY. Negative controls of CellStab were also included. 100 µL of serially diluted FSL was aliquoted into a 96-well plate to measure the fluorescent intensity and signal at each concentration.

Preparation of kodecytes and recovery of supernatant

RBC kodecytes were prepared at increasing concentrations of FSL constructs over a period of 2 hours (Table 12). A fresh aliquot of RBC and FSL was used for each time point (5 to 120 minutes for FSL-FLRO4 and 15 to 120 minutes for FSL-BODIPY). Post-koding, the solution used for transformation was recovered as a supernatant, and the (unknown) concentration of residual FSL construct was measured and quantitated using fluorescence spectrophotometer.

Table 12: Fluorescence spectrophotometer quantification of residual FSL in post-transformation solution. Table contains various concentrations and koding durations used for the preparation of kodecytes and the respective time points at which, post-transformation, the supernatant was harvested and quantitated for the residual FSL construct.

FSL constructs	concentration (µM)	koding duration (minutes)	quantification of residual FSL by (minutes)
FSL-FLRO4	6, 13, 25, 50	5, 15, 30, 60, 120	5, 15, 30, 60, 120
FSL-BODIPY	6, 13, 25, 50	15, 30, 60, 120	15, 30, 60, 120

Detection and quantitation of FSL in recovered post-transformation solution

Post-koding, the supernatant was harvested, and the (unknown) concentration of FSLs in the recovered supernatant was calculated from the standard curve with the appropriate dilution required to get the concentration within the measurable range of the standard curve (as fluorescence signal generated by the supernatant was too high and outside of the range of the chosen standard curve).

Results:

FSL-FLRO4

Figure 61 shows a standard curve of fluorescence intensity versus concentration of FSL- FLRO4, acquired by fluorescence spectrophotometer. A concentration range of 0.002 to 1.56 µM was able to be measured for FSL-FLRO4.

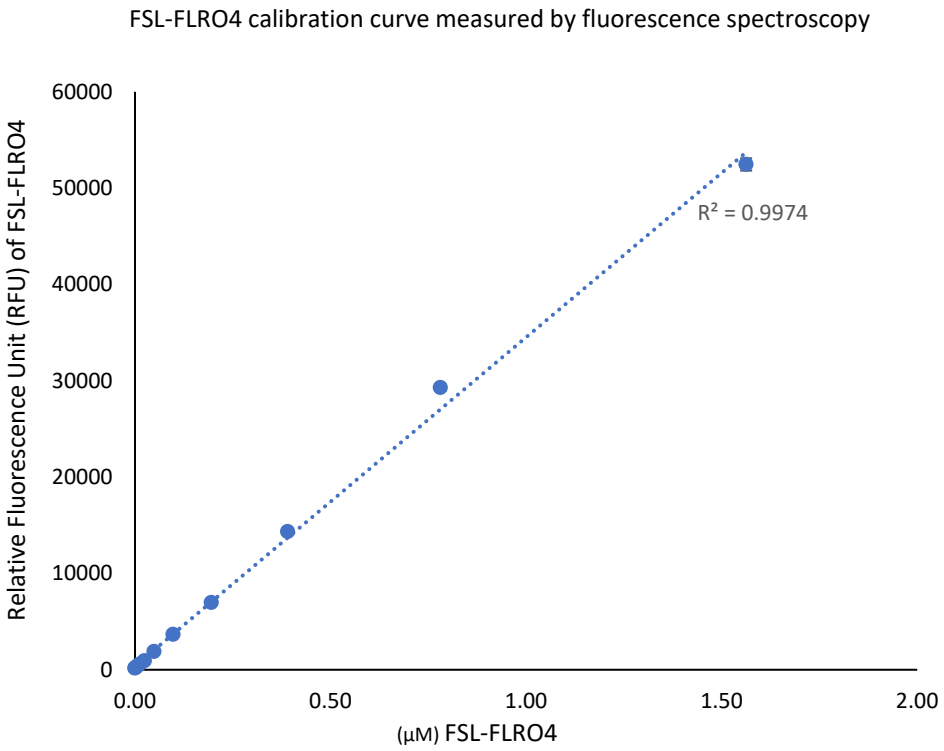

Figure 61: Calibration curve of FSL-FLRO4 fluorescence intensity versus concentration, measured by fluorescence spectrophotometer. Excitation and emission wavelength were set at 495nm and 520nm. FSL-FLRO4 was prepared from 0.002 to 1.56 µM. Experiments were performed three times, and results shown are mean ± standard deviation.

Figure 61 shows that the fluorescence signal was linearly proportional to the respective tested FSL construct concentration, and saturation in the signal at tested concentrations was not observed. Hence, a fluorescence spectrophotometer-based assay could establish that FSL-FLRO4 working stock showed an expected dose-dependent signal generation and aid in determining the linear range of detection. This respective standard or calibration curve was used to measure the unknown concentration of residual FSL construct in post-transformational solution obtained from different koding times.

Earlier in Section 4.2.1, the post-transformation solution was examined for its ability to kode fresh RBCs by flow cytometry. In here, (alternatively) quantifying the residual FSL-FLRO4 in the post-transformation solution by fluorescence spectrophotometer, the rate of uptake of FSL-FLRO4 post-labelling of RBCs with FSL-FLRO4 was analysed indirectly (Figure 63A). Here it can be seen that as the koding time increases, the concentration of residual FSL-FLRO4 in the post-transformation solution decreases. This trend was observed regardless of the concentration from which the residual constructs were harvested.

In Figure 62B, the same data (as in Figure 62A) is shown, but in percentage. It summarises the percentage of residual FSL-FLRO4 (left behind) in the post-transformation solution at each koding time (by quantifying the amount of FSL remaining in the supernatant). In Figure 62B, it could be seen that FSLs were acquired the fastest in the first hour of incubation, as only 30% of residual FSL-FLRO4 was remaining in the post-transformation solution. With respect to concentrations, it can be noted that for lower concentration, 6 µM, a smaller amount remains in the supernatant post-koding, compared to higher concentrations (13 µM onwards), suggesting that koding is more efficient at lower concentration. For example, after 5 minutes of koding with 6 µM FSL-FLRO4, around 65% of FSL remains in the supernatant, whereas for 50 µM, approximately 80% remains in the supernatant. This difference in koding efficiency among concentrations decreases or levels off when koding time approaches 2 hours. It is important to mention that similar results were observed when koding efficiency was analysed by flow cytometry (Section 3.3.3).

A two-way ANOVA with Tukey's multiple comparison test was used to examine the statistical significance of the observation that lower concentration FSL-FLRO4 (6 µM) had more effective koding efficiency (and thus lesser amount of residual FSL in the post-transformation solution) than higher concertation (13 µM and above) up until 60 minutes of koding. A change in the koding efficiency or residual amount of FSL is considered significant at *P<0.05, **P<0.005, ***P<0.0005, ****P<0.0001. For this, koding efficiency of 6 µM FSL-FLRO4 was compared to all other tested concentrations at all tested koding durations. The statistical analysis (Figure 62 B) revealed that 6 µM FSL-FLRO4 had significantly higher koding efficiency (although with a different P value) than all other concentrations up to 60 minutes of koding duration. However, this difference is not significant after 120 minutes of koding.

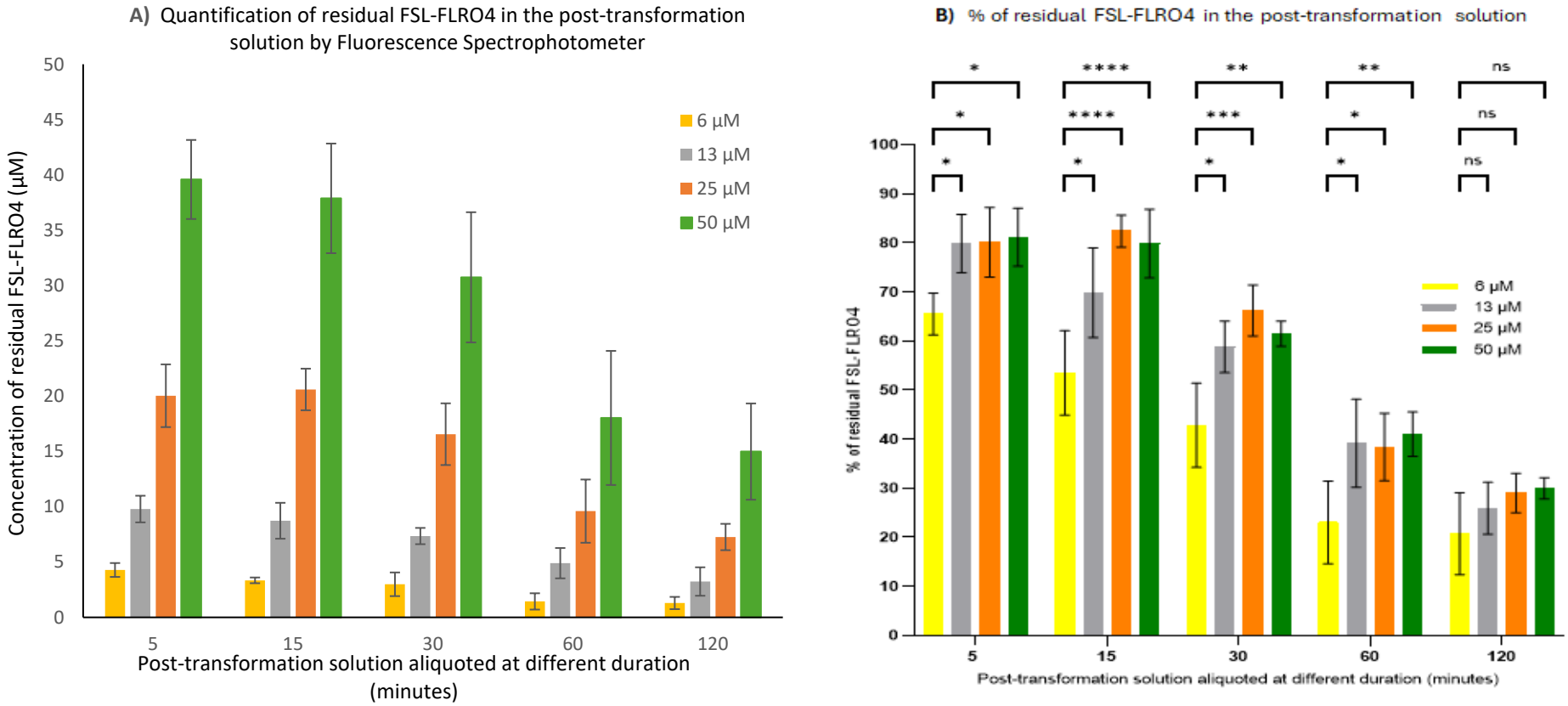

Figure 62: Fluorescence spectrophotometer quantification of residual FSL-FLRO4 in post-transformation solution. **A**) Amount of residual FSL-FLRO4 quantified post koding in the post-transformation solution. **B**) The percentage of residual FSL-FLRO4 remaining in the post-transformation solution. Residual FSL-FLRO4 was harvested after different koding duration (5, 15, 30, 60, and 120 minutes). Experiments were performed thrice, and the data is expressed as the mean ± SD. ANOVA with Dunnett's multiple comparison test is carried out to test the statistical significance. *P<0.05, **P<0.005, ***P<0.0005, ****P<0.0001

FSL-BODIPY

Figure 63 shows a standard curve of fluorescence intensity verses concentration of FSL-BODIPY, acquired by fluorescence spectrophotometer. Figure 64 establishes that FSL-BODIPY showed an expected dose-dependent signal and aided in determining linear range of detection based on fluorescence spectrophotometer. This respective standard or calibration curve was used to measure the unknown concentration of residual FSL construct in post transformation solution obtained after different koding duration.

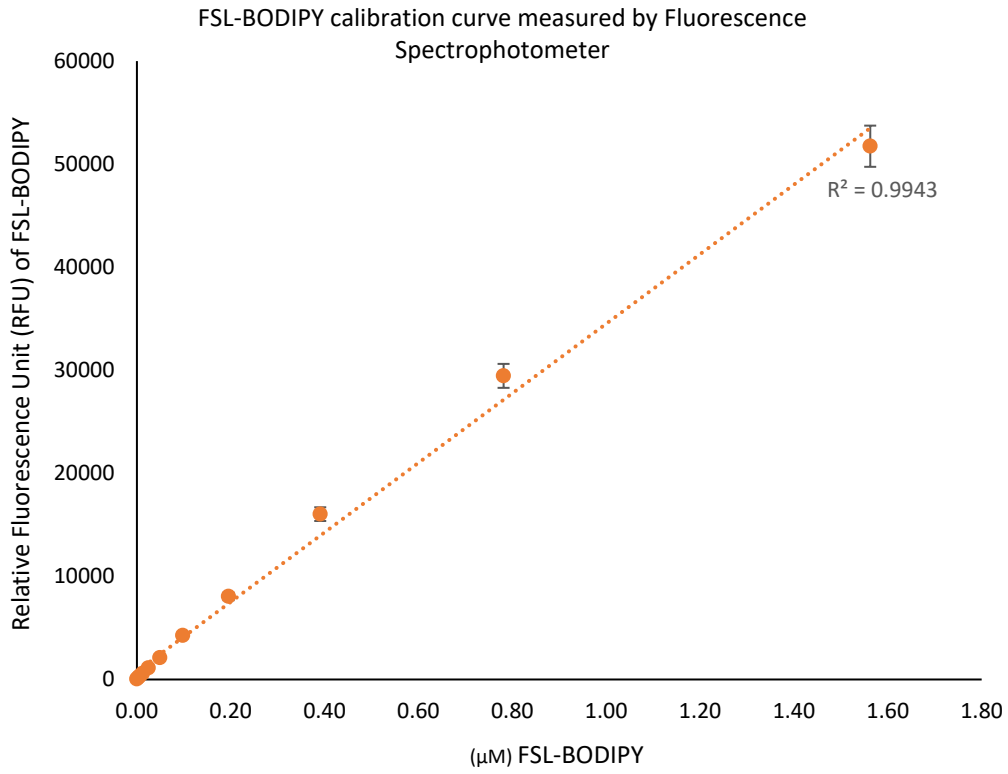

Figure 63: Calibration curve of FSL-BODIPY fluorescence intensity versus concentration, measured by fluorescence spectrophotometer. The excitation and emission wavelengths were set at 495nm and 520 nm, respectively. FSL-BODIPY was prepared from 0.003 to 1.56 µM. Error bars = ± SD (n = 3).

The amount of FSL-BODIPY remaining in the post-transformation solution following koding of RBCs with (6, 13, 25, and 50 µM) FSL-BODIPY is shown in Figure 64A. It can be seen that as the koding time increases, the concentration of residual FSL- BODIPY in the post-transformation solution decreases. For example, out of 6, 13, 25, and 50 µM after 15 minutes of incubation, approximately 2, 5, 8, and 14 µM remain in the post-transformation solution, and after 120 minutes, it decreases down to 0.8, 2, 5, and 10 µM. From the results shown in Figures 64A, it could be proposed that uptake of FSL-BODIPY starts to approach a plateau after 30 minutes of incubation/koding, i.e.,

FSL- BODIPY reaches the fastest uptake within 30 minutes of incubation; following this time point, only a minimum increase in uptake was observed.

In Figure 64B, the same data (as in Figure 64A) is shown, but in percentage. After 30 minutes of koding, approximately 75% of FSL was taken up by RBCs, as only around 25% remained behind in the post-transformation solution. This trend was observed regardless of the concentration from which the residual constructs were harvested. A two-way ANOVA with Tukey's multiple comparison test was used to examine the statistical significance of the observation that koding efficiency of FSL-BODIPY was very similar across the tested concentrations at similar koding durations. The statistical analysis revealed that there was no significant difference in the koding efficiency (or residual amount of FSL-BODIPY in the post transformation solution) among different concentrations of FSL at similar koding durations (i.e., after 15 minutes of koding, the koding efficiency or residual amount of FSL in the post-transformation solution was very similar across tested concentrations of FSL-BODIPY, Figure 64B).

When results in Figures 62 and 64 were compared with respect to the amount of residual FSL remaining in the post-transformation solution, under similar circumstances, FSL- BODIPY uptake was faster than FSL-FLRO4. For example, after 30 minutes of koding, only 25% of residual FSL-BODIPY remained in the post-transformation solution (accounting for 75% koding), whereas for FSL-FLRO4, it was nearly 50%. Similar results were seen by flow cytometry as well (Section 3.3.3). This observation was also tested for statistical significance. For this, a two-way ANOVA with Tukey's multiple comparison test was used. The statistical analysis revealed that up until 60 minutes of koding, FSL- BODIPY koding efficiency was statistically significantly (different) and better (with varying P value) than FSL-FLRO4 across tested concentrations.

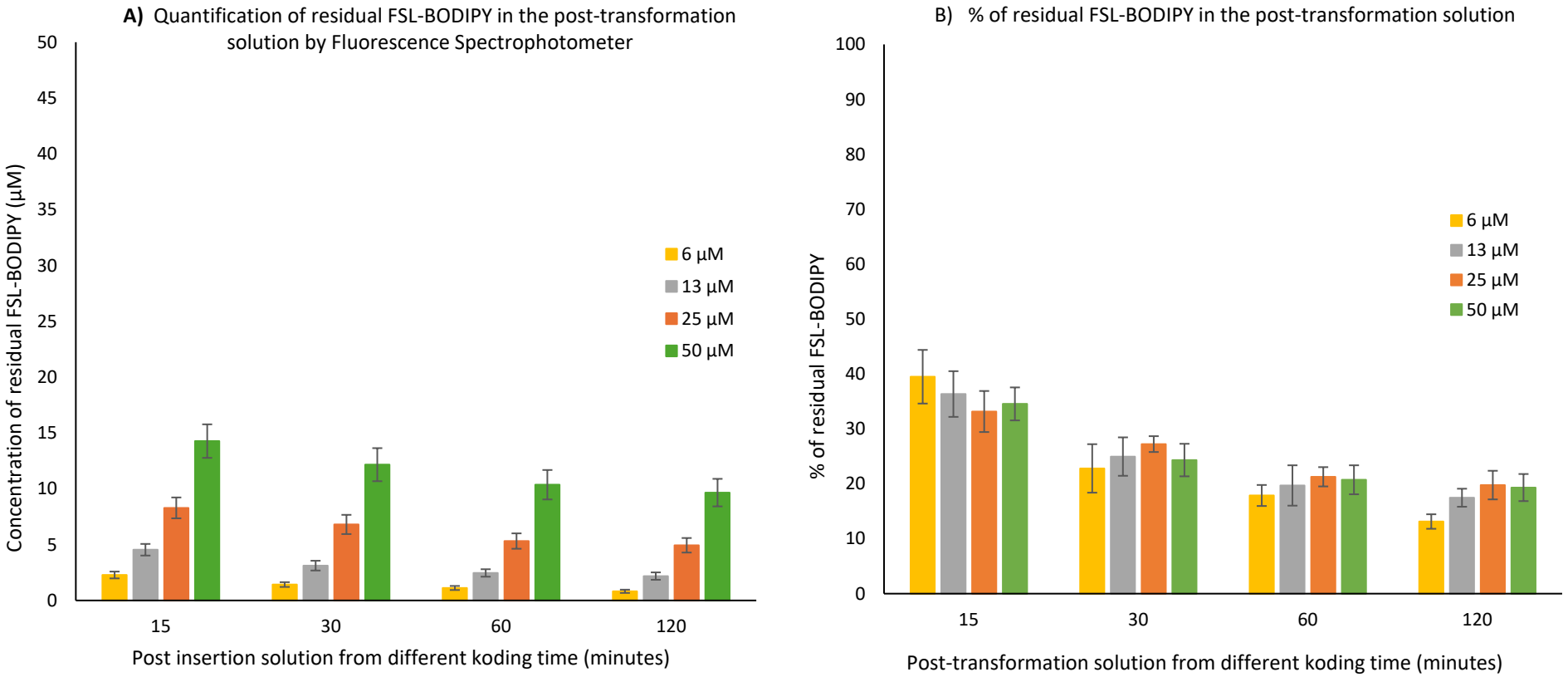

Figure 64: Fluorescence spectrophotometer quantitation of residual FSL-BODIPY in post-transformation solution. **A)** Amount of residual FSL-BODIPY quantified post koding. **B)** The percentage of residual FSL-BODIPY remaining in the post-transformation solution. Residual FSL-BODIPY was harvested after different koding duration (15, 30, 60, and 120 minutes). Experiments were performed thrice, and the data is expressed as the mean ± SD.

Summary:

The (improved) methodology based on fluorescence spectrophotometer examining the residual FSL in the solution post koding highlighted the following aspects:

- There is a detectable amount of residual FSL remaining in the recovered post- transformation solution. The concentration of residual FSLs decreases with increasing koding duration. At a standard koding duration of 2 hours, 25% of FSL- FLRO4 remains in the post-transformation solution, whereas it is nearly 13% for FSL-BODIPY (statistically significant).
- Under similar experimental conditions, fluorescence spectrophotometer results are correlated with those generated by flow cytometry.
- Based on the overall findings, it could be said that irrespective of the koding duration of RBCs with FSL, a (varying degree of) residual FSL remains in the post-transformation solution. This finding was observed both for flow cytometry and fluorescence spectrophotometer. This possibly suggests that the koding process could be occurring through equilibrium binding, i.e., FSL uptake into the membrane continues until some kind of stabilisation is attained between free and membrane bound FSL.

4.3 Effect of glycocalyx on FSL uptake

This experiment was designed to test if the presence of glycocalyx is a rate-determining step during the FSL modification process, i.e., does the glycocalyx affect the rate of the FSL transformation? To evaluate this purpose, experiments were designed to determine whether partially depleting glycocalyx before preparing kodecytes and after kodecyte preparation would influence koding.

Methodology: For this experimental set-up, two scenarios were tested. In the first scenario, RBCs were initially incubated with papain (treated/glycocalyx potentially depleted) and without papain (untreated/glycocalyx non-depleted), and then the respective RBCs (treated and untreated) were used for preparing kodecytes.

- Packed RBCs were washed and diluted to 25% v/v in CellStab.
- Equal volumes of RBCs were incubated with CellStab and papain at 37°C for 0.5 h. This created glycocalyx-non-depleted native RBCs (untreated) and glycocalyx-depleted RBCs (treated).
- After incubation, RBCs were washed twice with 1× PBS and once with CellStab.
- 6 and 50 µM FLRO4-kodecytes were prepared by incubating untreated and treated RBCs with 6 and 50 µM FSL-FLRO4 for 2 h at 37°C.
- MFI generated from respective kodecytes was compared to observe the effect of glycocalyx depletion and its subsequent effect on koding, i.e., cells with and without glycocalyx depletion and its effect on FSL uptake.

In the second scenario, first kodecytes were prepared, and then kodecytes were treated with papain (glycocalyx depleted) and without papain to analyse the effect of glycocalyx depletion on the kodecytes fluorescence signal.

- Packed RBCs were washed and diluted to 25% v/v in in CellStab.
- 6 and 50 µM FLRO4-kodecytes were prepared by incubating an equal volume of native RBCs with 6 and 50 µM FSL-FLRO4 for 2 h at 37°C. After incubation, kodecytes were washed twice with 1 × PBS and once with CellStab and resuspended in CellStab.
- FLRO4-kodecytes were incubated with CellStab (untreated) and papain (treated) at 37°C for 0.5 h.

- Respective kodecytes were washed and MFI analysed using flow cytometry.

The schematic overview of the method is presented in Figure 65.

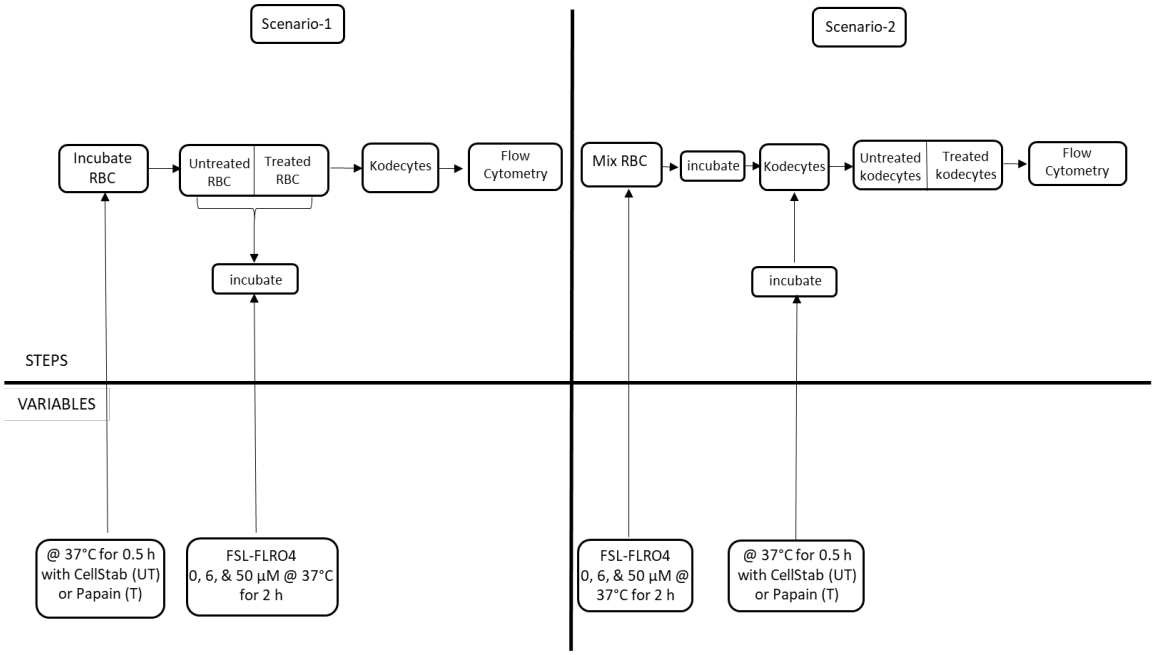

Figure 65: Schematic overview of method testing the effect of glycocalyx, (the co-relationship between FSL uptake and the presence of glycocalyx).

Results: Data generated from scenario 1 is shown in Figure 66, where papain-treated RBCs had a greater degree of transformation than untreated RBCs; that is, the depletion of glycocalyx accelerated the uptake of FSL-FLRO4. Overall, glycocalyx-depleted RBCs had approximately 30–50% higher fluorescence signals than non-treated RBCs, indicating that glycocalyx depletion accelerates the uptake of FSL-FLRO4. There was a difference in signal generated from two concentration variants of kodecytes; 6µM FLRO4- kodecytes (representing lower concentration, free FSLs) produced roughly 15% higher signal than 50µM FLRO4-kodecytes (concentration above CMC). This difference in signal generation suggests that glycocalyx may have some interaction with micelles.

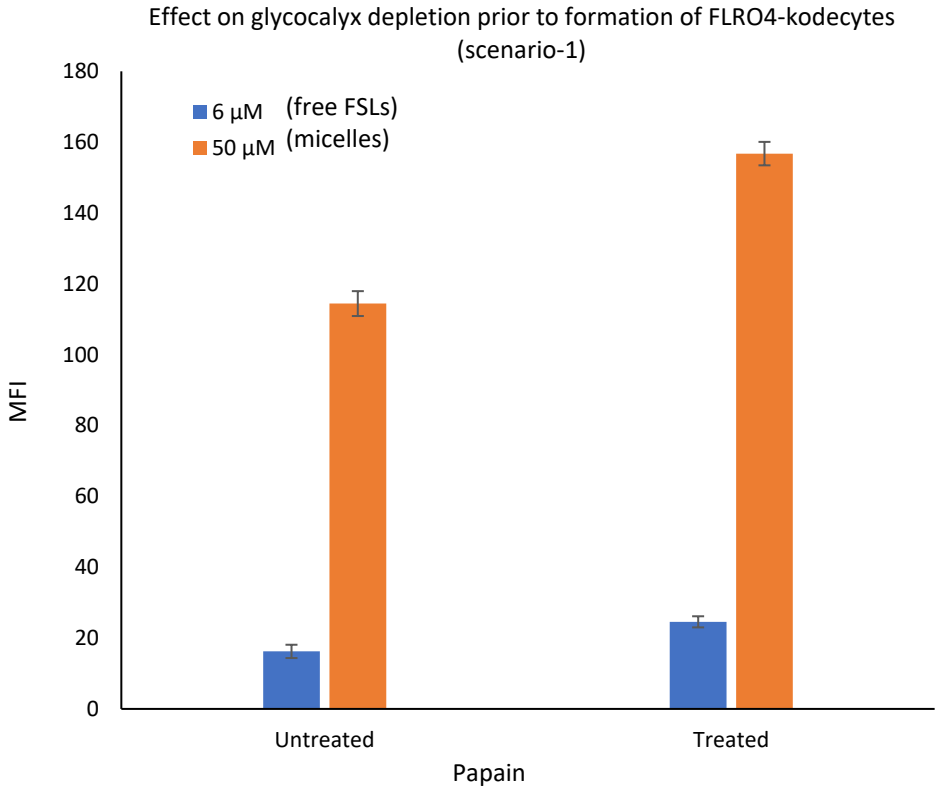

Figure 66: Effect of glycocalyx depletion on FSL-FLRO4 uptake (scenario-1) prior to the formation of FLRO4-kodecytes. RBCs were incubated with papain (treated, glycocalyx-depleted) and without papain in CellStab (untreated) before transformation of RBCs with FSL-FLRO4. MFI measured by flow cytometry.

Figure 67 shows the MFI generated from the second scenario, where the effect of glycocalyx depletion on FLRO4-kodecytes was examined (by a comparative representation of the fluorescence signal generated from glycocalyx-depleted and non-depleted FLRO4-kodecytes). The data suggests that papain-treated FLRO4-kodecytes (glycocalyx-depleted) have a less fluorescence signal than non-treated kodecytes, thus suggesting that the removal of the glycocalyx likely removed the glycocalyx-associated FSL construct. It is of note that the rate of decrease of signal was not similar between the tested concentrations; for example, 6µM FLRO4-kodecytes treated with papain showed a decline in fluorescence signal of only 5% (and within the margin of error), whereas for 50 µM FLRO4-kodecytes, almost 35% of the signals were lost. This supports the entrapment FSL (micelles) in the glycocalyx.

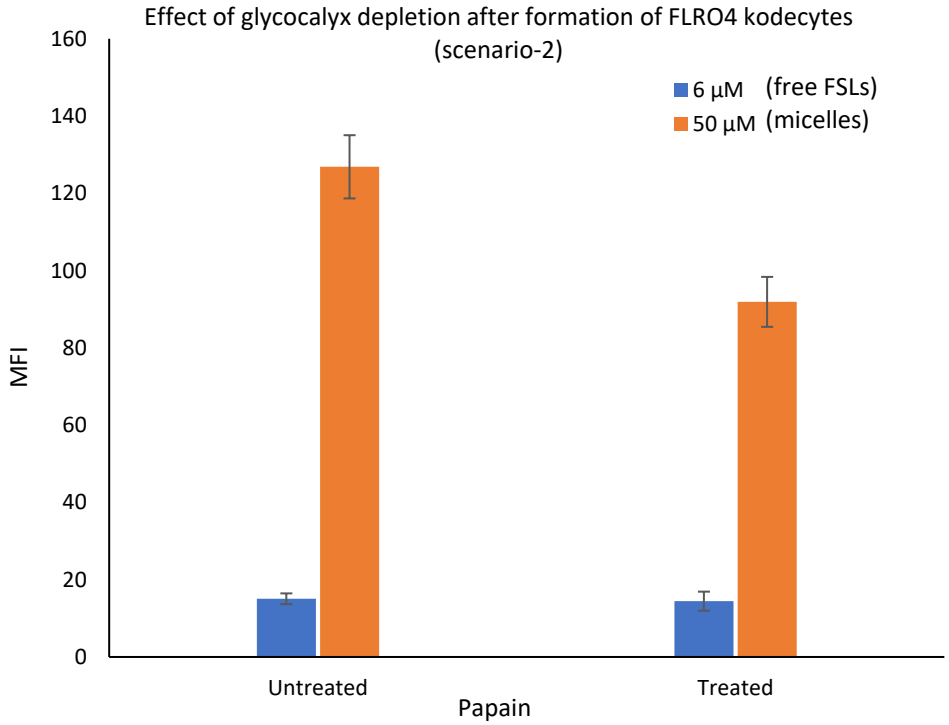

Figure 67: Effects of glycocalyx depletion on FSL-FLRO4 uptake (scenario-2) after the formation of FLRO4-kodecytes. Kodecytes were incubated with papain (treated with glycocalyx depletion) and without papain in CellStab (untreated), and the MFI of treated and untreated FLRO4-kodecytes was measured by flow cytometry.

From the results shown in Figures 66 and 67, the following conclusions could be drawn: Firstly, the removal of glycocalyx prior to the formation of kodecytes improves the uptake of FSL by more than 30%. Hence, it could be proposed that cells' glycocalyx interacts with FSL constructs and plays a role in determining the rate of labelling of cell membranes.

Secondly, when the glycocalyx of the kodecytes is removed following the koding process, a reduction in the fluorescence signal is observed (for the 50 µM kodecytes). This finding implies that FSL constructs (probably as micelles) are resident in glycocalyx. However, as all the signals were not lost after glycocalyx depletion of kodecytes, some FSL must therefore be in the plasma membrane.

4.4 Chapter summary:

The following conclusion could be deduced from the mechanism of the FSL construct study in different scenarios.

- Unlike FSL-FLRO4, FSL-BODIPY, and FSL-biotin, uptake approaches maximum and within 1 h of incubation at 37°C.
- An estimation of residual construct in the post-transformation study concludes that at any time point of analysis, there is a detectable amount of residual FSL left in the post-transformation solution of the kodecytes. The concentration of residual FSLs decreases with increasing koding duration. At a standard koding duration of 2 hours, 25% of FSL-FLRO4 remains in the post-transformation solution, whereas it is nearly 13% for FSL-BODIPY.
- At similar experimental conditions, the fluorescence spectrophotometer results (Section 4.2.2) correlate with those generated by flow cytometry (Section 3.3.3).
- The glycocalyx is a rate-determining step during the FSL modification process, as the removal of glycocalyx before kodecyte formation enhances FSL uptake by suggesting glycocalyx interacts with FSL constructs and influences cell membrane labelling rate. Additionally, kodecytes' glycocalyx partial removal reduces the fluorescence signal (for concentrations above CMC), suggesting FSL constructs are resident in glycocalyx, but some FSL must be in the plasma membrane as well.

Chapter 5 Investigating into FSL-FLRO4 signal loss during koding

Overview: The time-dependent uptake study of FSL-FLRO4 during 24 h incubations at 37°C showed that FSL-FLRO4 uptake reaches a maximum after 4 h of incubation (as the fluorescence signal MFI was highest, Section 3.3.3). After this incubation time point, the fluorescence signal starts decreasing. Compared to 4 h, FLRO4-kodecytes at 24 h lose approximately half of their fluorescence signal.

It is also important to highlight that, with FSL-BODIPY and FSL-biotin, there was no fluorescence signal loss during extended incubation at 37°C; however, there was a loss with FSL-FLRO4. Hence, initially, experiments were set up to measure and explain the reasons behind FSL-FLRO4 signal loss during 24-hour incubations at 37°C using flow cytometry.

Methodology overview: The following methodology was designed to test the hypothesis that post-transformation solution harvested after 24 h would account for the lost FSL-FLRO4 signal. The schematic overview of the methodology is presented in Figure 68, followed by a detailed explanation of the experimental protocol.

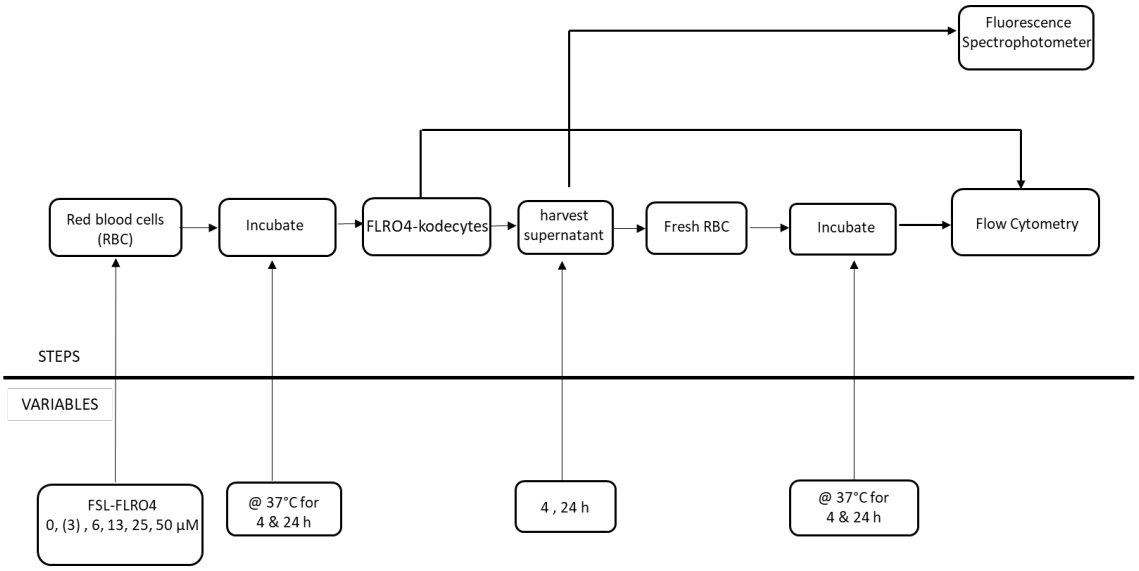

Figure 68: Schematic of methodology for exploring lost FSL-FLRO4 while koding.

The following protocol outlines the steps.

- RBC kodecytes were prepared at increasing concentrations of FSL-FLRO4 for time periods of 4 h and 24 h. A fresh aliquot of RBC and FSL was used for each time point (4 and 24 h).
- Post-transformation (after 4 h and 24 h incubation time points), the solution used for transformation was recovered as a supernatant.
- Respective supernatant or post-transformation solution was examined for the lost FSL-FLRO4 signal by two methodologies: flow cytometry and fluorescence spectrophotometer (fluorescence plate reader).
- For the flow cytometry analysis, the post-transformation solution was analysed for the presence of missing FSL-FLRO4 by measuring its ability to transform fresh RBCs into kodecytes using flow cytometry.
- The fluorescence signal generated by FLRO4-kodecytes prepared from transformation solutions (working stock) and supernatant at 4 h and 24 h was measured by flow cytometry.
- To determine FSL-FLRO4 signal loss, the MFI of kodecytes prepared from different transformation mediums (working stock and supernatant) was compared at respective time point.
- For fluorescence spectrophotometer analysis, supernatant recovered from 4 h and 24 h time points were measured for fluorescence signal readouts by fluorescence microplate-based assays.
- A comparative analysis of readouts from 4 h and 24 h supernatant would aid in determining if the 24 h harvested supernatant would account for FSL-FLRO4 signal loss (from 24 h time point kodecytes).
- It is important to note that the experiment concerning fluorescence spectrophotometer was performed in a separate setting (i.e., in separate scenarios). This was done to test and support the unexpected result that was observed in the following experiment.
- First flow cytometry result is explained, followed by the fluorescence spectrophotometer result.

Results: Figure 69 compares the MFI generated from FLRO4-kodecytes obtained after 4 h and 24 h of RBC incubation with FSL-FLRO4 at 37°C and kodecytes prepared with post-transformation solution, which was harvested after 24 h of incubation. From Figure 78, it could be seen that FLRO4-kodecytes obtained after 24 h of incubation generate nearly half of the fluorescence signal with respect to 4 h of incubation at 37°C. For example, compared to 4 h kodecytes, 24 h FLRO4-kodecytes produce approximately 45% less fluorescence signal at 3 and 6 µM and 55% at 13, 25, and 50 µM. MFI of kodecytes prepared from post-transformation solution harvested at 24 h was virtually negligible (around 1%). As 45–55% fluorescence signals were unaccounted for, it could be observed that MFI obtained from kodecytes prepared from a 24 h post- transformation solution did not match up to the level of fluorescence lost from 24 h working stock kodecytes.

A two-way ANOVA with Tukey's multiple comparison test was used to examine the statistical significance of the observation that MFI of 24 h post-transformation kodecytes is lesser than 4 and 24 kodecytes and different for 4 h and 24 h kodecytes. A change in fluorescence intensity is considered significant at **P<0.003, and highly significant at ****P<0.0001. The statistical analysis revealed that compared to 4 and 24 kodecytes, the difference in the MFI of 24 h post-transformation kodecytes was statistically significant. However, this was not observed at 3µM FSL-FLRO4. It was also observed that there was a significant difference between MFI of 4 h and 24 h kodecytes.

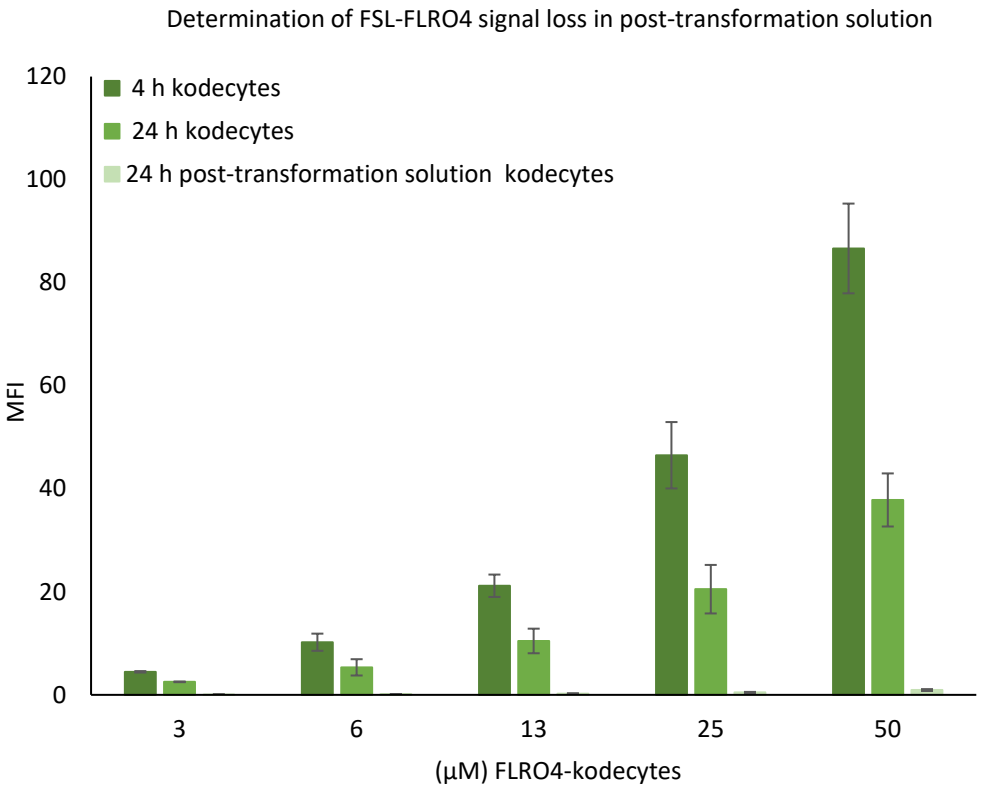

Figure 69: Determination of FSL-FLRO4 signal loss in a 24 h post-transformation solution. MFI of FLRO4-kodecytes obtained after 4 h and 24 h of incubation at 37°C (dark and light green bars, respectively) MFI of kodecytes prepared from a 24-hour post-transformation solution is represented by a lighter green bar.

From Figure 69, it could be surmised that there was loss in FLRO4-kodecytes lost fluorescence at 24 h and the flow cytometry methodology could not account for the fluorescence signals lost in the post-transformation solution (obtained at 24 h). Hence, the following questions arose:

- Whether lost FSL-FLRO4 was present in the 24 h post-transformation solution,
- and if the lost FSL-FLRO4 was present in the 24 h post-transformation then why did it not account for the lost signals i.e., unable to transform fresh red cells into new kodecytes.

Thus, to test these questions, further experiments were conducted to seek an explanation for the lost FSL-FLRO4 signal and specifically answer the following questions:

- Is lost FSL-FLRO4 degraded in the process of 24 h incubation at 37°C.

- Is lost FSL-FLRO4 present in the supernatant but, due to various factors, unable to make new kodecytes.

5.1 Testing FSL-FLRO4 degradation concept

Overview: The objective of this analysis was to examine whether FSL-FLRO4 constructs would degrade when maintained at 37°C for prolonged time periods of 24 h.

Method overview: The methodology was designed to examine whether FSL-FLRO4 constructs, in the absence of RBCs, would degrade if maintained at 37°C for an extended period of 12 h and 24 h. The schematic overview of the methodology is presented in Figure 70, followed by a detailed explanation of the experimental protocol.

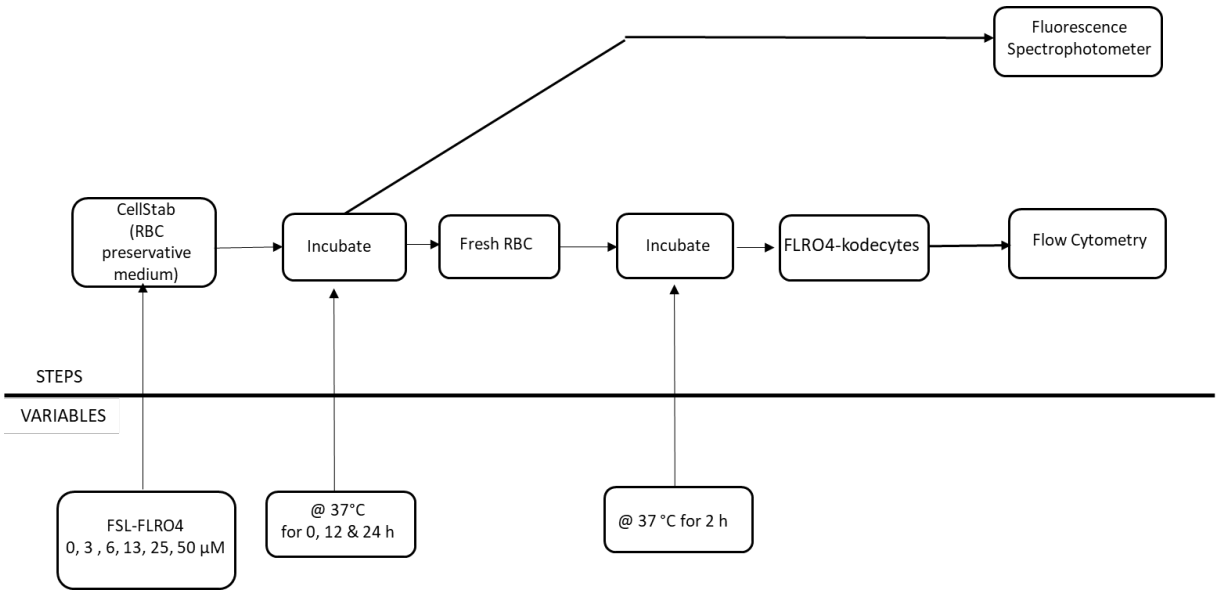

Figure 70: Schematic overview of method testing FSL-FLRO4 degradation concept.

The following protocol gives an overview of the steps involved.

- FSL-FLRO4 working stock of different concentrations was prepared and incubated at 37°C for 12 h and 24 h.
- A fresh batch of FSL-FLRO4 working stock was also prepared on the day of the experiment, representing 0 h.

- Freshly prepared (0 h), 12 h, and 24 h preincubated (at 37°C) FSL-FLRO4 working stocks were aliquoted into two sets.
- The first set was used to prepare kodecytes, and MFI generated from the respective kodecytes was measured by flow cytometry.
- The second set was quantified for its fluorescence signal by fluorescence spectrophotometer in a microplate-based assay.

Results: Figure 71 shows that comparable fluorescence signal was generated from FLRO4- kodecytes prepared from 12 h and 24 h (pre) incubated working stock and freshly prepared (0 h) working stock. This was observed across all the tested concentrations. Hence, it could be summarised from the flow cytometry result that in the absence of red cells the FSL-FLRO4 construct does not degrade during the prolonged incubation period of 12 h and 24 h at 37°C as freshly prepared and extended incubated working stock koded RBC generated similar MFI.

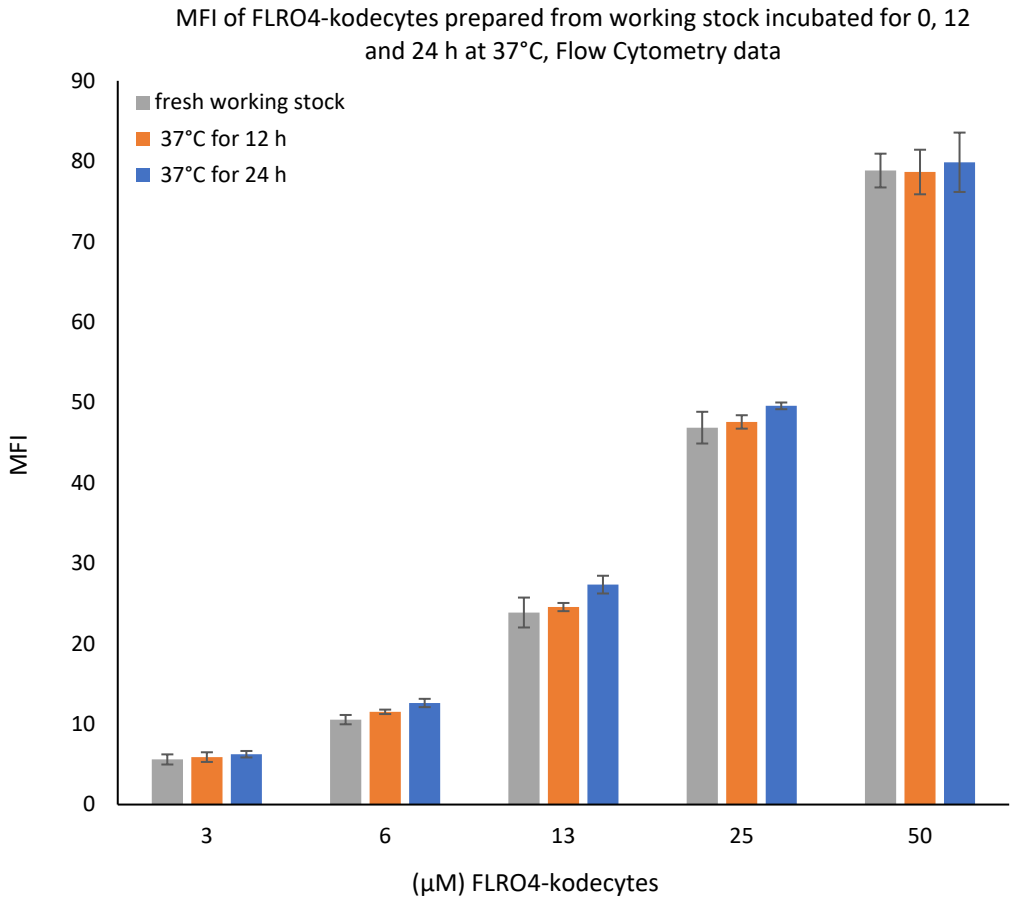

Figure 71: Analysis of degradation of the FSL construct using flow cytometry during prolonged incubation at 37°C. MFI of FLRO4-kodecytes prepared from working stock prepared freshly (0 h) and after 12 and 24 h incubation at 37°C. Experiments were performed thrice, and the data is expressed as the mean ± SD.

Alternatively, the fluorescence signal of FSL-FLRO4 constructs was also measured (and compared) by fluorescence spectrophotometer. The fluorescence intensity of different concentrations of FSL-FLRO4 (100µL aliquots) (obtained with and without incubation at 37°C) was measured using Tecan Spark® 10M in triplicate. In the fluorescence spectrophotometer (fluorescence microplate reader set up), the fluorescence intensity of a given sample is measured in relative fluorescence units (RFU), which account for the amount of fluorescence light signal emitted by the sample.

Figure 72 shows data obtained from a fluorescence spectrophotometer-based assay. Working stock of FSL-FLRO4 prepared freshly (0 h) and after 12, and 24 h incubation at 37°C generated approximately equivalent relative fluorescence. Hence, it could also be proposed that the FSL-FLRO4 construct does not degrade if maintained at 37°C for 12 h and 24 h, as the freshly prepared and 37°C incubated working stock generates very

similar fluorescence. From Figure 72, it could also be observed that RFU does not increase linearly with increasing concentrations of 3 to 50 µM. This effect is likely due to the self-quenching of the fluorophore [162,163].

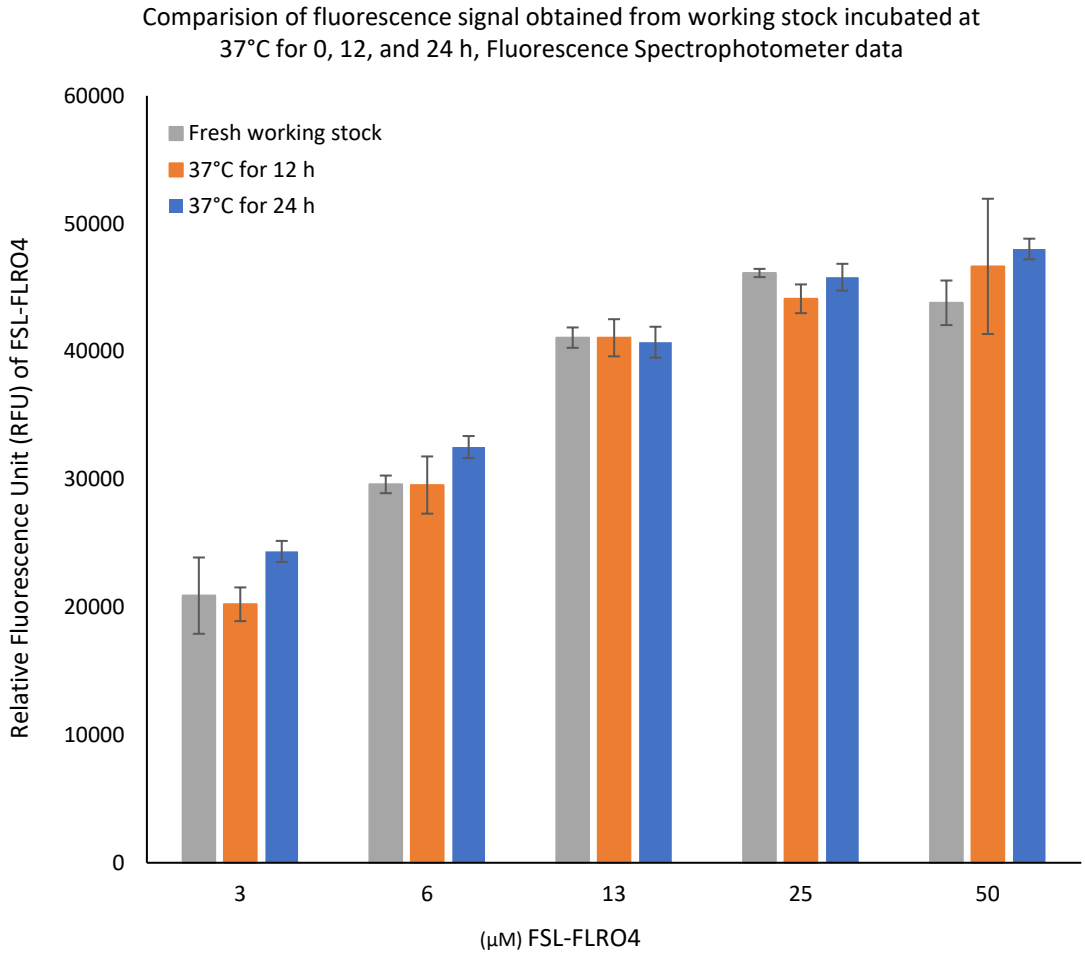

Figure 72: Analysis of degradation of the FSL construct using spectrophotometer during prolonged incubation at 37°C. Relative fluorescence of FSL-FLRO4 working stock prepared freshly and after 12, and 24 h incubation at 37°C.

5.2 Testing for lost FSL-FLRO4 in the post-transformation solution.

Overview: Based on the previous results (Figures 71 and 72) obtained by two methodologies, it was determined that FSL-FLRO4 does not degrade if maintained at 37°C for 12 h and 24 h (in the absence of red cells). Hence, it is possible that the missing FSL constructs are present in the harvested post-transformation solution, but in a form that is not able to transform fresh red cells into kodecytes. So, to test the second

hypothesis that the lost FSL is present in the post-transformation solution, the following experiment was set up.

Methodology: A schematic overview of methodology testing this concept is shown in Figure 70.

Results: Figure 73 shows the fluorescence signal obtained from post-transformation solution harvested after 4 and 24 hours of incubation of RBCs with FSL-FLRO4. Data was acquired by a fluorescence microplate-based assay. From the results, it could be observed that the post-transformation solution obtained after 24 h of incubation was more fluorescent than the 4 h post-transformation solution. The probable reason for the 24-hour post-transformation solution being more fluorescent than 6 h could be the comparatively more shedding off (or release) of the FSL-FLRO4 construct at 24 h (from the kodecytes) into the supernatant. The study confirms the hypothesis that lost FSL constructs are present in the harvested post-transformation solution, as evidenced by the consecutive rise of fluorescence in the 24-hour post-transformation solution. In other words, fluorescence signal loss from 24 h time point kodecytes and the consecutive rise of fluorescence in the 24 h post-transformation solution confirms the tested hypothesis that the lost FSL constructs are present in the harvested post- transformation solution.

Summary: FSL-FLRO4 signal loss study highlighted the fact that the missing (shed) FSL- FLRO4 was present in the post-transformation solution (supernatant) as measured by fluorescence spectrophotometer. However, they are present in the supernatant in a form that is not able to kode fresh RBCs (as shown in Figures 74 and 78). Therefore, it was proposed that FSL- FLRO4 lost from kodecytes or/and residual unacquired FSL was present in the post-transformation solution and is not able to kode fresh RBCs (at least very efficiently).

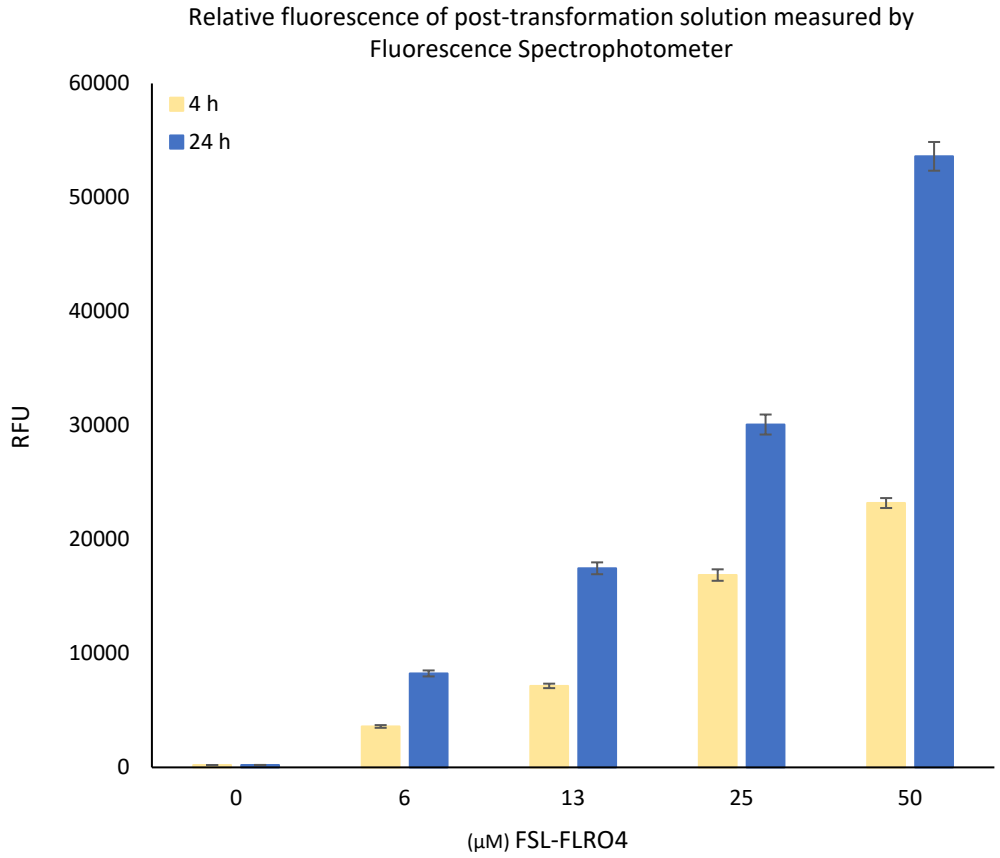

Figure 73: Relative fluorescence of post-transformation solution harvested after 4 and 24 h of incubation of RBCs with FSL-FLRO4. Results obtained by a fluorescence spectrophotometer.

5.3 Factors regulating koding ability of FSL-FLRO4

Overview: In the previous section, with reference to the FSL-FLRO4 signal loss study from 24 h post-transformation solution, it was shown that the lost FSL-FLRO4 did not degrade and was present in the post-transformation solution (as measured by spectrophotometer readout). Although FSL-FLRO4 were present in the post-transformation solution, they were not able to transform fresh RBCs into kodecytes suggesting that they may be associated with different RBC-derived (shed) bioactive proteins, lipids, and microparticles or microvesicles (referred to as membranous entities), which make up the interfering factor and which may also further regulate the uptake of shed FSL-FLRO4. The accumulation of interfering factors in the post- transformation solution could be either due to prolonged incubation at 37°C or additional associated factors (storage lesions).

Two hypotheses were suggested to test for the presence of these interfering factors. Firstly, it was proposed that membranous entities could be either generated by the RBCs or kodecytes in the process of koding which involved incubation at 37°C. Secondly, they may have been associated with the RBC membrane (in the form of RBC-associated microvesicles) before the koding process (despite washing), and ultimately ending up in the transformation solution. Due to extended incubation at 37°C, these membranous entities probably interact and associate with the available FSL. Hence, it could be suggested that during prolonged incubation at 37 °C, all different entities (released FSLs, membranous entities) could work in tandem to impact and change the dynamic of FSL uptake (from the post-transformation solution), ultimately controlling the availability of released FSL and further obstructing the FSL-FLRO4 koding process. The following experiments were conducted to explore factors regulating the koding ability of FSL- FLRO4 (which are mostly present in the post-transformation solution), and the results were analysed by flow cytometry and fluorescence spectrophotometer to understand this proposed phenomenon.

5.3.1 Potential membranous entities during the 37°C incubation of RBCs

Method overview: Experiments were set up to examine the first hypothesis that (interfering) membranous entities were being generated in the process of extended incubation of RBCs in CellStab at 37°C (in the absence of FSL constructs). The schematic overview of the methodology testing this concept is shown in Figure 74, followed by a detailed explanation of the experimental protocol.

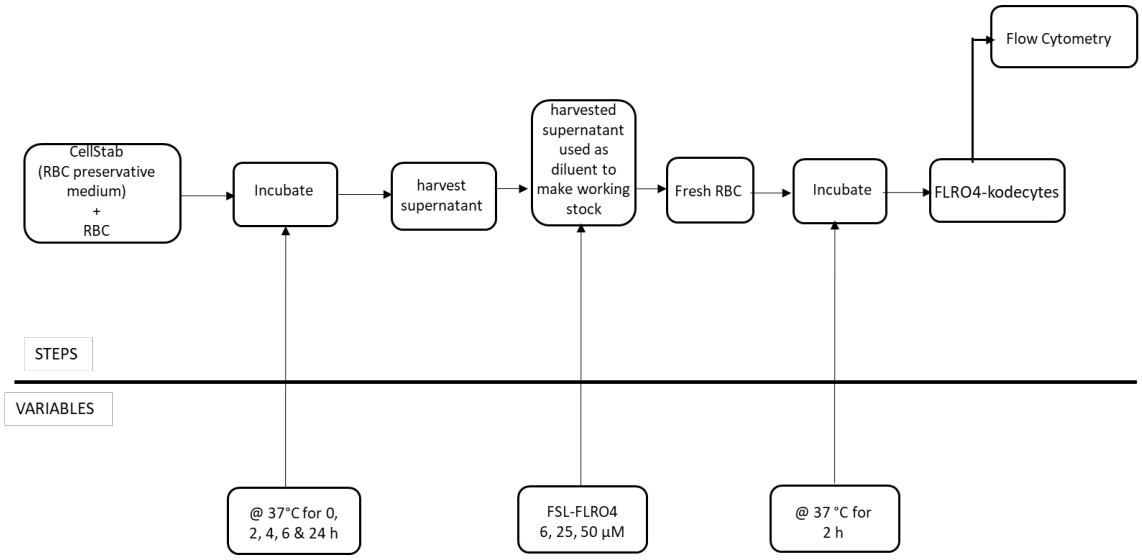

Figure 74: Schematic of method testing the concept of membranous entities created during at 37°C.

The following protocol was used to test the first hypothesis:

- RBCs were incubated with CellStab at 37°C for 0, 2, 4, 6, and 24 h. Separate tubes were maintained for each combination.
- Post 0, 2, 4, 6, and 24 h of incubation, respective supernatants were separated (referred to as CellStab supernatants).
- FSL-FLRO4 working stock or transformation solution was prepared using the CellStab supernatant as a diluent (obtained post 0, 2, 4, 6, and 24 h).
- Respective FSL-FLRO4 transformation solution were examined for its ability to transform fresh RBCs into kodecytes (at 37°C for 2 h) by flow cytometry.
- Fluorescence signal (MFI) generated from kodecytes prepared by the respective CellStab supernatant was compared with kodecytes prepared from the 0 h FSL- FLRO4 working stock (standard kodecytes).

Flow cytometry result

Figures 75A and 75B shows the impact on FSL-FLRO4 uptake (making of kodecytes) from the transformation solution prepared from buffer (CellStab) previously incubated for 2, 4, 6, and 24 h with RBC at 37°C. FSL-FLRO4 working stock was prepared across the tested concentrations of 6, 25, and 50 µM. The MFI of kodecytes prepared using the corresponding transformation solution was measured using flow cytometry (Figure 75A). Kodecytes prepared from working stock that used buffer, previously incubated for 2, 4, 6, and 24 h with RBCs, generated a lower fluorescence signal than conventional kodecytes (0 h) prepared with fresh CellStab.

In Figure 75B, the same data (as in Figure 75A) was normalised against 0 h kodecytes to allow a direct comparison of MFI change (i.e., MFI obtained from kodecytes made from supernatants obtained after 2, 4, 6, and 24 h incubation of RBCs at 37°C were normalised against 0 h incubation, then indicated as % change). The result shows that irrespective of FSL concentration (6–50µM), the fluorescence signal reduced at approximately the same rate, which is about 10% for 2 h, increasing to 20–25% for 4-6 h. Finally, at 24 h, it reduced by around 35%.

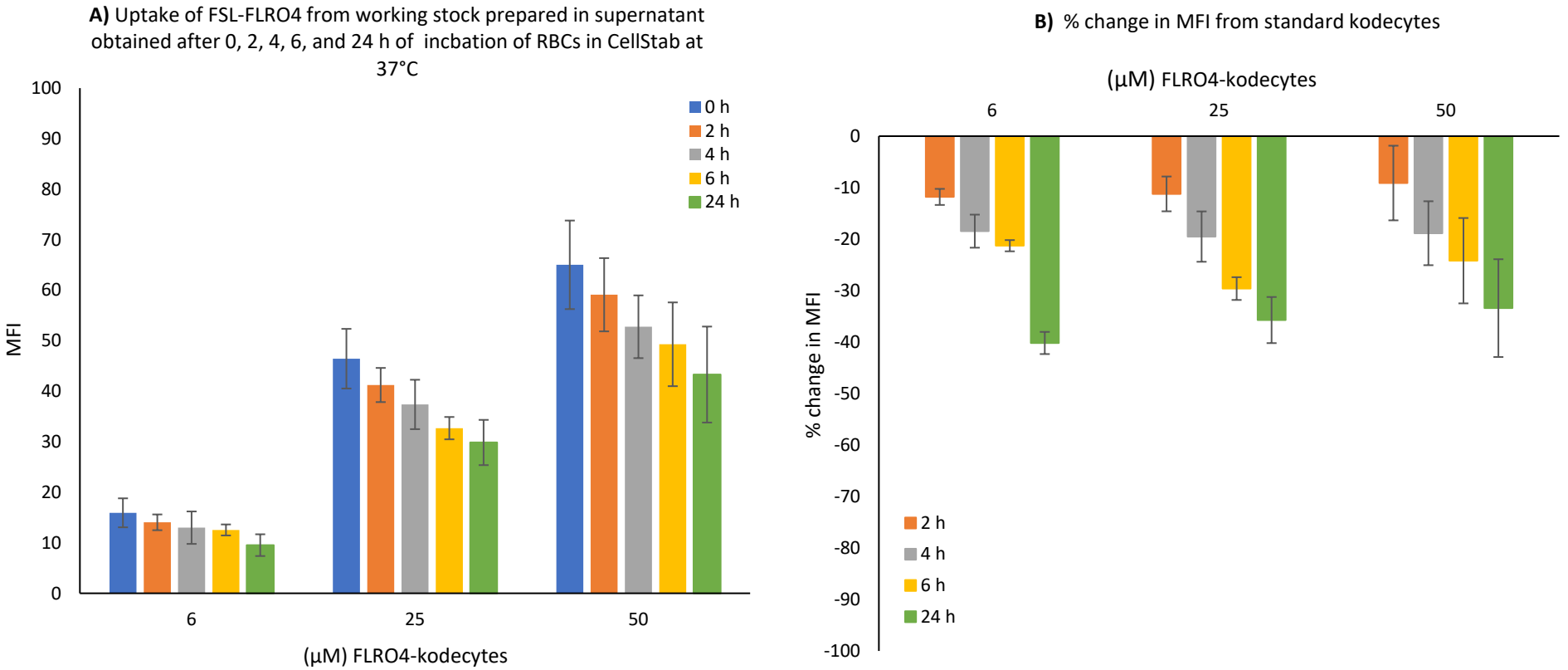

Figure 75: Potential membranous entities production in the absence of FSLs. Examining the concept of membranous entities generated during the 37°C incubation of RBCs without FSLs. Analysis of FSL-FLRO4 uptake from working stock (ws) prepared from diluent harvested from previously incubated buffer (CellStab) for 2, 4, 6, and 24 h with RBC at 37°C, flow cytometry data. **A**) MFI of RBC FLRO4-kodecytes generated from different working stocks. **B**) Change in FLRO4-kodecytes MFI compared to standard kodecytes (freshly prepared FSL-FLRO4 working stock), indicated as %.

From the above results, it could be suggested that the probable reason behind the decrease in MFI and hence the uptake of FSL-FLRO4 from working stock is due to incubation at 37°C. Thus, incubation of RBCs at 37°C probably facilitates the release of RBC-associated membranous entities, which interfere with and delay the efficient uptake of FSL-FLRO4 in suspension (as FSLs were suspected to be taken up or entrapped within these membranous lipids and hence were not available for further labelling of RBCs). This interference in FSL uptake was found to be of lesser extent (compared to prolonged incubation duration with FSL-FLRO4, Figure 69), and hence probably represents only part of the problem, and possibly the FSL koding process contributes to this issue. Thus, it was decided to perform experiments where different FSL constructs (along with FSL-FLRO4) would be tested for their respective influence or outcome when RBCs were incubated with FSL for an extended period of time.

5.3.2 Potential membranous entities generated in the process of koding

Methodology: To verify the possibility that the FSL koding process itself contributes or increases the generation of interfering membranous entities in the process of extended incubation of RBCs at 37°C, experiments were set up wherein two non-fluorescent FSL constructs, FSL-GB3 and FSL-Zero (FSL-0), were used. FSL-GB3 was chosen to match FSL-FLRO4 as they both have adipate-based spacers and similar molecular weights. FSL-0 was also chosen as it does not possess a significant functional group but does have a substantial spacer and is representative of most FSL constructs thus representing the spacer and lipid parts of the study. Two concentrations (6 and 50 µM) were used for FSL-GB3 and FSL-0, as theses be expected to establish the effect of FSL concentration on the rate of the release of membranous entities.

The methodology was designed to examine whether interfering membranous entities were being generated in the FSL koding process. The schematic overview of the methodology is presented in Figure 76, followed by a detailed explanation of the experimental protocol.

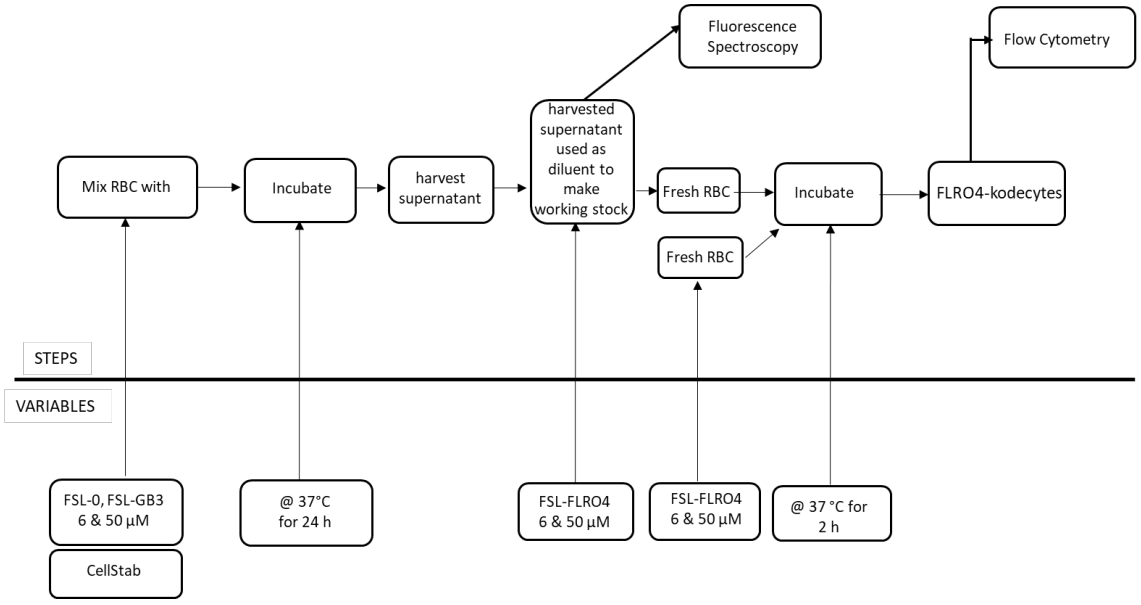

Figure 76: Examining the effect of koding on generation of membranous entities (testing whether incubation of RBCs with FSLs generates more membranous entities than without FSLs).

To test the proposed hypothesis, the following protocol was set up:

- RBCs were incubated with CellStab and 6 and 50 µM FSL-GB3 and FSL-0 at 37°C for 24 h. Separate tubes were maintained for each combination.
- After 24 h incubation, the solution used for transformation was recovered as a supernatant.
- FSL-FLRO4 working stock or transformation medium was prepared using these supernatants as diluents. Additionally, a fresh FSL-FLRO4 working stock (using fresh CellStab as diluent) was also prepared. These respective working stocks were examined by two methodologies: flow cytometry, and fluorescence spectrophotometer.
- For flow cytometry analysis, these different FSL-FLRO4 supernatants working stock was examined for the interfering factor by measuring its ability to transform fresh RBCs into kodecytes i.e., the efficiency of FSL-FLRO4 uptake by fresh RBCs.
- FLRO4-kodecytes prepared with different transformation media were compared against standard FLRO4-kodecytes (prepared by incubating RBC with fresh FSL- FLRO4 working stock) to establish the contribution of the FSL construct and koding process in generating interfering membranous entities in the process of extended incubation of RBCs at 37°C.

- For fluorescence spectrophotometer analysis, different FSL-FLRO4 supernatants working stocks were measured for relative fluorescence signal readouts.
- Data is represented after readouts from various FSL-FLRO4 supernatant working stocks were compared to fresh FSL-FLRO4 working stock.
- First flow cytometry result is explained, followed by the fluorescence spectrophotometer result.

Flow cytometry result

Figure 77 shows the impact of the FSL koding process (i.e., FSL constructs) on RBCs during extended incubation at 37°C. Here, fluorescence signals generated by FLRO4- kodecytes with FSL-FLRO4 transformation medium wherein the diluents (to prepare FSL- FLRO4 working stock) were harvested after 24 h of incubation of RBCs in CellStab, and 6, 50 µM of FSL-GB3 and FSL-0 were compared with standard FLRO4- kodecytes (fresh working stock) using flow cytometry. As shown in Figure 77, standard kodecytes generated the most fluorescent signals, and kodecytes prepared with FSL- FLRO4 transformation medium, where diluent was obtained from CellStab 24 h incubation (no FSLs), generated the least fluorescence signal.

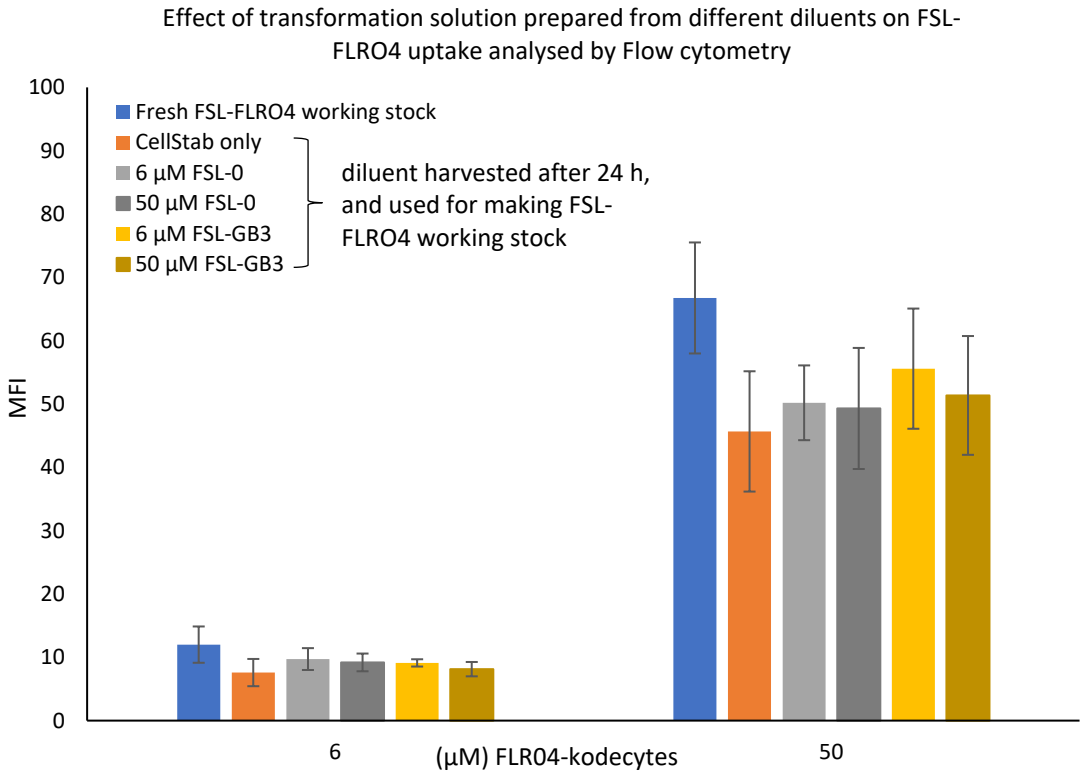

Figure 77: Potential Membranous entities production in the presence of FSLs (FC). Examining the concept of membranous entities generated during the 37°C incubation of RBCs with FSLs. Effect on uptake of FSLs from FSL-FLRO4 working stock prepared from different diluents harvested after 24 h incubation of RBCs with and without different FSL constructs (CellStab and 6 and 50 µM of FSL-GB3 and FSL-0). MFI of FLRO4-kodecytes prepared from different working stock were compared against MFI of FLRO4-kodecytes prepared using fresh working stock.

With respect to standard kodecytes, kodecytes prepared using FSL-FLRO4 transformation medium (diluent from 0 µM CellStab post 24 h) generated approximately 35% less signal, and kodecytes prepared using FSL-FLRO4 transformation medium (diluents from 6, 50 µM FSL-GB3 and FSL-0 post 24 h) generated approximately 12% less signal. This trend was observed irrespective of the strength of the FSL used (6 and 50 µM). Hence, based on the fluorescence signal generated by different kodecytes using flow cytometry, it could be summarised that there was more uptake of FSL-FLRO4 when diluent for transformation medium was prepared from supernatant harvested after 24 h incubation of RBCs with FSL-GB3 and FSL-0 than CellStab only.

An explanation for the observed phenomenon could be that the presence of FSL constructs (during an extended incubation at 37°C) helps maintain RBC membrane integrity as fewer membranous entities (and, in turn, interfering factors) could be generated. In contrast, in the absence of the FSL construct, interference-causing entities were more significant (thus regulating FSL-FLRO4 uptake). Hence, it could be concluded

that transforming red cells into kodecytes did not make them more likely to shed the product.

Fluorescence spectrophotometer result

Figure 78 demonstrates a comparative representation of the fluorescence signal generated by FSL-FLRO4 working stock/transformation medium, prepared from six different diluents: supernatant obtained after 24 h of incubation of RBCs in CellStab, 6 and 50 µM of FSL-0 and FSL-GB3 at 37°C. Here, quantification of fluorescence signals were performed by fluorescence spectrophotometer.

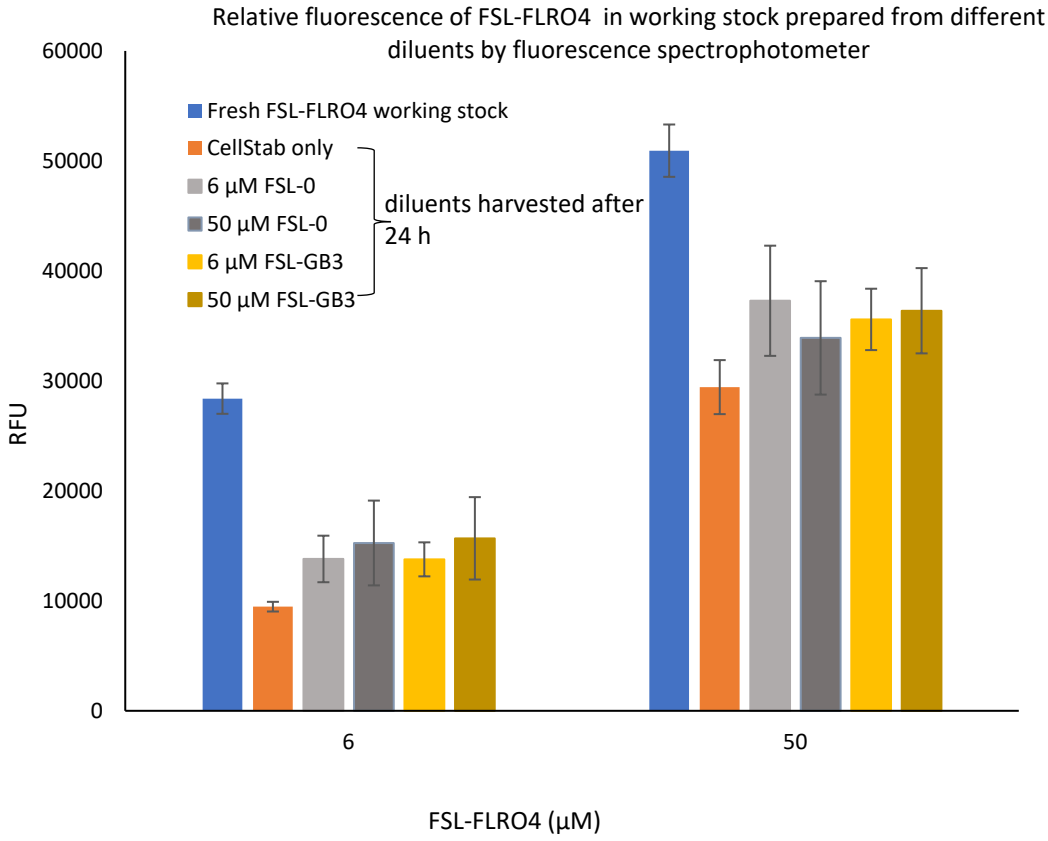

Figure 78: Spectrophotometer data interpretation of membranous entities generated in the process of koding process. Relative fluorescence of FSL-FLRO4 working stock prepared from diluents obtained after 24 h of incubation of RBCs in CellStab and 6, 50µM of FSL- 0 and FSL-GB3 at 37°C. Freshly prepared FSL-FLRO4 working stock was used for comparative purposes.

From Figure 78, it could be observed that FSL-FLRO4 working stock prepared freshly generated significantly more fluorescence signal than working stock prepared with diluents harvested after 24 h. For example, 6 µM FSL-FLRO4 working stock prepared

from supernatant harvested after 24 h incubation of RBCs with CellStab generated approximately 42% less signal than standard working stock. This difference was found to be around 60% for 50 µM FSL-FLRO4 working stock. Additionally, FSL-FLRO4 working stock prepared from diluent harvested after 24 h of incubation of RBCs in FSL generated more signals compared to when RBC was incubated without FSL. Fluorescence spectrophotometer findings mostly correlate with the results obtained by flow cytometry (Figure 77, when the same working stock aliquots were used for preparing kodecytes).

The present tested hypothesis could not establish the complete cause behind the factor causing FSL-FLRO4 fluorescence signal loss. It should be noted here that the FSLs considered for testing this assumption resembled FSL-FLRO4 but was not FSL-FLRO4; hence, the actual effect of prolonged RBC incubation with FSL-FLRO4 at 37°C could not be discarded.

The second hypothesis aimed to examine the possible link between RBC-derived extracellular membranous vesicles (probably associated with the RBC membrane since the start of the transformation process) and their interference with the uptake of FSL-FLRO4 during prolonged incubation at 37°C. The generation of RBCs-associated membranous vesicle has been shown to be linked to *in vitro* storage and, subsequently, the age of RBCs [148,164,165]. The concern that extended *in vitro* storage of RBCs at 4°C may generate RBCs-associated MVs (proposed interfering factor) and resultant usage of old RBCs would impact the uptake of FSL constructs was already comprehended in the early course of this study (detailed study in Section 3.2). Based on the results obtained from the RBC storage age-based uptake study: as RBCs age during *in vitro* storage, their ability to uptake FSL-FLRO4 decreases, so it was decided to use RBCs no older than 10 days of storage at 4°C for making kodecytes. Since RBCs aged less than 10 days were always used in this study, RBCs-associated membranous entity theory has a minimal role to play in being the source or reservoir of interfering factors which, would impact the dynamics of FSL-FLRO4 uptake and control the availability of missing or shed FSL.

5.4 Chapter summary:

The following conclusion could be deduced from the study, where factors that regulate the koding ability of shed FSL-FLRO4 (present in the post-transformation solution) were examined. Conclusions are based on the flow cytometry and fluorescence spectrophotometer results.

- The time-dependent uptake study of FSL-FLRO4 during 24 h incubations at 37°C showed that FSL-FLRO4 uptake reaches a maximum after 4 h of incubation; after this incubation time point, the fluorescence signal starts decreasing. Compared to 4 h, FLRO4-kodecytes at 24 h lose more than half of their fluorescence signal.
- Unlike FSL-FLRO4, FSL-BODIPY and FSL-biotin at concentrations less than 100 µM did not exhibit this behaviour of signal loss during extended koding.
- Based on results obtained by flow cytometry and fluorescence spectrophotometer, it could be seen that FSL-FLRO4 does not degrade if maintained at 37°C for 12 h and 24 h (in the absence of red cells), and the lost and/or residual FSL-FLRO4 are present in the harvested post-transformation solution but in a form that is not able to efficiently transform fresh red cells into kodecytes.
- Extended incubation of RBCs in CellStab at 37°C facilitates the release of more (interfering) RBC-associated membranous entities than when RBCs were incubated with FSL constructs (tested FSL-GB3 and FSL-0). Hence, it could be proposed that transforming red cells into kodecytes (i.e., the act of incubation at 37°C) make them more likely to shed their membrane and, in turn, the product.
- The tested hypothesis could not establish the full cause of FSL-FLRO4 fluorescence signal loss as the FSLs considered for testing the proposed hypothesis resembled FSL-FLRO4 but were not FSL-FLRO4; hence, the actual effect of prolonged RBC incubation with FSL-FLRO4 at 37°C could not be discarded.
- In summary, at 37°C, RBC-derived membranous entities (proteins, lipids, and microvesicles) make up or account for the interfering factor and further regulate the uptake of missing FSL-FLRO4 from the supernatant.

Chapter 6 Kodecytes morphology analysis and Cytotoxicity studies

Cells are sensitive to their environment. Application or uptake of exogenous molecules/probes has been reported to bring about significant cellular changes in shape, structure, functionality, viability, motility, and cytoskeleton remodelling [166]. The aim of this aspect of the study was to measure whether the uptake of FSL constructs under different koding conditions (i.e., temperature, duration, concentration, and cell type) visually impacts the integrity of the membrane or the vitality of the kodecytes. Additionally, the influence of the koding process on the viability of actively dividing Jurkat cells and PC-3 cells was also analysed. To examine the cytotoxicity profile of FSL constructs, different cell viability assays based on different methodologies and instrumentation were used.

6.1 Scanning electron microscope analysis of RBC kodecytes morphology

Overview: Optical microscopy has a limited resolution of approximately 200nm with maximum magnification of around 2000×. In contrast Scanning Electron Microscopy (SEM) provides tenfold improvement in resolution (nearly 1 nm) with magnification of about 15,00,000× allowing access to three-dimensional shape of cells.[167-170] The RBC membrane is paramount to its survivability and is widely chosen as a methodology to observe and examine its morphology.

In this study, Hitachi Ultra High-Resolution Analytical FE-SEM SU-70 was used to study the surface morphology of red cells and Jurkat cells pre and post koding. It is important to note that this SEM has advantage of not only providing ultra-high resolution (1.0 nm/15kV, 1.6nm/ 1 kV), but also reduced charge-up imaging, compositional-contrast imaging, and ultra-low voltage imaging.

SEM can be used to view the RBC membrane's morphological changes, which can be correlated to its functionality and survivability.[171] Hence, SEM was used to examine RBCs' morphological characteristics (diameter and shape) post-koding.

Methodology: The following methodology was used for SEM (Hitachi SU-70) sample preparation and analysis. A schematic overview of the methodology is presented in Figure 79, followed by a detailed description of the experimental protocol.

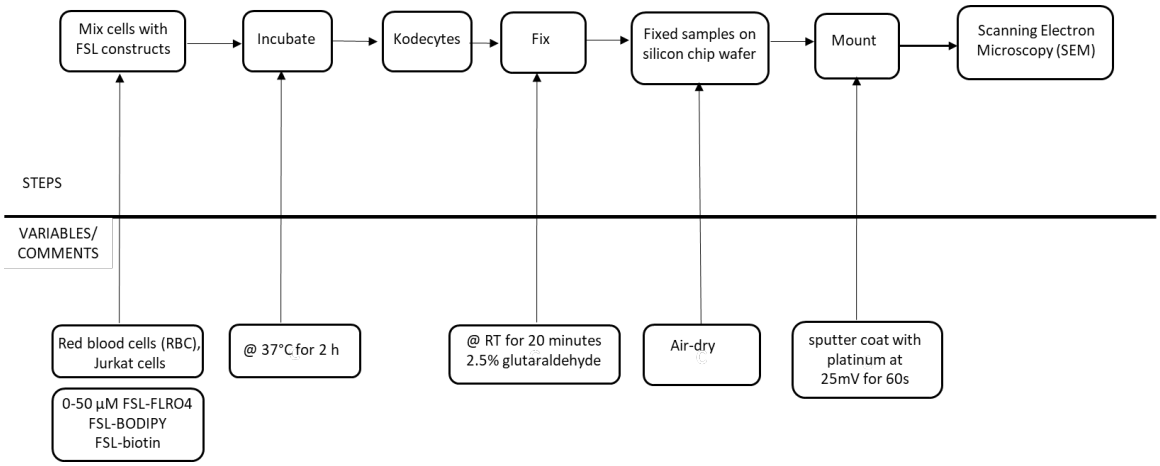

Figure 79: Schematic overview of methodology used for SEM sample preparation.

Procedure of SEM sample preparation for RBC kodecytes.

- FSL constructs were diluted to the required concentration in CellStab.
- One volume of FSL at a given concentration was incubated with one volume of packed RBC at 37°C for 2 h. Unkoded cells were also prepared simultaneously. For the RBC storage duration study (5.1.1), day-0 and day-15 old RBCs were used for preparing kodecytes.
- In section 5.1.3, different koding incubation periods were used (0-24 h).
- RBC kodecytes were washed 2× and made into a 5% suspension.
- Kodecyte samples were fixed with 2.5% glutaraldehyde for 20 minutes at RT.
- Fixed kodecytes were washed 3× with DI water. Samples were placed on a silicon chip wafer and allowed to dry completely.
- Prior to viewing with SEM, the dried samples were mounted using a double-sided carbon tape and sputter coated with platinum at 25mV for 60s (Hitachi; E-1045).
- SEM images were taken using the standard voltage of 5KV.
- Kodecytes and unkoded cells were counted and categorised by shape and graded based on the nomenclature of Bessis [169] explained in detail in Section 1.10, Figure 80 and summarized in Table 13. Results are shown as percentage of normal cells.

Table 13: Red cells categorised by shapes based on nomenclature of Bessis. [169]

Red cells shape names	Abbreviation	Description
Discocyte	D	normal biconcave red cells
Type I Echinocyte	EI	an irregularly countoured discocyte
Type II Echinocyte	EII	a flat red cell with spicules
Type III Echinocyte	EIII	ovoid or spherical cell with 30 to 50 conical spicules evenly distributed over its surface
Type I Sphero-Echinocytes	SEI	a sphere with ~50 threadlike spicules
Type II Sphero-Echinocytes	SEII	a smooth sphere
Type I Stomatocytes	SI	cup shape red cells with a shallow circular invagination, rim is thicker compared with the shorter circular invagination
Type II Stomatocytes	SII	cup shape with a deeper invagination, nearly circular
Type III Stomatocytes	SIII	cup shape with a deep invagination, often elongated into a mouth or pit-like slit

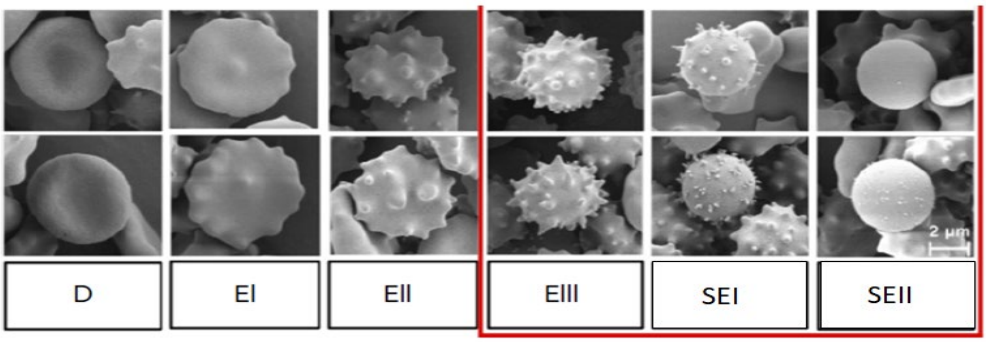

A) SEM micrographs of red blood cells with normal and altered morphology during 40d *in-vitro* storage

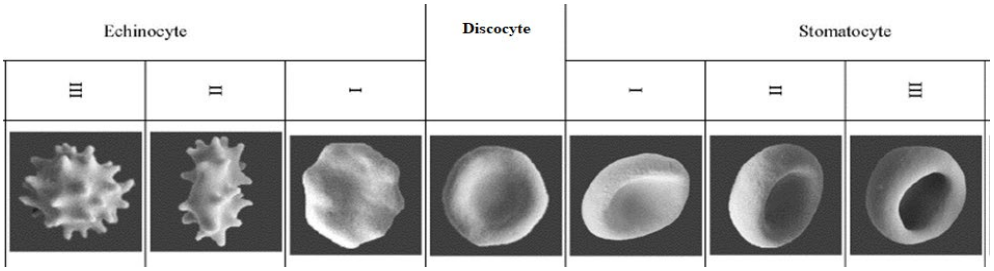

B) The reversible discocyte-echinocyte and discocyte-stomatocyte transformation

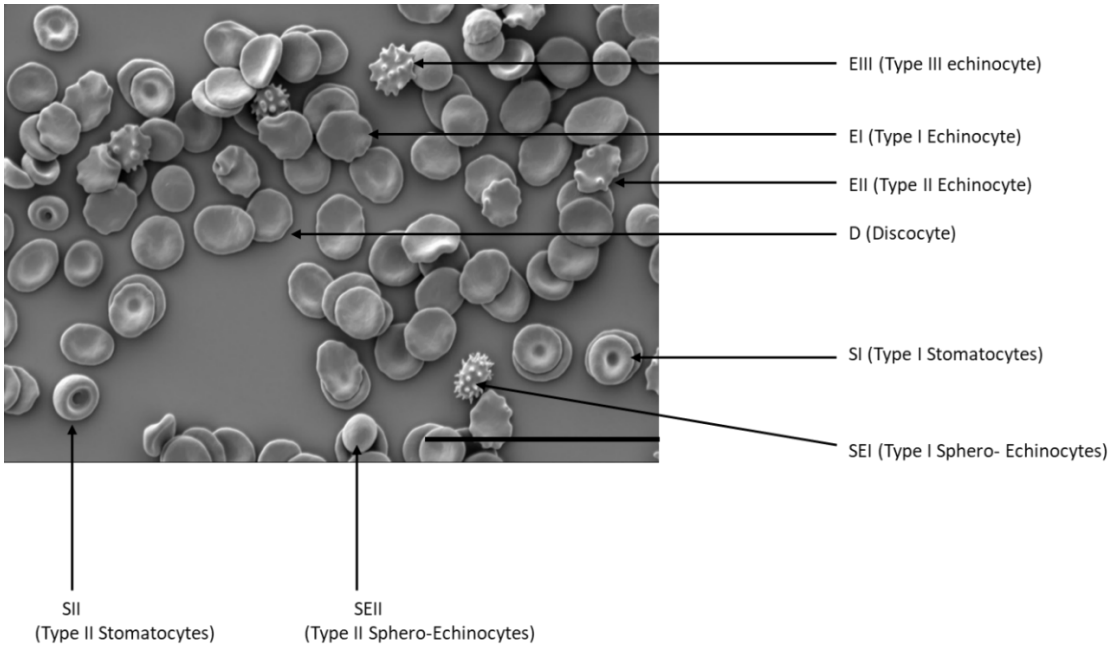

C) SEM micrographs of red blood cells prepared at AUT

Figure 80: SEM micrographs of RBC with normal and altered morphology. Abbreviations used for respective red cells are discocyte (D), type I echinocyte (EI), type II echinocyte (EII), type III echinocyte (EIII), type I sphero-echinocytes (SEI), type II sphero-echinocytes (SEII), type I stomatocytes (SI), and type II stomatocytes (SII) and detailed description is in table 13. Scale bar = 30 µm. **A)** During *in vitro* storage for 40 days. **B)** Reversible transformation stages C) SEM preparation during the course of the study at AUT

It is important to mention here that echinocyte subtypes (EI, EII, and EIII) and spherо-echinocyte subtypes (SEI and SEII) were easier to differentiate and categorise based on different shapes; hence, their subtypes have been used to grade kodecytes and unkoded cells in this study. However, for stomatocytes, their subtypes have been grouped and analysed as one. The reason behind doing so was the lack of very clear demarcation in the shape of the respective stomatocyte subtypes. It is important to note that kodecytes and unkoded cells diameter measuring > to 6µm in diameter are determined as discocytes, and < 6µm are determined as stomatocytes.

Procedure of SEM sample preparation for Jurkat kodecytes.

- Equal volumes of Jurkat cell suspension were added to an equal volume of FSL working stock and serum-free medium (negative control) and incubated for 2 h at 5% CO_2 and 37°C.
- Kodecytes were washed 2× and then fixed by incubating with 2.5% glutaraldehyde for 20 minutes at RT.
- Fixed kodecytes were washed with DI water 3× by centrifugation at 130× g for 3 minutes.
- After final washing, kodecytes were processed the same as RBCs.

For characterising the diameter, the mean diameter of both kodecytes and control cells was measured manually using an SEM micrograph and the analysis tool, Image J. For this, a straight line (chosen as the diameter) was drawn in 4 separate directions across several axes of the same cell. The mean diameter was then measured using the automated measurement function in Image J. The diameters of at least 100 random cells per image were measured, and the mean diameter of kodecytes and unkoded cells was plotted. For each image, 4 random fields with representative 100 cells were counted. Counting was done from left to right and a consistent pattern of counting cells was followed. Each experiment was repeated at least twice.

During the course of the study, it was observed that kodecytes and unkoded cells graded as stomatocytes (and their subtypes) on average have a smaller diameter. Hence, kodecytes, or unkoded cells, were classified as stomatocytes based on their altered shape and size (measuring ≤ 6µm in diameter).

6.1.1 RBC storage-age effect on FLRO4-kodecytes morphology

Extended *in vitro* storage of RBC at 4°C and, in turn, usage of relatively older RBC for the koding process have been shown to impact the uptake of FSL-FLRO4 (section 3.2). Experiments were designed to analyse if the slower uptake of FSL constructs was corelated to any change in the morphology of RBC. In summary, this section investigates how the duration of RBC storage affects the morphology of RBCs and, in turn, the morphology of FLRO4-kodecytes. The results would establish if the selection of RBC to make kodecytes (and results) were dependent on RBC storage age.

FSL-FLRO4

Figures 81 and 82 show the impact of the storage age of RBC (d0 and d15) on FLRO4-kodecyte morphology across the tested concentration range of 0–50 µM. Kodecytes made from different storage age RBCs were categorised by shape and graded based on the nomenclature of Bessis, summarised in Table 13 and Figure 80. Results are shown as a percentage of normal cells (discocytes), i.e., normal cells/abnormal cells. Abnormal cells account for a total of EI+EII+EIII+SEI+SEII.

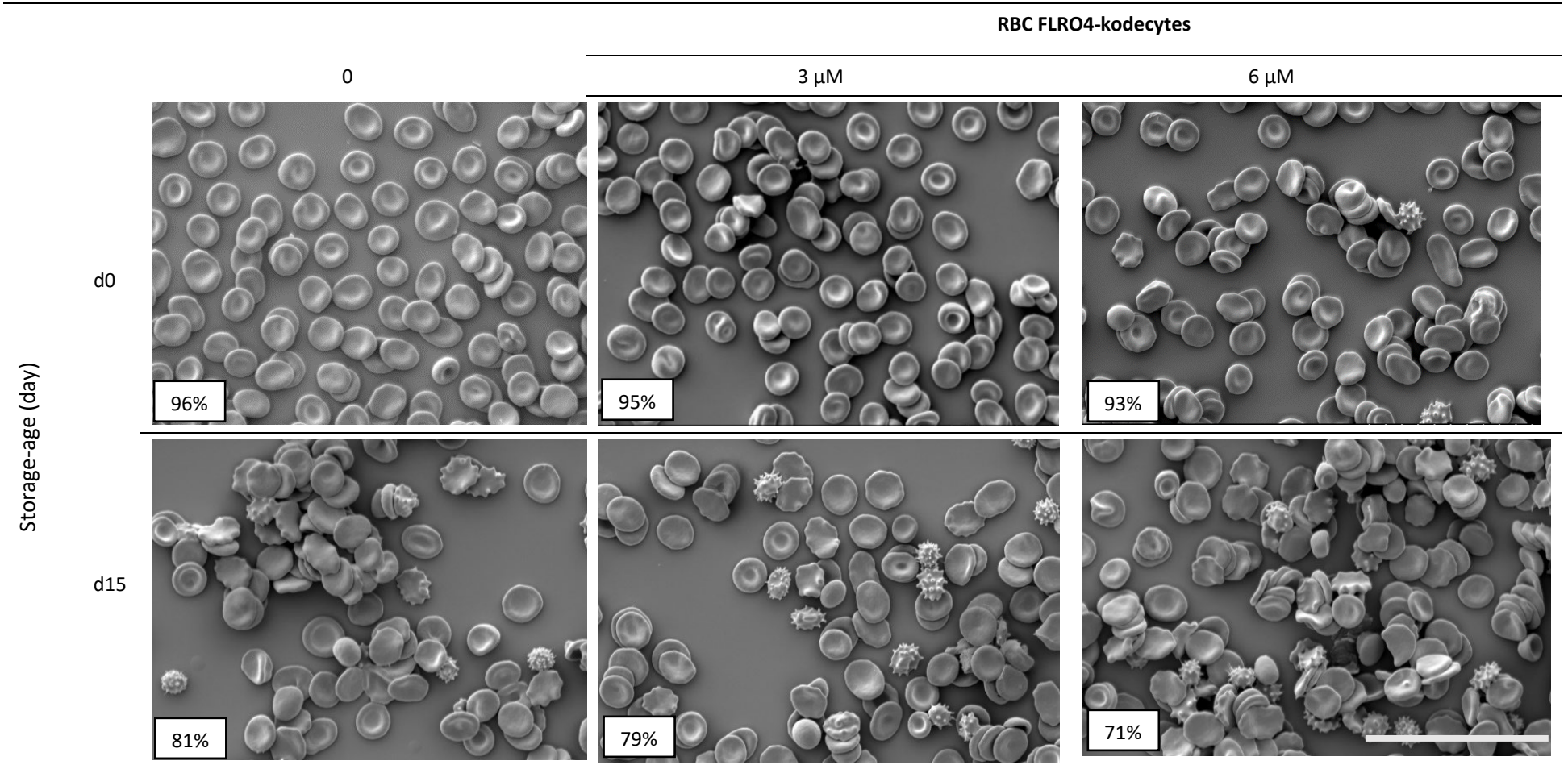

Figure 81: SEM micrograph analysing RBC storage-age effect on FLRO4-kodecytes morphology. Example SEM micrograph of unkoded RBC and 3-6µM FLRO4-kodecytes (scale bar = 30µm) prepared from RBCs stored at 4°C for 0 and 15 days. The inset box on the left of each micrograph is the approximate % of normal cells. Note: Box % relates to the average observed for all experiments, not just the micrograph shown.

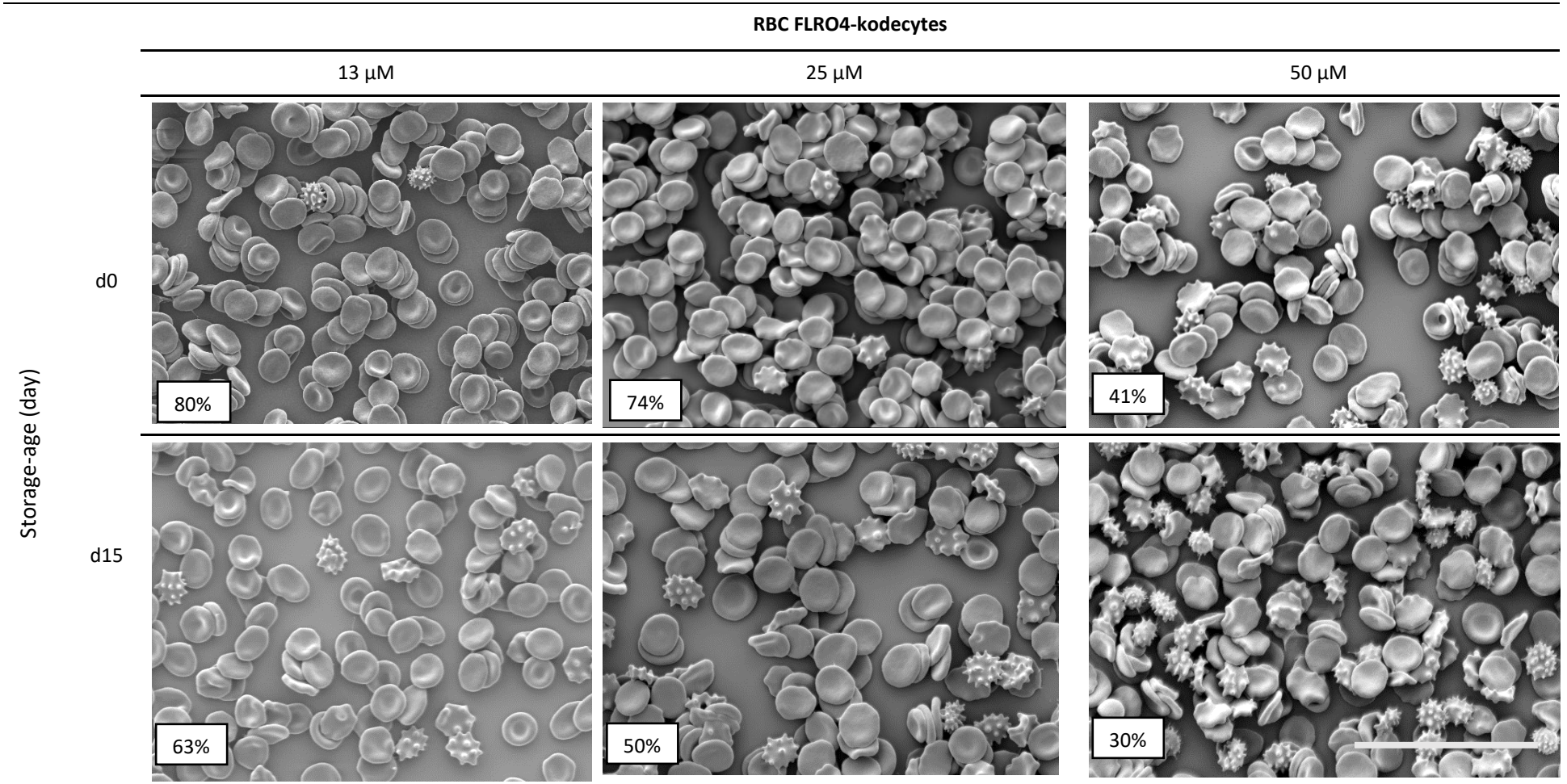

Figure 82: SEM micrograph analysing RBC storage-age effect on FLRO4-kodecyte morphology. Example SEM micrograph of 13-50µM FLRO4-kodecytes (scale bar = 30µm) prepared from RBCs stored at 4°C for 0 and 15 days. The inset box on the left of each micrograph is the approximate % of normal cells. Note: Box % relates to the average observed for all experiments, not just the micrograph shown.

From the results shown in Figures 81 and 82, the following conclusions were made: firstly, unkoded cells and (3–50 µM) kodecytes prepared from d0 or fresh RBCs had more discocytes, i.e., normal cells, than when d15 stored RBCs were used. Secondly, the transformation of RBCs with a concentration of >13µM FSL-FLRO4 resulted in a change in morphology from predominantly discocytes to an increasing percentage of type I-III echinocytes. Although this observation was displayed irrespective of the storage age of RBCs (used for preparing kodecytes), it was seen more for d15-stored RBCs at a 50µM concentration.

Table 14 summarises the various transitions in kodecytes and unkoded cell shapes and is categorised based on the nomenclature of Bessis. The results are shown as an approximate percentage of cells. The data in Table 14 shows that when kodecytes were prepared using older RBCs, more type II and type III echinocytes of flat and spherical shape with conical spicules were observed from 13 µM concentration onwards. This trend sets in as the concentration of FSL-FLRO4 increases, and more type III echinocytes, i.e., spherical cells with 30 to 50 conical spicules, start appearing.

Table 14: Effect of RBC storage-age on FLRO4-kodecyte. Unkoded cells and FLRO4-kodecytes prepared from d0 and d15 stored RBC were categorised by shape based on the nomenclature of Bessis. Results are shown as a percentage.

	RBC-storage age (days)											
	d0						**d15**					
		FLRO4-kodecytes (µM)						**FLRO4-kodecytes (µM)**				
Cell type (%)	**0**	**3**	**6**	**13**	**25**	**50**	**0**	**3**	**6**	**13**	**25**	**50**
D	96	95	93	80	74	41	81	79	71	63	50	30
EI	2	2	3	8	10	15	5	4	5	10	14	10
EII	0	2	2	6	8	22	5	6	8	11	19	17
EIII	1	1	1	4	6	18	7	8	8	7	12	31
SEI	0	0	0	1	0	1	0	3	6	6	2	8
SEII	0	0	0	0	1	1	1	0	1	2	3	1
S	1	0	1	1	1	2	1	0	1	1	0	3

6.1.2 Concentration-dependent effect

FSL-FLRO4

Based on SEM micrographs shown in Figures 81 and 82 and data shown in Table 14, it could be concluded that treatment of RBCs with concentrations of >13µM FSL-FLRO4 resulted in a change in morphology from predominantly discocyte to increasing percentage of type I-III echinocytes.

FSL-BODIPY

Figure 83 shows the SEM micrograph of unkoded and 3-50µM BODIPY-kodecytes. It can be seen that a concentration-dependent effect of FSL-BODIPY on kodecytes was not observed until the 50µM concentration. For example, with respect to unkoded cells, the appearance of abnormal cells like type I and II echinocytes (which are irregularly contoured discocytes) were observed when RBCs were transformed with FSL-BODIPY at a 50µM concentration. Hence, it can be concluded that BODIPY-kodecytes mostly appeared to behave similarly to control, i.e., unkoded cells.

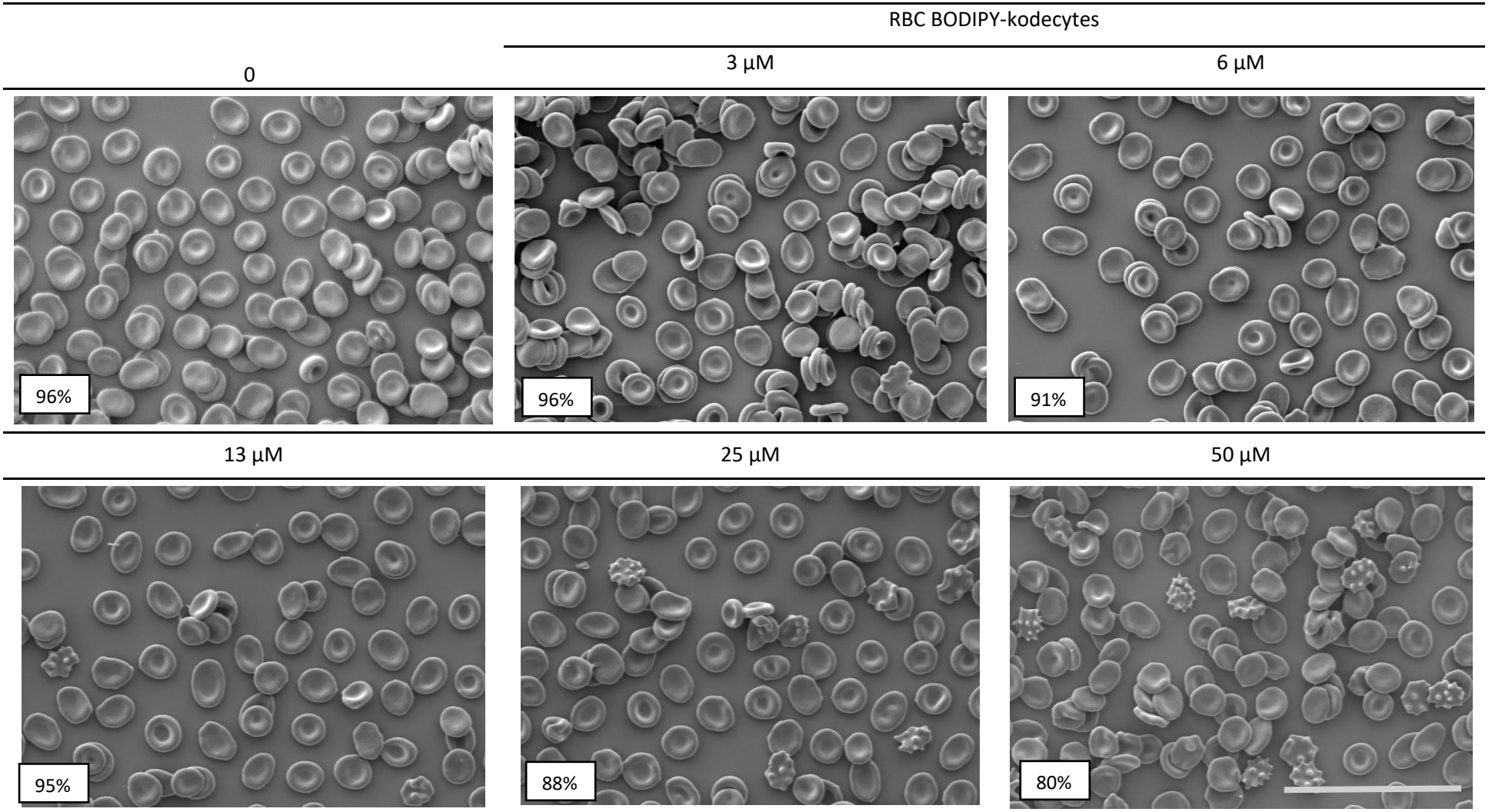

Figure 83: Example SEM micrograph of unkoded and 3-50µM BODIPY-kodecytes (scale bar = 30µm). The inset box on the left of each micrograph is the approximate % of normal cells. Note: Box % refers to the average observed for all experiments, not just the micrograph shown.

FSL-biotin

The standard procedure for detecting RBC biotin-kodecytes is by conjugation of Streptavidin, Alexa Fluor™ 488 conjugate (SAF488). Hence, it was essential to examine both the initial FSL-biotin labelling and the effect of the addition of the secondary label SAF488 on biotin-kodecytes. To do this, various controls were prepared by incubating unkoded cells (obtained by preincubation of RBC with CellStab at 37°C for 2 h) with and without 1 mg/mL of SAF488 conjugate for 30 minutes at RT in the dark. Simultaneously, 1, 13, and 50µM biotin-kodecytes (representing low, intermediate, and high concentrations) were incubated with 1 mg/mL of SAF488 conjugate and CellStab for 30 minutes at RT in the dark.

Figure 84 shows a comparative illustration of the SEM micrographs of unkoded cells, biotin-kodecytes, and subsequent secondary modification with SAF488 conjugate plus controls (without SAF488). From the results shown in Figure 85, it can be seen that adding SAF488 conjugate to unkoded cells and biotin-kodecytes only brings about small (<5%) changes to the respective unkoded cells and kodecytes. Therefore, it is concluded that the FSL-biotin must be responsible for most of the changes in the resulting kodecytes, and subsequent secondary treatment of these kodecytes with SAF488 conjugate only adds small additional (cumulative) modifications (predominantly of type I and II echinocytes). The data from various studies suggests that avidin binds to biotinylated membrane polyvalently [172,173]; therefore, it is possible that multipoint streptavidin attachment to FSL-biotin induces further rearrangement in the membrane.

Table 15 summarises the approximate % of normal cells found in unkoded cells and biotin-kodecytes after secondary treatment of these kodecytes with and without SAF488 conjugate. Table 15 also shows the change in the % of normal cells compared with unkoded cells that were not treated with (-) SAF488 and the change in the % of normal cells when treated with SAF488. This analysis was performed for both unkoded cells and 1-50 µM biotin-kodecytes. Table 16 lists the percentage of different grades of abnormal shapes for the experiment. From Table 15, it can be seen that additional modification by SAF488 increases the % of abnormal cells by approximately 5%.

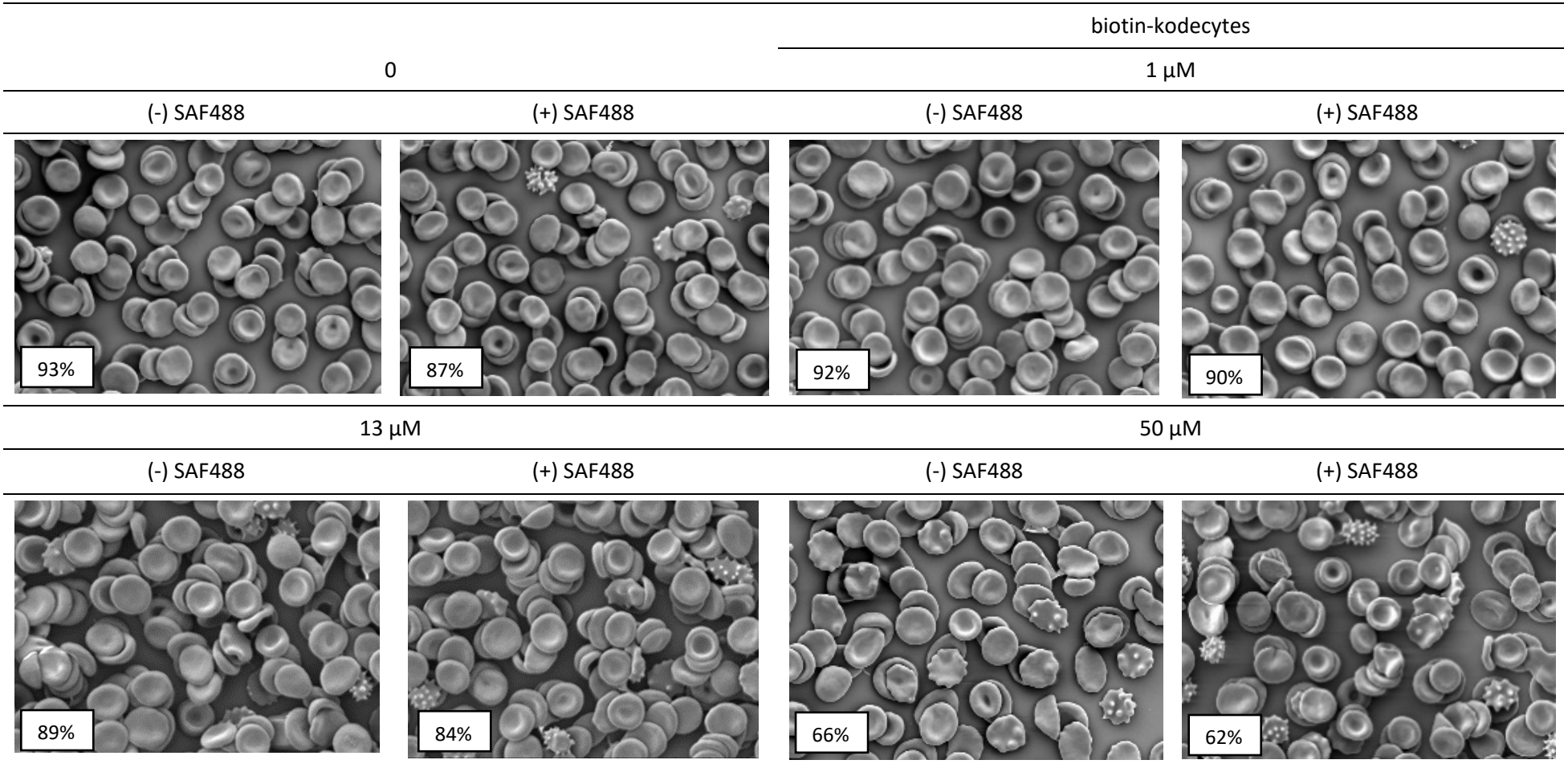

Figure 84: Testing the effect of the secondary label SAF488 on biotin-kodecytes. A comparative representation of SEM micrographs of 1-50µM biotin-kodecytes and unkoded (scale bar = 50µm) incubated with SAF488 conjugate plus control (without SAF488). The inset box on the left of each micrograph is the approximate % of normal cells. Note: Box % refers to the average observed for all experiments, not just the micrograph shown.

From the data shown (Tables 15 and 16), it is concluded that more abnormal cells result when RBCs are transformed with FSL-biotin at higher concentrations, and subsequent SAF488 treatment only brings about minor additional changes.

Table 15: The effect of the secondary label SAF488 on biotin-kodecytes (part 1). Unkoded cells and 1-50 µM biotin-kodecytes incubated with (+) and without (-) SAF488 conjugate, categorised by shape, cells are graded on the basis of nomenclature of Bessis. Results are shown as a percentage. The change in the % of normal cells from unkoded cells without (-) SAF488 is shown. Change in the % of normal cells in the presence of SAF488 for unkoded cells and 1- 50 µM biotin-kodecytes is also shown.

			biotin-kodecytes					
	0		1 µM		13 µM		50 µM	
Cell type	SAF488		SAF488		SAF488		SAF488	
	(-)	(+)	(-)	(+)	(-)	(+)	(-)	(+)
D (%)	93	87	92	90	89	84	66	62
Δ from (-) SAF488 unkoded cells (%)		6	1	3	6	9	27	31
Δ from (-) and (+) SAF488 (%)		6		2		3		4

Table 16: The effect of the secondary label SAF488 on biotin-kodecytes (part 2). The percentage of different grades of abnormal shapes for analysing the effect of the addition of the secondary label SAF488 on biotin-kodecytes.

			biotin-kodecytes					
	0		1 µM		13 µM		50 µM	
Cell type (%)	SAF488		SAF488		SAF488		SAF488	
	(-)	(+)	(-)	(+)	(-)	(+)	(-)	(+)
EI	3	8	3	3	5	5	13	15
EII	2	3	1	4	5	4	14	17
EIII	0	1	2	2	1	5	5	3
SEI	1	1	0	1	0	2	1	1
S	1	0	1	0	0	0	1	2

Following the initial analysis measuring the effect of the secondary labelling of SAF488 conjugate on biotin-kodecytes, a more comprehensive range of concentrations (0, 3, 6, 13, 25, and 50µM) of biotin+SAF488 kodecytes were tested for evidence of when the concentration-dependent morphological changes occur. There was no major change in the shape of biotin+SAF488 kodecytes up to 25 µM, but at 50 µM, morphology changed from discocytes to echinocytes (Figure 85).

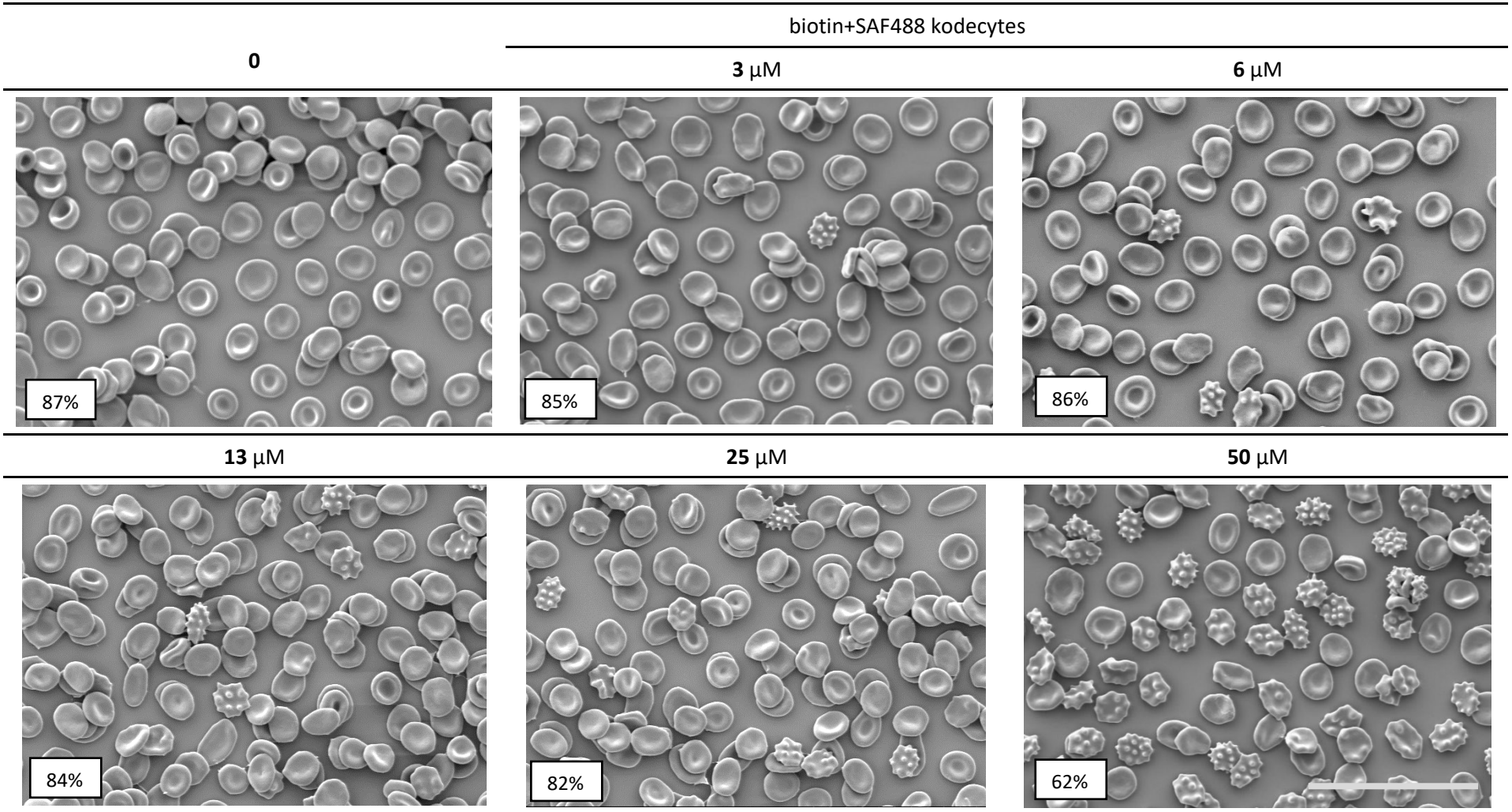

Figure 85: Example SEM micrograph of 3-50μM biotin+SAF488 kodecytes and unkoded cells (scale bar = 30μm). The inset box on the left of each micrograph is the approximate % of normal cells. Note: Box % relates to the average observed for all experiments, not just the micrograph shown.

In summary, the data in Table 17 (and Figures 81, 82, 83, and 85) show that an FSL concentration-dependent changes in kodecyte morphology is observed, and are most noticeable for FSL-FLRO4, followed by FSL-biotin. Although BODIPY-kodecytes did show concentration-dependent morphological changes at higher concentrations (e.g., 50 µM), they appeared relatively minor when compared to unkoded cells.

Table 17: Summary of shapes of different RBC kodecytes and unkoded cells counted, categorised and graded based on the nomenclature of Bessis. The results are shown as percentages.

		µM FLRO4-kodecytes					µM BODIPY-kodecytes					biotin+SAF488 kodecytes				
Stage	**0**	**3**	**6**	**13**	**25**	**50**	**3**	**6**	**13**	**25**	**50**	**3**	**6**	**13**	**25**	**50**
D	96	95	93	80	74	41	96	91	95	88	80	85	86	84	82	62
EI	2	2	3	8	10	15	2	4	2	6	9	3	4	5	6	12
EII	0	2	2	6	8	22	1	2	1	4	7	5	4	4	7	14
EIII	1	1	1	4	6	18	0	1	0	0	2	2	1	5	4	5
SEI	0	0	0	1	0	1	0	1	0	0	1	2	2	2	0	3
SEII	0	0	0	0	1	1	0	0	1	0	0	2	2	0	0	2
S	1	0	1	1	1	2	1	1	0	2	1	1	1	0	1	2

The following conclusion could be deduced from the SEM analysis of RBCs kodecytes post-labelling with different FSL constructs.

- FLRO4-kodecytes prepared from d15 stored RBC had more changes in their morphology than when kodecytes were prepared with d0 RBCs.
- RBC transformation with a concentration of >13µM FSL-FLRO4 resulted in a change in morphology from predominantly discocytes to an increasing percentage of type I-III echinocytes.
- BODIPY-kodecytes did not show any substantial concentration-dependent morphological changes compared with unkoded cells.
- The transformation of RBCs with FSL-biotin causes change in the resulting kodecytes as well. The secondary treatment of biotin-kodecytes with SAF488 conjugate adds a small but cumulative alteration (<5%), i.e., FSL-biotin brings major changes, and subsequent SAF488 treatment brings minor changes.
- With respect to changes in the shape of unkoded cells, concentration- dependent change in kodecyte morphology was observed. It was most noticeable for FSL-FLRO4, followed by FSL-biotin.

6.1.3 Time-dependent effect

A time course uptake study and subsequent SEM analysis were set up to determine the effect of different koding times on RBC/kodecytes morphology at 37°C. For this, RBCs were incubated with FSL constructs at 37°C for up to 24 h. Kodecytes and unkoded samples were aliquoted at the respective times and prepared for SEM analysis (Table 18). Morphological changes in kodecytes were compared to unkoded cells. For information regarding characterising the diameter of kodecytes and unkoded cells, refer to Section 6.1.

Table 18: Time-course uptake study and subsequent SEM analysis of kodecytes and unkoded cells at 37°C over a period of 24 h.

FSL constructs	Concentration (µM)	SEM analysis (h)
FSL-FLRO4	0, 6, 25, 50	0, 0.5, 1, 2, 3, 4, 6, 24
FSL-BODIPY	0, 6, 25	0, 0.25, 0.5, 1, 2, 4, 24
FSL-biotin	0, 6, 25	0, 0.25, 0.5, 1, 2, 4, 24

FSL-FLRO4

Figure 86 shows the effect of FSL-FLRO4 uptake on the resulting kodecyte morphology over an increasing incubation time. Only representative time points (0 h, 2 h, and 24 h) showing apparent changes in the kodecyte morphology are shown.

The following conclusions were drawn from the experimental data (Figure 86). Firstly, incubation of RBCs without FSL constructs results in approximately 2% abnormal cells at 2 h and approximately 80% at 24 h. Secondly, as the koding period increases from 0 h to 2 h, kodecytes morphology changes from discocytes to an increasing percentage of type I-III echinocytes. This observation was clearly seen for 25 and 50 µM FLRO4-kodecytes. Post 2 h incubation, a transformation in shape from discocytes and echinocytes to stomatocytes was observed. At 24 h, kodecytes were found to have few discocytes (<15%) and more type I and II stomatocytes (>85%), i.e., during the course of the incubation duration, kodecytes showed a gradual transformation from standard biconcave shape to echinocytes (irregularly contoured discocytes with spicules of varying degree; from 0-2 h) to stomatocytes, which are smaller, more normal-looking cup-shaped red cells with a thicker rim and a varying degree of central depression.

Based on the results shown in Figure 86 and Table 19, it could be proposed that although extended koding duration at 37°C induces shape change in the kodecytes, at 24 h, unkoded cells were also shown to have a nearly similar morphology as FLRO4-kodecytes. This time-dependent morphology change, essentially post-2 h, could be proposed because of prolonged incubation at 37°C rather than the effect of FSL.

During the 0–4 h koding duration, the appearance of spiculated or crenated red cells or echinocytes could be an indirect sign of the transformation or koding of cells with FSL- FLRO4, as seen in the case of certain amphiphiles incubated with red cells[174,175]. Additionally, one of the most important observations from this aspect of the study is the time-dependent reversible transformation of RBC FLRO4-kodecytes from discocytes to echinocytes to a combination of abundant stomatocytes.

The average diameter of unkoded cells and 6–50 µM FLRO4-kodecytes prepared during different koding durations at 37°C was also measured. The unmodified cells started at approximately 7 µm and gradually decreased in diameter to approximately 5 µm. Irrespective of koding time, compared to unkoded cells, there was no considerable difference in the average diameter (Figure 87) of kodecytes. A two-way ANOVA with Tukey's multiple comparison test was used to investigate the statistical significance of the result that, when compared to unkoded cells, there was no significant difference in the average diameter of kodecytes between the various koding durations. The statistical study revealed no significant variation in the average diameter of kodecytes generated at varied koding times when compared to unkoded cells. This was observed across all tested FSL-FLRO4 concentrations.

A decrease in the diameter of FLRO4-kodecytes is probably the result of the conversion of echinocytes to stomatocytes, and the natural effect of becoming smaller is what causes echinocytes to become more normal-looking stomatocytes. Additionally, as the unkoded cells became smaller in diameter with increasing incubation duration at 37°C, the effect seen was due to incubation at 37°C, not FSL modification.

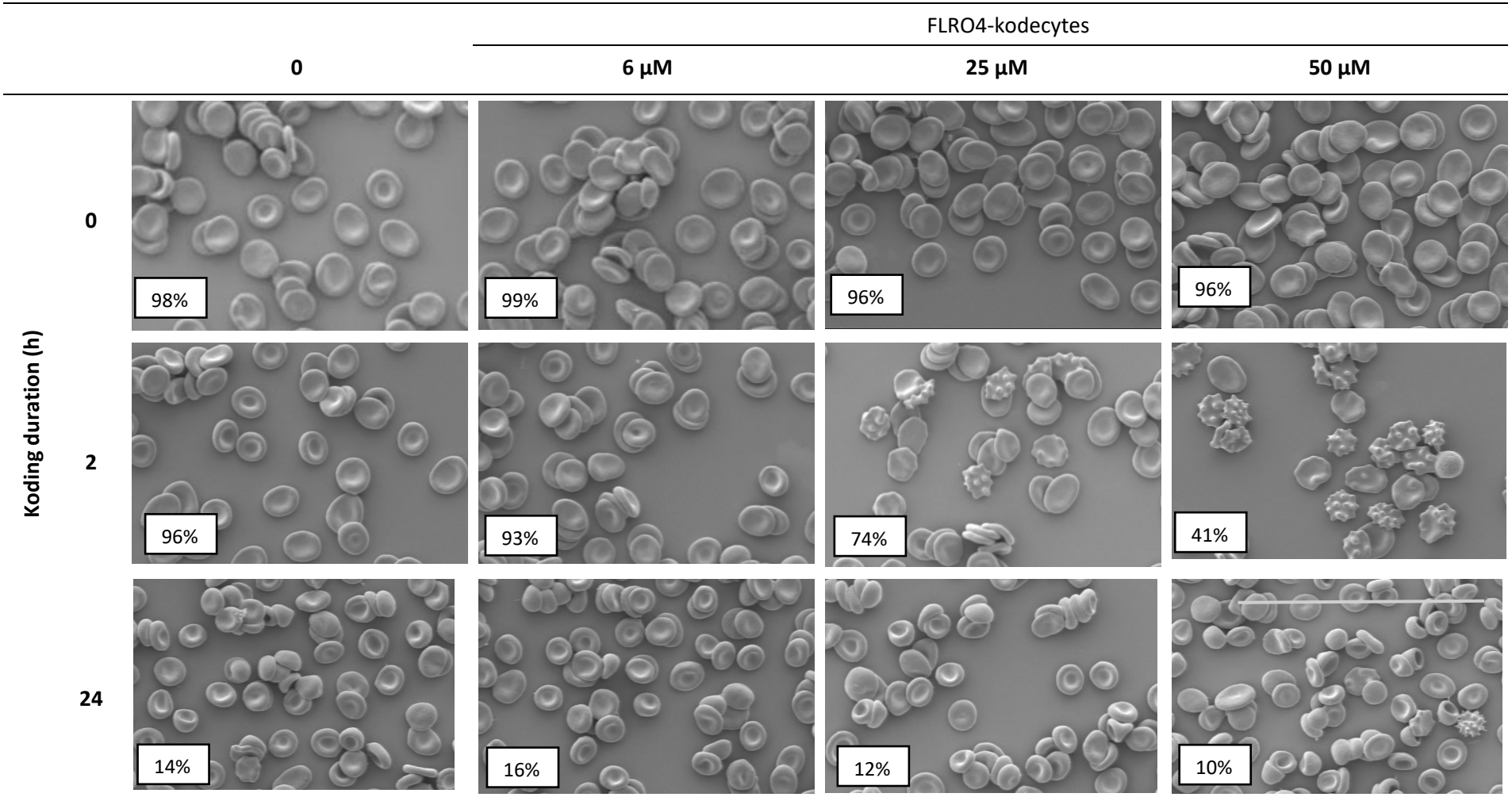

Figure 86: RBC FLRO4-kodecytes SEM micrograph and effect of koding duration. Example SEM micrograph of unkoded cells and 6–50µM FLRO4-kodecytes showing the effect of different koding duration at 37°C (scale bar = 50µm). SEM micrographs are shown only at 0, 2, and 24 h. The inset box on the left of each micrograph is the approximate percentage of normal cells. Note: Box % refers to the average observed for all experiments, not just the micrograph shown.

Table 19: Effect of koding duration on RBC FLRO4-kodecytes (from SEM micrograph). Summary of the effect of different koding durations on the morphology of RBC FLRO4- kodecytes and unkoded cells at 37°C. The results are shown as a percentage of normal cells.

	Koding duration (h)											
	0				2				24			
		FLRO4-kodecytes (µM)				FLRO4-kodecytes (µM)				FLRO4-kodecytes (µM)		
stage	0	6	25	50	0	6	25	50	0	6	25	50
D	98	99	96	96	96	93	74	41	14	16	12	8
EI	1	0	2	1	2	3	10	15	3	4	3	2
EII	1	1	2	3	0	2	8	22	6	5	2	5
EIII	0	0	0	0	1	1	6	18	0	0	0	0
SEI	0	0	0	0	0	0	0	1	0	0	0	0
SEII	0	0	0	0	0	0	1	1	0	0	0	0
S	0	0	0	0	1	1	1	2	77	75	83	85

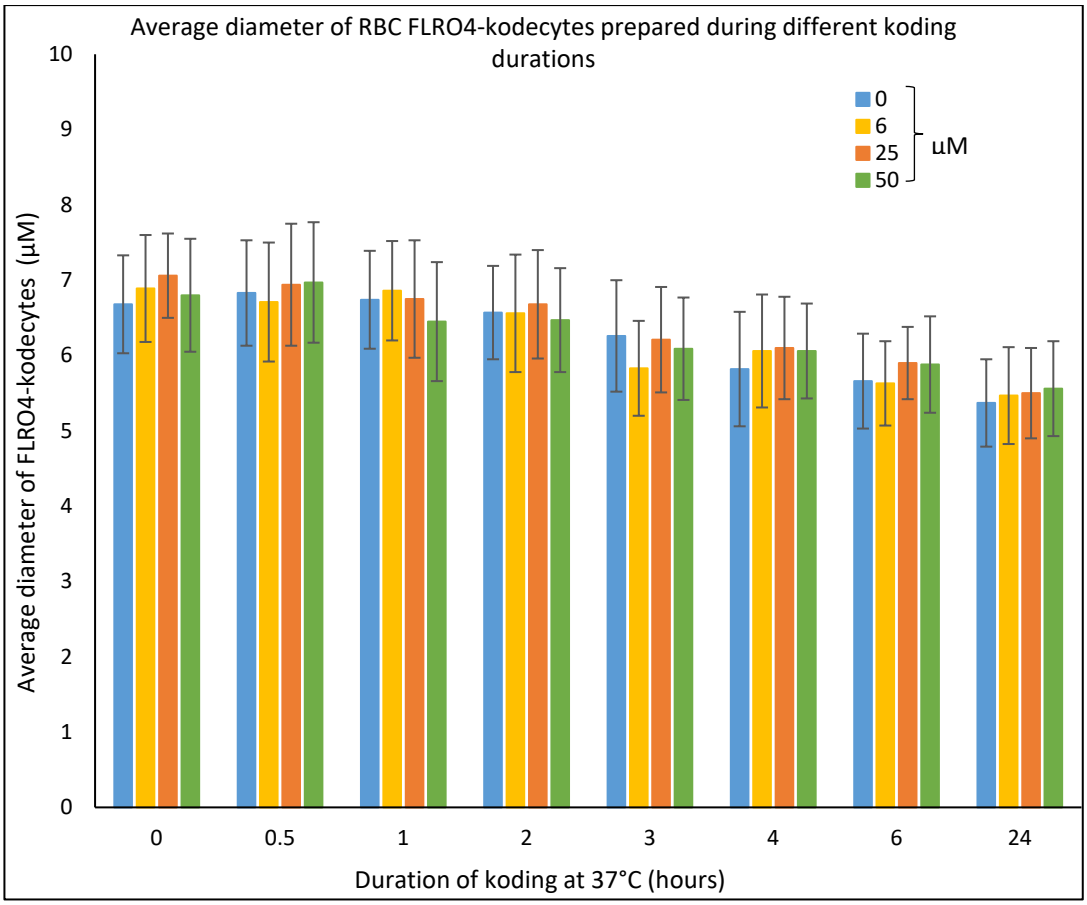

Figure 87: SEM analysis of the average diameter of RBC FLRO4-kodecytes prepared at 37°C during different koding durations. RBCs were incubated with 0, 6, 25 and 50 µM of FSL-FLRO4 for 0, 0.5, 1, 2, 3, 4, 6 and 24 hours.

FSL-BODIPY

Figure 88 shows the SEM micrographs of FSL-BODIPY uptake on the resulting kodecyte morphology during different koding durations at 37°C. SEM micrographs from all the studied time points are not shown; only representative time points (0 h, 2 h, and 24 h) showing apparent changes in the kodecyte morphology are shown in Figure 88. The following conclusions were drawn from the SEM micrograph: FSL-BODIPY does not cause any major shape alteration post 2 h incubation at 37°C, but at 24 h, a combination of stomatocytes, echinocytes, and discocytes were observed (Table 20). The occurrence of approximately 20–25% echinocytes post-24-h incubation is in contrast to FLRO4- kodecytes. Unkoded cells showed a similar trend, except for the absence of any considerable number of echinocytes post-24-h incubation at 37°C.

Table 20: Effect of koding duration on RBC BODIPY-kodecytes (from SEM micrograph). Summary of the effect of different koding durations on the morphology of RBC BODIPY- kodecytes and unkoded cells at 37°C. The results are shown as a percentage of cells.

	Koding duration (h)								
	0			2			24		
		BODIPY- kodecyte (μM)			BODIPY- kodecyte (μM)			BODIPY- kodecyte (μM)	
stage	0	6	25	0	6	25	0	6	25
D	98	94	92	96	91	88	14	9	12
EI	1	3	6	2	4	6	3	10	6
EII	1	2	2	1	2	4	6	13	12
EIII	0	1	0	0	1	0	0	9	12
SEI	0	0	0	0	1	0	0	0	0
SEII	0	0	0	0	0	0	0	0	0
S	0	0	0	1	1	2	77	59	58

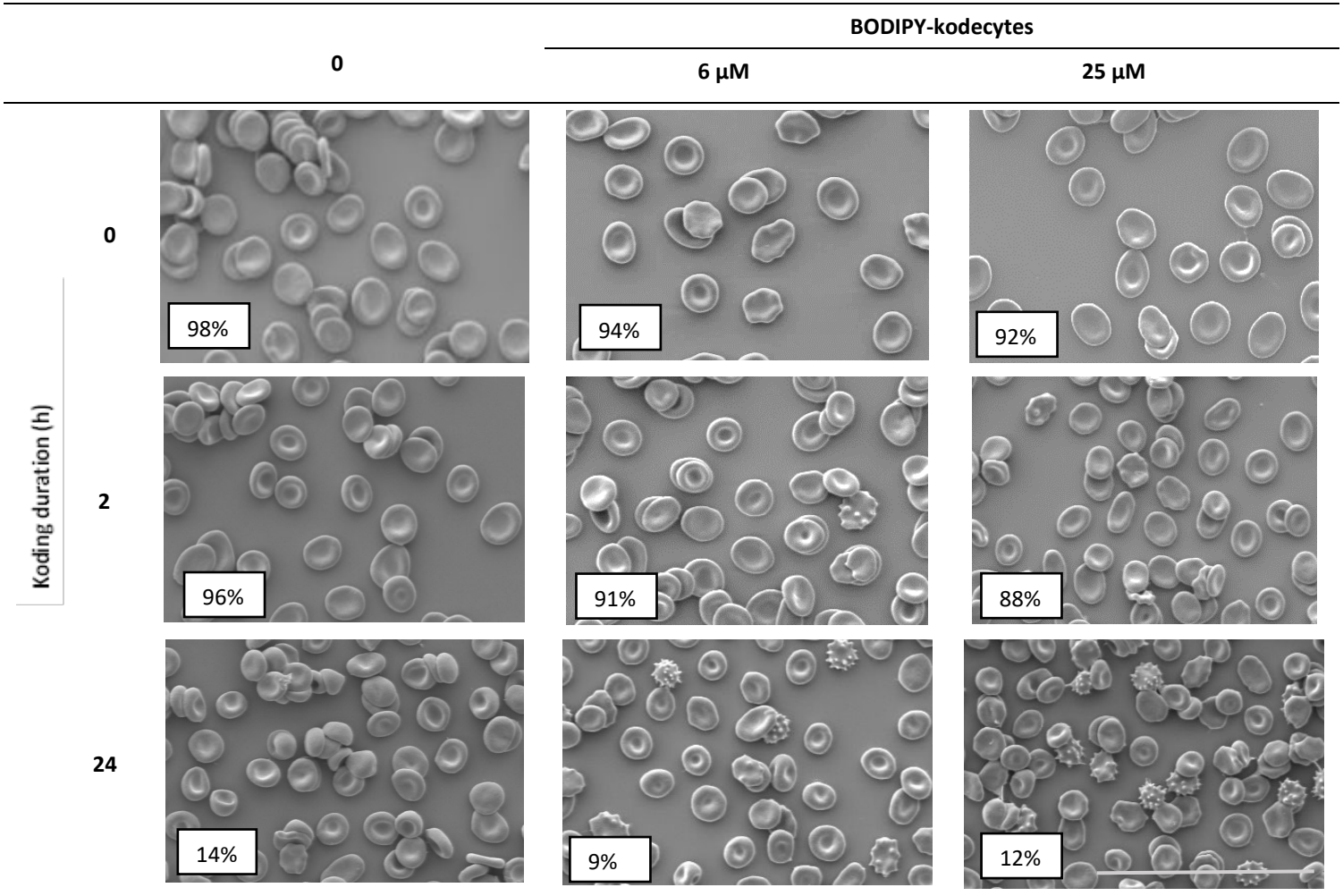

Figure 88: RBC BODIPY-kodecytes SEM micrograph and effect of koding duration. Example SEM micrograph of 6, 25µM BODIPY-kodecytes and unkoded cells, showing the effect of different koding durations at 37°C (scale bar = 50µm). SEM micrographs are shown only at 0, 2, and 24 h. The inset box on the left of each micrograph is the approximate % of normal cells. Note: Box % refers to the average observed for all experiments, not just the micrograph shown.

Figure 89 shows the average diameter of unkoded cells and 6, 25 µM BODIPY-kodecytes prepared during different koding durations at 37°C. Initially (i.e., at 0 h), the unmodified cells were approximately 7 µm in diameter, and after 24 h of koding, they were reduced to 5 µm. Simultaneously, the average diameter of BODIPY-kodecytes decreased at the same rate. The overall results imply that the decrease in average diameter of kodecytes and unkoded cells is related to prolonged incubation at 37°C rather than the FSL koding process. A two-way ANOVA with Tukey's multiple comparison test was used to investigate the statistical significance of the result that, when compared to unkoded cells, there was no significant difference in the average diameter of BODIPY-kodecytes between the various koding durations. The statistical study revealed no significant variation in the average diameter of kodecytes generated at varied koding times when compared to unkoded cells. This was observed across all tested FSL-BODIPY concentrations.

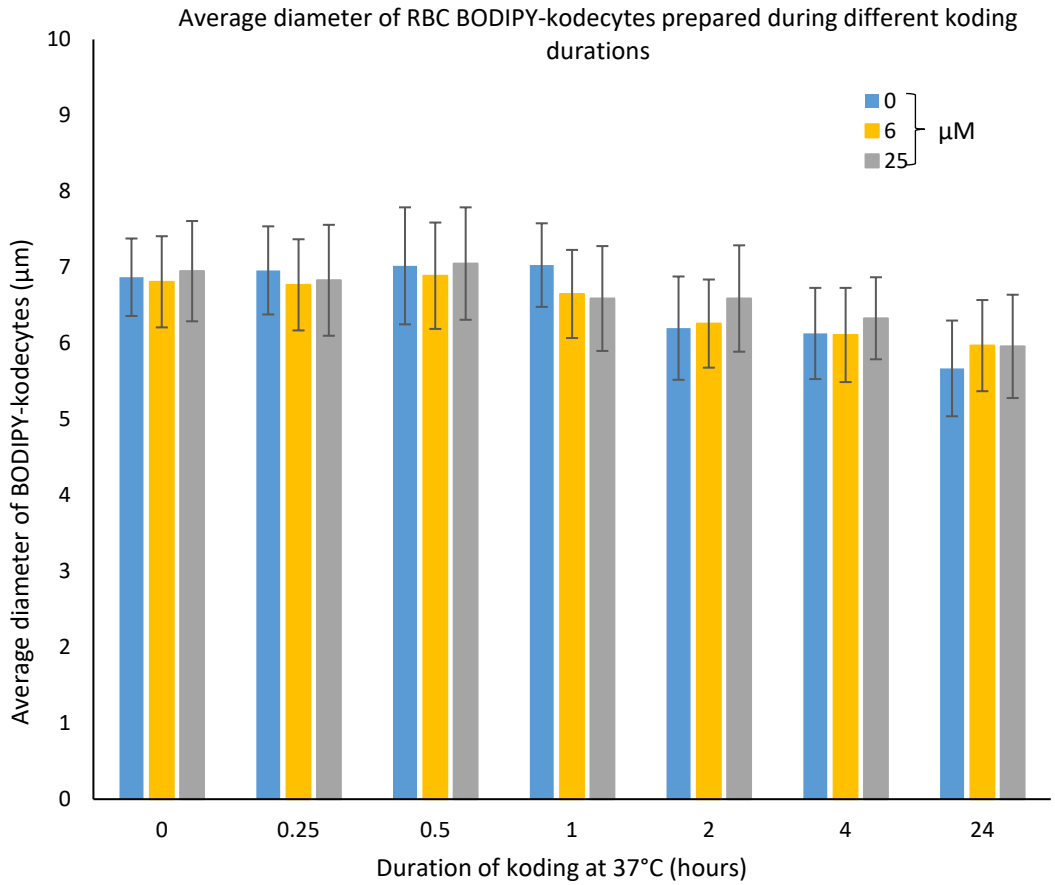

Figure 89: SEM analysis of average diameter of RBC BODIPY-kodecytes prepared during different koding duration at 37°C. RBCs were incubated with 0, 6, and 25 µM of FSL-BODIPY for 0, 0.25, 0.5, 1, 2, 4, and 24 hours.

FSL-biotin

SEM micrographs in Figure 90 show the effect of FSL-biotin uptake and subsequent secondary modification by SAF488 on the resulting biotin+SAF488 kodecytes. RBCs were incubated with (and without) FSL-biotin at 37°C for up to 24 h, followed by secondary modification with SAF488 conjugate. Only representative time points (0 h, 2 h, and 24 h) showing apparent changes in the kodecyte morphology are shown. From Figure 91 (and Table 21), it could be summarised that, with respect to unkoded RBCs, FSL-biotin did not seem to induce any major shape alteration during 2 h of incubation at 37°C. At 24 h, stomatocytes (>50%) along with echinocytes (>20%) and discocytes (<25%) populations were seen. The presence of echinocytes after 24 h of incubation at 37°C was also observed for BODIPY-kodecytes, but not in the case of FLRO4-kodecytes. Additionally, at 24 h, the SEM micrograph of unkoded cells modified with SAF488 showed similar trends and proportions of different cell shapes.

Table 21: Effect of koding duration on RBC biotin+SAF488-kodecytes (from SEM micrograph). Summary of the effect of koding durations on biotin+SAF488-kodecytes and unkoded cells at 37°C. The results are shown as a percentage of cells.

	Koding duration (h)								
	0 h			**2 h**			**24 h**		
	+SAF488								
		biotin kodecytes (µM)			**biotin kodecytes (µM)**			**biotin kodecytes (µM)**	
stage	**0**	**6**	**25**	**0**	**6**	**25**	**0**	**6**	**25**
D	90	90	89	87	86	82	25	14	11
EI	3	2	2	4	4	5	8	13	11
EII	2	4	4	3	4	7	15	12	12
EIII	2	1	1	2	1	4	0	4	8
SEI	1	2	1	2	2	0	0	2	0
SEII	1	0	2	1	2	0	0	0	0
S	1	1	1	1	1	1	52	55	58

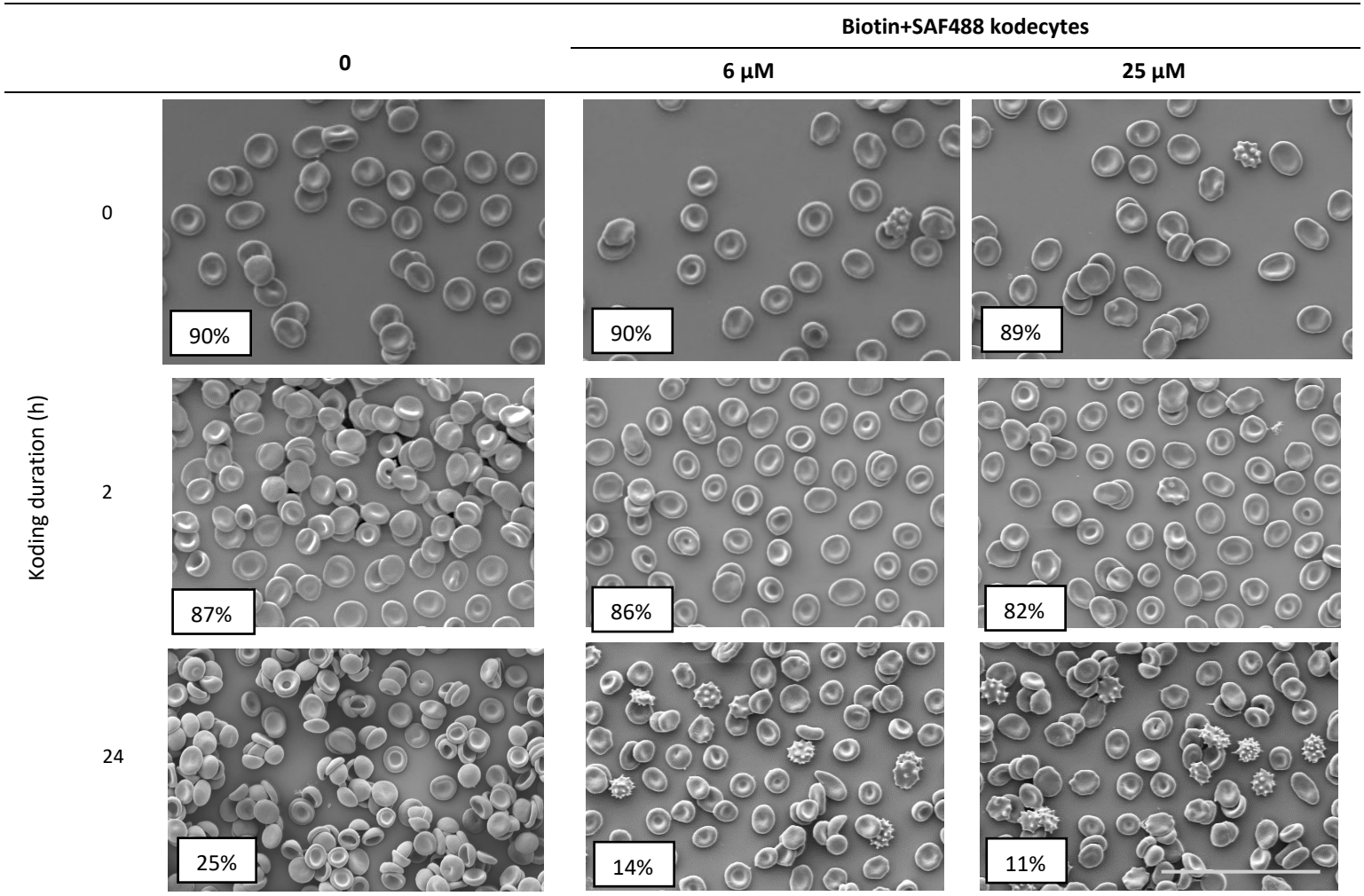

Figure 90: RBC biotin-kodecytes SEM micrograph and effect of koding duration. Example SEM micrograph of unkoded cells and 6, 25µM biotin+SAF488 kodecytes, showing the effect of different koding times at 37°C (scale bar = 50µm). SEM micrographs are shown only at 0, 2, and 24 h. The inset box on the left of each micrograph is the approximate percentage of normal cells. Note: Box % refers to the average observed for all experiments, not just the micrograph shown.

Figure 91 shows the average diameter of unkoded cells and 6, 25 µM biotin+488 kodecytes prepared during different koding durations at 37°C. As the koding duration increased, the average diameter of unmodified cells and biotin+SAF488 kodecytes decreased gradually. For example, immediately after koding, the average diameter was found to be approximately 7, which changed to nearly 5 µm during 24 hours of koding. A two-way ANOVA with Tukey's multiple comparison test was used to examine the statistical significance of the observation that compared to unkoded cells, there was no considerable difference in the average diameter of biotin+488 kodecytes at respective koding time. The statistical analysis revealed that there was no significant difference in the average diameter of kodecytes formed at different koding times with respect to unkoded cells. This was found to be true across tested concentrations of FSL-biotin.

Overall, the data in Figures 87, 89, and 91 show that regardless of the FSL used to prepare kodecytes, the average diameter of kodecytes and unkoded cells decreases with an increase in koding duration. This indicates that the decrease in the average diameter of kodecytes and unkoded cells was due to prolonged incubation at 37°C rather than the effect of FSL or FSL koding process. This observation was also verified by statistical analysis. A two-way ANOVA with Tukey's multiple comparison test was performed to determine the statistical significance of the observation that, when compared to unkoded cells, there was no significant difference in the average diameter of kodecytes generated with varied FSL at different koding periods. The statistical study revealed no significant variation in the average diameter of kodecytes prepared from different FSL generated at different koding times when compared to unkoded cells. This was found to be true across tested concentrations of FSL.

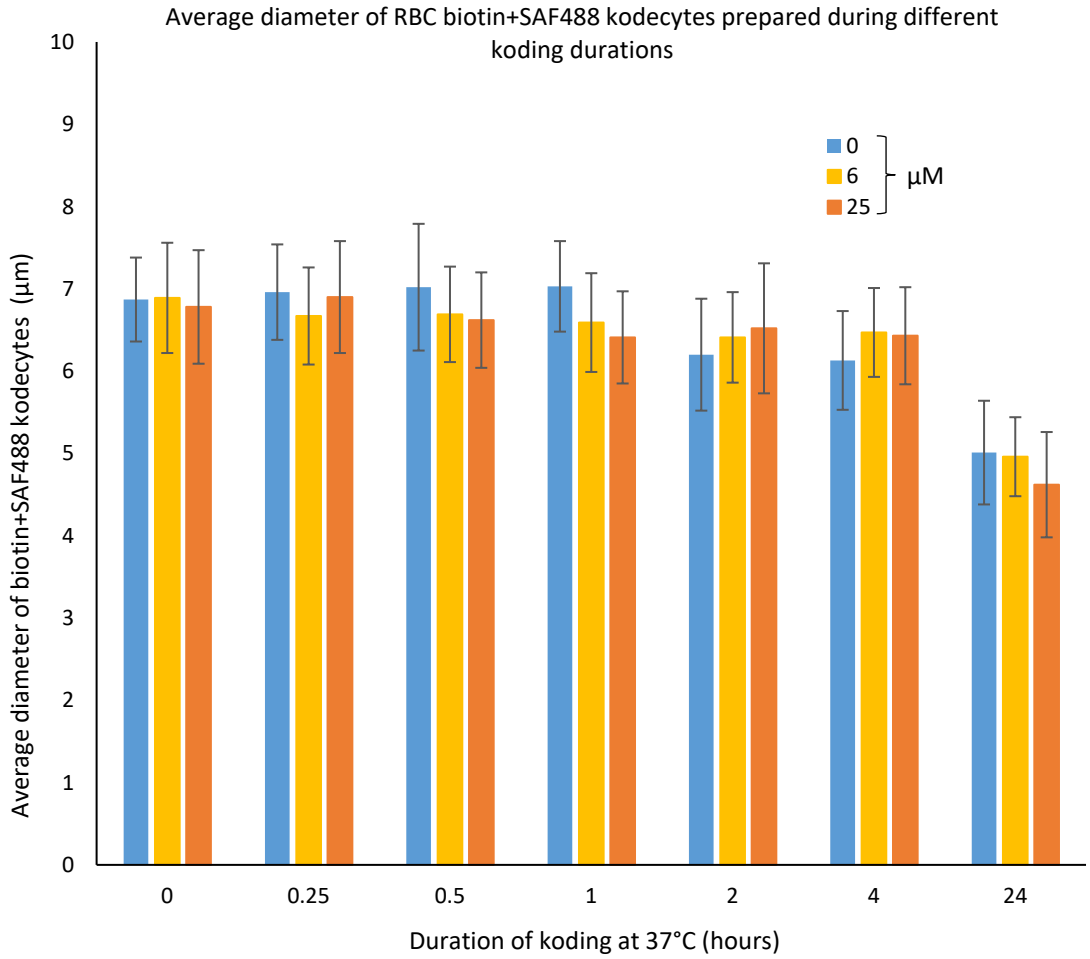

Figure 91: SEM analysis of average diameter of RBC biotin+SAF488-kodecytes prepared during different koding duration at 37°C. RBCs were incubated with 0, 6, and 25 µM of FSL-biotin for 0, 0.25, 0.5, 1, 2, 4, and 24 h.

6.2 SEM analysis of Jurkat kodecytes

6.2.1 Effect of uptake of different FSL constructs and concentrations.

SEM was used to examine the morphological characteristics of Jurkat kodecytes post-labelling with different FSL constructs, as examined with RBC kodecytes. The results shown in Figure 92 show the SEM micrographs of Jurkat FLRO4, BODIPY, and biotin+SAF488 kodecytes formed after 2 h of incubation of FSL constructs with Jurkat cells at 37°C. Two types of unkoded cells were also analysed and are represented in Figure 92: one batch of unkoded cells was prepared by incubating Jurkat cells in serum-free media, and the other batch of unkoded cells was obtained by subsequent secondary incubation of unkoded Jurkat cells with 1 mg/mL SAF488. The second batch of unkoded cells accounts for any structural changes due to the SAF488 conjugate.

The SEM micrographs in Figure 92 show Jurkat kodecyte morphology at different concentrations of FSL constructs. The micrographs showed that FLRO4 and BODIPY kodecytes and unkoded cells mostly display a round or spherical morphology with even cell surfaces without any noticeable breakage, indicating preserved cell morphology. This was found to be the same across all tested concentrations. Hence, it was concluded that there is no observable difference between unkoded cells and kodecytes at 6– 50 μM.

Jurkat biotin+SAF488 kodecytes and SAF488-modified unkoded cells appear more flattened than unkoded cells and FLRO4 and BODIPY-kodecytes. A SEM micrograph of biotin-kodecytes showed a nearly rounded morphology at a lower concentration. However, at a higher concentration of 50 μM, rounded morphology started to flatten out but was not very significant (data not shown for FSL-biotin only). Hence, this flattened morphology could be argued to be a result of either SAF488 conjugation, FSL-biotin modification itself, or both. Thus, it could be proposed that both FSL-biotin uptake and SAF488 secondary conjugation may be playing a part (in tandem or cooperative action) in bringing about the flattened morphology of Jurkat biotin+SAF488 kodecytes.

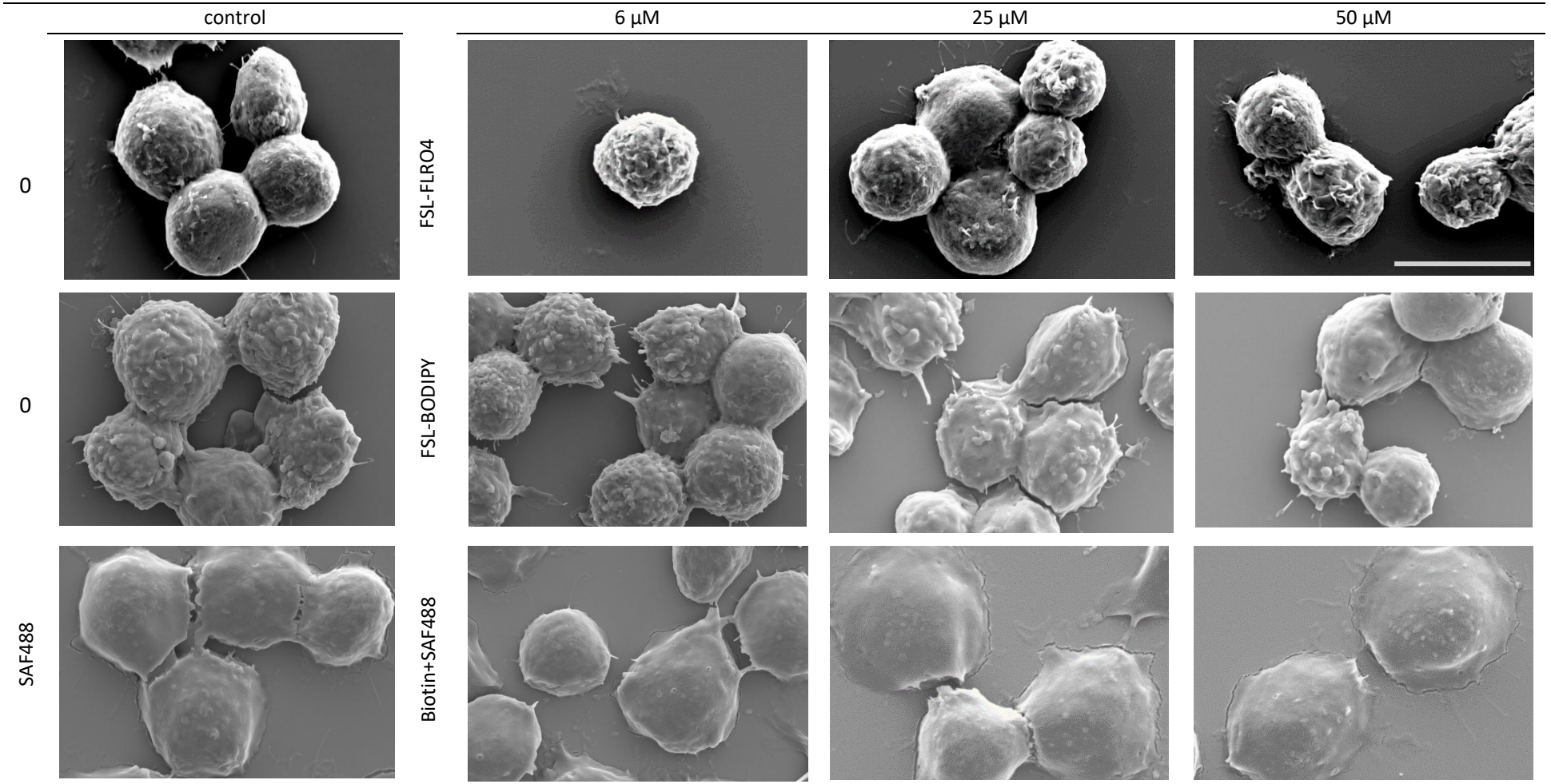

Figure 92: SEM micrographs analysis of Jurkat kodecytes (FLRO4, BODIPY, and biotin+SAF488 kodecytes) formed after 2 h of koding duration at 37°C. SEM micrographs of unkoded Jurkat cells and subsequent secondary modification with SAF488 conjugate (controls) were also analysed (unkoded cells and kodecytes scale bar = 10µm).

Figure 93 shows the change in average diameter of Jurkat kodecytes prepared after 2 h of koding with FSL-FLRO4, FSL-BODIPY, and FSL-biotin at 37°C. The respective kodecytes were measured and compared with those of unkoded cells. FLRO4 and BODIPY- kodecytes average diameter changed marginally (<5%) compared to unkoded cells. In the case of 25 and 50 µM BODIPY kodecytes, the average size changed only by <2% and is similar to unkoded cells. Jurkat biotin+SAF488 kodecytes show an increase in the average diameter with increasing concentrations. For example, 25-50 µM biotin+SAF488 kodecytes became approximately 15% larger in diameter compared to SAF488-modified unkoded cells (statistically significant). However, this increase in size appears to be due to the flattening and not enlarging of the biotin+SAF488 kodecytes. Overall, it can be concluded that (except for biotin+SAF488 kodecytes), the koding process had no negative impact on the morphology of the resulting kodecytes.

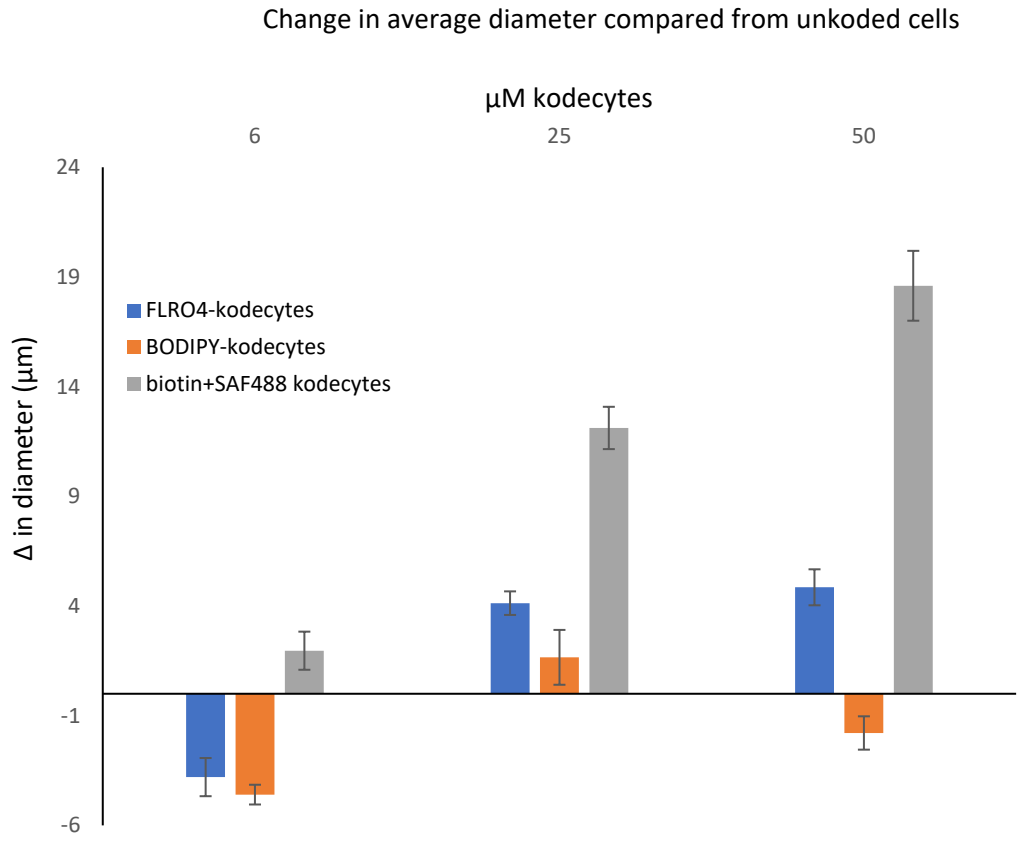

Figure 93: Change in kodecytes diameter with respect to unkoded cells. Difference in average diameter of Jurkat FLRO4 and BODIPY-kodecytes were compared to unkoded cells. For biotin+SAF488-kodecytes, difference in average diameter was compared to SAF488-modified unkoded cells after 2 h of incubation with the respective FSL construct at 37°C.

Summary

The following conclusion could be drawn from the SEM micrographs of RBCs and Jurkat kodecytes post-labelling with FSL constructs.

- FLRO4-kodecytes prepared from d15-stored RBCs had more changes in their morphology than when kodecytes were prepared with d0 RBCs. Based on the results obtained, it was decided to use RBC no older than 15 days of storage at 4°C for making kodecytes. This would help ensure reliable and reproducible results by minimising experimental variables.
- RBC transformation with a concentration of >13µM FSL-FLRO4 resulted in a change in morphology from predominantly discocytes (stage 0) to an increasing percentage of stage 1–3 echinocytes. However, there was no observable difference between unkoded cells and Jurkat kodecytes morphology prepared from 3–13 µM.
- RBC BODIPY-kodecytes did not show any substantial concentration-dependent (3–25 µM) morphological changes compared with unkoded cells. However, 50µM BODIPY kodecytes showed an increasing percentage of stage 1–3 echinocytes.
- Compared to other kodecytes, the transformation of RBCs with FSL-biotin causes intermediate change in the resulting kodecytes (more than FSL-BODIPY and less than FSL-FLRO4). The secondary treatment of biotin-kodecytes with SAF488 conjugate adds cumulative modification (<5%), i.e., FSL- biotin brings major changes, and subsequent SAF488 treatment brings minor changes.
- One more interesting observation from the extended (0–24 h) incubation study at 37°C is the time-dependent reversible transformation of RBC kodecytes from discocytes to echinocytes to a combination of abundant stomatocytes.
- Additionally, the unkoded cells and kodecytes became smaller in diameter with increasing incubation duration at 37°C. These consequences observed were due to simple incubation at 37°C rather than the extended koding process (duration) with FSL constructs.

6.3 Viability of Jurkat and PC-3 kodecytes

Overview: This aspect of the study aimed to measure the impact of FSL uptake on Jurkat and PC-3 kodecyte viability under different koding conditions. Three assays were chosen to examine the cytotoxic profile of FSL constructs: Trypan blue cell exclusion assay, Muse™ Count & Viability assay, and MTT cell proliferation assay. The Trypan blue and Muse™ Count and Viability assays determine cell viability by considering the integrity of the cellular membrane. In contrast, the MTT assay measures cellular metabolism and, in turn, the proliferation status of the cells. It is important to note that these assays are based on different methodologies; Trypan blue assay uses a manual hemocytometer, while the Muse™ Count & Viability assay uses a Muse™ Cell Analyzer (a cytometry-based instrumentation), and the MTT assay uses spectrophotometry.

6.3.1 Trypan blue cell exclusion assay

The Trypan blue cell exclusion assay is based on the principle that Trypan blue solution selectively stains dead cells blue; hence, it is helpful in the differentiation and counting of the cells and estimating cell death. A schematic overview of the methodology for testing the Jurkat kodecyte viability under different conditions is presented in Figure 94, followed by the experimental protocol.

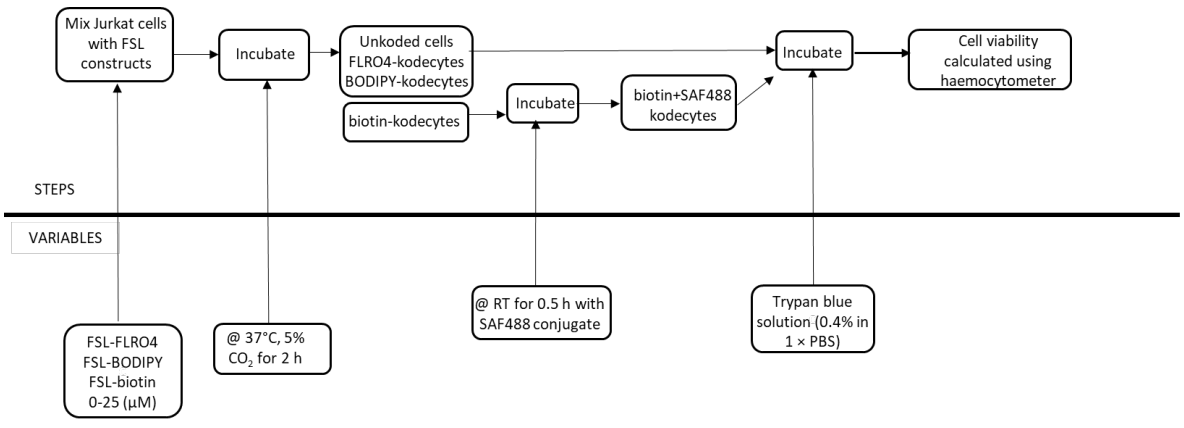

Figure 94: Schematic overview of method testing the viability of Jurkat kodecyte by Trypan blue cell exclusion assay under different koding variables and conditions.

- Jurkat cells were incubated with different concentrations of FSL for 2 h at 37 °C (in serum-free koding solution). Control or unkoded cells were also prepared simultaneously. From this stage onwards, unkoded cells were subjected to the same treatment as kodecytes.
- After a 2 h incubation, kodecytes were washed and resuspended in RPMI medium. An equal volume of kodecytes was added to an equal volume of trypan blue solution (0.4% in 1× PBS) and mixed well.
- 10 µL of this mixture was loaded into the V-shaped groove of the hemocytometer counting chamber.
- The hemocytometer was placed in the inverted microscope under a 10× objective, and unstained (viable) and stained (non-viable) cells were counted separately within each of the four large quadrants of the hemocytometer and then averaged. The total number of viable cells/mL, total number of cells/mL, and cell viability were determined using the following formulas:

Viable cells/mL = Average number of viable cells × 2 (dilution factor) × 10^4

Total cells/mL = Average number of viable and non-viable cells × 2 (dilution factor) × 10^4

Cell viability (%) = (total viable cells (unstained) /total cells (unstained and stained)) ×100

Effect of primary FSLs used in this study on Jurkat kodecytes viability

Figure 95 shows the difference in viability of FLRO4, BODIPY, and biotin+SAF488 kodecytes from unkoded cells. For this, Jurkat cells were incubated with and without FSL constructs (0–25 µM) for 2 h at 37°C. Here, kodecyte viability obtained at respective concentrations has been compared to controls, i.e., unkoded cells (indicated in %). From the data, it could be seen that with respect to unkoded cells, there is an increase in BODIPY and biotin+SAF488 kodecyte viability at a lower concentration range (0.5–6 µM). However, beyond 6 µM, BODIPY kodecyte viability decreased by <4%, and for 6 to 25 µM biotin+SAF488 kodecyte, viability decreased gradually by 4–14%. In contrast, with increasing concentrations of FSL-FLRO4, kodecyte viability decreased, however, it was about 10% by 6 µM and increased 24% by 25 µM. Hence, it can be concluded that for FSL-FLRO4 (and to a lesser extent for biotin+SAF488 kodecyte), decrease in viability is

most evident at 25 µM. Under similar testing concentrations, BODIPY-kodecytes were the most viable, with approximately 95% viability at 25 µM.

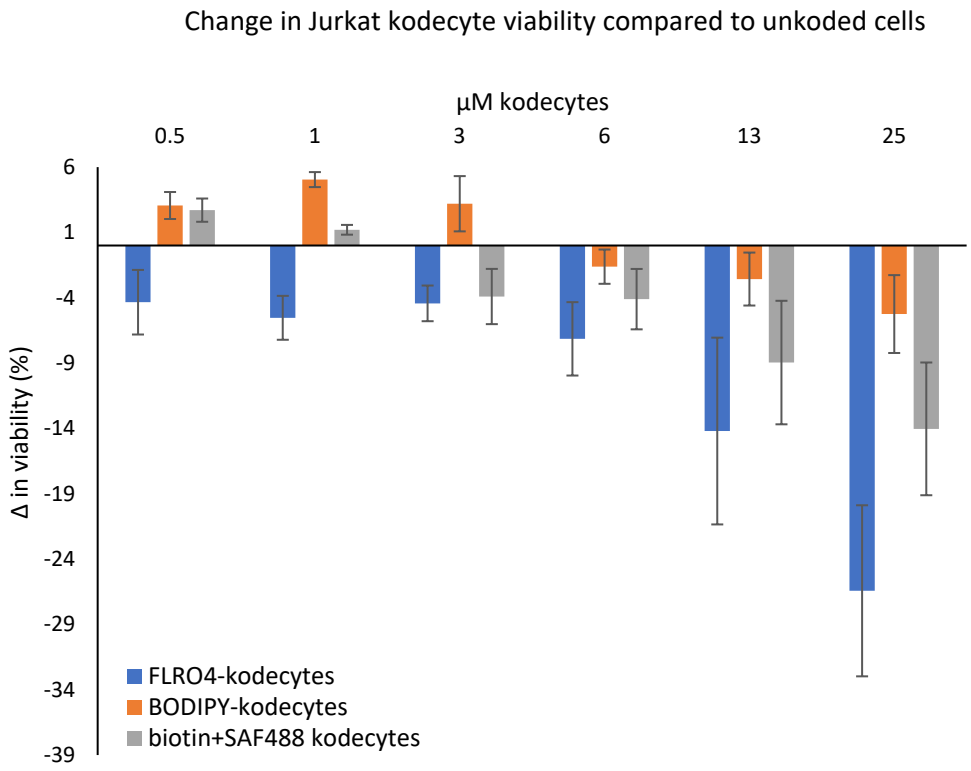

Figure 95: Trypan blue cell exclusion assay examining the viability of kodecytes. The changes in Jurkat FLRO4, BODIPY, and biotin+SAF488-kodecyte viability were compared with unkoded cells. Cell viability was analysed after 2 h of incubation of the FSL construct (0–25 µM) with Jurkat cells at 37 °C.

To explore the possible reasons behind decreased FLRO4-kodecyte viability, the following aspects were considered: Firstly, is serum-free koding medium having an impact on viability? Secondly, as the FSL constructs used for this study differ in their spacers, are different spacers having a more negative impact? Hence, FSL constructs with different spacers were tested for their impact on respective kodecytes. Additionally, the impact of serum deprivation on FLRO4-kodecytes was also analysed in a more detailed manner.

Effect on Jurkat kodecytes viability post koding (over 24 h)

The previous results (Figure 95) showed that, (after 2h koding) compared to FSL-BODIPY and biotin, FLRO4-kodecytes had lower viability. To examine this issue and to have an

overall idea of the viability of FLRO4-kodecytes after koding, FLRO4-kodecytes viability was examined over 24 h in serum-free and serum-supplemented resuspension media. The overview of the methodology testing the viability of Jurkat FLRO4-kodecytes over a period of 24 h is shown in Figure 96, followed by the experimental protocol.

- Jurkat cells were incubated with and without FSL-FLRO4 transformation solution (0–50 µM) for 2 h at 37°C (0 h). Following this, unkoded cells and FLRO4-kodecytes were washed and resuspended in serum-free and serum-supplemented Jurkat cell culture media and incubated at 37°C for 24 h.
- Trypan blue assay was used to measure the cell viability of Jurkat kodecytes and unkoded cells at the following time points: initially, at 0 h, i.e., immediately after 2 h of incubation of RBCs with and without FSL-FLRO4, and secondly, after 24 h of incubation of kodecytes and unkoded cells at 37 °C in the respective media.

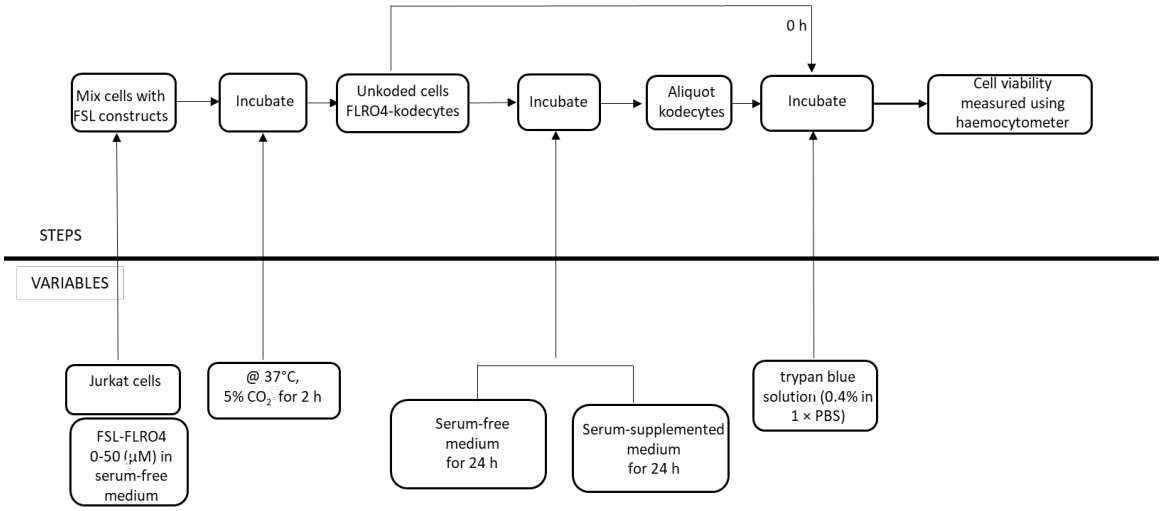

Figure 96: Schematic of method testing the effect of serum on kodecytes viability. Jurkat FLRO4-kodecytes viability was tested over a period of 24 h (in serum-free and serum-supplemented resuspension medium by Trypan blue cell exclusion assay).

From Figure 97A, it can be seen that at the 0 h time point, unkoded cells were the most viable, and increasing concentrations of FLRO4-kodecytes reduced viability. Similarly, after 24 hours of incubation, unkoded cells were most viable in both serum-free and serum-supplemented resuspension media. However, the difference in viability between serum-free and serum-supplemented resuspension media was noticeable. Additionally, irrespective of the resuspension medium, kodecyte density decreased with increasing

concentration. Compared to the serum-supplemented medium, kodecyte viability decreased when maintained in the serum-free medium. The effect of serum deprivation increased with increasing FSL concentrations and was very prominent at 50 µM.

For direct comparison, the raw data shown in Figure 97A was normalised against unkoded cells (indicated as %). Figure 97B shows the change in the viability of kodecytes at 0 h and 24 h in serum-free and serum-supplemented media. This result highlights that, compared to unkoded cells, with increasing concentrations of kodecytes (e.g., 25 and 50 µM kodecytes), viability decreased by nearly 25% to 56% in serum-supplemented medium and approximately 30 to 70% in serum-free medium (24 h). Based on the results it can be proposed that viability of kodecytes is primarily affected due to koding whereas serum deprivation adds an additional negative impact on kodecytes viability. Overall, the negative effect on kodecytes viability was proposed to be a combination of FSL concentration (major) and serum deprivation (minor).

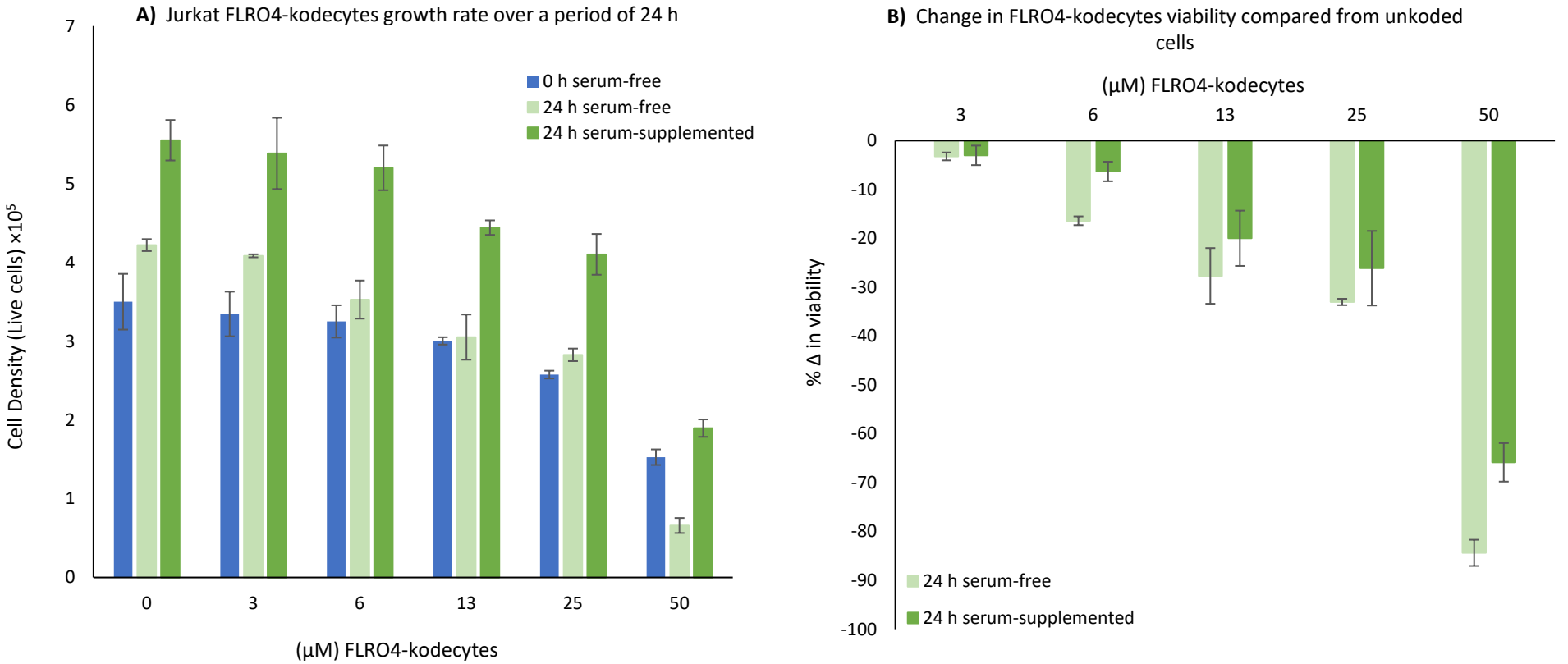

Figure 97: Effect of serum on kodecytes viability examined over 24 h. Jurkat FLRO4-kodecytes viability over 24 h in serum-free and serum-supplemented media determined by Trypan blue cell exclusion assay. Unkoded cells were also examined simultaneously. **A**) Jurkat cells were incubated with (3–50 µM) FSL-FLRO4 transformation solution for 2 h at 37 ˚C (represented as 0 h serum-free) and the increase in the kodecytes and unkoded cell density in 24 h was quantified. **B**) Change in FLRO4- kodecytes viability compared to unkoded cells (indicated as %).

6.3.2 Muse™ Count & Viability assay

The Muse™ Count & Viability assay is a cytometry-based assay that determines cell viability by considering the integrity of the cellular membrane. It is widely used as an alternative to traditional methods like the Trypan blue assay. It uses pre-optimised DNA binding dyes that differentially stain viable and non-viable cells based on their permeability to ensure reproducible and consistent results. The overview of the methodology used to investigate the impact of different FSL uptakes on the viability of respective Jurkat kodecytes is presented in Figure 98, followed by the experimental protocol.

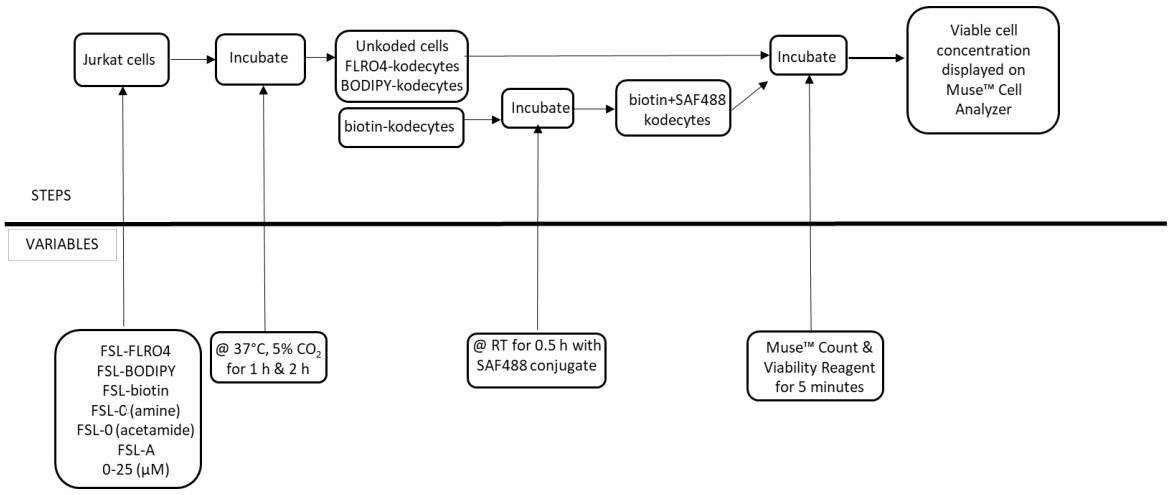

Figure 98: Schematic overview of method testing the Jurkat kodecyte viability by the Muse™ Count and Viability assay.

- Jurkat cells were incubated with different concentrations of FSL for 2 h at 37 °C. Control or unkoded cells were also prepared simultaneously.
- After a 2 h incubation, kodecytes were washed and resuspended in RPMI medium. Kodecyte suspensions were incubated with Muse™ Count and Viability reagent (1:10) for 5 minutes at RT. Muse™ Count & Viability reagent contains two fluorescent nucleic acid stains in a buffered, saline solution that is physiologically compatible. Workflow and test principles are shown in Figure 99.
- Kodecytes and Muse™ Count and Viability reagent mixture was loaded into the Muse™ Cell Analyzer, and samples were acquired.

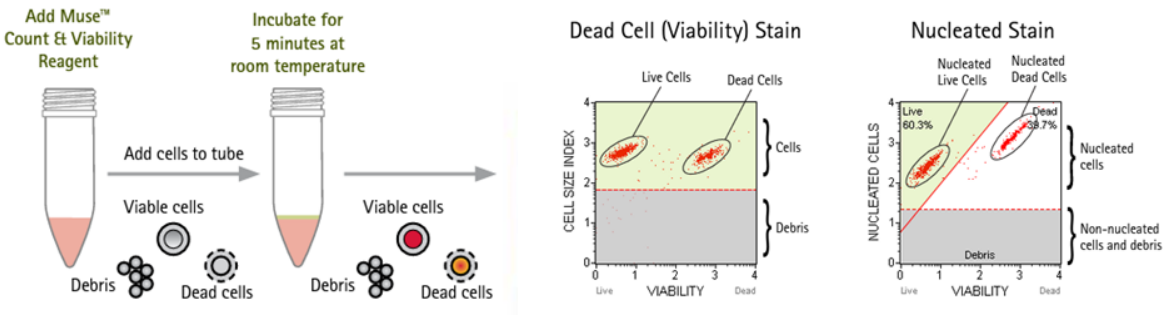

Figure 99: Workflow used in Muse™ Count and Viability assay.The assay uses two DNA intercalating dyes, membrane impermeant and membrane permeant dyes. Adapted from Kiselev MA. [176]

FSL constructs and viability by Muse™ Count & Viability assay

The concentration-dependent response of FLRO4, BODIPY and biotin+SAF488 on respective kodecytes viability is shown in Figure 100. Data displayed is obtained after 2 h incubation of Jurkat cells with and without FSL construct (0-25 µM) at 37˚C. Here, the viability obtained at respective concentrations is compared against unkoded cells (% of control). Muse™ Count & Viability assay showed that compared to unkoded cells, kodecytes viability was very similar (<5%) up to 6 µM concentration. This trend was seen irrespective of the FSL construct used. Additionally, compared to unkoded cells, the viability of 25 µM FLRO4, BODIPY and biotin+SAF488 kodecytes decreased by approximately 35%, 6% and 15%, respectively. Of all the tested FSL constructs, BODIPY- kodecytes seems to maintain their viability quite consistently with under 6% drop across the concentration range.

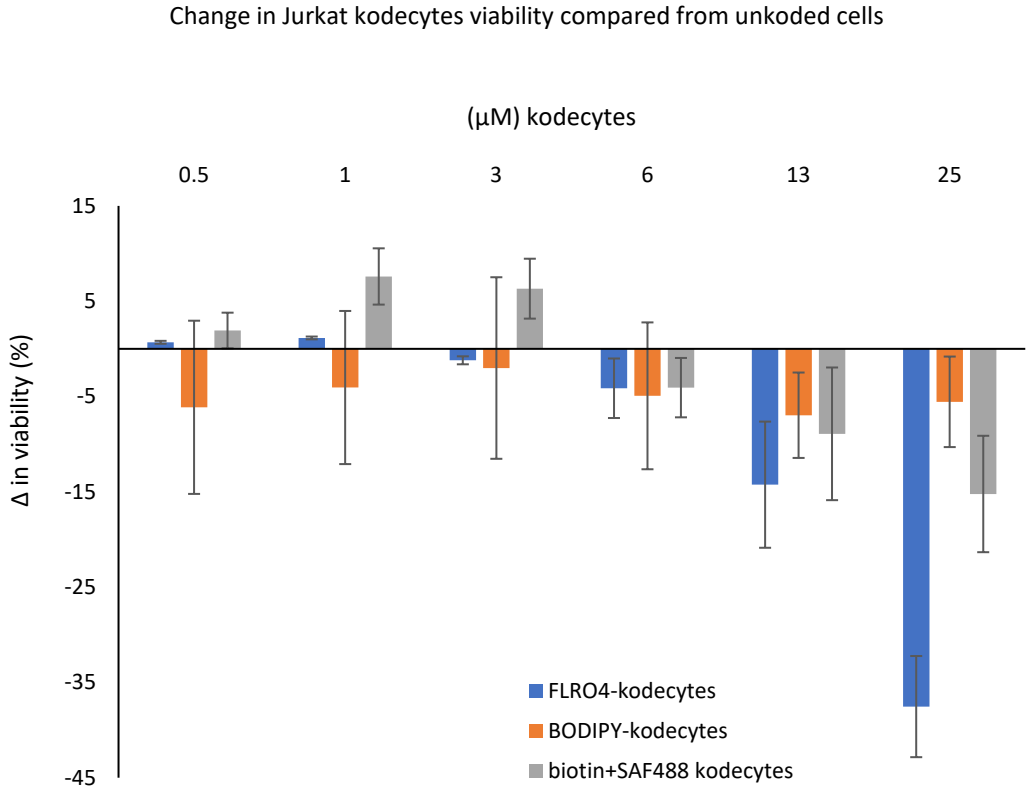

Figure 100: Muse™ Count & Viability assay examining the viability of kodecytes. The changes in Jurkat FLRO4, BODIPY, and biotin+SAF488 kodecytes viability were compared with unkoded cells. Cell viability was analysed after 2 h of incubation of the FSL construct (0–25 µM) with Jurkat cells at 37 °C.

Automated Muse™ Cell Analyzer versus manual haemocytometer

Trypan blue assay is a manual hemocytometer-based assay that allows for very few cells to be analysed at a time. However, data attained from the Muse™ Cell Analyzer is obtained after examining a sizable number of cells at a time. Therefore, in order to determine the comparability (and reliability) of the results obtained from both assays, the viability of FLRO4, BODIPY, and biotin+SAF488 kodecytes (with respect to unkoded cells) was assessed simultaneously.

Figure 101 shows a comparative analysis of Jurkat FLRO4-kodecytes viability obtained by the Muse™ Count & Viability assay (Muse™ Cell Analyzer) and Trypan Blue assay (manual hemocytometer). Based on the results, the following conclusions can be drawn: More kodecytes (<5%) were found to be viable when the automated Muse™ Cell Analyzer was used for accessing viability than the manual hemocytometer. However, this was the trend up to concentrations of only 13 µM, and at 25 µM, kodecytes viability determined by the hemocytometer was approximately 12% higher than the Muse™ Cell

Analyzer. This difference in kodecyte viability that was obtained from two different analysis techniques could be attributed to the sample preparation steps required for the automated Muse™ Cell Analyzer (like sample dilution for the assay to be run in the optimal event range and additional incubation of kodecytes with the Muse count and viability reagent). Based on the result shown in Figure 101, it could be concluded that at similar experimental conditions, Trypan blue assay results, in general, correlated with those of Muse™ Count & Viability assay results.

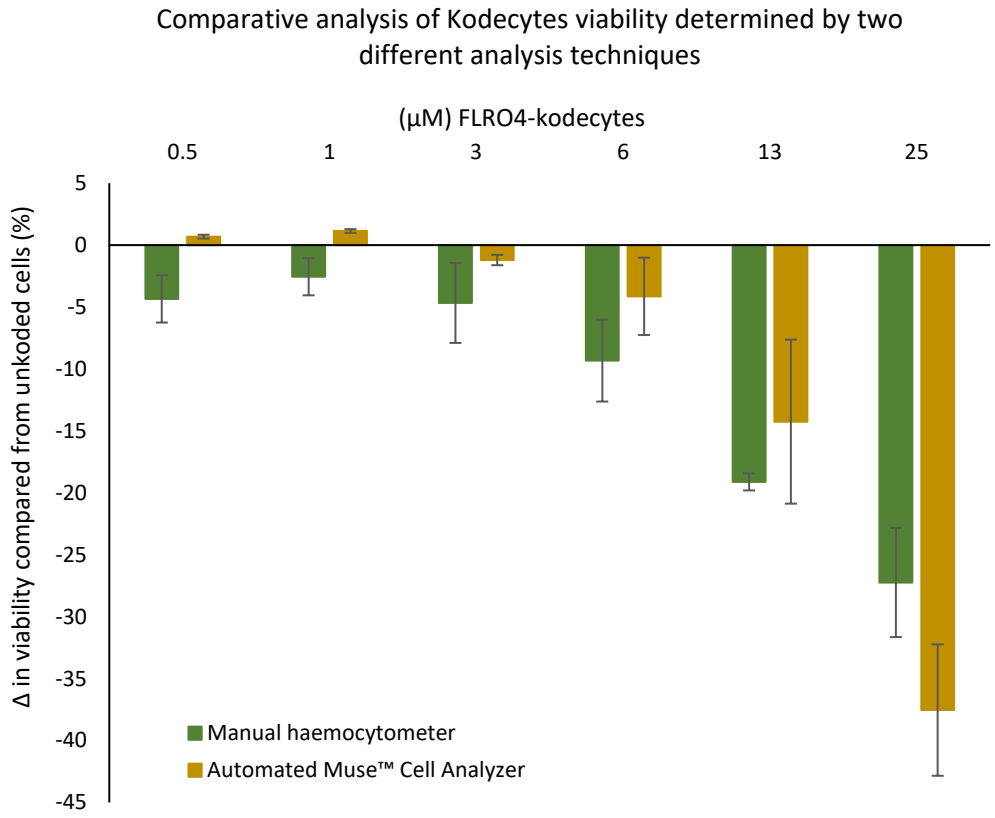

Figure 101: Comparative representation of Jurkat FLRO4-kodecytes viability measured by Trypan Blue Assay (manual hemocytometer) and the Muse™ Count & Viability assay (automated Muse™ Cell Analyzer). Kodecytes were formed after 2 h of incubation (0–25 µM) with and without FSL- FLRO4 with Jurkat cells at 37°C. Viability is compared to the control (%).

Effect of FSL construct with different spacers on kodecytes viability

Based on the data shown in Figures 95 and 97, it was found that the koding process had a more negative impact on the viability of FLRO4-kodecytes than BODIPY and biotin-kodecytes. It was proposed that perhaps this was due to either spacers or a functional head group. Hence, to understand the cytotoxicity generated by FSL constructs in

general, more FSL constructs (with different spacers) should be tested for their viability profile.

Additional FSL constructs with different complexity of functional heads were tested for their cytotoxicity profile during koding on Jurkat cells. From previous results shown in the concentration and time-dependent uptake study of the FSL construct in Jurkat cells (see Sections 3.3.1 and 3.3.3), it was concluded that a 25 µM concentration and 1 h incubation duration was optimal for fluorescence signal generation and were chosen to measure the influence of different FSL constructs on respective kodecyte viability. It is important to note that FSL-A (tri) and FSL-FLRO4 have adipate-based spacers, whereas all other constructs have CMG2 based spacers. Jurkat cells were incubated with 25 µM of FSL-zero (amine), FSL-zero (acetamide), FSL-biotin, FSL-BODIPY, FSL-FLRO4, and FSL-A (tri) for 1 h at 37 °C. Viability was measured by two different analysis techniques, i.e., using a manual hemocytometer and an automated Muse™ Cell Analyzer. Overall, kodecytes viability was compared to unkoded cells (indicated as %).

Figure 102 shows a comparative analysis of kodecyte viability prepared using various FSL constructs, revealing the following conclusions: Compared to unkoded cells, the viability of zero (amine and acetamide)-kodecytes and BODIPY-kodecytes (CMG2-based spacers) decreased by only 3%. Whereas the viability of A (tri)-kodecytes and FLRO4-kodecytes (adipate-based spacers) decreased by 15%.

Moreover, biotin-kodecytes, which have a CMG2-based spacer, were shown to be less viable (<12%) than other CMG2-based kodecytes (zero and BODIPY-kodecytes). However, possibly the difference in viability is because of the functional head group (as the spacer is a common entity here). Hence, it could be said that the biotin residue is counterproductive and affects the viability of biotin-kodecytes. Based on the results, it was proposed that CMG2-based kodecytes were more viable than adipate-based constructs.

Overall, it could also be concluded that, compared to the 2 h koding duration, FSL- constructs have a lesser cytotoxicity effect at 1 h; thus, 1 h is suggested to be the optimal koding duration for active cells. Additionally, based on the results, it could be

summarised that the Muse™ Cell Analyzer demonstrates agreement and provides comparable results to the manual hemocytometer.

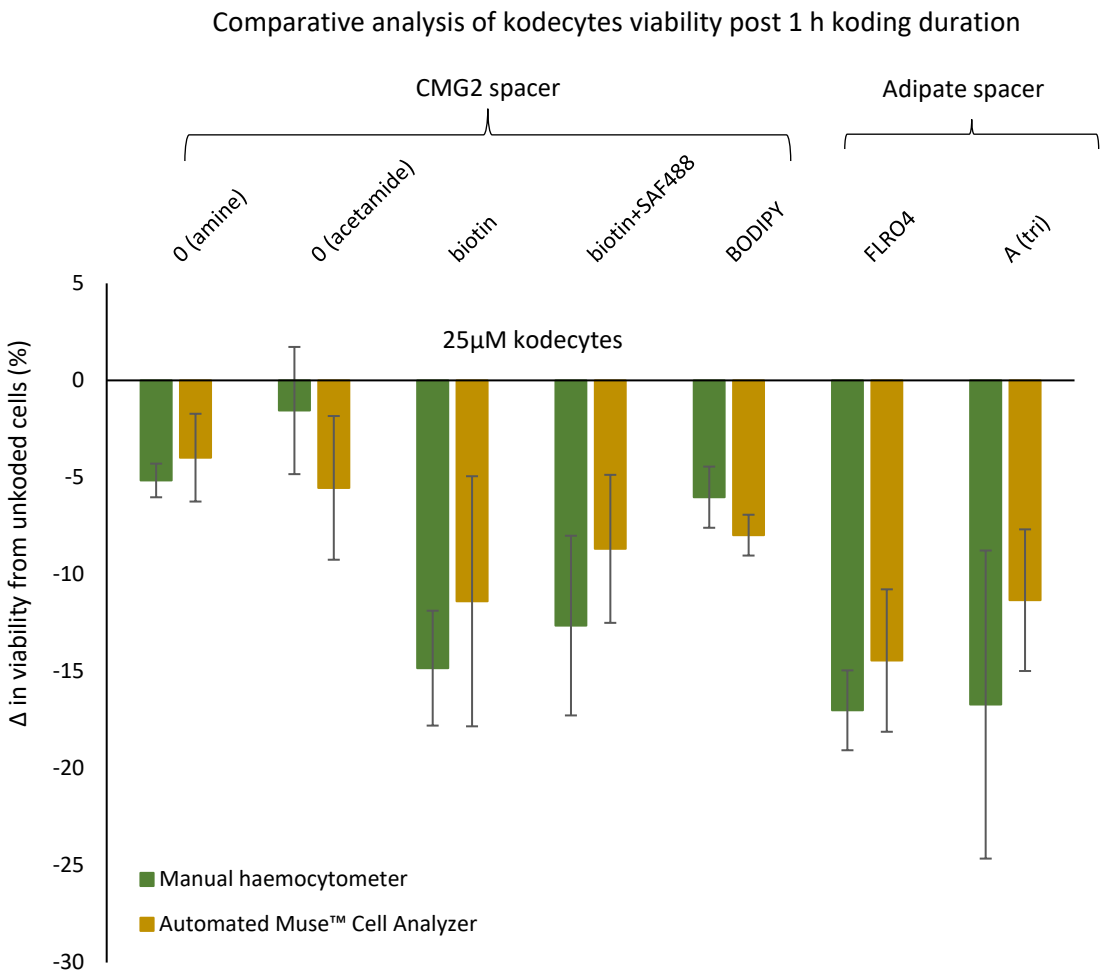

Figure 102: A comparative analysis of the viability of different kodecytes. The viability was measured and compared by the Trypan Blue assay and the Muse™ Count & Viability assay. Kodecytes were formed after 1 h of incubation of 25 µM FSL constructs with Jurkat cells at 37°C. Viability is compared to the control (%).

6.4 MTT cell proliferation assay

Overview: The MTT cell proliferation assay assesses cellular metabolism and, in turn, the proliferation status of cells (in question). It differentiates metabolically active and proliferating cells from metabolically inert and non-dividing cells. The MTT assay is a colorimetric assay and is based on the conversion of a water-soluble MTT (3-(4, 5-dimethylthiazol-2-yl)-2, 5-diphenyltetrazolium bromide) compound to an insoluble formazan product. In this assay, viable cells with active metabolism convert MTT into formazan, whereas non-proliferating and dead cells lose this ability and therefore show

no signal. Thus, colour formation is a marker of viable cells. The resulting intracellular purple formazan (directly proportional to the number of viable cells) is solubilized and quantified by measuring the absorbance or optical density at 540 nm using spectrophotometry.

In this section, the MTT assay was first used to determine if the FSL-FLRO4 koding process (at different koding durations) affects the kodecyte proliferation/metabolism status, i.e., if the koding process stimulates or inhibits kodecyte proliferation. Once the implication of different koding durations was examined, the viability of PC-3 kodecytes, i.e., viable kodecytes with active metabolism (after koding), was measured by the MTT cell proliferation assay over a period of 72 h.

6.4.1 Effect of different koding duration on PC-3 kodecytes

Methodology: A time-course FSL-FLRO4 uptake study and subsequent cell proliferation analysis were set up to determine the effect of different koding duration on PC-3 FLRO4- kodecytes viability at 37°C. A schematic overview of the methodology is presented in Figure 103, followed by the detailed experimental protocol.

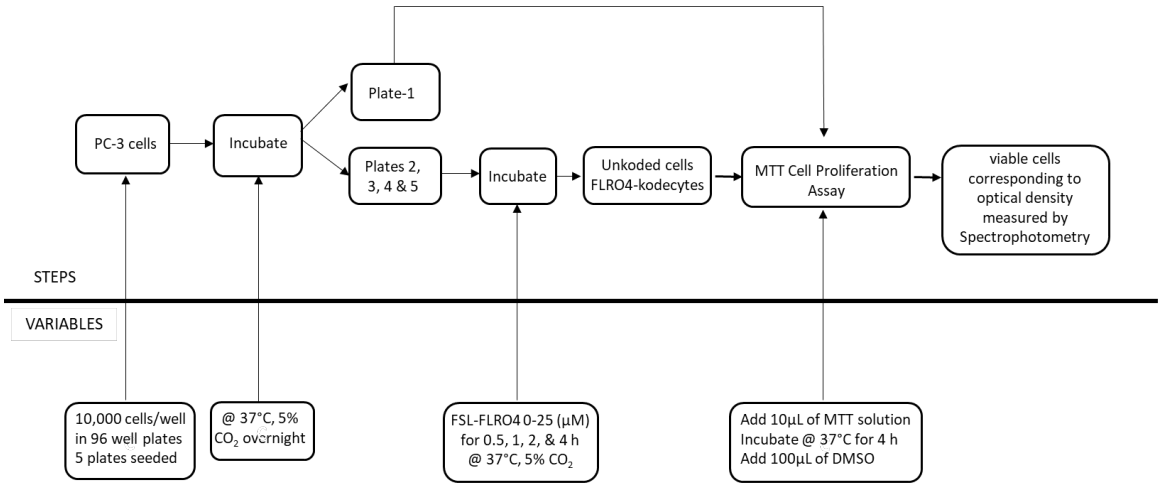

Figure 103: Schematic overview of method testing the effect of koding durations on PC-3 kodecyte proliferation by the MTT cell proliferation assay.

- PC-3 cells were detached from culture flasks, and an optimal cell count of preferably 1×10^4 cells were placed in 100 µL of complete medium per well in a 96-well plate. The MTT assay plate design included a blank well-containing medium only, unkoded control cells, and test cells transformed with FSL-FLRO4 to be assayed.
- 5 plates were seeded for 0, 0.5, 1, 2, and 4 h time point analysis. Prior to the addition of FSL-FLRO4, the cells were incubated overnight at 37°C, 5% CO_2 (for proper cell attachment).
- The following day, all 96-well plates were washed with serum-free medium, and FSL-FLRO4 transformation solution was prepared.
- FSL-FLRO4 working stock was not added to plate-1 (representing 0 h). 0 h provides the reference point from which cell proliferation is calculated.
- 100 µL of 6, 25 µM FSL-FLRO4 were added to plates 2, 3, 4 and 5, and incubated for 0.5, 1, 2 and 4 h prior to performing the MTT assay. Six replicates for each concentration were tested. 100 µL of the serum-free medium was added to the column marked as blank and control.
- After the respective incubation of cells with FSL-FLRO4 transformation solution, 10 µL of MTT solution (5mg/mL in 1×PBS) was added into each well and incubated for 3 h at 37°C. The plate was incubated for a few minutes to ensure proper dissolution of the MTT formazan complex, and viability was determined by measuring the photometric absorbance at 540nm using a microtiter plate reader.
- For analysing the effect of time over a period, the 0 h time point (plate 1) was also analysed by MTT (0 h provides the reference point from which cell proliferation is calculated).

Results

FSL-FLRO4

The effect of different koding durations on the proliferation (or cellular metabolism) of 6 and 25 µM PC-3 FLRO4-kodecytes (and unkoded cells) at 37°C is shown below (Figure 105). It is important to note that 0 h provides the reference point from which cell proliferation was measured. As the MTT assay allows for quantification of cell viability through cellular metabolism, the following inferences can be made from the results

presented in Figure 104. Firstly, with respect to 0 h unkoded cells, after 0.5-2 h incubation, unkoded cells (and 6 µM kodecytes) were found to be metabolically active and proliferating, with a slight increase after 1 h (> 8%). However, after 4 h of incubation, proliferation decreased by approximately 6%. Secondly, except after 4 h of incubation (and after-2 h for 25 µM kodecytes), no difference in cell metabolic pattern was observed between unkoded cells and FLRO4-kodecytes. Finally, based on the cellular proliferation quantification, it could be proposed that the 1 h koding duration was the most suitable, as kodecytes were found to be most viable and proliferating after 1 h koding.

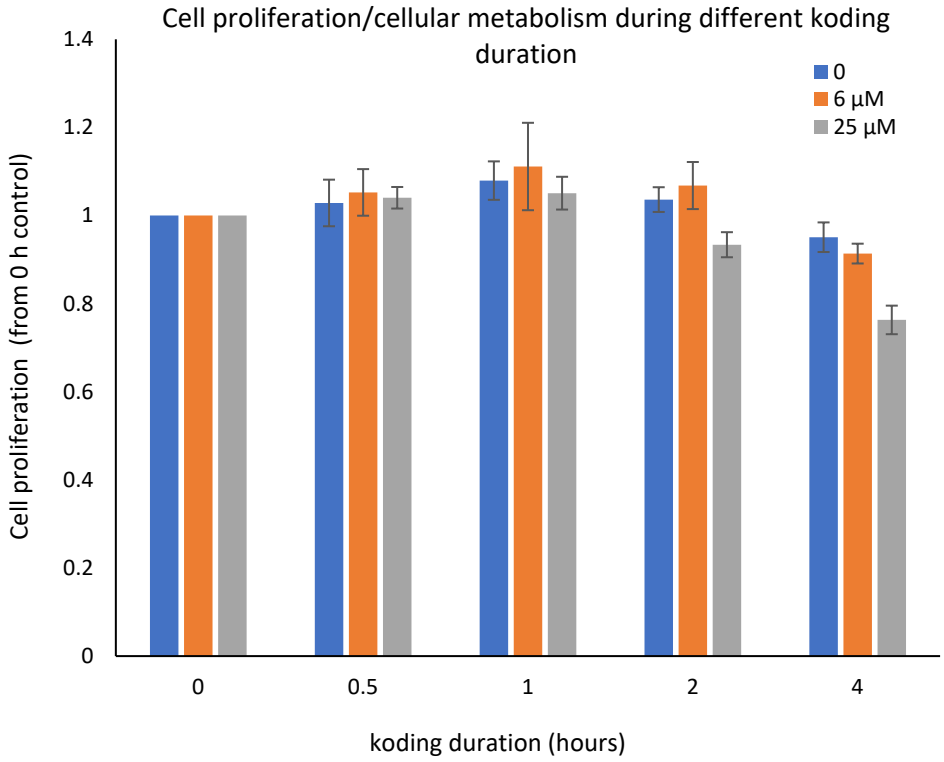

Figure 104: Effect of different koding durations on PC-3 kodecyte proliferation/metabolism. Unkoded cells were also quantified for proliferation after 0, 0.5, 1, 2, and 4 h of incubation in a serum-free medium. PC-3 cells were transformed with (6 and 25 µM) FSL- FLRO4 for 0.5, 1, 2, and 4 h in serum-free medium, and cell proliferation was compared to the 0 h unkoded cells (reference point).

6.4.2 Effect on PC-3 kodecytes proliferation post koding (over 72 h)

In the earlier result (section 6.3.1), the effect of koding process and storage media on Jurkat-kodecytes viability was examined over 24 h by Trypan blue cell exclusion assay. Based on the results, it was proposed that the negative effect on Jurkat kodecytes

viability was due to a combination of FSL concentration (koding process) and serum deprivation.

Compared to the Trypan blue cell exclusion assay, the MTT cell proliferation/metabolism assay is less labour-intensive. Hence, in this section, after 1 h of koding, the proliferation rate of a different kodecyte (PC-3 kodecyte) in serum-supplemented storage media was examined over a longer duration (72 h).

The methodology overview is presented in Figure 105, and the detailed experimental protocol is as follows.

- PC-3 cells were seeded in 96-well plates at a cell density of 10×10^4 cells/well and incubated overnight at 37°C with 5% CO2 (for proper cell attachment).
- After overnight incubation, PC-3 cells were koded with (6 and 25 µM) and without FSL-FLRO4 transformation solution for 1 h at 37°C. Following this, unkoded cells and FLRO4-kodecytes were washed and resuspended into serum-supplemented PC-3 culture medium and incubated at 37˚C for 0, 24, 48, and 72 h.
- The MTT proliferation assay was performed at 0 h, i.e., immediately after 1 h of koding with FSL-FLRO4, and after completion of 24, 48, and 72 h of incubation of kodecytes and unkoded cells at 37 ˚C in the serum-supplemented medium. Here, kodecytes and unkoded cells' proliferation ability was quantified, and the proliferation rate was determined by measuring the photometric absorbance at 540nm using a microtiter plate reader.

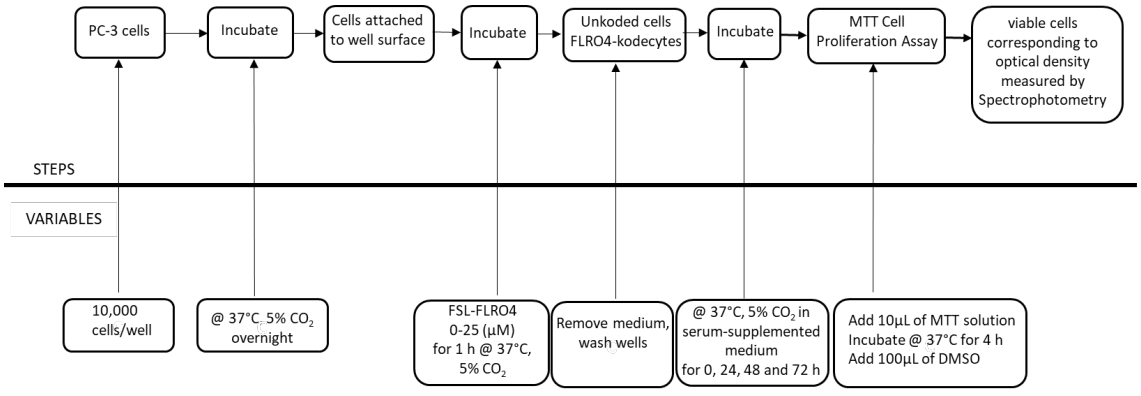

Figure 105: Schematic overview of method testing for proliferation post-koding. The proliferation of PC-3 kodecyte was examined by the MTT cell proliferation assay over a period of 72 hours post-koding.

The effect of the koding process on PC-3 kodecyte proliferation over 72 hours is shown in Figure 106. Here, after 1 h of koding of PC-3 cells, the time-dependent response of unkoded cells and PC-3 kodecyte proliferation over a period of 24, 48, and 72 h in the serum-supplemented medium was analysed. The result presented showed that over a period of 72 h, both unkoded cells and kodecytes were metabolically active, as proliferation was not majorly affected adversely. For example, after 24, 48, and 72 h of culture in serum-supplemented medium, the number of kodecytes and unkoded cells increased consistently. However, compared to 25 µM kodecytes, the rate of proliferation of unkoded cells was higher (nearly 10%).

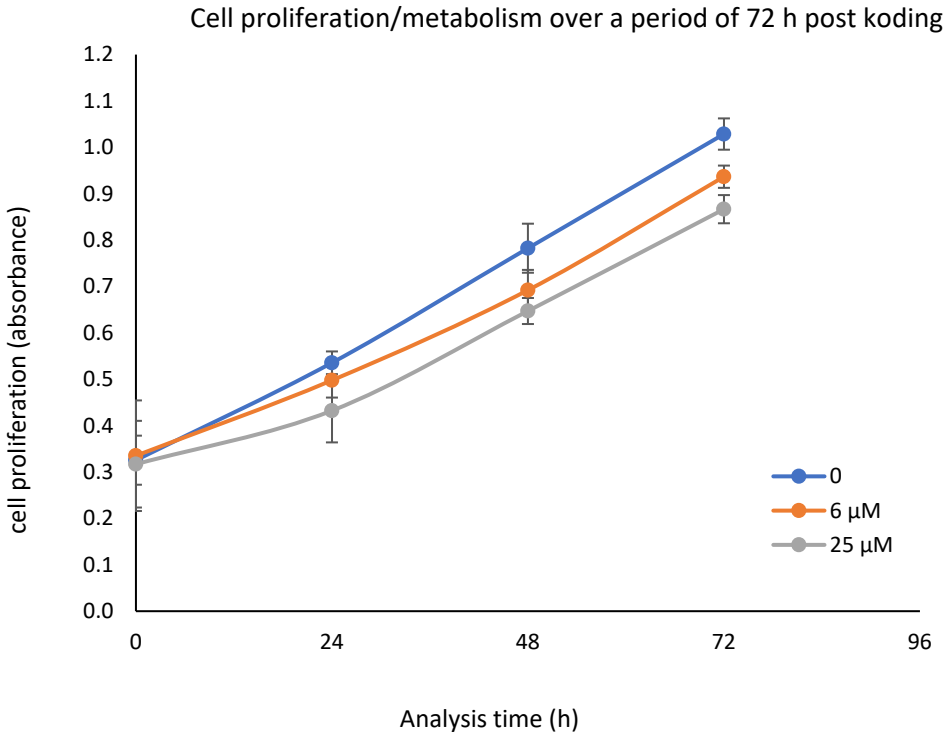

Figure 106: Effect of koding process on PC-3 kodecytes proliferation/metabolism (over 72 h). Unkoded cells and PC-3 kodecytes proliferation over a period of 72 h in the serum-supplemented medium. PC-3 cells were transformed with (6 and 25 µM) and without FSL-FLRO4 transformation solution for 1 h at 37 °C, and cell proliferation was measured over a period of 72 h by the MTT cell proliferation assay.

Based on results from Sections 7.4 and 7.5, it was shown that Jurkat-kodecytes lost more than half of their acquired FSLs within 3 hours of culture in resuspension media. Hence, the results in Figure 107 show a consequence of koding on the long-term proliferation of PC-3 kodecytes, which eventually lose FSL and continue growing as PC-3 cells. Overall, the koding process had a marginal effect on the proliferation of cells that were once kodecytes.

6.5 Chapter summary:

Following summary could be drawn from the FSL constructs cytotoxicity study:

- The SEM study of RBC kodecytes suggests that the morphology of kodecyte changes in response to FSL concentrations greater than 13 µM. This change is most pronounced for FSL-FLRO4 and is detected to a lesser extent for FSL-biotin and FSL-BODIPY. The change in morphology from predominantly discocytes (stage 0) and an increasing percentage of stage 1–3 echinocytes is probably due to the uptake of FSL constructs.
- There was no observable difference between unkoded cells and Jurkat kodecytes morphology and diameter prepared from 3–13 µM FSL constructs
- An interesting observation from the extended (0–24 h) koding duration study at 37°C is the time-dependent reversible transformation of RBC kodecytes from discocytes to echinocytes to a combination of abundant stomatocytes. Additionally, the unkoded cells and kodecytes became smaller in diameter with increasing koding duration at 37°C. These observed consequences were due to simple incubation at 37°C rather than the extended koding process (duration) with FSL constructs.
- Results obtained from the Trypan blue cell exclusion assay, Muse™ count viability assay, and MTT cell proliferation assay (on Jurkat and PC-3 kodecytes) suggest that FSL-constructs have low cytotoxicity at 1 h of koding, making 1 h the optimal duration of koding for active cells.
- A study comparing the viability of kodecytes made from different FSL constructs found that overall, CMG2-based kodecytes were more viable than adipate-based constructs.
- The effect of the koding process on PC-3 kodecyte proliferation over 72 hours showed that the number of kodecytes and unkoded cells increased consistently. However, a concentration-dependent effect on kodecyte proliferation was observed post-koding, suggesting that koding with higher concentrations could possibly affect the viability post-koding.

Chapter 7 Retention and cell-to-cell transfer of FSL constructs

Overview: An ideal cell labelling and tracking agent should not only label a wide range of cell types with minimum or no cytotoxicity but also exhibit minimum cell-to-cell transfer (membrane retainability) and have reliable chemical and metabolic stability over the relevant period. This aspect of the study aimed to:

Examine the retention of FSL constructs on kodecytes by flow cytometry.

- Examine whether FSL constructs transfer from kodecytes to unkoded cells when co-incubated. It was anticipated that this experiment might led to further understanding of the dynamics of loss and relabelling of kodecytes.
- Compare the retention and transfer of FSL constructs in a co-incubation (and co-culture) scenario when kodecytes are prepared from cells with a dormant membrane (RBC) and active membrane (Jurkat cells).

The different criteria during which retention, cell-to-cell interaction and transfer phenomena were tested are:

- FSL constructs differing in functional head groups and spacers:
    - two functional head group; fluorophore (FSL-FLRO4 and FSL-BODIPY) and vitamin (FSL-biotin)
    - two different spacers; one short adipate (FSL-FLRO4), one long CMG2 (FSL-BODIPY and FSL-biotin).
- Different storage temperatures: 37°C, and 4°C
- Different storage media: effect of protein (BSA), plasma-lipids and plasma-protein (plasma) and serum on retention of FSLs in RBC and Jurkat kodecytes.
    - for RBC-kodecytes; CellStab (glycine buffered saline used for RBC preservation) with different concentration of BSA and 50% plasma
    - for Jurkat-kodecytes; two concentrations of serum in cell culture medium.

Table 22 provides a summary of the experiments conducted in this section, outlining their objectives, tested variables. Outcomes from respective study is discussed in result section.

Table 22: A summary of the experiments conducted in retention study section outlining their objectives, and tested variables. JC: Jurkat cells, RBC: Red Blood Cells.

Sections	Cells	FSL	Objective	Variables
7.1	RBC	FLRO4 BODIPY biotin	Factors influencing retention of FSL	• 37°C and 4°C • 0, 5, 15% BSA and 50% plasma • storage time: 0 - 24 h • FSL (µM): 6 and 25
7.2	RBC	FLRO4 BODIPY biotin	Transfer of FSL in co-incubation dynamics of loss and re-labelling of kodecytes	• 37°C and 4°C • CellStab with 0, 5, 15% BSA and 50% plasma • storage time: 0 - 24 h • FSL (µM): 6 and 25
7.3	RBC	FLRO4 BODIPY biotin	FSL retention in long-term storage 4°C	• 0, 5, and 15% BSA • Storage time: 0 -12 weeks • FSL (µM): 6 and 25
7.4	RBC	FLRO4	Glycocalyx contribution on retention of FSL at 37°C	• storage time: 0 - 24 h • FSL (µM): 6 and 25
7.5	JC	FLRO4 BODIPY	Contribution of active membrane on retention	• koding duration: 1 h and 2 h • storage time: 0 – 24 • FSL: 6µM
7.6	JC	FLRO4 BODIPY biotin	Contribution of serum on the retention of FSL	• 5% and 10% serum • storage time: 0 - 48 h
7.7	JC	FLRO4 BODIPY	Interaction of Jurkat kodecytes with unkoded cells in co-culture	• storage time: 0 - 24 h

Methodology: A schematic overview of the methodology examining the retention of FSL-FLRO4, BODIPY and biotin on respective red blood cell kodecytes is shown in Figure 107, followed by the detailed experimental protocol.

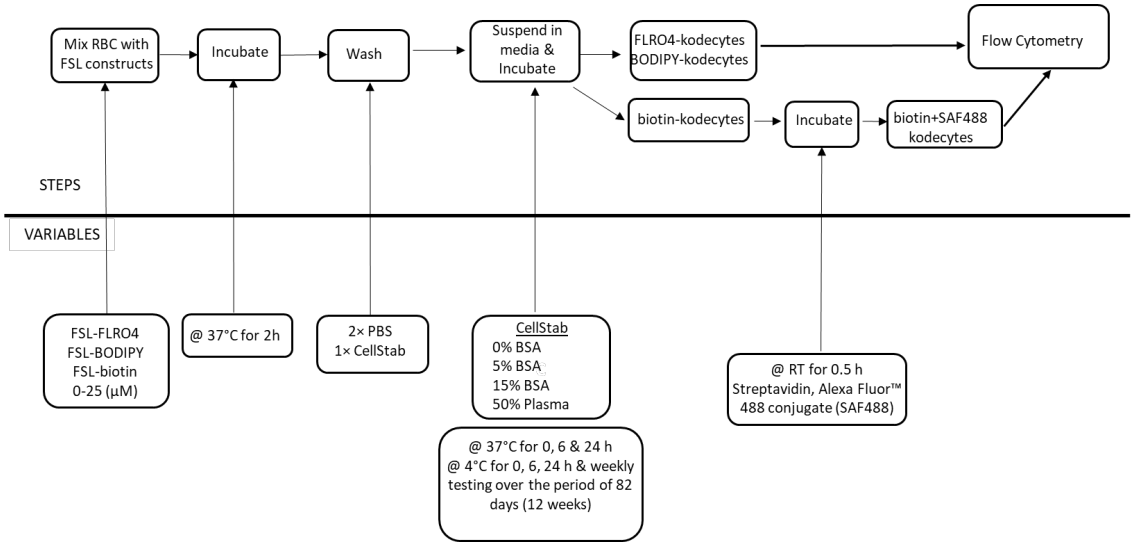

Figure 107: Schematic overview of method testing the retention of FSLs (FSL-FLRO4, BODIPY, and biotin) on their respective RBC-kodecytes by flow cytometry.

- FSL koding solution was prepared using red cell preservative solution (CellStab) as a diluent.
- Kodecytes were prepared with 6 and 25 µM FSL koding solution at 37°C for 2 h. Control or unkoded cells were prepared by incubating RBCs with CellStab at 37°C for 2 h.
- After completion of incubation duration, kodecytes and control cells were washed 2× with PBS and once with CellStab.
- Four red cell storage or resuspension medium were prepared: 0, 5, and 15 % BSA prepared in CellStab. For 50% plasma preparation in CellStab, first plasma was separated by centrifugation from whole blood and diluted in a 1:1 with CellStab.
- To examine the retention of FSL constructs in kodecytes: the kodecytes were finally resuspended at 5% v/v in respective red cell storage or resuspension medium as mentioned above. Relevant samples were divided equally into three sets and maintained at 37°C, RT, and 4°C. Finally, retention or stability of FSL constructs was assessed by flow cytometry over a period of 0, 6, and 24 h.
- Retention of FSL constructs on kodecytes at 4°C was extended and tested over 12 weeks. The resuspension or storage medium was changed every 4 weeks.

- The change in the retention of FSL constructs in kodecytes under different tested scenarios (over a period) was correlated with a shift in the mean fluorescence intensity of kodecytes.
- To allow for a more direct comparison of MFI change over a specific period of time, the raw data was normalised against 0 h. For this, the change in MFI and, consequently, the retention of the FSL construct was determined using the formula [(Fi / F0) × 100] -100, where F0 and Fi represent the kodecytes fluorescence intensity at 0 h or a specific period of analysis. Negative values indicate a decrease in the retention of the FSL construct from the 0 h time point, whereas positive values represent an increase in the retention of the FSL constructs.

7.1 Retention of FSL in RBC kodecytes

7.1.1 FSL-FLRO4

This section explores the impact of media and temperature variations on the retention of FSL. Figure 108 shows the effect of different storage media and temperatures over a period of 24 h on the retention of FSL-FLRO4 in FLRO4-kodecytes. The following conclusions are made based on the data: Firstly, the fluorescence signal of kodecytes stored in 0 and 5% BSA CellStab and 50% plasma CellStab remained nearly consistent over 24 h of incubation at 4°C. Secondly, within 24 h, when the storage temperature was increased to 37°C, the fluorescence signal of kodecytes maintained in a similar storage medium decreased substantially. For example, when kodecytes were stored in CellStab only, the fluorescence signal decreased by 13% in the first 6 h and 75% by 24 h.

The signal decreased even more in the presence of BSA or plasma. From Figure 108, it could be summarized that at 37°C storage temperature, in the presence of BSA in the storage medium, the fluorescence signal decreased by approximately 72% in the first 6 h and 90% by 24 h. Additionally, in 50% plasma, signals decreased by nearly 50% and 85%, respectively. Notably, in the first 6 h of storage, the fluorescence signal relatively decreased more for 6 µM kodecytes than 25 µM kodecytes (approximately 21%). This trend was also observed when kodecytes were stored in 50% plasma.

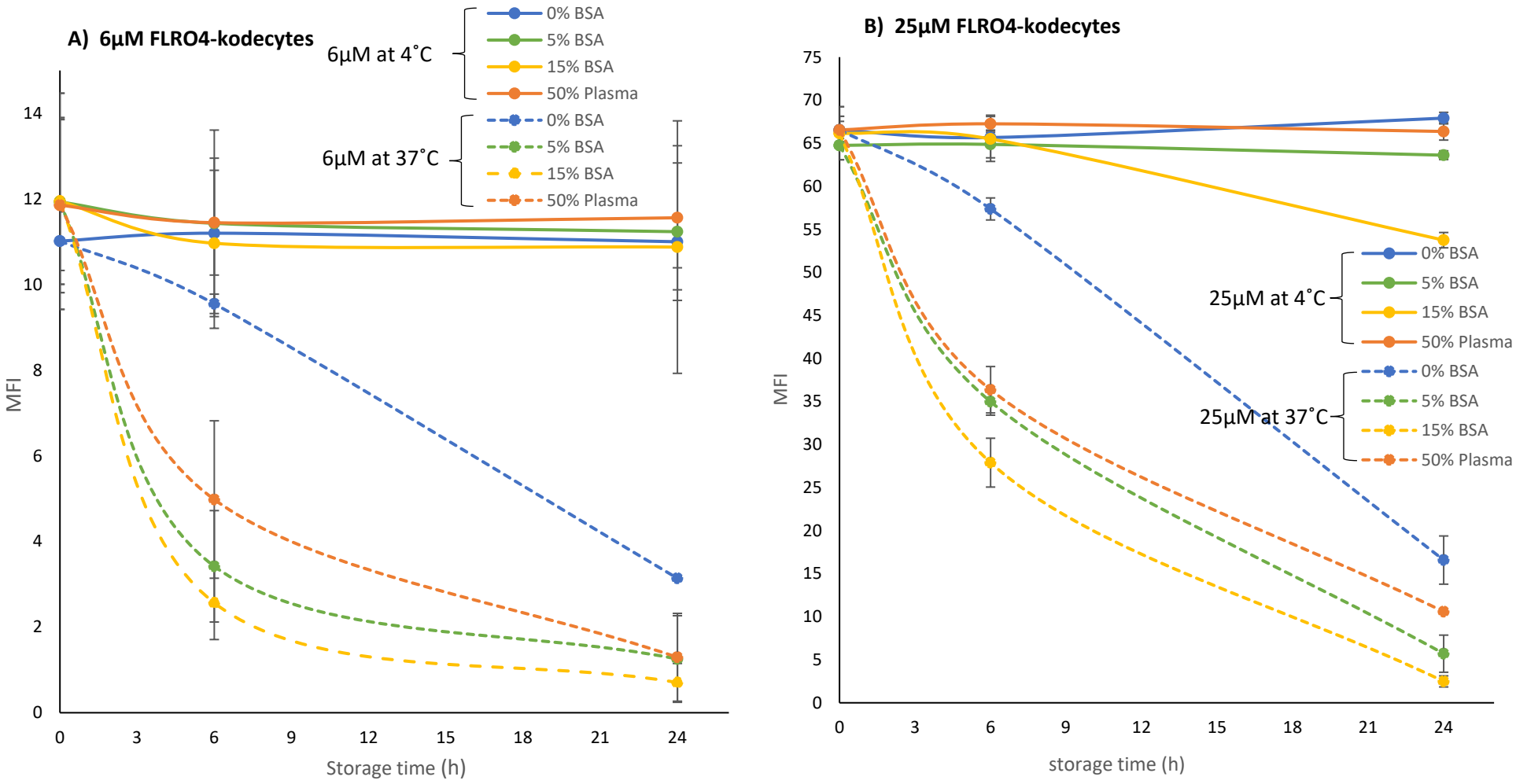

Figure 108: The retention of FSL-FLRO4 in RBC FLRO4-kodecytes over 24 h in 0, 5, 15% BSA and 50% plasma in CellStab at 37°C, and 4°C. Results shown are mean ± standard deviation, n=3. The MFI generated by **A**) 6 µM FLRO4-kodecytes **B**) 25 µM FLRO4-kodecytes over 24 h

In Table 22, the data shown in Figure 108 was normalised against 0 h to allow a more direct comparison of MFI change (at different incubation temperatures and storage media). Overall, the results showed that at 37°C, FSL-FLRO4 was lost from the kodecytes much quicker, thus decreasing the retention of FSLs on FLRO4-kodecytes. This observation could be because, at 37°C, the membrane becomes more fluid, favouring FSL movement and facilitating the release of FSL. Additionally, within 6 h of storage in the presence of BSA or plasma, more than 40% of FSLs were lost from the kodecytes, indicating that the presence of BSA/plasma increases the loss of FSLs from the kodecytes. However, it is important to note that the presence of BSA/serum is not necessarily causing the loss of FSL from the kodecytes but may instead be hindering the ability of the released FSL to re-label the kodecytes.

Table 23: Change in MFI of 6 and 25 µM FLRO4-kodecytes at 6 and 24 h from 0 h (%)in 0, 5, 15% BSA, and 50% plasma in CellStab at 37°C and 4°C. The change in MFI and, consequently, the retention of the FSL were determined using the formula [(Fi / F0) × 100] -100, where F0 and Fi represent the kodecytes MFI at 0 h or a specific period of 6 and 24 h. Negative values indicate a decrease in the retention of the FSL construct from the 0 h time point, whereas positive values represent an increase in the retention of the FSL constructs.

		Change in MFI from 0 h (%)							
		FLRO4-kodecytes							
		4˚C				**37˚C**			
		6 µM		**25 µM**		**6 µM**		**25 µM**	
	CellStab	**6 h**	**24 h**	**6 h**	**24 h**	**6 h**	**24 h**	**6 h**	**24 h**
cell storage solution	**0% BSA**	2	0	-1	2	-13	-71	-14	-75
	5% BSA	-4	-5	0	-2	-71	-89	-46	-91
	15% BSA	-8	-10	-1	-9	-79	-94	-58	-96
	50% plasma	-3	-2	1	0	-58	-89	-45	-84

7.1.2 FSL-BODIPY

Figure 109 shows the effect of different storage media (with temperature variation) on the retention of FSL-BODIPY in BODIPY-kodecytes over 24 h. The data in Figure 109 has been normalised against 0 h and is shown in Table 23 for clarity. It shows the change in BODIPY-kodecytes fluorescence signal from 0 h (%) over a period of 24 h storage, indicating the retention of FSL-BODIPY. The following conclusions can be drawn from the data shown in Figure 109 and Table 23: Firstly, at 4°C, irrespective of different

concentrations of BSA in the storage media, the MFI of BODIPY-kodecytes remains stable, and in the presence of 50% plasma, the MFI decreases by 5%.

Secondly, at 37°C, within 6 h of storage, the MFI of BODIPY-kodecytes decreases by nearly 9% in CellStab, while it decreases further to 15% in the presence of BSA and 25% in the presence of plasma. Further incubation for 24 h in CellStab increased the signal loss by 6%, whereas in the presence of BSA and plasma, it increased to 45%.

This result highlights that at 37°C, within 6 h of storage, the presence of BSA or plasma does not have a major impact on the retention of FSL-BODIPY, but after 24 h of storage, the presence of proteins or plasma lipids significantly decreases the retention of FSL-BODIPY in kodecytes. Hence, it could be said that an elevated temperature of 37°C causes a minor impact on FSL-BODIPY retention, and the effect of protein and plasma lipids amplifies its negative effect mostly after 24 h of storage.

Table 24: Change in MFI of 6 and 25 µM BODIPY-kodecytes at 6 and 24 h from 0 h (%) in 0, 5, 15% BSA and 50% plasma in CellStab at 37°C, and 4°C.

		Change in MFI from 0 h (%)							
		BODIPY-kodecytes							
		4˚C				**37˚C**			
		6 µM		**25 µM**		**6 µM**		**25 µM**	
	CellStab	6 h	24 h	6 h	24 h	6 h	24 h	6 h	24 h
cell storage solution	**0% BSA**	2	0	2	-2	-9	-15	-7	-12
	5% BSA	4	1	3	0.5	-26	-71	-16	-65
	15% BSA	4	-1	3	2	-35	-92	-21	-79
	50% plasma	-6	-5	-4	-2	-38	-80	-35	-86

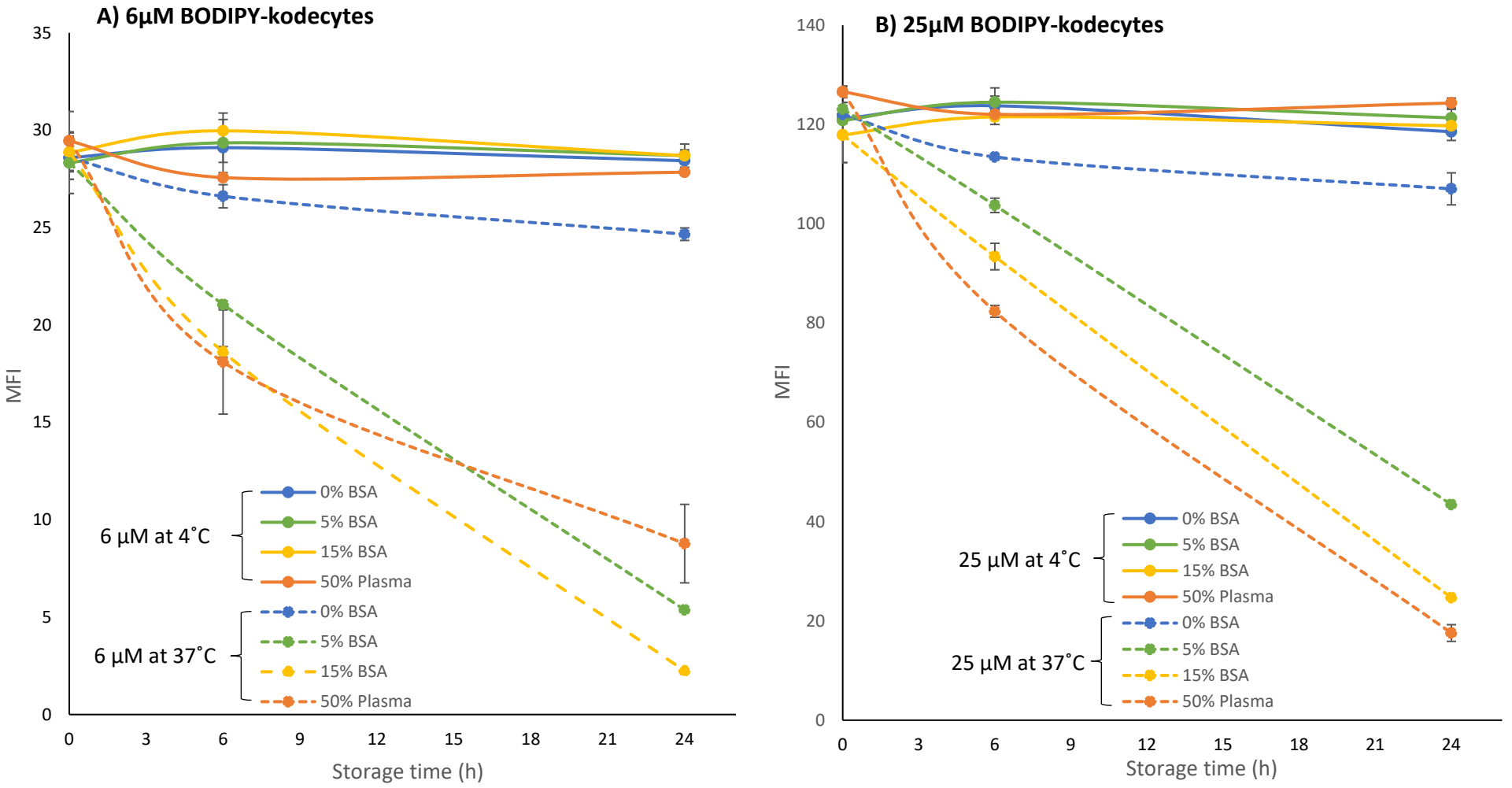

Figure 109: The retention of FSL-BODIPY in BODIPY-kodecytes over 24 h in 0, 5, 15% BSA and 50% plasma in CellStab at 37°C, and 4°C. Results shown are mean ± standard deviation, n=3.Change in the MFI of **A**) 6 µM BODIPY-kodecytes **B**) 25 µM BODIPY-kodecytes.

7.1.3 FSL-biotin

Similar to FSL-FLRO4 and FSL-BODIPY, the retention of FSL-biotin in biotin+SAF488 kodecytes was examined over a period of 24 h in different storage media at 37°C and 4°C. Results (Figure 110) showed that when biotin+SAF488 kodecytes were stored at 4°C, the MFI of kodecytes decreased, indicating a decrease in retention (by 8%). Additionally, irrespective of the FSL concentration (6 and 25µM) tested, the fluorescence signal changed at approximately the same rate under a similar incubation temperature and storage media.

The data in Table 24, normalised against 0 h, provides a direct comparison of the retention levels of FSL-biotin at 6 and 24 h. Compared to 4°C, biotin+SAF488 kodecytes lost more FSLs when kodecytes were maintained at 37°C. Compared to CellStab within 6 h of storage, the MFI of biotin+SAF488-kodecytes decreased by more than 10% in the presence of BSA. However, the impact of BSA in storage media was clearly established after 24 h of storage, as the MFI of biotin+SAF488-kodecytes decreased further by 40%. Hence, it could be concluded that after 24 h at 37°C, the retention of FSL-biotin is impacted mostly by the presence of BSA in the storage media, and this negative effect is enhanced by elevated temperature.

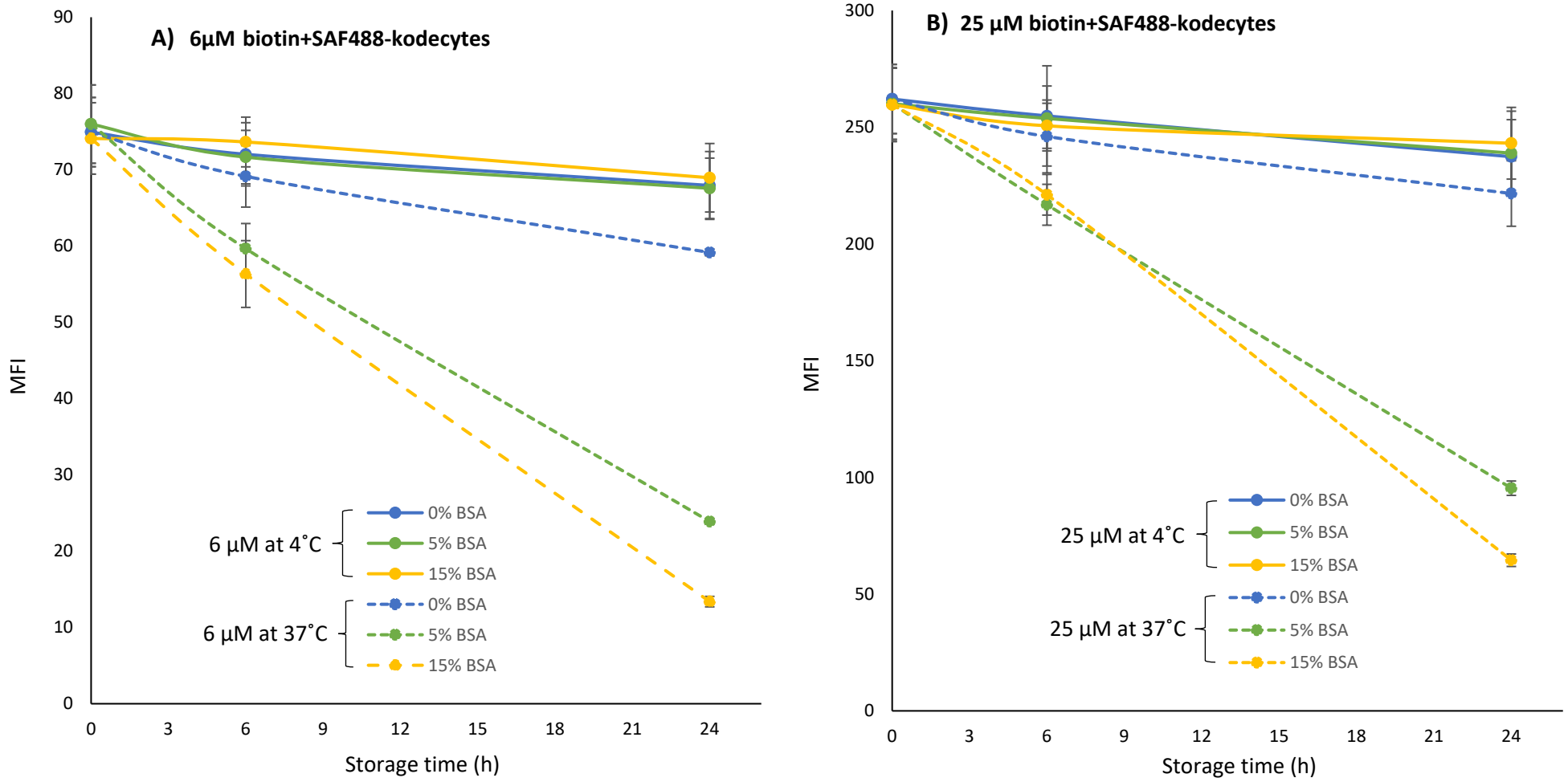

Figure 110: The retention of FSL-biotin in RBC biotin+SAF488 kodecytes over 24 h in 0, 5, and 15% BSA in CellStab at 37°C, and 4°C. Results shown are mean ± standard deviation, n=3. Change in the MFI of **A**) 6 µM biotin+SAF488 kodecytes **B**) 25 µM biotin+SAF488 kodecytes.

Similar results were observed in the case of FSL-BODIPY retention study. A possible explanation behind this finding could be the presence of a hydrophobic head group in both FSLs, which have more affinity towards protein and plasma-lipid, thus may facilitate more release of FSLs from kodecytes.

Table 25: Change in MFI of biotin+SAF488 kodecytes at 6 and 24 h from 0 h (%) in 0, 5, and 15% BSA in CellStab at 37°C, and 4°C. 6 and 25 µM of biotin+SAF488 kodecytes were prepared.

		Change in MFI from 0 h (%)							
		biotin+SAF488 kodecytes							
		4˚C				**37˚C**			
		6 µM		**25 µM**		**6 µM**		**25 µM**	
	CellStab	**6 h**	**24 h**	**6 h**	**24 h**	**6 h**	**24 h**	**6 h**	**24 h**
cell storage solution	**0% BSA**	-4	-9	-3	-9	-8	-21	-6	-15
	5% BSA	-6	-10	-2	-8	-21	-69	-17	-63
	15% BSA	-1	-7	-3	-6	-24	-82	-15	-75

7.1.4 Comparative analysis of retention between different FSL constructs

The data shown in Tables 23, 24, and 25 are potted in Figure 111 to allow for a more direct comparison between the different FSL constructs and reveal which FSL constructs are retained most efficiently in kodecytes when stored at 37°C. The data in Figure 111 is calculated by normalising the MFI generated by the 25 µM kodecytes over a specific period against the MFI of the 0 h time point.

From Figures 108–111, the following conclusion could be drawn: Firstly, when kodecytes are stored at 37°C in BSA (protein) or plasma (plasma lipid and protein) free medium, within 24 h of storage, approximately 75% of acquired FSL-FLRO4 is lost from the kodecytes, whereas the loss was only around 12% for the FSL-BODIPY and FSL-biotin constructs. This implies that an increase in temperature has a minor effect on the retention of FSL-BODIPY and FSL-biotin in the respective kodecytes. Overall, the loss of signal suggests the possibility that lost FSL constructs are being retained by the storage media (i.e., unable to relabel the kodecytes). Additionally, in protein/serum-lipid free media at 37 °C, the loss of signal (and hence the decrease in relabelling of kodecytes) could be attributed to the fact that the storage medium in which the reaction is taking

place actually acquires proteins and lipids shed from 37°C-incubated cells and captures the released FSLs (see Chapter 5).

Secondly, irrespective of the FSL constructs used to prepare kodecytes, BSA supplementation in the media led to more loss of FSL construct than in the BSA-free media. Within 24 h of storage, in BSA-supplemented media, FLRO4-kodecytes lost 90% of their FSL constructs, whereas BODIPY and biotin+SAF488 kodecytes lost approximately 65% of their FSL constructs. Thus, it could be seen that at 37°C, the protein-supplemented media has a greater impact on FSL-FLRO4 than FSL-BODIPY and FSL-biotin. Additionally, FSL-FLRO4 and FSL-BODIPY had comparable losses of respective constructs in a 50% plasma-supplemented medium. Overall data indicates that relatively more FSL constructs are lost in protein and plasma-lipid supplemented storage media. However, it is essential to note that possibly, the protein or plasma-lipids are not necessarily causing or increasing the loss of FSL from the kodecytes but are probably hindering their ability to re-label the kodecytes. This is supported by evidence in Chapters 3, 5 and 7, where the impact of membrane lipids and protein/plasma-lipid on the koding process and retention of FSL constructs is discussed.

A comparison of these FSL constructs in large scenarios is not shown for 4°C storage, as the retention of most FSL constructs remained largely unchanged over the period of 24 h.

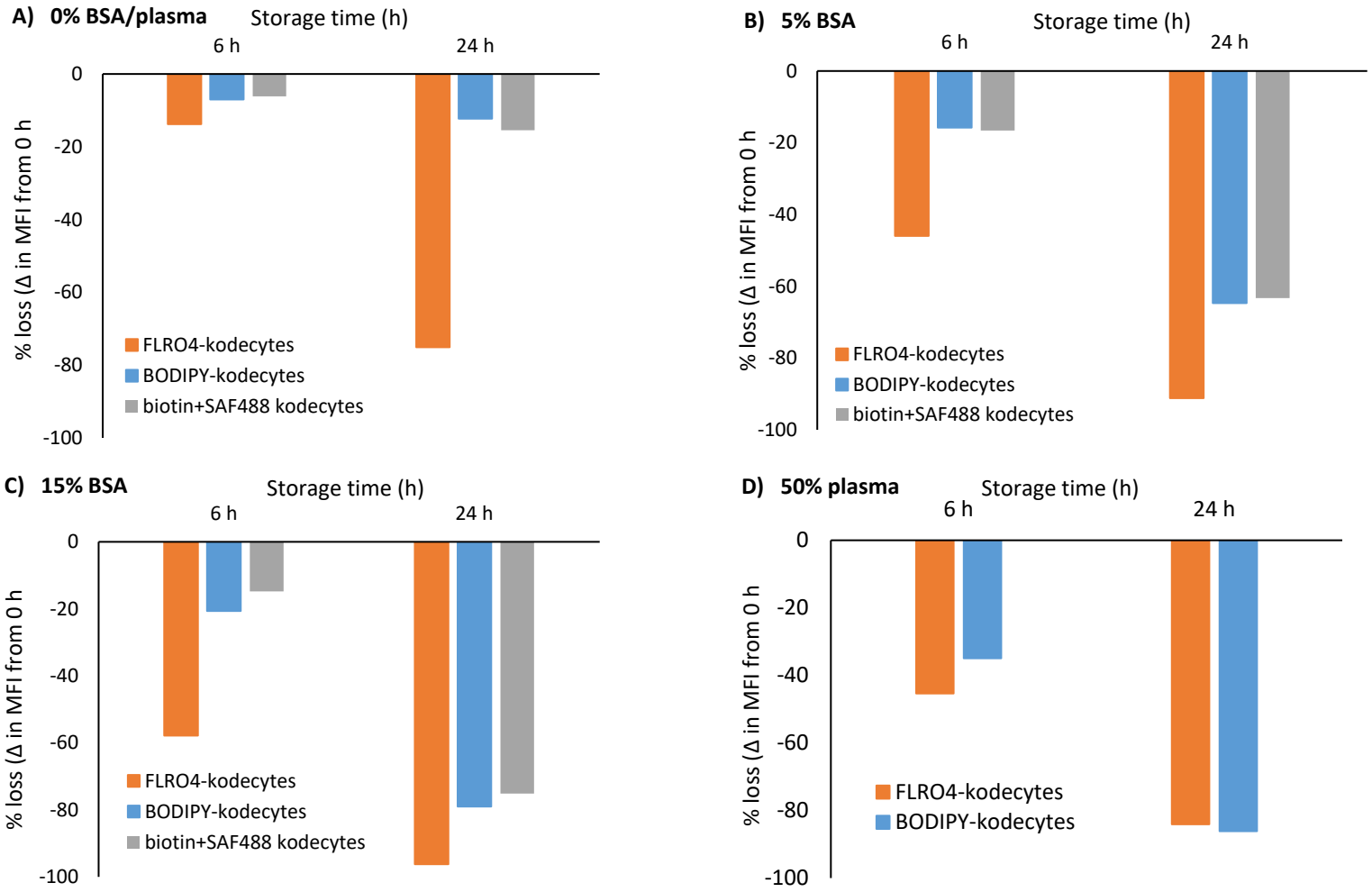

Figure 111: Comparative analysis of FSL retention in RBC kodecytes at 37°C. Kodecytes were prepared using FSL-FLRO4, FSL-BODIPY, and FSL-biotin. RBC kodecytes were stored in **A**) 0% BSA or plasma, **B**) 5% BSA **C**) 15% BSA and **D**) 50% plasma in CellStab. Change in MFI is compared from 0 h (%).

7.2 Co-incubation study

This experiment was designed to analyse the interaction and transfer of FSL constructs from kodecytes to unkoded cells when co-incubated in equal proportions. It was anticipated that this experiment might led to further understanding of the dynamics of loss and relabelling of kodecytes. The methodology is described in detail below, and a schematic overview is shown in Figure 112.

- Kodecytes were prepared with 6 and 25 µM FSL koding solution at 37°C for 2 h.
- After koding, kodecytes were washed 2× with PBS and once with CellStab.
- To examine the transfer of FSL constructs from kodecytes to unkoded cells, a co-incubation set-up was prepared, wherein an equal volume of kodecytes and unkoded cells (1:1) was mixed and thereafter resuspended at 5% v/v in respective resuspension media.
- The resulting samples were divided equally into three sets and maintained at 37°C, RT, and 4°C.
- 6 and 25 µM kodecytes were also maintained in isolation at similar conditions.
- To establish the evidence of transfer of FSL-construct, two comparisons were made.
- Firstly, FSL-construct transfer was examined during the 24 h co-incubation of what initially contained an equal mixture (1:1) of kodecytes and unkoded cells. For this, the MFI of kodecytes and unkoded cells were measured by flow cytometry at 0, 6, and 24 h co-incubation. Change in MFI of respective unkoded cells and kodecytes (after 0, 6 and 24 h) determined if FSL constructs were either:
    - lost from kodecytes and acquired by unkoded cells, i.e., an increase in the MFI of the unkoded cell population and the concomitant decrease in the MFI of kodecytes during 24 h of co-incubation served as an indication of the complete transfer of FSL construct (from kodecytes to unkoded cells).
    - lost from kodecytes and not taken up by unkoded cells, (indicating) a loss to the storage media, where the lost FSL could no longer label unkoded cells.

- lost from kodecytes and are partially taken up by unkoded cells, indicating some constructs were lost to the storage media and some constructs partially label unkoded cells.

- There is also a fourth possibility that there is no change in the MFI of kodecytes and unkoded cells throughout co-incubation, indicating no loss of FSL constructs by kodecytes and, hence, no uptake of FSL constructs by kodecytes. However, all experimentation data so far supports the loss of FSL constructs from the kodecytes with varying degrees (owing to 4°C and 37°C storage), so this scenario is highly unlikely.
- Second, the MFI of kodecytes in isolation would be compared with the MFI of kodecytes stored in co-incubation to determine if the presence of unkoded cells regulates the retention of FSL constructs.

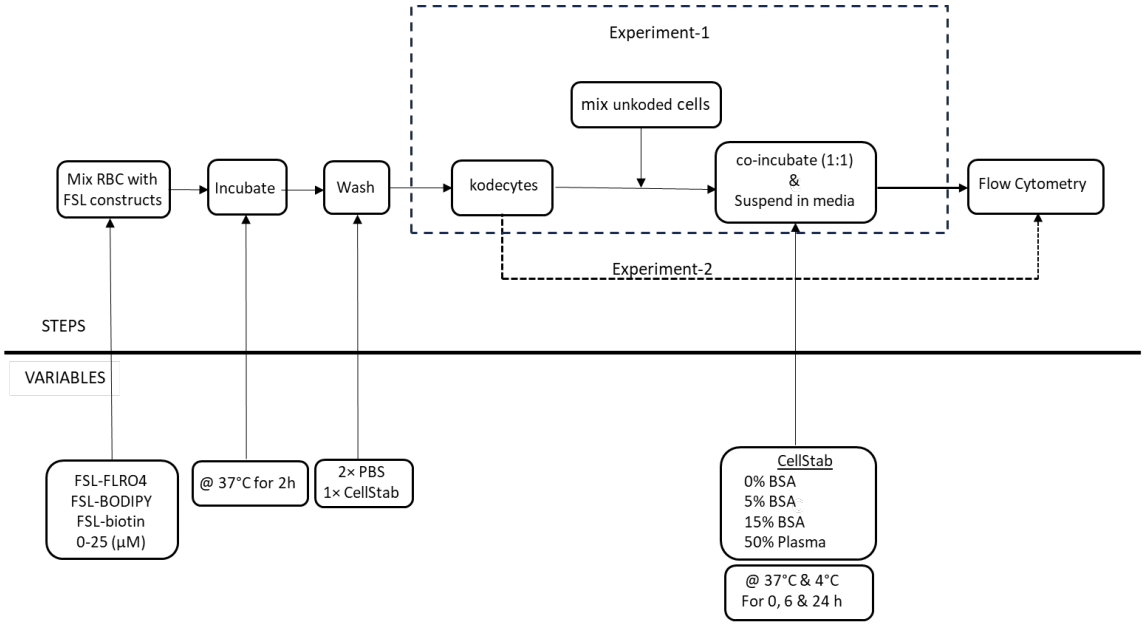

Figure 112: Schematic overview of methodology examining co-incubation scenario. The transfer of FSL-FLRO4, FSL-BODIPY, and FSL-biotin from RBC kodecytes to unkoded cells was studied in a co-incubation set up by flow cytometry.

7.2.1 FSL-FLRO4

Figures 113and 114 show the effects of various storage media and storage temperatures on RBC kodecytes and unkoded cells in the co-incubation experiment. In order to investigate the differences caused by two distinct concentrations of FSL-FLRO4 (6 and 25µM), two co-incubation scenarios (equal mixtures (1:1) of RBC kodecytes and unkoded cells) were set up and are denoted as (0+6) and (0+25), where 0 represents the unkoded part, and 6 and 25 represent the koded part. The MFI from unkoded and kodecytes components was measured over 24 h using flow cytometry.

The following observations were made using the data shown in Figures 113 and 114: Firstly, the MFI of unkoded cells and RBC kodecytes experienced minimal change over the testing period at 4°C. This was observed regardless of the tested storage media (0% BSA, 5% BSA, 15% BSA, and 50% plasma). This suggests that FSL-FLRO4 constructs are largely retained in FLRO4-kodecytes at 4°C, as observed in Section 7.1.1 (Figure 108).

Secondly, at 37°C, in the co-incubation experiment, the MFI of unkoded cells increased over the 24 h period. The increase in MFI by the unkoded cells was greater when the co-incubation was maintained in 0% BSA rather than 5% BSA, 15% BSA, and 50% plasma. This indicates that BSA and plasma in the storage media decrease the likelihood of FSL- FLRO4 transferring from kodecytes to unkoded cells.

Finally, throughout 24 h, the amount of fluorescence signal lost from kodecytes in any scenario did not represent the fluorescence signal gained by the unkoded cells. For example, in co-incubation after 24 h at 37°C in 0% BSA storage medium, 6 and 25 µM kodecytes lost approximately 75% of their fluorescence signal, whereas unkoded cells gained only around 5%. This suggests the lack of total FSL transfer from kodecytes to unkoded cells and retention of FSL constructs by the media. It was also observed that as the concentration of BSA in the storage media increases, the fluorescence signals produced by unkoded cells further decrease, indicating that a higher concentration of BSA has a greater capacity to retain FSL constructs, and interfere with them from being able to relabel (refer to Section 3.3.4)

An important observation in this data is that in 0% BSA/plasma at 37 °C, the relabelling rate, although higher than when plasma or protein were present in the media was not

as high as could be expected. This means that FSLs shed by kodecytes into media without added lipid or protein are still poorly labeled. This could be due to the fact that the storage medium in which the reaction is taking place actually acquires proteins and lipids shed from 37°C-incubated cells and captures the released FSLs.

It needs to be appreciated that the loss-relabelling process is very dynamic, as FSL lost from kodecytes can relabel either another kodecyte or an (initially) unlabelled cell. Additionally, the unkoded cells, which become labelled, also probably lose their FSLs to the media. Furthermore, it is not known if kodecytes or unkoded cells would have a labelling preference. Overall, it can be concluded that FSL constructs lost from kodecytes in the presence of protein (BSA) or plasma-lipid (plasma) do not relabel adjacent cells, at least to any significance.

To ensure that the co-incubation experiment was not influenced by the presence of unkoded cells (i.e., the koded cells lost their constructs at any different rate in the presence of unkoded cells), a full set of experiments for each FSL construct was done (kodecytes only). A comparative analysis of kodecytes when maintained in isolation or when maintained with unkoded cells (in co-incubation) established that the rate of loss of FSL constructs from koded cells was the same regardless of the presence or absence of unkoded cells (results not shown).

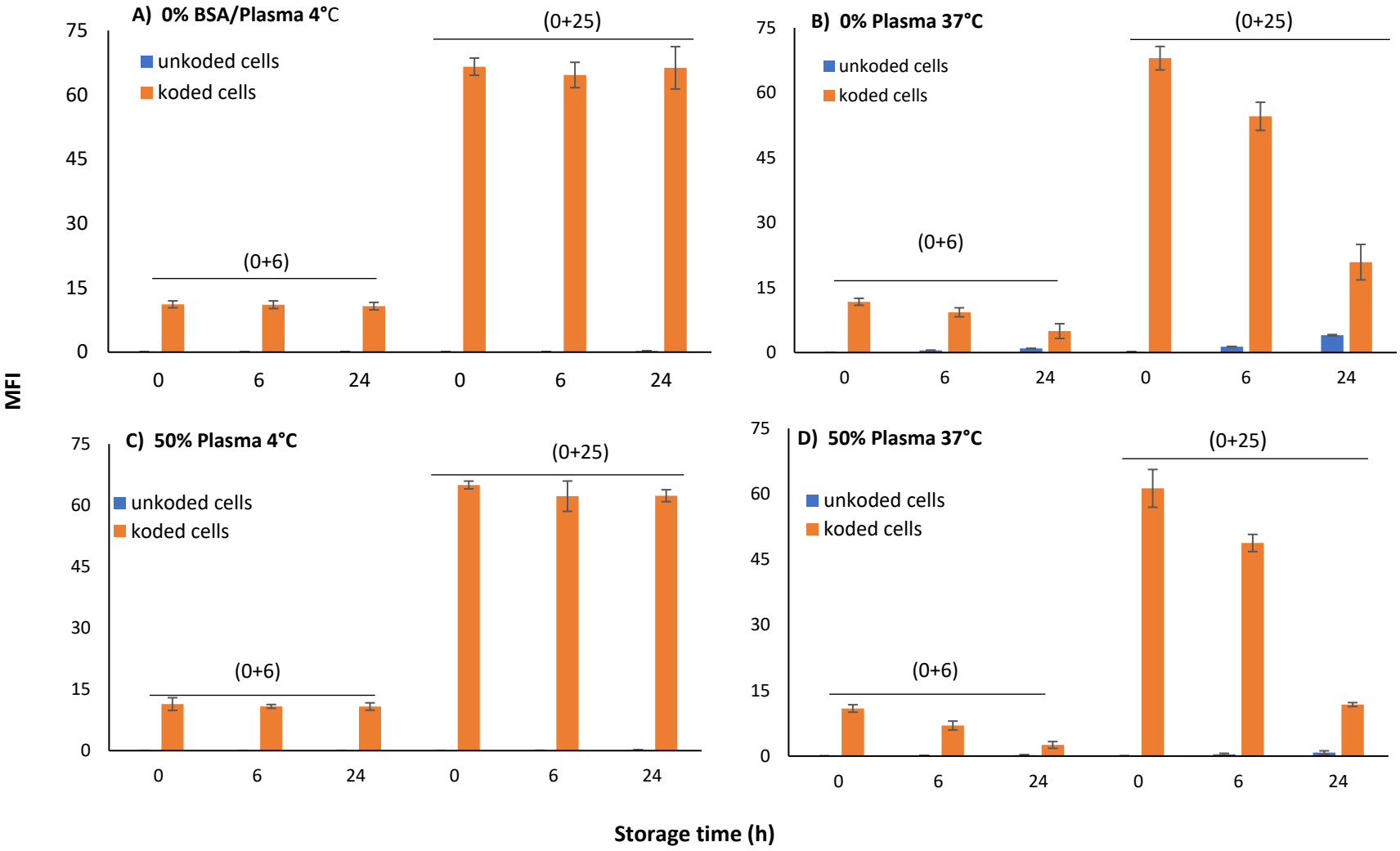

Figure 113: Change in MFI of FLRO4-kodecytes and unkoded cells in coincubation. Koded and unkoded cells were co-incubated and stored in **A**) 0% BSA/Plasma 4°C and **B**) 0% BSA/Plasma 37°C **C**) 50% Plasma 4°C and **D**) 50% Plasma 37°C for 0, 6 and 24 h. (0+6) and (0+25) represent a co-incubation experiment.

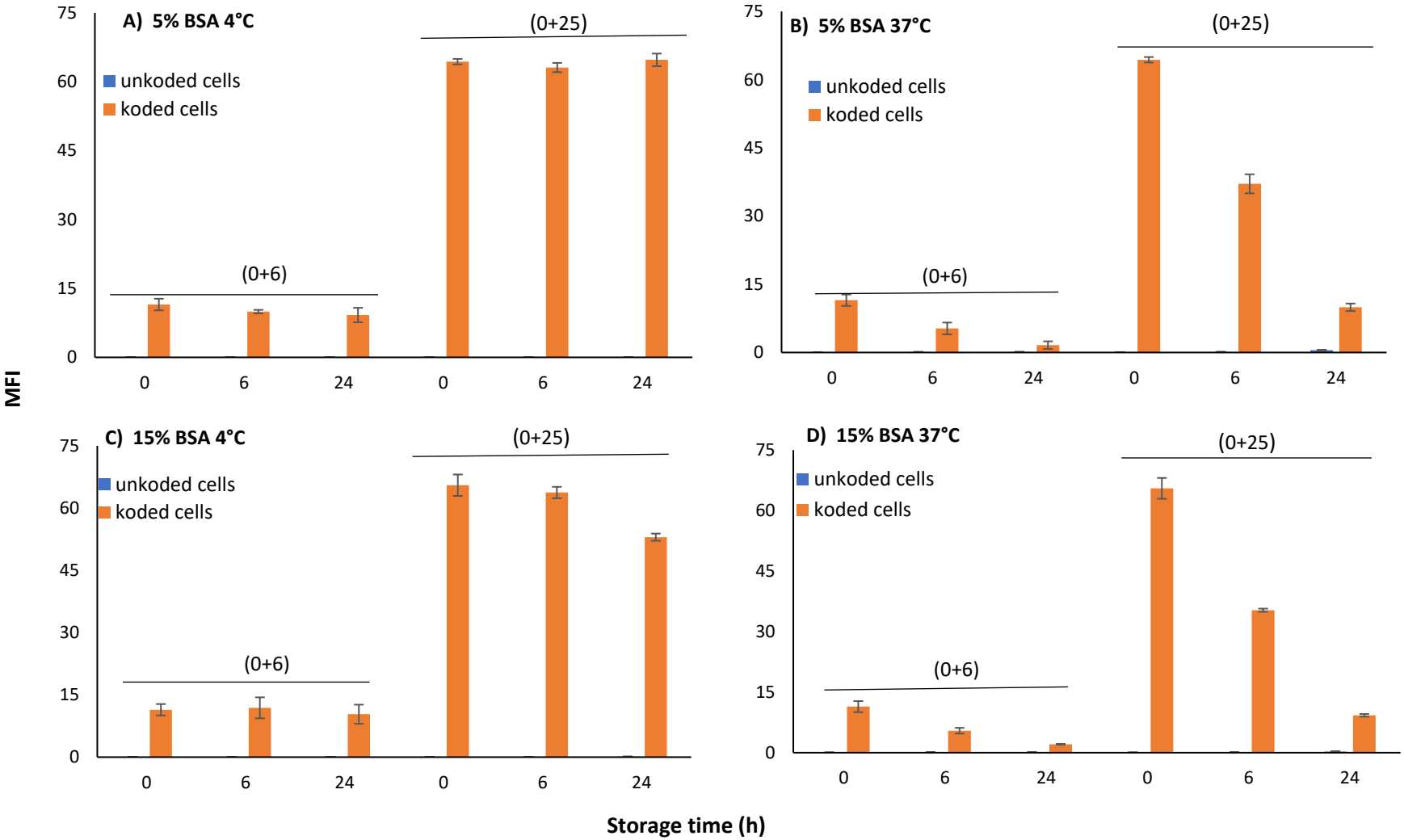

Figure 114: Change in MFI of FLRO4-kodecytes and unkoded cells in coincubation. Co-incubated koded and unkoded cells were stored in **A**) 5% BSA 4°C and **B**) 5% BSA 37°C **C**) 15% Plasma 4°C and **D**) 15% Plasma 37°C for 0, 6 and 24 h. (0+6) and (0+25) represent a co-incubation experiment.

7.2.2 FSL-BODIPY

Figures 115 and 116 show the effect of different resuspension media and incubation temperatures on RBC BODIPY-kodecytes and unkoded cells in the co-incubation set-up. Two different concentrations of FSL-BODIPY (6 and 25μM) were tested for their kodecytes membrane retention in the co-incubation set-up. The co-incubation set-up is indicated as (0+6) and (0+25), where 0 represents the unkoded part, and 6 and 25 represent the koded part. The following conclusions can be made from the co-incubation data obtained during 24 h storage in various conditions: Firstly, at 4°C, irrespective of different concentrations of BSA in the storage media, the MFI of BODIPY-kodecytes remain primarily unchanged (< 1%), indicating higher membrane retention of FSL-BODIPY. The MFI of unkoded cells increased by 0.4%.

Secondly, at 37°C, in the absence of BSA or plasma, the MFI of BODIPY-kodecytes decreased by nearly 30%. In BSA or plasma, the MFI of BODIPY kodecytes decreased by considerable margin of 70-80%. The MFI of unkoded cells increased by 20% in the absence of BSA and plasma and by 4% in the presence of BSA and plasma.

This result highlights that comparatively, more FSL-BODIPY was taken up by the unkoded cells in the absence of BSA and plasma, which is predominantly observed at 37°C. Hence, increased temperature and absence of BSA and plasma enhance the uptake of FSL-BODIPY by unkoded cells. Additionally, in the co-incubation set-up, the stability of FSL-BODIPY in kodecytes was predominantly negatively influenced by the presence of BSA and plasma, i.e., at increased storage temperature, the presence of BSA/plasma has a significant negative impact on the retention of FSL-BODIPY.

Like the FSL-FLRO4 co-incubation study, the FSL-BODIPY co-incubation study also supports the fact that BSA plays a role in preventing the FSL construct from relabelling unkoded cells.

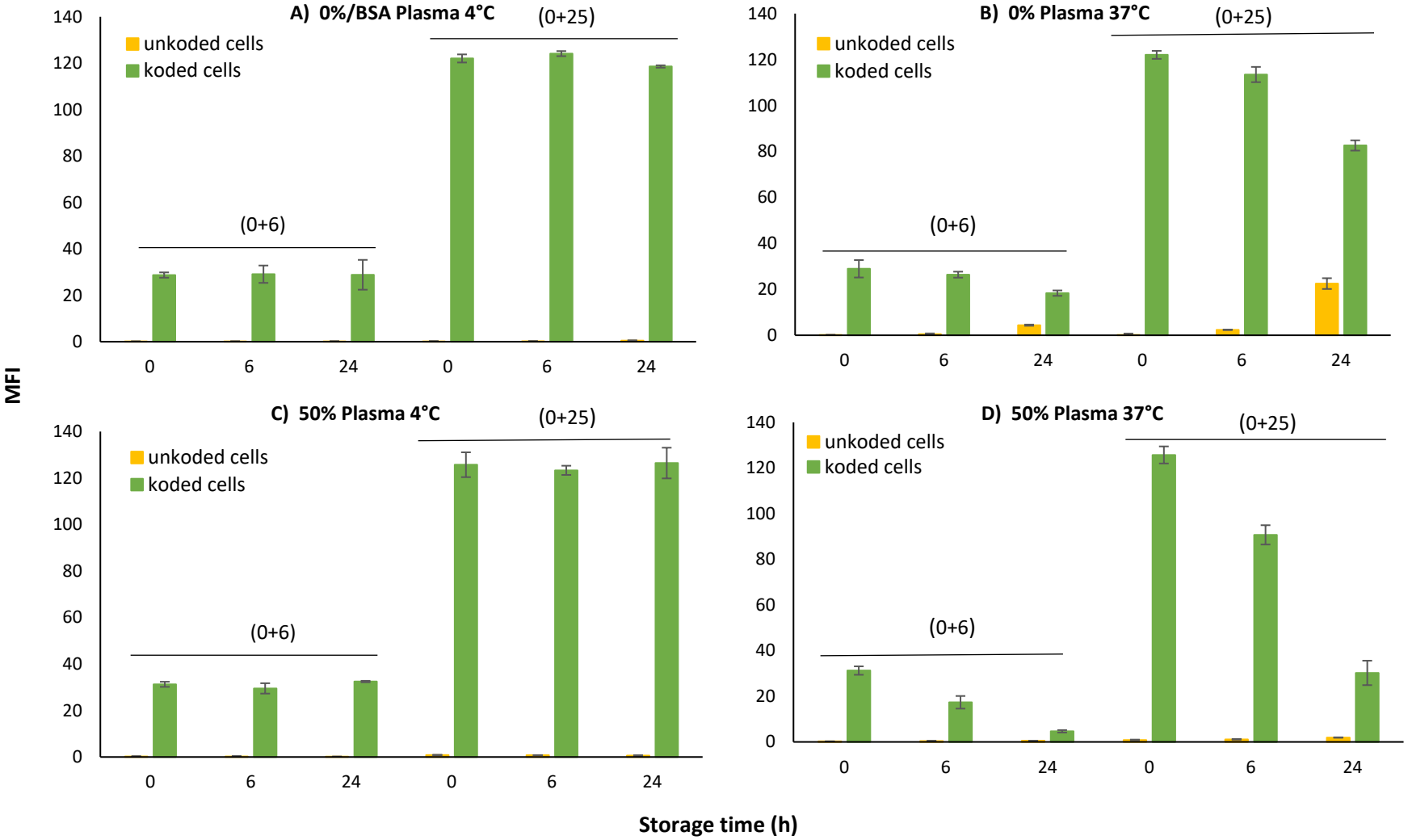

Figure 115: Change in MFI of BODIPY-kodecytes and unkoded cells in coincubation.Co-incubated koded and unkoded cells were stored in **A**) 0% BSA/Plasma 4°C and **B**) 0% BSA/Plasma 37°C **C**) 50% Plasma 4°C and **D**) 50% Plasma 37°C for 0, 6 and 24 h (0+6) and (0+25) represent a co-incubation experiment.

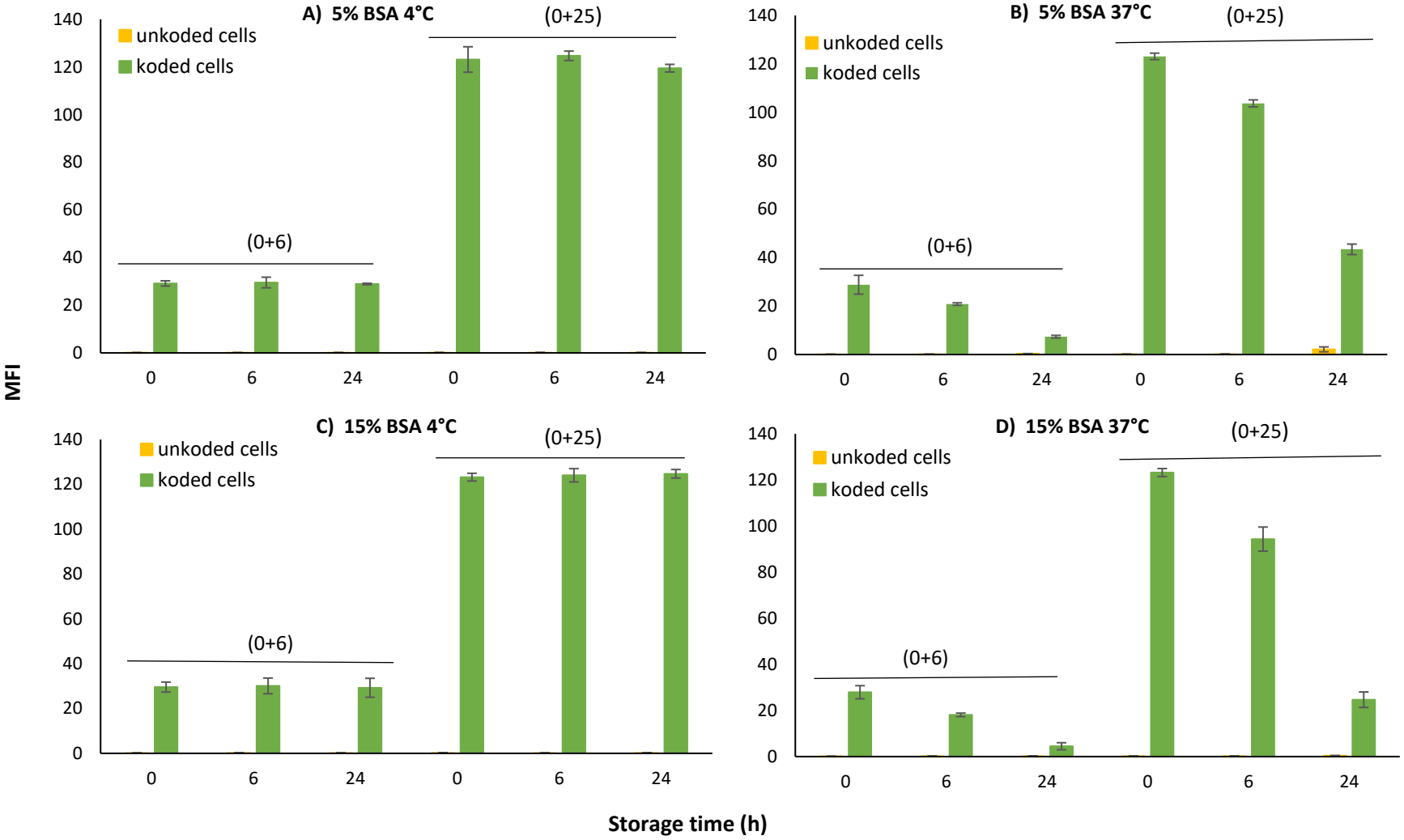

Figure 116: Change in MFI of BODIPY-kodecytes and unkoded cells in coincubation. Co-incubated koded and unkoded cells were stored in **A**) 5% BSA 4°C and **B**) 5% BSA 37°C **C**) 15% Plasma 4°C and **D**) 15% Plasma 37°C for 0, 6 and 24 h. (0+6) and (0+25) represent a co-incubation experiment.

7.2.3 FSL-biotin

Similar to FSL-FLRO4 and FSL-BODIPY, the retention of FSL-biotin in RBC biotin+SAF488 kodecytes in a co-incubation set-up was examined over a period of 24 h when stored in 0, 5, and 15% BSA CellStab storage media at 37°C, and 4°C.

Figures 117 and 118 showed that, regardless of storage media, the MFI of co-incubated biotin+SAF488 kodecytes dropped by around 7% (±2) after 24 h storage at 4°C, indicating a marginal decline in retention. The MFI of unkoded cells increased by 1% in the absence of BSA and by 0.1% in its presence.

At 37°C, the MFI of biotin+SAF488 kodecytes dropped by over 55% when BSA was not present in the storage medium. It further decreased to 70-80% in 5-15% BSA. In the absence of BSA, the MFI of unkoded cells rose by 25%, whereas in the presence of 5-15% BSA, it increased by only 4 - 0.4%. In addition, under similar incubation temperature and storage medium, the fluorescence signal changed at about the same pace regardless of FSL concentration (6 and 25µM). Following conclusion can be made from the overall data. Increase in storage temperature decreased the retention of FSL-biotin in biotin+SAF488 kodecytes and the presence of BSA further decreases retention.

The amount of fluorescence signal lost from kodecytes in any scenario did not represent the fluorescence signal gained by the unkoded cells. This signifies the lack of total FSL transfer from kodecytes to unkoded cells and supports the retention of constructs in the media. Presence of BSA further impedes the acquisition of FSL construct by unkoded cells indicating that a higher concentration of BSA has a greater capacity to retain FSL constructs and prevents them from being able to relabel.

Overall, it could be concluded that, during co-incubation at 4°C, the MFI of the biotin+SAF488 kodecytes dropped by 7%. In the case of FLRO4 and BODIPY kodecytes, this was less than 1%. This indicates that at 4°C, over the period of 24 h, out of all tested FSL constructs, FSL-biotin is the least retainable, Hence, the long-term analysis of proteins' impact on FSL construct retention in kodecytes at 4°C is crucial to determining their lasting effect.

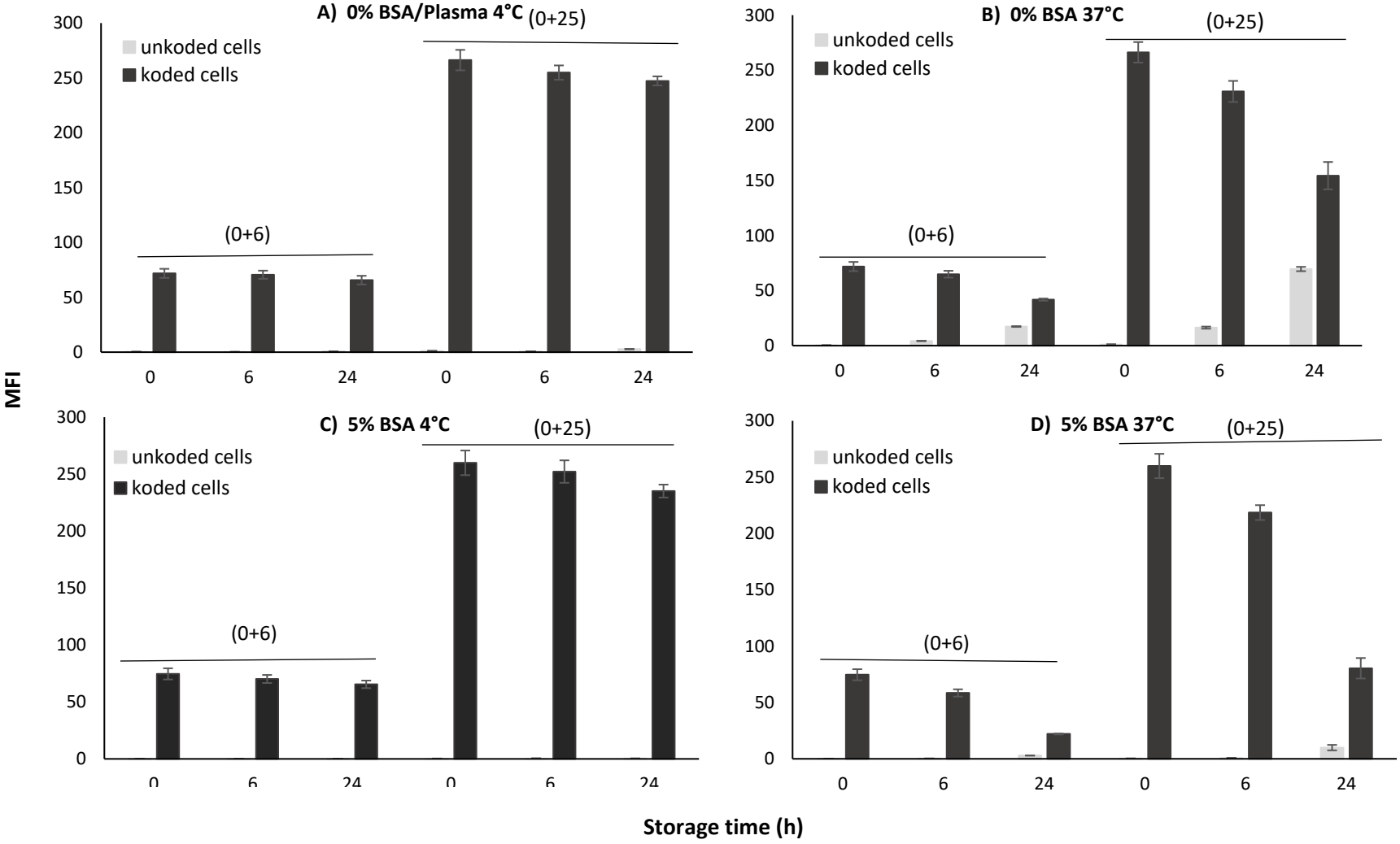

Figure 117: Change in MFI of biotin kodecytes and unkoded cells in coincubation. Co-incubated koded and unkoded cells were stored in **A**) 0% BSA/Plasma 4°C and **B**) 0% BSA/Plasma 37°C **C**) 5% BSA 4°C and **D**) 5% BSA 37°C for 0, 6 and 24 h. (0+6) and (0+25) represent a co-incubation set-up.

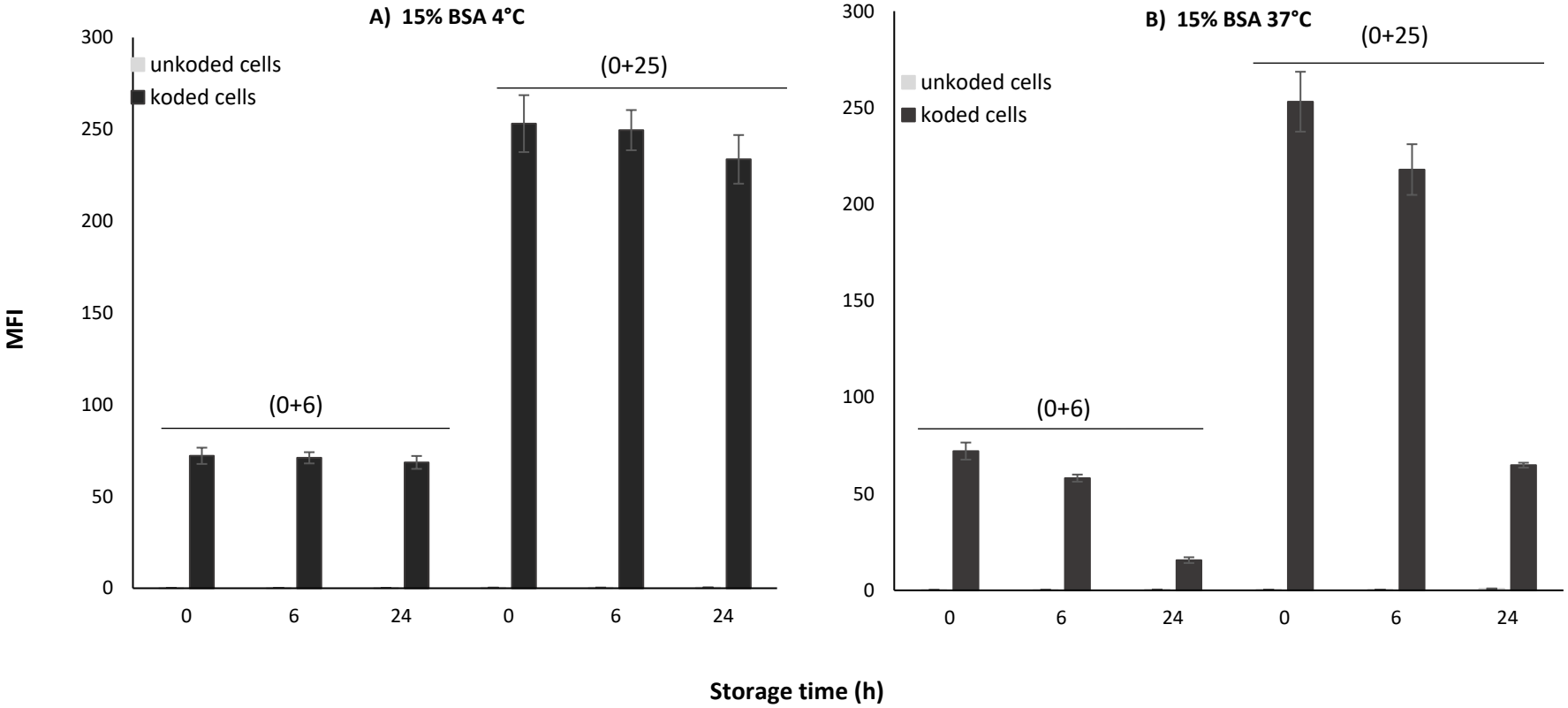

Figure 118: Change in MFI of biotin kodecytes and unkoded cells in coincubation. Co-incubated koded and unkoded cells were stored in **A**) 15% BSA 4°C and **B**) 15% BSA 37°C for 0, 6 and 24 h (0+6) and (0+25) represent a co-incubation set-up

7.2.4 Comparative analysis of FSL uptake by unkoded cell in co-incubation

To summarise how unkoded cells (RBC) behave differently when co-incubated with different RBC kodecytes, the uptake of the FSL construct by unkoded cells from various co-incubation experiments was compared using the data generated from previous experiments (Figures 113 to 118).

Figure 119 shows the signal gain by unkoded cells when (different) kodecytes were stored with unkoded cells in co-incubation at 37°C. To determine the amount of FSL acquired by unkoded cells, the change in the MFI (%) of unkoded cells was calculated by normalising the MFI generated by unkoded cells over a specific period (0, 6, 24 h) against the MFI of 0 h kodecytes. The MFI generated by koded cells at the 0 h time point was considered the maximum signal (100%).

The overall co-incubation study allows for the following conclusion: Primarily, there was a noticeable increase in fluorescence signal and, in turn, the FSL constructs by unkoded cells at 37°C when co-incubation experiments were incubated in BSA (protein) and plasma (serum-lipid)-free storage media. Unkoded cells acquired the most FSLs when co-incubation was with biotin-kodecytes (approximately 26%). The acquisition of FSLs decreased (by unkoded cells) slightly with BODIPY-kodecytes (15%). In contrast, unkoded cells acquired the fewest FSLs when co-incubated with FSL-FLRO4 kodecytes (nearly 6%). The amount of FSL acquisition by unkoded cells decreased significantly (<2%) when the co-incubation experiments were stored in protein and serum-lipid-free media. Based on the results, the following three questions need to be answered:

- Why, in protein or plasma-lipid free storage media, the acquisition of lost FSLs occurs but is not complete, indicating that the transfer process is not entirely efficient?
- Why does the acquisition of lost FSLs by unkoded cells decrease even more in protein or serum-lipid-supplemented media?
- Why were different FSL constructs acquired differently by unkoded cells?

Overall, it could be seen that (Figure 119) the amount of fluorescence signal or FSLs lost from kodecytes in any scenario did not represent the fluorescence signal gained or acquired by the unkoded cells. Compared to protein/serum-lipid supplemented storage

media, unkoded cells acquired more shed or lost FSLs in protein/serum free media, but this does not account for all lost FSLs (by kodecytes). This indicates the possibility of interfering factors in the media that may retain and further regulate the uptake of shed FSLs and prevent the acquisition of FSLs by unkoded cells. The accumulation of interfering factors (membranous entities) in the storage media could be due to prolonged incubation at 37°C. Thus, probably, these membranous entities present in the storage media were interfering with the acquisition of (shed) FSLs by unkoded cells (and also the relabelling of kodecytes).

Additionally, in protein or plasma-lipid supplemented storage media, unkoded cells acquired even fewer lost FSLs. This indicates the possibility of FSL constructs being retained by the storage medium even more. This suggests that proteins and serum may bind to the FSL construct, thus preventing unkoded cells from acquiring it. Additionally, the scavenging and storing action of BSA and plasma for the lost FSL construct is also supported by the observation that as the percentage of BSA in the storage media increased, the fluorescence signals acquired by unkoded cells decreased further (Figure 119), implying that retention of the FSL construct by the storage mediums increased proportionally with the increasing percentage of BSA (and plasma). Hence, the presence of BSA and plasma in a storage media adds to the cumulative change and delays the acquisition of lost FSLs by unkoded cells even further.

Finally, the nature of the FSL construct itself (like the degree of hydrophobicity of the head group, length of the spacer, etc.) could be responsible for the observation that in different FSL construct co-incubation setups, the unkoded cells acquired lost FSLs differently. FSL-related factors are discussed in Section 7.

Overall, the unkoded cells at 4°C did not show any significant change in fluorescence signal over 24 h of co-incubation; hence, the comparison for this scenario is not shown.

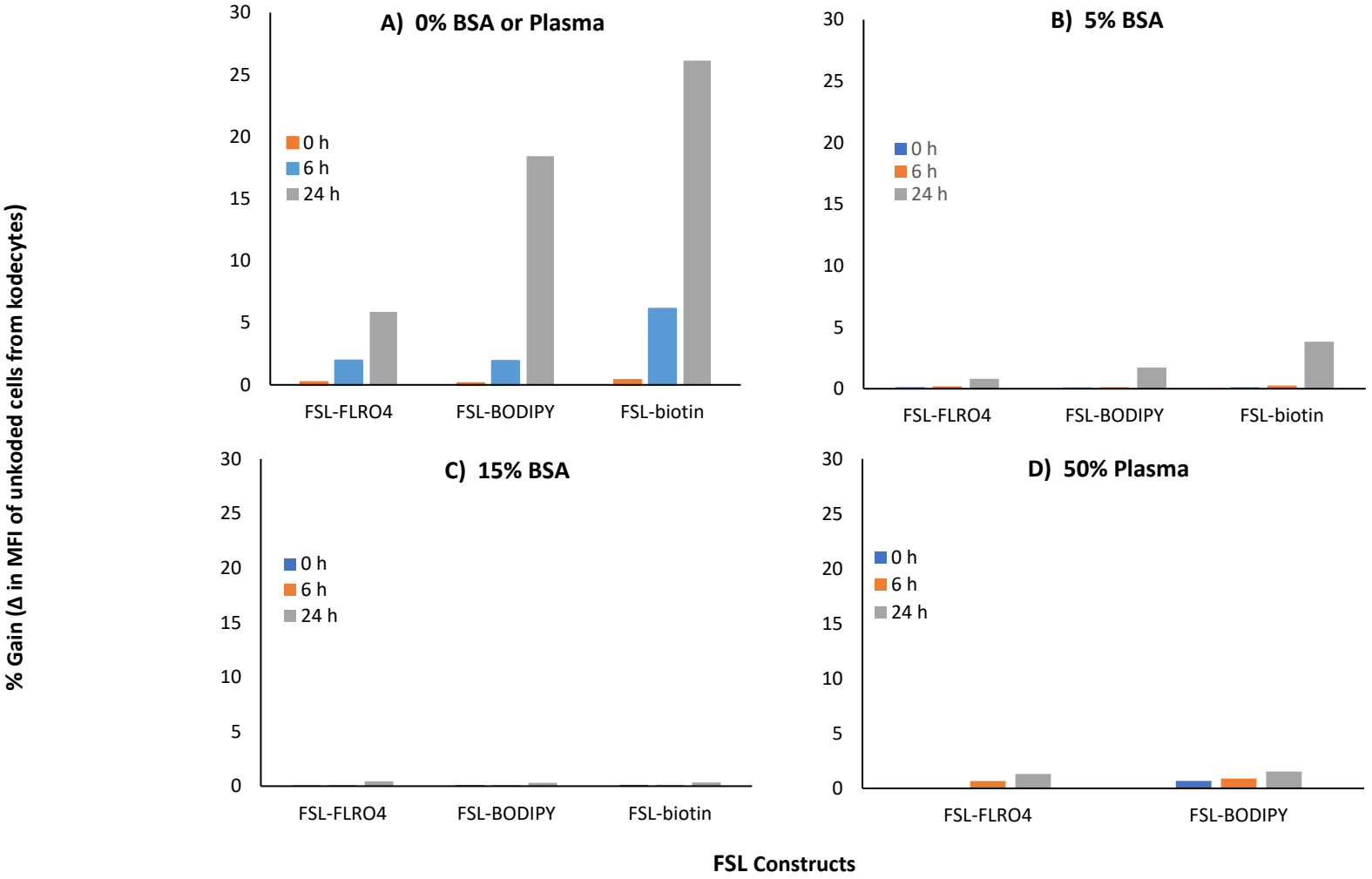

Figure 119: Uptake of FSLs by unkoded cells in co-incubation experiments stored at 37°C.The Y axis shows change in MFI (%) of unkoded cells at specific periods (0, 6 and 24 h) with respect to the MFI of RBC (25µM) kodecytes at 0 h only (100%). Data shown correspond to co-incubation set-up when stored in **A**) 0% BSA **B**) 5% BSA, **C**) 15 % BSA and **D**) 50% plasma in CellStab.

7.3 Retention of FSL constructs in Jurkat kodecytes

In the previous section, the retention of various FSL constructs in RBC kodecytes was examined. Since it is important to investigate the retention of FSL constructs and examine the dynamics of loss in actively growing cells, Jurkat cell cultures were established, and the retention of FSL-FLRO4, FSL-BODIPY, and FSL-biotin in Jurkat kodecytes at 37°C in different culture media was examined. Initially, two different koding durations were tested to analyse if koding duration regulates the retention of FSL constructs in kodecytes. Moreover, various serum concentrations in culture media were investigated for their significance in the retention of FSL constructs once the influence of varying koding durations on retention effectiveness was established.

7.3.1 Koding duration and retention of FSL constructs

Methodology

Two different koding durations were used to examine the retention of 6 µM FSL-FLRO4 and FSL-BODIPY on their respective kodecytes over a 24 h timeframe. To do this, 6 µM FLRO4 and BODIPY kodecytes were formed during a koding time of 1 and 2 h. Following the formation of the corresponding kodecytes, they were washed, resuspended in the complete media, and subsequently cultured at 37°C. At regular intervals of 0, 2, 4, and 24 h, kodecytes were harvested, and the retention of each kodecyte was assessed. Flow cytometry was used to determine the retention of FSL constructs in kodecytes.

Results

The study demonstrates the impact of different koding durations on the retention of FSL-FLRO4 and FSL-BODIPY in respective kodecytes over 24 h (Figures 120 A, B, and C). The same data in Figures 120 A and B is represented in Figure 120 C as percentage for clarity. In the case of FLRO4-kodecytes, a 2 h koding duration generated a greater initial signal at time point 0 h (0 h signifies MFI obtained just after koding). However, throughout the course of a 24 h retention test, koding duration had nearly no influence on the retention of FSL-FLRO4. Further, for BODIPY-kodecytes, a 2 h koding duration resulted in improved retention of FSL-BODIPY over a 2 and 4 h testing period. Additionally, over 24 h, the MFI of FLRO4 and BODIPY-kodecytes decreased gradually but showed a different pattern of loss. For example, post 2 and 4 h in the culture

medium, BODIPY-kodecytes lost approximately 25–45% of their FSL constructs, whereas in the case of FLRO4-kodecytes, this increased from 75–85%. It could be summarised that post 2 or 4 h in culture medium, FSL-BODIPY was approximately 40% more retained than FSL-FLRO4. However, irrespective of the different koding durations and post-24 h retention in culture media, approximately 90% of signals were lost for FSL constructs. As 2 h of koding duration provided better retainability for FSL-BODIPY and had no obvious adverse effect on FSL-FLRO4, it was used for koding hereafter.

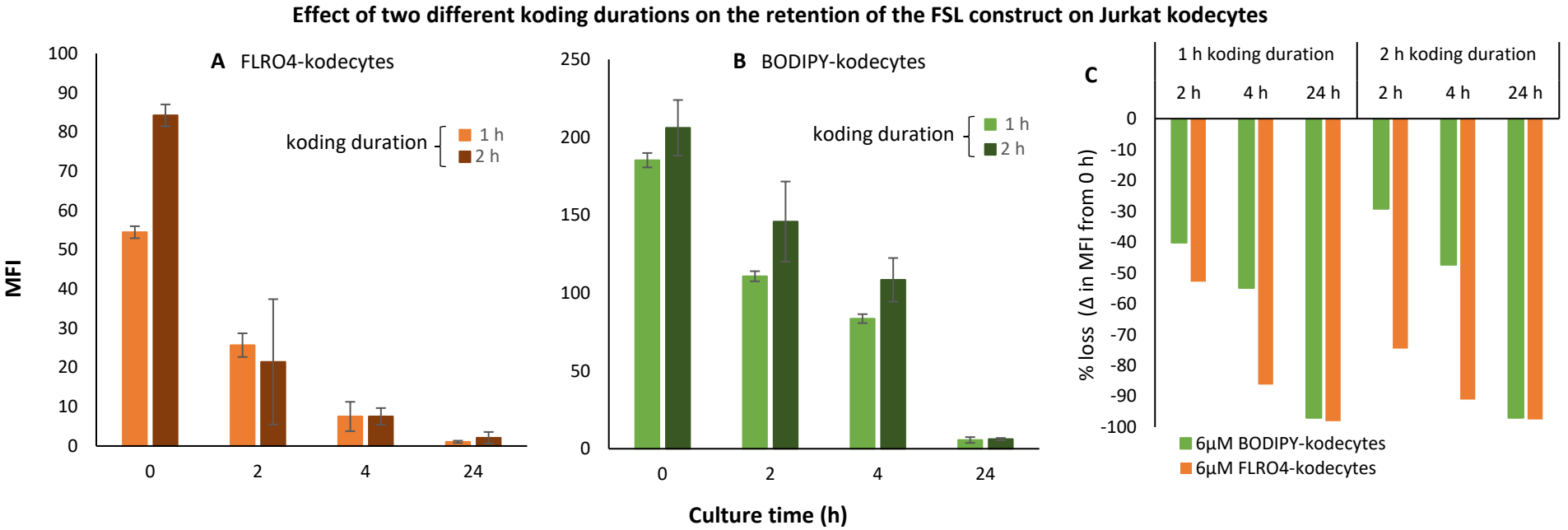

Figure 120: Effect of koding durations on the retention of FSLs in Jurkat-kodecytes at 37°C. Two different koding durations of 1 h and 2 h were tested for establishing their effectiveness on retention of 6 µM **A)** FSL-FLRO4 and **B)** FSL-BODIPY over a period of 0, 2, 4 and 24 h; where 0 h signifies MFI obtained just after either 1 h or 2 h koding. **C)** Change (loss) in MFI (%) of 6µM FLRO4 and BODIPY-kodecytes from 0 h, depicting effectiveness of retention of respective FSL constructs after 1 and 2 h of koding duration. The change in MFI, was determined using the formula [(Fi / F0) × 100] -100, where F0 and Fi represent the kodecytes fluorescence intensity at 0 h or a specific period of 2, 4, and 24 h. Note: scales are different across the graphs.

Factors probably affecting the retention of FSL constructs are: the expected refreshment or recycling of the cell membrane, including cells growing in a continuous culture; or the loss of FSL constructs to the media, which may be either temperature-dependent (37°C) or the constituent of the storage media, like 10% serum or both.

Lipids, along with other membrane constituents, are recycled between the membrane constituents and intracellular compartments. Depending upon the hydrophobicity of lipids, this process could be of a varied rate (rapid or slow). As FSL constructs are lipid-based constructs, this phenomenon could play a role in maintaining the retention of the FSLs in the kodecyte membrane. Additionally, Jurkat cells have a doubling time of 20.7 ± 2.2 h so it is unlikely that the loss observed within 2 and 4 h of incubation in culture is because of cell proliferation. From Figure 123 C, it could be seen that the FLRO4-kodecytes lost nearly 80% of their construct within 4 h of incubation in culture medium, whereas the BODIPY-kodecytes lost 45% of FSL-BODIPY. This result indicates that though both FSLs were lost into the media due to greater membrane fluidity at 37°C (enabling quick movement of FSLs from membrane to media), at similar testing conditions, incubation at 37°C had a more negative impact on FLRO4-kodecytes than the BODIPY-kodecytes. Moreover, cell proliferation could be the probable cause of the loss of FSL constructs from kodecytes at 24 h.

7.3.2 Different culture medium and retention of FSL construct

Serum provides vital nutrients and growth factors that help cells grow more effectively. Thus, this section investigates the effects of culture medium with varying serum gradients (5, and 10% serum) on the retention of FSL constructs. In order to achieve this, 6 µM FLRO4 and BODIPY kodecytes were formed after 2 h of koding of Jurkat cells. Following the formation of the corresponding kodecytes, they were washed, resuspended in two different culture mediums, either containing 5% or 10% serum, and subsequently cultured at 37°C. At regular intervals of 0, 3, 24, and 48 h, respective kodecytes were harvested, and the retention of the FSL construct was assessed. Flow cytometry was used to establish the presence of FSL constructs in kodecytes.

The impact of culture media with different gradients of serum (5 and 10% serum) on the retention of FSL constructs in kodecytes over a 48 h period is shown in Figure 121. Post 3 h incubation in a storage medium, in the case of FLRO4-kodecytes, a rapid decline in

MFI was observed, whereas a more gradual decrease in MFI was noted for BODIPY and biotin+SAF488-kodecytes. Although after 24 h FLRO4 and BODIPY-kodecytes lost most of their signal, biotin+SAF488-kodecytes managed to maintain a noticeable amount. Probably the rapid decline in MFI could be attributed to a less retained FSL construct, and the gradual decline in MFI could be attributed to the anticipated recycling of the cell membrane and cell proliferation for cells growing in continuous culture.

Overall, a comparative study on MFI from various kodecytes suggests that serum gradients of 5-10% in culture medium does not affect FSL construct retention over the 48 h testing period. Additionally, it could also be summarized that of all three tested FSL constructs, FSL-biotin was more effectively retained in the corresponding kodecytes.

It is important to note that in Section 6.3, where the viability of Jurkat kodecytes was analysed under similar circumstances, it was shown that kodecytes were largely viable and metabolically active, and proliferation was not affected adversely. This suggests factors (such as internalization of FSLs) other than degradation of the kodecytes are involved in the decrease in retention of FSL constructs over the period of 24 h.

To conclude, FSL-FLRO4 does not appear to be suitable for long-term tracking of active cells at 37°C, as approximately 80% of signals was lost within 3 h of koding. However, FSL-BODIPY retained about 60% of their signal for up to 3-4 h and thus retained for longer. Finally, as observed FSL-biotin was the best retainable construct tested and can be used as a long-term tracking agent for actively dividing cells. Additionally, 10% serum, which is the usual concentration of serum used in standard cell culture conditions, is acceptable if used post-koding.

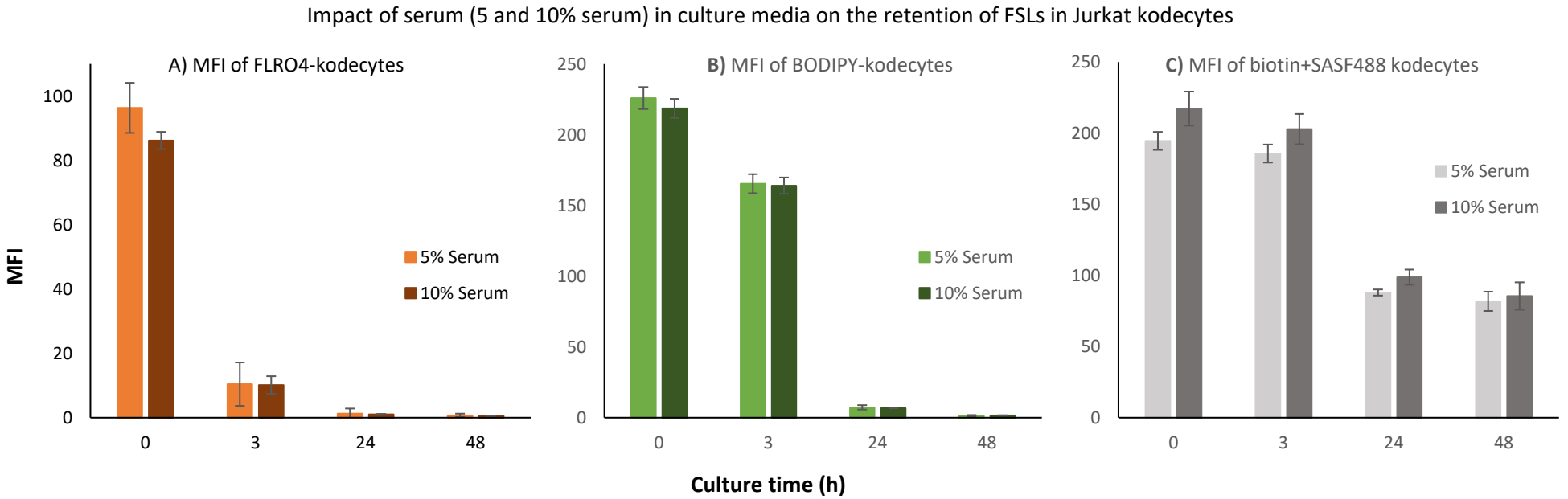

Figure 121: The effect of serum on the retention of FSL in Jurkat kodecytes over 48 h (5, and 10% serum in culture media). MFI of 6 µM **A)** FLRO4-kodecytes, **B**) BODIPY-kodecytes and **C**) biotin+SAF488-kodecytes generated over a period of 0, 3, 24 and 48 h at 37°C was determined using flow cytometry. Experiment was repeated twice, mean ± SD. Note: scales are different across the graphs.

7.4 Assessment of FSL constructs transfer with co-culture studies

To ensure cell tracking or proliferation monitoring, it is crucial to avoid the transfer of probes from labelled cells to unlabelled cells. In this work, 6 µM FLRO4 and BODIPY- kodecytes were formed after 2 h of koding of Jurkat cells. Following the formation of the corresponding Jurkat kodecytes, they were washed and maintained in an *in vitro* culture in complete media with either koded cells in isolation or an equal mixture of koded and unkoded cells to examine the transfer of FSL from kodecytes to unkoded cells. Samples were harvested at 0, 2, 4, and 24 h following the start of the co-culture. The MFI (in turn, the stability of the binding of FSL constructs to kodecytes) of koded in isolation and co-culture was determined by flow cytometry. It is important to note that the results shown could not be performed another time because of COVID lockdown and the unavailability of flow cytometry.

As can be seen in Figure 122, the MFI of unkoded cell populations does not rise during the 24 h co-culture period, suggesting that none of the tested FSL constructs (FSL-FLRO4 and FSL-BODIPY) shows any appreciable transfer from kodecytes to unkoded cells. The FLRO4-koded cell populations in co-culture exhibited a rapid decrease in MFI, indicating a faster decrease in retention of FSL-FLRO4. In comparison, the BODIPY-kodecytes showed a gradual decrease in signal hence, loss of FSLs construct was slower and gradual.

Additionally, the MFI of kodecytes in co-culture with unkoded cells and isolation was comparable. This was observed for both FSL-FLRO4 and FSL-BODIPY. This suggests that the presence of unkoded cells with kodecytes in co-culture does not influence the decrease in fluorescence signal and, consequently, the decrease in FSL stability. The loss in signal and, thus, retention of respective FSL could align partly with the loss of FSL constructs to media and partly with the anticipated refreshment or recycling of the cell membrane, including cells growing in a continuous culture.

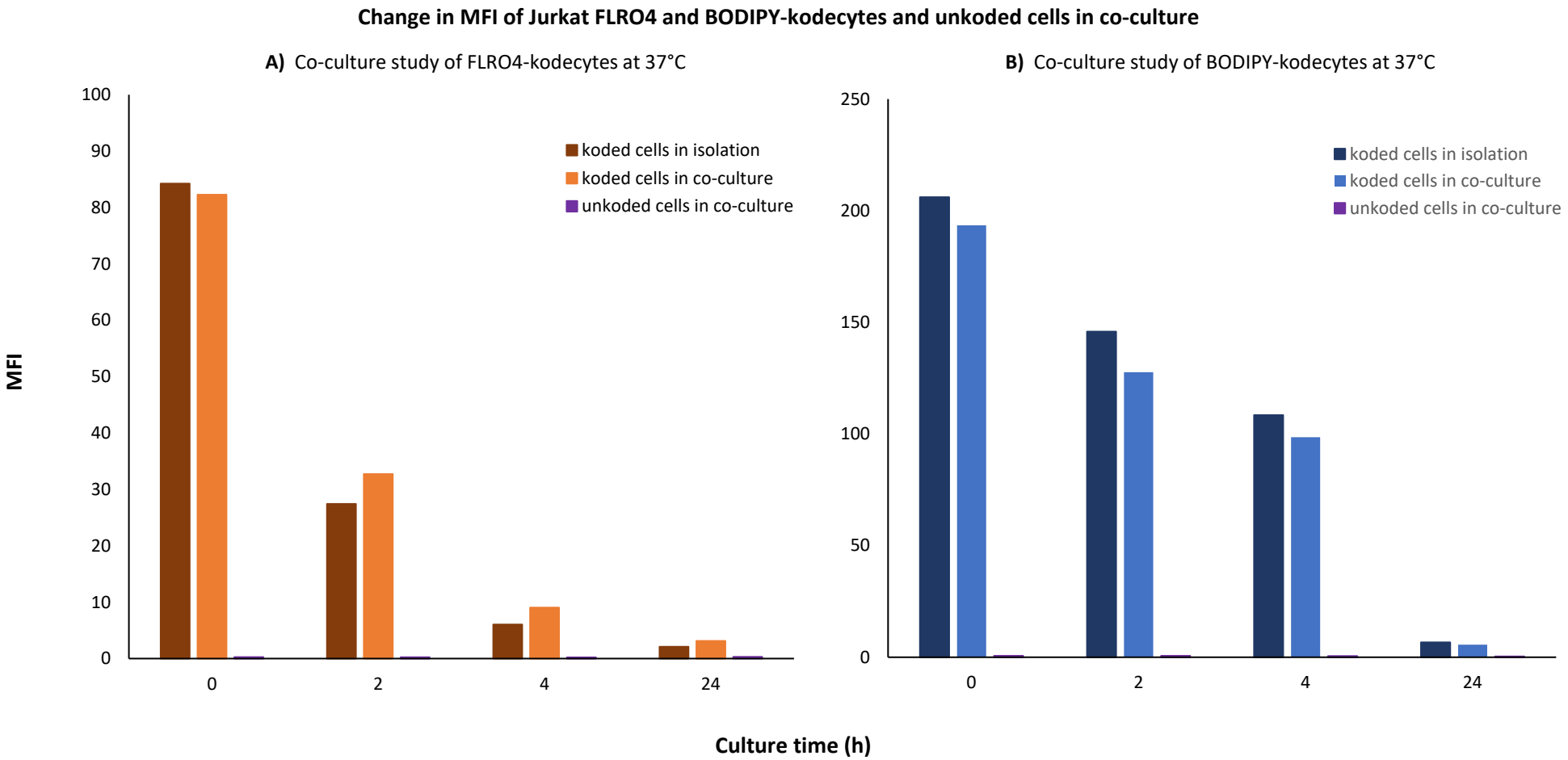

Figure 122: Change in MFI of Jurkat kodecytes and unkoded cells in coincubation. **A**) FLRO4-kodecytes **B**) BODIPY-kodecytes, and unkoded cells were cultured in complete medium at 37°C for 0, 2, 4 and 24 h. Both FSLs (FSL-FLRO4 and FSL-BODIPY) were tested at similar coincubation set-up. Kodecytes were maintained in isolation and tested simultaneously for a comparative analysis. Note: scales are different across the graph.

7.5 Chapter summary:

- Initial experiments established that kodecytes stored at 4°C retain FSL constructs in the kodecyte efficiently. This was true regardless of the presence of protein or plasma in storage media. In contrast, at 37°C, the FSL constructs were lost from kodecytes over time more rapidly.
- Overall data indicates that relatively more fluorescence signal was lost in protein and plasma-supplemented storage media. However, it is essential to note that the protein/plasma-lipid may not necessarily cause the loss of FSL from the kodecytes but may instead be hindering its ability to re-label the kodecytes.
- Regardless of the presence of protein or plasma in storage media, at 37°C, FSL-BODIPY and FSL-biotin are better retained in their respective kodecytes than FSL-FLRO4.
- The retention of FSL-FLRO4 in kodecytes is primarily influenced by the presence of BSA and plasma in storage media, as within 6 h of storage, nearly 70% of the signal is lost. In the case of FSL-BODIPY and FSL-biotin, the presence of protein or plasma lipid in the storage media also impacts the retention of FSL constructs, but at a slower pace.
- FSL-FLRO4 is not very suitable for tracking of active cells at 37°C due to quick signal loss. Comparatively, FSL-BODIPY retained more signal under similar conditions, making it more suitable for short-term tracking of cells (< 1 day). Finally, FSL-biotin is the best retainable construct, retaining approximately 40% of its signal even after 48 h of koding and could potentially serve as a long-term tracking agent.
- Jurkat kodecytes were found to be viable with intact membranes and active metabolism, suggesting factors other than degradation may be affecting the decrease in FSL construct retention over 24 hours. These factors could include expected membrane refreshment or recycling, continuous culture, and loss of FSL construct to media, indicating the importance of these factors in maintaining FSL construct integrity.

- The co-incubation study, where the interaction and transfer of FSL constructs from koded to unkoded cells were examined, found that the unkoded cells did not account for the total loss, hence there was no significant transfer. This indicates that the lost FSLs were probably partially labelling unkoded cells, and storage media could account for the rest of the lost FSLs.
- The finding that protein and serum-supplemented media prevent or slow down the acquisition of shed FSLs by unkoded cells in a co-incubation setup supports the previous hypothesis that protein/serum are not necessarily causing the loss of FSL from the kodecytes. However, it may instead be hindering its ability to re-label the kodecytes.
- None of the tested FSL constructs showed any appreciable transfer when Jurkat kodecytes were co-cultured with unkoded cells, suggesting that a similar phenomenon is preventing the acquisition (or relabelling) of lost FSLs.
- Generally, the MFI of koded cells in co-incubation (or co-culture in the case of Jurkat kodecytes) and isolation were comparable. This suggests that the presence of unkoded cells in co-incubation usually does not influence FSL retention.
- Overall, it could be summarised that the retention of the FSL construct is negatively affected by an elevated temperature of 37°C, and this effect is even more pronounced when protein and plasma-lipid are present in storage medium. Hence, the optimal storage conditions for kodecytes are crucial for their optimal performance and longevity.

Chapter 8 Discussion

8.1 The biological membrane

Life exists because of biological membranes.[1] The molecular landscape of the biological membranes that wrap cells is astonishingly similar in primitive unicellular prokaryotes to sophisticated multicellular eukaryotes like humans. It is made up of a diverse array of molecules, including lipids, proteins, and glycans. Each of these molecules is essential to the organism's continued existence and integrity. [1]

The biological membranes molecular landscape manages almost all interactions of the cell with its environment. [2] It regulates cell-cell interactions and maintains optimum cell function. Thus, manipulating biological membranes has the potential to improve our understanding of how cells interact with one another and provide new avenues for diagnosis and treatment. Given the intricate and dynamic nature of the cell membrane, bioengineering cell surfaces without impacting their viability, function, or antigenicity has been a problem. [2]

8.2 Bioengineering the molecular landscape of the biological membrane

Modification of the molecular landscape of the biological membrane with exogeneous material can potentially be achieved through three main methods: chemical conjugation, genetic modification, and passive modification using hydrophobic anchors.[2,3] While most chemical methods harm the cell's already-existing functional components, genetic alteration is often exceedingly complicated, difficult to manage, and confined to single allele mutations. On the other hand, the molecular landscape of the biological membrane can be modified without (significant) damage by using hydrophobic anchors in passive modification.[2]

Kode technology offers modification of any cells, organisms, viruses, or surfaces by means of the incorporation of desired functional components with biocompatibility and functionality.[3] Various FSL constructs have been known for several years for effective cell modification.[111] Despite the *in vitro* and *in vivo* use of several FSL constructs, many aspects of their dynamics of cell modification, cytotoxicity profile, and subsequent fate are not well understood. Additionally, mechanism of FSL construct uptake during the

koding process and their retention behaviour after koding have yet to be explored and are complicated as comparisons between methodologies is challenging. Furthermore, if the dynamics of cellular uptake are understood, improved methods of time of transformation may be possible, or at least the impact of the variable on the experiments will be better understood.

Previous work based on agglutination using serology has established some parameters (temperature, resuspension media, antibody variant) for labelling of RBC primarily with blood group based FSL constructs. However, the serology-based technique are restricted in applicability to non-blood group FSL constructs and to other cells. Thus, it is critical to use other sensitive technologies to understand the mechanism (and associated limitations) underlying FSL construct cell modification processes.

This research project explores in detail the interaction dynamics of FSL constructs, the mechanism of FSL uptake, the cytotoxicity profile of FSL constructs (based on different key indicators), and the retention of FSL constructs on inactive (RBCs) and actively dividing cell (Jurkat, PC-3) membranes using flow cytometry, fluorescence spectrophotometer, fluorescence microscopy, and scanning electron microscopy. Flow cytometry, being a very sensitive technology, has a wide range of detection, and the data generated by flow cytometry can help quantify the result by measuring the physical and chemical characteristics of kodecytes. This study was designed to optimise parameters for FSL construct uptake and retention on inactive and dormant cell membranes.

In brief, the most important findings of this study were that FSL modification of inactive and active cell membranes did not have any significant detrimental effects on the viability of the cells, and various factors (storage temperature and time, lipids, proteins, and different cell types) which effect the retention of FSL constructs on kodecytes have now been established. This study also established in detail the differences in the dynamics of uptake and retention detected between different FSL constructs (FSL-FLRO4, FSL- BODIPY and FSL-biotin).

8.3 RBC storage age and its effect on uptake of FSL constructs

RBC concentrates used for this study were stored at 4°C, and according to various literature, prolonged storage of RBC at 4°C causes changes known as "RBC storage lesions".[177-180] Hence, this study investigated the impact of RBC storage age on FSL construct uptake, aiming to determine if the selection of RBC for kodecyte preparation is RBC storage age dependent. The results obtained by flow cytometry showed that FSL-FLRO4 was taken up less efficiently by older stored RBCs (> d10 storage age) than younger stored RBCs. This indicates that FSL-FLRO4 show RBC storage-age-dependent uptake. However, unlike FSL-FLRO4, the storage age of RBC does not impact the uptake of FSL-BODIPY, as there was no significant difference in the uptake of FSL-BODIPY when different-aged RBCs were used. Potential explanations for the abovementioned findings are as below.

Human RBC have an average lifespan of 120 days in circulation, and at the time of blood donation, blood contains a heterogeneous population of both recently enucleated younger and older RBC[180] as reticulocytes, which are immature nucleated RBC precursors that constantly renew the mature enucleated RBC in the bone marrow. [181] The first hypothesis that could be proposed for the observation that FSL-FLRO4 uptake was more intense for d0 RBC (freshly processed blood) than d15 (storage-age) could be attributed to the age of RBCs at collection, i.e., to the difference in uptake efficiency of young and old RBC in the blood collected and processed for preparing kodecytes.[182] This hypothesis could have been tested if young and old RBCs were able to be separated from blood after collection and were further examined for their uptake efficiency of FSL constructs. However, this experiment was not done as the methodology for isolation of young red cells is restricted to isolating reticulocytes, and the processing to achieve this could potentially influence the results.

Secondly, the effect of storage lesions on RBC probably is the major contributor to koding efficiency of storage age RBCs. Cells that are stored for longer periods will have more storage lesions, and , thus when incubated will release more bioactive proteins, lipids, and RBC-derived microparticles or microvesicles (MP/MV).[164] This concept was clearly established when supernatant of incubated red cells was able to reduce FSL uptake. In retrospect ideally, this method would have been extended to examine old

verses young storage age supernatant as it is probable storage age will increase the number of MVs in the supernatant.

At the same, various studies have reported that microvesicles (MV) is produced during RBC storage and that its production is closely related to adverse morphological changes (i.e., changes in the asymmetry of the lipid bilayer of the cellular membrane).[180,181,183] Additionally, it has also been documented that MV accumulation gradually increases with storage time, and timings could be variable. [164,184].

Irrespective of the different storage ages of RBC, FSL-BODIPY uptake was found to be similar. The differences between FSL-FLRO4 and FSL-BODIPY was unexpected; however, this could be attributed to the fact that FSL-BODIPY has a highly lipophilic neutral functional group, which has been reported to be highly photostable and retainable.[150,151] As a result of the relative high lipophilicity of BODIPY dye, it tends to bind and localise onto the cellular membrane.[150-153] Hence, it could be suggested that prolonged storage of RBC at 4°C did not impact the uptake of FSL-BODIPY because it has a slightly different mechanism of labelling from the other FSLs (i.e., the functional head can interact with the lipid membrane) Most FSL constructs (except FSL-biotin and FSL-BODIPY) have a hydrophilic head; thus, experiment results from FSL-FLRO4 are probably most applicable to generic FSL.

8.4 Interaction of FSL constructs with biological membranes

Although the biological use of FSL has been addressed in several papers [5,126,185], the factors involved in the koding process has not been systematically investigated. Hence, one of the primary aims of this research was to examine the dynamics of cellular uptake of FSL-FLRO4, FSL-BODIPY, and FSL-biotin by inactive (RBCs) and actively dividing cells (Jurkat cells and PC- 3 cells) using flow cytometry. For this, initial experiments were carried out to examine various factors which would affect the uptake of FSL constructs.

8.4.1 Potential Factors affecting the uptake of FSL constructs

The uptake of lipid conjugates or lipid analogue probes (amphiphilic molecules) by biological membranes has been shown to be affected by their conformation in the solution phase.[86-88] In particular, they could be present in aqueous solution as either monomers, micelles (mixture of monomers and micelles), or aggregates.[87,88] The nature

of their conformation is determined by the structure of the compound including lipid, spacers and functional head. Additionally, various other factors like concentration, temperature and length of incubation process, presence of protein, serum, cell shape, cell age, membrane fluidics and cellular activity (dormant of actively dividing cells) would also affect the net uptake of lipid conjugates. [87]

Thus, understanding the conformation (free or micelle) of FSL in the solution phase (i.e., FSL characterization) is usual to understanding the koding process. Previous studies involving the characterization of FSLs in aqueous solutions (dispersed in PBS pH 7.4) have shown that in the absence of lipids and detergents, FSL constructions reside in aqueous solutions as free molecules when below their critical micelle concentration (CMC) [112] and when above CMC as micelles. Additionally, the exact conformation an FSL takes in solution is typically unknown and variable depending upon the functional head group, spacer, medium used for transformation, temperature, etc.[111]

According to Schwarzmann G., the CMC regulates the uptake of lipid conjugates into the biological membrane.[88] Lipid conjugates at or above CMC have reduced are shown to reduce their uptake compared to when present in the monomer form. As FSL constructs are lipid analogue constructs, they could be proposed to have a similar effect. Additionally, it also needs to be appreciated that the CMC point measurement is influenced by the chosen method and interpretation of the data, with no universally applicable or accepted method for determining it.[88] The CMC of FSL-biotin and FSL- FLRO4 ranged between 14-30 µM and 5-130 µM. [111] The CMC analysis of FSL-BODIPY has not been reported previously.

During this research, initial experiments were carried out to examine factors that would potentially impact the uptake of FSL construct, including:

- FSL concentration: FSL-FLRO4 (0.5 to 50µM), FSL-BODIPY (0.1 to 50 µM) and FSL- biotin (6 to 50 µM)
- Temperatures (4°C, RT, 37°C)
- Koding duration (5 minutes to 24 hours)
- BSA (accounting for protein) or serum (accounting for lipids and proteins)
- Glycocalyx (intact verses partially depleted)

Concentration dependent uptake

In this aspect of the study, a wide range of FSL construct concentrations were tested for their uptake by cells, and they mostly included concentrations below and above their CMC. At the standard koding scenario (koding duration of 2 h at 37 °C), the concentration-dependent uptake study of FSL constructs showed an expected dose-dependent cellular uptake with negligible background signals. At tested concentrations (≤ 50μM), uptake of FSL was linear for FSL-FLRO4, FSL-BODIPY, and FSL-biotin. A plateau of saturation in the fluorescence signal was not observed with the highest concentration used in this study, indicating that flow cytometry allowed for the dynamic range of sample concentrations to be analysed. Additionally, concentration-dependent cellular uptake was observed for both RBC-kodecytes and Jurkat-kodecytes.

Preferably stained (or exogenously labelled/probed) populations should have a relatively homogenous Gaussian distribution on a log scale, with as low a peak width (CV) as can be obtained.[186] Hence, CV can be said to signify staining uniformity. A symmetrical CV is associated with uniform, homogeneous staining, and a broader CV is associated with a non-uniform, asymmetrical, dimly stained subpopulation.[154] It should be noted that both RBC and Jurkat kodecytes reacted as homogenous, uniform, symmetrical populations, and subpopulations of kodecytes with non-homogeneous (multiple peaks) staining were not detected.

Temperature-dependent uptake

A previous temperature-dependent uptake study of blood group-based FSL constructs for red cell modification using agglutination methodology found that koding efficiency improves with temperature.[187] However, temperature-dependent uptake of FSL-FLRO4, FSL-BODIPY, and FSL-biotin has not been analysed before. In this study, three different koding temperatures (37°C, RT, and 4°C) were examined and compared for their effectiveness in making RBC kodecytes at a range of representative concentrations (i.e., low: 6 μM, medium: 25 μM, and high: 50 μM concentrations of FSL). Additionally, the koding efficiency of these FSLs and concentration was analysed over a range of koding durations of 1, 2, 4, 6, and 24 h.

The results confirmed, as expected that the uptake of FSL constructs increases with temperature. At 37°C, FSLs were the more readily acquired, followed by koding at RT and 4°C. This was observed regardless of the different FSL constructs used for koding RBCs and at all tested concentrations (6, 25, and 50 µM). Additionally, regardless of different koding temperatures, FSL-biotin koding efficiency was superior to that of FSL- FLRO4 and FSL-BODIPY. In marked contrast to FSL-FLRO4 and FSL-BODIPY, the labelling efficiency of FSL-biotin even at 4°C was much faster and more efficient. For example, within seconds of mixing RBC with FSL-biotin (0 h), biotin+SAF488 kodecytes accounted for nearly 15% of the uptake, whereas for FSL-FLRO4 and FSL-BODIPY, the respective kodecytes acquired less than 1% of the FSLs (Section 3.3.1).

There could be multiple factors that might impact the temperature-dependent uptake of FSL constructs. These factors may work in tandem or separately. The fluid state of the lipid bilayer is affected by temperature.[48] At 37°C, the membrane has been shown to be more fluid than at RT and 4°C, and probably the greater fluidity of the biological membrane facilitates the rapid uptake of the FSL construct. Hence, it could be suggested that the smaller degree of FSL construct incorporation at lower temperatures was due to a decrease in membrane fluidity.[48,86] Additionally, higher temperatures could also increase the availability of FSL constructs to incorporate into the RBC membrane. It is probable that higher temperature affects how quickly monomers leave from their micellar form. Overall, at 37°C and RT, FSL constructs could be proposed to be in rapid motion, colliding more constantly with the surrounding RBC, hence increasing the effectiveness of labeling and uptake.

The results obtained from the temperature-dependent uptake study of FSL constructs were in good agreement with literature investigating the uptake of various lipid analogue probes like exogenous glycolipid by biological membranes.[48] It was previously reported that exogenous glycolipid and lipid analogue probe (amphiphilic molecules) incorporation is significantly reduced at low temperatures, most likely as a result of the membrane's decreased fluidity.[48,89]

Another important insight from this study was the determination of temperature uptake equivalences, i.e., equivalence points of FSL uptake at RT and 4°C with respect to 37°C (after 1 h). This study proposes the approximate equivalence uptake points for

FSL- FLRO4, FSL-BODIPY, and FSL-biotin. For FSL-FLRO4 and FSL-BODIPY, it was estimated to be 1-2 h at 37°C ≈ 4-8 h at RT ≈ 200-300 h at 4°C, whereas for FSL-biotin, it was 1 h at 37°C ≈ 2 h at RT ≈ 24 h at 4°C. These results suggest that uptake efficiency differs among FSL constructs (at least those tested here).

Time-dependent uptake

Currently, the standard koding duration is 2 hours. In this aspect of the study, kodecytes were prepared at 37°C with koding durations ranging from 5 minutes to 24 h, with a range of FSL concentrations. The results confirmed, as expected that the uptake of FSL constructs increases with increasing koding duration. FSL construct uptake was fastest in the first hour, and then slowed. In, the case of FSL-FLRO4, uptake reaches a maximum at 4 h of koding, and after 4 h of koding duration, the fluorescence signal (MFI) surprisingly starts decreasing. Compared to 4 h, FLRO4-kodecytes at 24 h lose approximately half of their fluorescence signal. In contrast It is also important to FSL- BODIPY and FSL-biotin, did not show any significant fluorescence signal loss with extended incubation at 37°C. Additional experiments were then designed to evaluate mechanism for FSL-FLRO4 loss (See Chapter 5),

The impact of CMC on the uptake of FSL construct became much clearer from the time - dependent uptake study. Results showed that in the case of FSL-FLRO4, lower concentrations, especially 3 and 6 µM (below CMC), seem to be taken up faster within the initial incubation/koding period than higher (above CMC) concentrations (≥ 25 µM), and as the incubation period progresses, the rate of uptake becomes more uniform across the concentration range. It is possible to speculate that the difference in koding efficiency is due the (CMC), and monomers more efficiently label the cells.[112] As the micelle form is said to be more stable as it does not readily dissociate or exchange monomers in the solution phase.[88]

This the slower uptake rate at higher concentrations (> 25 µM) of FSL- FLRO4 during preliminary incubation time points could be attributed to the presence of micelles. It could be proposed that during the initial phase of incubation, FSL-FLRO4 at higher concentrations are in micellar form (or transitioning) with a low off-rate, owing to which they are more stable and do not allow exchange or dissociation of their monomers

readily in the solution phase. As the incubation/koding time progresses, micelles will have more time to incorporate into the membrane's surface, levelling off the uptake efficiency of lower concentrations. The CMC of FSL-FLRO4 has been proposed to be in the range of 14–30 μM. [111]

To further investigate the micelle phenomenon, an experiment was run wherein a non-fluorescent FSL construct, FSL-GB3, was used along with FSL-FLRO4 (in two different ratios) to attain a strength of 50 μM (representing micelles). FSL-GB3 was chosen for this study as it has an adipate-based spacer (like FSL-FLRO4); hence, confounding effects generated because of structural dissimilarities could be avoided. Results (3.3.3) show that, when RBC FLRO4-kodecytes were made in the presence of FSL-GB3 inducing the formation of micelles due to total lipid contained the fluorescence signal decreased. This was observed at both 5 and 60 minutes of koding duration. Based on the results (see Section 3.3.3), it could be hypothesised that FSL-GB3 induced micelle formation thus affecting the uptake of FSL-FLRO4 by retaining the FSL-FLRO4 in a micellar form and reducing its interaction with the RBC.

However, in contrast to FSL-FLRO4 uptake, FSL-BODIPY uptake reached its optimum quicker for higher concentrations (50, 25, and 13 μM) than lower concentrations (6 and 3 μM). This is not surprising as the FSL-BODIPY micelle would be expected to be significantly different to other micelle as it is more hydrophobic, and the stability of the micelle is probably much lower.[188,189] Hence, the inferred observation in the case of FSL-BODIPY (Section 2.6.3) may be due to the presence of less stable micelles, and /or their enhanced interaction with the cell lipid layer

The CMC of FSL-BODIPY has not been previously determined. During this study, a fluorescent plate reader-based experiment was set up to determine a potential CMC for FSL-BODIPY. When the fluorescence of FSL-BODIPY dispersions at increasing concentrations was analysed, it was shown that at increasing concentrations, FSL-BODIPY dispersions showed increased fluorescence until ≈13 μM; above this concentration, the change in fluorescence signal was not significant. This result suggests that the CMC of FSL-BODIPY could be around 13 μM, which is within the range expected. However, other methods are required to determine this value more accurately.

In the case of FSL-biotin, only two concentrations (6 and 25 µM) were tested for the time-dependent uptake study. Results showed that FSL-biotin uptake at different koding durations was very similar, suggesting (unlike FSL-FLRO4 and FSL-BODIPY) that possibly micelles have less impact the rate of FSL-biotin uptake. However, according to earlier studies, it was proposed that the CMC of FSL-biotin ranged between 14 and 30 µM, but the results obtained in this study do not relate to it. This could probably be because: Firstly, of all tested FSLs in this study, FSL-biotin has the least stable micelle form with a higher off-rate. Thus, FSL-biotin micelles would dissociate faster and release monomers with the quickest uptake rate. Based on the results shown in sections 3.3.2 and 3.3.3, it could be proposed that FSL-biotin was acquired with the highest koding efficiency, followed by FSL-BODIPY, and finally by FSL-FLRO4. Thus, the concept of FSL-biotin having the least stable micelle with a higher off-rate seems possibly.

Additionally, during the process of koding, microvesicles are released into the koding medium, which can change the CMC of FSL-biotin. Therefore, understanding how the process of koding affects micellar stability and degradation is of crucial importance for proper understanding of the interaction of FSLs with biological membranes. Due to a lack of appropriate instruments and difficulties in studying micellar assemblies, experiments testing the stability of FSL constructs in micelle were not performed.

Experiments were also conducted to examine the time-dependent cellular uptake of FSL-FLRO4 and FSL-BODIPY by Jurkat cells at 37°C. Overall, the results from Jurkat kodecytes showed that within 30 minutes of incubation or koding, approximately 40% of FSL-FLRO4 and FSL-BODIPY were acquired by Jurkat cells. Thereafter, within an hour of incubation, it increased to about 90% and 70% for FSL-FLRO4 and FSL-BODIPY, respectively, suggesting the fluorescence signal has plateaued for FSL-FLRO4. Jurkat cells acquired FSL-FLRO4 faster than FSL-BODIPY, whereas during the RBC koding process, FSL-BODIPY outperformed FSL-FLRO4. These observations could probably be attributed to the difference in the biological membrane of RBCs and Jurkat cells (non-active vs. actively dividing.

In summary, the uptake of FSL by the biological membrane is time, temperature, concentration, and FSL construct dependent. Additionally, the koding efficiency of FSLs is influenced by the presence of the micelle, which in turn is influenced by factors like

functional group, spacer, lipid, concentration, temperature, size, and hydrophobicity/hydrophilicity.

Impact of BSA (protein) and serum (protein or lipid) on koding process

Serum and serum components like albumin, protein, LDLs, and HDLs have been documented to form stable complexes with various lipid compounds include glycolipids.[86,87] Thus serum and lipid-probe complexes can affect availability (and uptake) to the cell membrane. The uptake of the lipid probes has been shown to be dependent on both the concentration of serum and the time of cell membrane exposure to the lipid analogue probe.[48] Additionally, these complexes could be of variable strength depending on the strength of the interaction between the lipid analogue probe and protein or lipid components.[14,32] These complexes are important as they determine the labelling and relabelling of lipid analogue probes by virtue of the release of the bound probe, which could further depend upon the micellar concentration of the lipid probe. Similarly, these interactions could possibly be involved in labelling and relabelling of cells with FSLs.

BSA is a serum albumin protein and is often used as a model for human serum albumin (HSA) due to its 76% structural homology to HAS [14,32,48] and is a good candidate for the studying the impact of components of protein. Also BSA is known to associate with protein.[190]

In section 3.3.4, the impact of BSA (protein) on the uptake of FSL constructs by RBCs was investigated. Result shows that as the concentration of BSA in the FSL transformation medium increased, its koding effectiveness decreased. The uptake of FSL by RBCs decreases significantly with 0.4% BSA, plateauing around 6% BSA, suggesting a saturation effect at higher concentrations. This negative impact on the uptake of FSL construct was more apparent at higher concentration. This implies that BSA is interacting with FSLs and interfering with labelling RBCs. This result is in good agreement with the findings reported in Saqr H et al. [48]

Another important finding from this aspect of the study was that protein had lesser impact on FSL- FLRO4 uptake than FSL-BODIPY and thus in the presence of BSA in transformation media, FSL-FLRO4 was capable of faster transformation (>30%)

compared to FSL-BODIPY constructs (Section 3.3.4). The phenomenon observed with FSL-BODIPY could be attributed to the lipophilic functional group of FSL-BODIPY. It has been known in literature that albumin has affinity for binding a variety of hydrophobic ligands such as fatty acids, tryptophan, steroids, anaesthetics, and several dyes it is the main transport agent in the plasma.[191] Additionally, it also been shown that serum albumins has several lipid binding site and due to a hydrophobic cleft, albumin tends to bind to lipophilic drugs.[192] Thus, it could be proposed that in the presence of BSA (in the transformation medium), FSL- BODIPY constructs are more likely to be interacting with BSA, resulting in an FSL-BSA complex, and as the FSL constructs are not readily available for labelling or relabelling of RBCs.

FSL-glycan were not examined in this study. It has been known (personal communication) that at 4°C, FSL-Glycan does not interact with BSA and thus does not associate with BSA. However, this interaction has not been studied at 37°C; hence, to establish the effect of BSA at physiological conditions (37 °C), the impact of BSA on FSL-Glycan still needs to be studied.

Glycocalyx and its effect on FSL uptake

From this aspect of the study, it was shown that the glycocalyx is a rate-determining step during the FSL modification process in RBC, as the reduction in the glycocalyx before kodecyte formation enhances FSL uptake, suggesting the glycocalyx interacts with FSL constructs. Additionally, when the kodecytes' glycocalyx is partially removed fluorescence signal is reduced (for concentrations above CMC), suggesting FSL constructs as micelles are possibly resident in glycocalyx. However, as other cells that differed in their glycocalyx thickness were not examined (only RBCs with a 0.015 µm glycocalyx was studied), it could be suggested that, in addition to the presence of glycocalyx, a number of additional parameters (possibly more important), like the relative bulk of the FSL, its charge and relative hydrophobicity/hydrophilicity could also influence the rate at which FSLs would interact with glycocalyx and eventually modify the cell membranes.

8.5 SEM analysis of kodecytes

SEM provides resolution on the order of 1-2 nm allowing access to the three-dimensional shape of cells.[193] However, it is difficult to process biological specimens for SEM without the process causing changes in the cellular morphology.[194] Hence, in this study, an alternative methodology for SEM sample preparation was used. Difficult steps like the usage of OsO_4 and different-grade ethanol dehydration steps were replaced to make the method safer and easier to perform.[194] The new procedure was used with two cell types, RBCs and actively dividing Jurkat cells, to examine their morphological characteristics (size and shape) postlabeling with different FSL constructs.

The ethanol dehydration step was also primarily omitted from the protocol because studies have shown that the use of ethanol in the dehydration step can affect lipids present on the cell membrane. Although it could be argued here that use of ethanol would have shown the same effect on unkoded and koded cells and the relative adverse effect would be proportional to both control and test, FSL being a lipid-based construct will cause the lipid content on kodecytes, and thus, application of ethanol could impact the kodecytes more adversely than to unkoded cells. However, the disadvantages of this alternative method cannot be ignored, as it could possibly lead to the appearance of artefacts on the cell surface.

The primary aim of the study was to determine if the uptake of FSL constructs under different koding conditions (i.e., temperature, duration, concentration, and cell type) *visually* impacts the cell membrane. Based on the results (Section 6.1.2), it was observed that RBC transformation with a concentration of >13µM FSL- FLRO4 resulted in a change in morphology from predominantly discocytes (normal biconcave shape) to an increasing percentage of type I-III echinocytes (increased spikiness). Moreover, concentration- dependent morphological changes were prominently observed for FLRO4-kodecytes, followed by biotin, and least for BODIPY-kodecytes.

This FSL concentration-induced phenomenon has been observed by Ferrell, who found that human RBCs incubated with certain phospholipids became spiculate echinocytes, and changes in the morphology of RBC are dependent on its concentration.[174,195] Moreover, Isomaa studied shape transformations induced by different amphiphiles and suggested that anionic amphiphiles like sodium alkyl sulphates and zwitterionic

amphiphiles like 3-(alkyldimethylammonio)-l-propanesulfonates) shown to be powerful echinocytogenic agents. In contrast, non-ionic amphiphiles were mostly stomatocytogenic agents.[175] Amphiphiles-induced shape change was proposed to be a protective mechanism against membrane bilayer collapse.[175]

Additionally, results (Tables 15 and 16) also showed that the secondary treatment of biotin-kodecytes with SAF488 conjugate adds cumulative morphological changes to biotin-kodecytes (predominantly of type I and II echinocytes). Previously, the data from studies showed that avidin binds to biotinylated membrane polyvalently [172,173]; therefore, it is possible that multipoint streptavidin attachment to FSL-biotin induces further rearrangement in the cell membrane.

A time-course FSL uptake study and subsequent SEM analysis were performed to determine the effect of different koding times on RBC/kodecytes morphology at 37°C. For this, RBCs were incubated with FSL constructs at 37°C for up to 24 h. Results from the extended (0–24 h) incubation study at 37°C showed a gradual transformation from standard biconcave shape to echinocytes to stomatocytes (from 7 to 5µm). Additionally, the unkoded cells and kodecytes became smaller in diameter with increasing incubation duration at 37°C, indicating the change in diameter is a consequence of incubation at 37°C. Isomaa showed strong time-dependent shape-alteration when RBCs were treated with cationic amphiphiles. They show that post-cationic amphiphile incubation, RBCs immediately induce strongly crenated erythrocytes, which, during further incubation, shift to less crenated erythrocytes or to stomatocytes. Thus, RBCs transformed from echinocytic stages before stomatocytic shapes were attained.[175]

SEM was also used to examine the morphological characteristics of Jurkat kodecytes post-labelling with different FSL constructs. Results from SEM micrographs showed that FLRO4 and BODIPY Jurkat kodecytes mostly display a round or spherical morphology with even cell surfaces without any noticeable breakage, indicating preserved cell morphology. Additionally, FLRO4 and Jurkat BODIPY-kodecytes average diameter changed only marginally (<5%) compared to unkoded cells. However, Jurkat biotin+SAF488 kodecytes show an increase in the average diameter with increasing concentrations although this change was probably associated with flattening and not enlarging the biotin+SAF488 kodecytes.

8.6 Examining cytotoxic effects of FSLs on Jurkat and PC-3 kodecytes

This aspect of the study aimed to measure and compare the impact of different FSL construct uptake on Jurkat and PC-3 kodecyte viability under different koding conditions (koding duration, concentration and FSL constructs spacers). Three assays were chosen to examine the cytotoxic profile of FSL constructs: the Trypan blue cell exclusion assay, the Muse™ Count & Viability assay (which measures viability based on the integrity of the cellular membrane), and the MTT cell proliferation assay (which measures cellular metabolism, accounting for the proliferation status of the cells). Moreover, the effect on the proliferation status of kodecytes post-koding was also examined.

Based on the results, it was established that FSL-constructs have low cytotoxicity after 1 h of koding, suggesting 1 h is the optimal duration of koding for active cells (Section 6.4.1). However, 2 h of koding duration (as recommended in the standard protocol) was shown to be more effective in koding with lower concentrations of FSL-FLRO4. The choice is therefore a compromise.

Additionally, compared to BODIPY and biotin-kodecytes, FLRO4-kodecytes had lower viability, and a concentration-dependent effect on kodecyte viability was clearly observed at 25 µM (Sections 6.3.1 and 5.3.2). At similar experimental conditions, it was also shown that Trypan blue assay results, in general, were correlated with those of Muse™ Count & Viability assay results (Figure 102).

The effect on kodecyte viability and proliferation status post-koding was also examined. This aspect of the study showed that the concentration of FSLs used to prepare Jurkat kodecytes has an impact on the viability of kodecytes post-koding (25–50 µM kodecytes survived poorly compared to 6–13 µM kodecytes; Figure 98). Moreover, similar results were observed when the proliferation ability of PC-3 kodecytes over 72 h was assessed post-koding (Section 6.4.2). From the results (Section 6.4.2), two important conclusions can be drawn: Firstly, unkoded cells and kodecytes proliferation increased over 72 h of culture suggesting normal process are unaffected. Secondly, a concentration-dependent effect on kodecyte proliferation was observed post-koding, suggesting that koding with higher concentrations could possibly affect the viability of PC-3 kodecytes post-koding.

Based on the results discussed, it can be proposed that the concentration of FSL used for preparing kodecytes is the most important factor in maintaining the viability and proliferation status of kodecytes post-koding and should be less than 25µM.

8.7 Predictive mechanism of FSL uptake

Dynamics of uptake, desorption and translocation

The mechanism by which FSL constructs, and biological membranes interact was unknown. Hence, the next aim of this project was to understand the mechanism of uptake of FSL-FLRO4, FSL-BODIPY, and FSL-biotin by inactive (RBCs) and actively dividing cells (Jurkat cells and PC-3 cells).

Since FSL constructs were originally designed to be synthetic analogues of natural glycolipids (amphiphiles), it is hypothesised that the FSL mechanism of uptake by the cell membrane could mimic the cell labelling process of biologically active amphiphiles. [112] Hence, based on the understanding of biologically active amphiphiles, the mechanism by which FSL constructs, and biological membranes would interact could be predicted. An overview of the interaction of biologically active amphiphiles with the cell membrane would be useful for predicting the mechanism of FSL uptake. Biologically active amphiphiles (metabolites) interact with the cell membrane substantially (if not preeminently) through passive transport.[14,88] However, the nature of the interactions between amphiphilic molecules and lipid bilayers is intricate and comprises multistep interactions (i.e., uptake, translocation, and desorption) that further regulate the extent and rate of uptake.[14]

There is limited information available on glycolipid interactions with lipid bilayers and biological membranes which is surprising considering their biological significance. Filipe HAL. (2014) proposed different models to explain the interaction of amphiphiles with biological or lipid membranes.[14] These models were based on the solubility of the solute (molecule of interest) in the aqueous medium and the lipid bilayer. The three different models [14] based on the solubility of the molecules of interest (amphiphiles) are :

- Solutes with high solubility in the aqueous media and insoluble in the lipid bilayer

- Solutes with very low solubility in the aqueous media and a high partition into the lipid bilayer
- Solutes with a moderate solubility in the aqueous media and lipid bilayer

The first model deals mostly with characterising the effects of charged peptides and surfactants. Here, the target molecule is completely soluble in the aqueous medium and insoluble in the lipid bilayer, thus it does not bind to or interact with the lipid bilayer. Additionally, the second model does not suit the vitals of our target molecule of interest, as the solute used for this model is highly soluble in the lipid bilayer with minimum or no solubility in aqueous media. Hence, these models cannot be fully utilised to characterise our molecules (amphiphilic) of interest, as these models do not suit the characteristics of FSLs of interest.

The third model requires the target molecule to be moderately soluble in aqueous media as well as in the lipid bilayer. This model could be proposed to be most relevant for this study (and aid in figuring out the overall mechanism of uptake of the FSL construct), as FSL constructs are amphiphilic molecules.

However, FSL constructs are highly soluble in aqueous medium owing to the presence of a spacer, which imparts a high degree of dispersibility in water, and the presence of a lipid-based tail aids in its interaction with the lipid membrane as well. Thus, the first and the second models could represent some aspects of the FSL construct, and possibly FSL constructs would resemble their mechanism of uptake.

According to the third model, it is hypothesised that the target amphiphilic molecules are unrecognisable by transporters in the membrane, and the amphiphilic molecules cross the membrane barrier by possibly passive mechanisms [14]. The target molecule binds with the lipid bilayer moderately, i.e., by the partition-diffusion mechanism, and the target molecule gradually equilibrates between the distinct compartments.

Schwarzmann, 2001; Wilchek & Bayer, 1987, reviewed the uptake of exogeneous glycolipids by red blood cells and actively dividing cells. [88,196] This review concluded that the uptake of exogeneous glycolipids varied depending upon the physical and chemical conformation of glycolipids in the transformation solution, cell type used for study, and complexity of glycocalyx, i.e., the form of exogeneous glycolipids (micelles, monomers,

and aggregates), membrane permeability, thickness of glycocalyx, etc. A study on the mechanism of exogeneous glycolipid uptake projected that there are three possible modes by which glycolipids can interact and be incorporated into the membrane: serum -sensitive loosely associated micelles; serum-resistance, trypsin-releasable forms, which consist of more firmly held monomers or micelles (interact via attachment to proteins exposed on the cell membrane/protein-bound); trypsin stable (impervious to proteolytic enzyme's attachment) mainly monomers acquired into the hydrophobic regions of the membrane. [88,197] Additionally, the physical and chemical properties of glycolipids regulate the three abovementioned modes of incorporation.

It is known that glycolipids freely exchange between plasma and RBC membranes, and glycolipids are thought to be distributed between membrane and plasma (in the lipoprotein fraction) compartments at an equilibrium of one-third to two-thirds. [88,197]

FSL constructs were originally designed to be synthetic analogues of natural glycolipids that are capable of mimicking the spontaneous cell labelling process, originally associated with natural glycolipids but designed to be used in PBS. There could be several ways for the FSL construct to attach to a surface; these will depend on the type of surface being tagged, the type of construct (including its functional group, type of spacer, and type of lipid), as well as the labelling environment. It is likely that some or all of the non-covalent forces (hydrophobic, electrostatic, van der Waals interactions) are involved in promoting and preserving FSL attachment to a surface. Owing to the lipid tail FSL constructs in aqueous solutions will rapidly associate with the lipid membrane. Overall, it is well established that the amphipathic FSL construct is able to self-assemble into lipid membranes.

To understand and predict the mechanism of uptake of FSL constructs, experiments were conducted aiming to comprehend the time period during which RBCs would acquire maximum FSL constructs and indicate clearer stabilisation of uptake and loss of FSLs from the membrane. For this, prolonged (undesirable) incubation at 37°C was replaced with a more favourable combination of RT and 4°C incubation. Henceforth, the koding efficiency of FSL constructs in different scenarios was analysed. The time frame in which the stabilisation of the fluorescence signal begins and remains unchanged foretells the maximum uptake of FSL. This would help in predicting whether stabilisation

of uptake of FSL constructs occurs or not, and in turn, it would help in forecasting the mechanism by which FSL uptake occurs.

Based on the experiments, the following conclusions were made: Firstly, for FSL-FLRO4, the maximum uptake seems to approach later than for FSL-BODIPY, and FSL- biotin. Hence, it could be proposed that FSL-BODIPY and FSL-biotin acquisition attain stabilisation (proposed) onto the RBC membrane at a much faster rate than FSL-FLRO4, with FSL-biotin being the fastest. In summary, it could be concluded that during the koding process, after a certain time period (which depends on the FSL used), saturation of signals occurs. This suggests that the FSL constructs, tested are mimicking the natural glycolipid uptake mechanism and acquired by the lipid bilayer via the partition-diffusion mechanism as the target FSLs gradually equilibrate between the distinct compartments.

To cross-check the abovementioned observation, further experiments were performed where the interrelationship between FSL constructs in the transformation solution pre- and post-koding was explored. Based on the results obtained from these experiments, it appears that RBCs did not take up all FSL constructs, and residual FSL constructs are available post-koding in the post-transformation solution. This was found, irrespective of the FSL constructs used and the harvesting time of the post- transformation solution; however, the strength of the FSL construct in the post- transformation solution varied and was found to be dependent on the time of harvest. Additionally, kodecytes prepared from transformation and post-transformational solution (for 5 minutes to 1 h time points) never accounted for the total fluorescence signal with respect to the 2 h time point. Some percentages of fluorescence signals were always unaccounted for. This difference in fluorescence signal loss was highest for FSL-FLRO4 and negligible for FSL-biotin. This suggests that FSL uptake into membrane continues until some kind of equilibrium is attained between free and membrane bound FSL (as they are actively exchanging). Therefore, it could be said that at certain time period when FSL constructs in the immediate vicinity of the bilayer are in equilibrium with the FSL constructs in the transformation solution (with free exchange between transformation medium and RBC membranes), a state of balance or saturation is achieved. This is usually around 1 h for the tested FSL constructs.

Additionally, an alternative methodology based on a fluorescence microplate assay was tested for examining the effectiveness of koding of FSL-FLRO4 and FSL-BODIPY and in turn the mechanism of FSL uptake by measuring the (unknown) concentration of FSL remaining in the kodecyte supernatant (i.e., post-transformation solution) after transformation. This methodology helped in the indirect detection and quantification of any residual FSL construct in the post-transformation solution and aided in further understanding whether FSL uptake, i.e., the koding process, occurs equilibrium binding into the cell membrane. At similar experimental conditions, fluorescence spectrophotometer results were highly correlated with those generated by flow cytometry.

Overall, it could be proposed that, the FSL constructs are acquired by the lipid bilayer via the partition-diffusion mechanism (free exchange of FSL between koding medium and cell membrane) as the target FSLs gradually equilibrate between the distinct compartments.

8.8 Potential explanation for (interfering) factor regulating koding process

The standard koding duration of cells is 2 h at 37°C. To analyse the koding duration where maximum FSLs are acquired in RBCs, FSL uptake was tested for extended koding duration over 24 h. During the (extended 24 h) koding process of RBCs with FSL-FLRO4 at 37°C, it was shown that FSL-FLRO4 uptake was maximum at 4 h of koding (as the fluorescence signal MFI was highest), and after this incubation period, the MFI started decreasing. Compared to 4 h, FLRO4-kodecytes at 24 h lose approximately half of their fluorescence signal (Figure 70). The study investigating the FSL-FLRO4 signal loss during koding showed that the missing (shed) FSL-FLRO4 construct did not degrade over the period of koding and are present in the harvested post-transformation supernatant (Sections 4.1 and 4.2). However, it was found that FSL lost from kodecytes or/and residual unacquired FSL is not able to kode fresh RBCs (at least very efficiently), suggesting that they are being captured by material in the supernatant. Thus, it was proposed that possibly these lost FSLs may be associated with different RBC-derived (shed) bioactive proteins, lipids, and microparticles or microvesicles (referred to as membranous entities), which make up the interfering factor and which may also further regulate the uptake of shed FSL. The accumulation of interfering factors in the post-

transformation solution could possibly be due to prolonged incubation at 37°C and additional associated factors (storage lesions).

Experiments were set up to examine whether, during prolonged incubation at 37°C, (interfering) membranous entities were generated or not. Additionally, it was also analysed whether membranous entities were generated in the absence of FSL constructs or in the presence of FSL constructs, i.e., during the koding process. Based on the results (Section 4.3), it was shown that the act of incubation of RBCs at 37°C probably facilitates the release of RBC-associated membranous entities, which interfere with and delay the efficient uptake of FSL-FLRO4 in suspension (i.e. FSLs are suspected to be taken up or entrapped within these membranous lipids and hence not available for further labelling of RBCs).

Overall, this aspect of the study showed that membranous entities (shed bioactive proteins, lipids, and RBC-derived microvesicles) are probably generated either by the RBCs and/or kodecytes in the process of involved incubation at 37°C. Any additional effect of koding due to the process of koding was not established. These membranous entities ultimately end up in the transformation solution and probably interact with and associate with the available FSL. Hence, it could be suggested that incubation at 37°C will change the dynamics of FSL uptake, ultimately affecting the koding process and this process is probably accelerated by the uptake of FSL constructs.

8.9 Retention of FSL constructs in kodecytes

This aspect of the study aimed to primarily examine the retention of FSL constructs on (mainly) RBC kodecytes when stored in different resuspension media with temperature variations. Experiments were also designed to analyse the interaction and transfer of FSL constructs from kodecytes to unkoded cells when co-incubated. These experiments, led to a further understanding of the dynamics of the loss and relabelling of kodecytes.

Based on the results it can be seen that over a period of 24 h, temperature impacts the retention of FSL construct on kodecytes. Compared to 4°C, the FSL constructs are lost from kodecytes over time more rapidly at 37°C (Section 7.1). Additionally, at 37°C more FSLs are lost in protein and plasma-supplemented storage media. However, the rate of loss was found to be different for different FSL constructs. Under any tested scenarios,

FSL-BODIPY and FSL-biotin are better retained in their respective kodecytes than FSL- FLRO4 (7.1.4).

An important observation from this study is that in 0% BSA/plasma at 37°C, the relabelling rate, although higher than when plasma or protein were present in the media was not as high as could be expected. This means that FSLs shed by kodecytes into media without added lipid or protein are still poorly labeled. This could be due to the fact that the storage medium in which the reaction is taking place actually acquires proteins and lipids shed from 37°C-incubated cells and captures the released FSLs. It needs to be appreciated that the loss-relabelling process is very dynamic, as FSL lost from kodecytes can relabel either another kodecyte or an (initially) unlabelled cell. Additionally, the unkoded cells, which become labelled, also probably lose their FSLs to the media

The co-incubation study, where the interaction and transfer of FSL constructs from koded to unkoded cells were examined, found that the unkoded cells did not account for the total loss, hence there was no significant transfer (Section 7.3.4). This indicates that the lost FSLs were probably partially labelling unkoded cells, and storage media could account for the rest of the lost FSLs. Additionally, the finding that protein and serum-supplemented media prevent or slow down the acquisition of shed FSLs by unkoded cells in a co-incubation setup supports the previous hypothesis (7.1.4) that protein/serum are not necessarily causing the loss of FSL from the kodecytes. However, it may instead be hindering its ability to re-label the kodecytes.

Overall, the loss of signal suggests the possibility that the lost FSL constructs are being retained by the storage media (i.e., unable to relabel the kodecytes). Additionally, in protein/serum-lipid free media at 37°C, the loss of signal (and hence the decrease in relabelling of kodecytes) could be attributed to the fact that the storage medium in which the reaction is taking place actually acquires proteins and lipids shed from 37°C incubated cells and captures the released FSLs (see Chapter 5). It is essential to note that the protein/plasma-lipid may not necessarily cause the loss of FSL from the kodecytes but may instead be hindering its ability to re-label the kodecytes.

Furthermore, it is not known if kodecytes or unkoded cells would have a labelling preference. Overall, it can be concluded that FSL constructs lost from kodecytes in the

presence of protein (BSA), or plasma-lipid (plasma) do not relabel adjacent cells, at least to any significance.

8.10 Conclusions

- RBC storage-age has an adverse impact on the koding efficiency of FSL-FLRO4, but no impact on FSL-BODIPY. Based on the results, it is advisable to use fresh RBCs for preparing kodecytes, or no older than 10 days of storage at 4°C.
- As expected, all examined FSL constructs exhibited concentration-dependent uptake of FSL, and irrespective of the concentration of FSL used to prepare kodecytes, they were labelled as homogeneous populations.
- The optimal koding duration for FSL is 1 h at 37°C or 4 h at RT. This was found to be true for the FSL tested in this research. However, a time-dependent study showed that the rate of koding is different among constructs (FSL-biotin>FSL-BODIPY>FSL-FLRO4). RBC and Jurkat kodecytes both showed comparable trends.
- The rate of uptake of FSL constructs by biological membranes appears depends on the presence of micelles in the transformation solution with monomers being acquired fastest.
- Lipophilic substances like serum and BSA may affect the uptake of FSLs especially if the functional group is lipophilic, e.g. BODIPY.
- The glycocalyx is a rate-determining step during the FSL modification process, as the partial removal of glycocalyx before kodecyte formation enhances FSL uptake by suggesting glycocalyx interacts with FSL constructs (and micelles) and thus influences cell membrane labelling rate.

- Extended koding duration at 37°C, found that FSL- FLRO4 uptake reaches a maximum after 4 h of incubation, and after this incubation time point, the MFI decreased. Lost and/or residual FSL-FLRO4 are present in the harvested post-transformation solution but in a form that is not able to efficiently transform fresh red cells into kodecytes. This study highlighted that the act of incubation at 37°C probably leads to the formation of RBC-derived membranous entities (proteins, lipids, and microvesicles). These entities further interfere with the uptake of FSL-FLRO4. Thus, the act of koding affects the uptake of the FSL construct, and primarily due to incubation at 37°C.
- As expected, 4°C, the FSL constructs are lost from kodecytes over time more rapidly at 37°C. Additionally, at 37 °C, and this is enhanced in the presences of protein and plasma-supplemented storage media for FSL-FLRO4. However, FSL- BODIPY and FSL-biotin are better retained in their respective kodecytes than FSL-FLRO4 possibly because of the hydrophobic head. It is not known if this applies to FSL-glycans
- The co-incubation study showed that unkoded cells became kodecytes over the period, but the strength of the kodecytes very slowly and do not acquire all the FSLs lost from the kodecytes.

The conclusions from this research are that although many stages of the koding process are predictable, the underlying mechanisms are complex and influenced by several external factors. Overall, this research has led to further in depth understanding of the koding process and will inform future experiments.

References

1. Watson H. Biological membranes. Essays in biochemistry 2015;59:43-69.
2. Stephan MT, Irvine DJ. Enhancing cell therapies from the outside in: cell surface engineering using synthetic nanomaterials. Nano today 2011;6(3):309-325.
3. Henry S, Perry H, Bovin N. Applications for kodecytes in immunohaematology. ISBT Science Series 2018;13(3):229-237.
4. Henry SM, Bovin NV. Kode Technology–a universal cell surface glycan modification technology. Journal of the Royal Society of New Zealand 2019;49(2):100-113.
5. Blake DA, Bovin NV, Bess D, Henry SM. FSL constructs: a simple method for modifying cell/virion surfaces with a range of biological markers without affecting their viability. JoVE (Journal of Visualized Experiments) 2011(54):e3289.
6. Georgakopoulos T, Komarraju S, Henry S, Bertolini J. An improved Fc function assay utilizing CMV antigen-coated red blood cells generated with synthetic function–spacer–lipid constructs. Vox Sanguinis 2012;102(1):72-78.
7. Ilyushina NA, Chernyy ES, Korchagina EY, Gambaryan AS, Henry SM, Bovin NV. Labeling of influenza viruses with synthetic fluorescent and biotin-labeled lipids. Virologica Sinica 2014;29:199-210.
8. Bagatolli LA, Ipsen JH, Simonsen AC, Mouritsen OG. An outlook on organization of lipids in membranes: searching for a realistic connection with the organization of biological membranes. Progress in lipid research 2010;49(4):378-389.
9. Bretscher MS. Asymmetrical lipid bilayer structure for biological membranes. Nature New Biology 1972;236(61):11-12.
10. Op den Kamp JA. Lipid asymmetry in membranes. Annual review of biochemistry 1979;48(1):47-71.
11. Mohandas N, Gallagher PG. Red cell membrane: past, present, and future. Blood, The Journal of the American Society of Hematology 2008;112(10):3939-3948.
12. Van Meer G, Voelker DR, Feigenson GW. Membrane lipids: where they are and how they behave. Nature reviews Molecular cell biology 2008;9(2):112-124.
13. Ali O, Szabó A. Review of Eukaryote Cellular Membrane Lipid Composition, with Special Attention to the Fatty Acids. International Journal of Molecular Sciences 2023;24(21):15693.
14. Chattopadhyay A. Membrane organization and Dynamics: Springer, 2017.
15. Yang L, Yatomi Y, Miura Y, Satoh K, Ozaki Y. Metabolism and functional effects of sphingolipids in blood cells. British journal of haematology 1999;107(2):282-293.
16. Minari O, Tsubono H, Akiyama M, Sakagami T. Sphingomyelins in human erythrocytes and plasma. The Journal of Biochemistry 1967;62(5):618-620.
17. Kojima N, Hakomori S-i. Cell adhesion, spreading, and motility of GM3-expressing cells based on glycolipid-glycolipid interaction. Journal of Biological Chemistry 1991;266(26):17552-17558.
18. Carson DD, Rohde LH, Surveyor G. Cell surface glycoconjugates as modulators of embryo attachment to uterine epithelial cells. International journal of biochemistry 1994;26(10-11):1269-1277.
19. Hakomori S-I. Bifunctional role of glycosphingolipids. Modulators for transmembrane signaling and mediators for cellular interactions. Journal of Biological Chemistry 1990;265(31):18713-18716.

20. Hakomori S-i, Nudelman E, Levery S, Solter D, Knowles BB. The hapten structure of a developmentally regulated glycolipid antigen (SSEA-1) isolated from human erythrocytes and adenocarcinoma: a preliminary note. Biochemical and biophysical research communications 1981;100(4):1578-1586.
21. Cooper GM, Hausman R. A molecular approach. The Cell 2nd ed Sunderland, MA: Sinauer Associates 2000.
22. Wang B, Boons G-J. Carbohydrate recognition: biological problems, methods, and applications: John Wiley & Sons, 2011.
23. Laine RA. Invited Commentary: A calculation of all possible oligosaccharide isomers both branched and linear yields 1.05× 1012 structures for a reducing hexasaccharide: the Isomer Barrier to development of single-method saccharide sequencing or synthesis systems. Glycobiology 1994;4(6):759-767.
24. Schenkel-Brunner H. Human blood groups: chemical and biochemical basis of antigen specificity: Springer Science & Business Media, 2000.
25. Xia Y, Peng L. Photoactivatable lipid probes for studying biomembranes by photoaffinity labeling. Chemical reviews 2013;113(10):7880-7929.
26. Guţu M, Rusu V, Ştefănescu C. Membrane fluidity--biophysical parameter in relation to membrane transport processes. Revista Medico-chirurgicala a Societatii de Medici si Naturalisti din Iasi 2011;115(1):153-162.
27. Ballweg S, Sezgin E, Doktorova M, et al. Regulation of lipid saturation without sensing membrane fluidity. Nature communications 2020;11(1):1-13.
28. Goldstein DB. The effects of drugs on membrane fluidity. Annual review of pharmacology and toxicology 1984;24(1):43-64.
29. Sok M, Šentjurc M, Schara M. Membrane fluidity characteristics of human lung cancer. Cancer letters 1999;139(2):215-220.
30. Jain MK, White III HB. Long-range order in biomembranes. Advances in lipid research 1977;15:1-60.
31. Hollan S. Membrane fluidity of blood cells. Haematologia 1996;27(3):109-127.
32. Filipe HAL. Following Amphiphilic Molecules on their Way Through Lipid Membranes: Development of a Kinetic Model of Passive Permeation Through the Blood-Brain Barrier. Universidade de Coimbra (Portugal); 2014.
33. Leidl K, Liebisch G, Richter D, Schmitz G. Mass spectrometric analysis of lipid species of human circulating blood cells. Biochimica et Biophysica Acta (BBA)-Molecular and Cell Biology of Lipids 2008;1781(10):655-664.
34. Esteban-Martin S, Risselada HJ, Salgado J, Marrink SJ. Stability of asymmetric lipid bilayers assessed by molecular dynamics simulations. Journal of the American Chemical Society 2009;131(42):15194-15202.
35. Daleke DL. Regulation of phospholipid asymmetry in the erythrocyte membrane. Current opinion in hematology 2008;15(3):191-195.
36. Sims PJ, Wiedmer T. Unraveling the mysteries of phospholipid scrambling. Thrombosis and haemostasis 2001;86(07):266-275.
37. Daleke DL. Regulation of transbilayer plasma membrane phospholipid asymmetry. Journal of lipid research 2003;44(2):233-242.
38. Daleke DL, Huestis WH. Erythrocyte morphology reflects the transbilayer distribution of incorporated phospholipids. The Journal of cell biology 1989;108(4):1375-1385.
39. Schroit AJ, Madsen JW, Tanaka Y. In vivo recognition and clearance of red blood cells containing phosphatidylserine in their plasma membranes. Journal of Biological Chemistry 1985;260(8):5131-5138.

40. Schwartz RS, Tanaka Y, Fidler IJ, Chiu D, Lubin B, Schroit A. Increased adherence of sickled and phosphatidylserine-enriched human erythrocytes to cultured human peripheral blood monocytes. The Journal of clinical investigation 1985;75(6):1965-1972.
41. Setty BY, Kulkarni S, Stuart MJ. Role of erythrocyte phosphatidylserine in sickle red cell–endothelial adhesion. Blood, The Journal of the American Society of Hematology 2002;99(5):1564-1571.
42. Singer SJ, Nicolson GL. The Fluid Mosaic Model of the Structure of Cell Membranes: Cell membranes are viewed as two-dimensional solutions of oriented globular proteins and lipids. Science 1972;175(4023):720-731.
43. Laude AJ, Prior IA. Plasma membrane microdomains: organization, function and trafficking. Molecular membrane biology 2004;21(3):193-205.
44. Waheed AA, Freed EO. The role of lipids in retroviral replication. Retrovirus-Cell Interactions: Elsevier; 2018:353-399.
45. Martinez-Outschoorn UE, Sotgia F, Lisanti MP. Caveolae and signalling in cancer. Nature reviews Cancer 2015;15(4):225-237.
46. Hsu K. Exploring the Potential Roles of Band 3 and Aquaporin-1 in Blood CO2 Transport–Inspired by Comparative Studies of Glycophorin BAB Hybrid Protein GP. Mur. Frontiers in Physiology 2018;9:733.
47. Wang DN. Band 3 protein: structure, flexibility and function. FEBS letters 1994;346(1):26-31.
48. Saqr H, Pearl D, Yates A. A review and predictive models of gang ioside uptake by biological membranes. Journal of neurochemistry 1993;61(2):395-441.
49. Park J, Andrade B, Seo Y, Kim M-J, Zimmerman SC, Kong H. Engineering the surface of therapeutic “living” cells. Chemical reviews 2018;118(4):1664-1690.
50. Simons K, Lingwood D, Coskun U, Grzybek M. Lipid rafts and membrane organization. FEBS Journal: Wiley-Blackwell Publishing, Inc Commerce Place, 350 Main St, Malden 02148 …; 2009:53-53.
51. Custódio CA, Mano JF. Cell surface engineering to control cellular interactions. ChemNanoMat 2016;2(5):376-384.
52. Liu L, He H, Liu J. Advances on non-genetic cell membrane engineering for biomedical applications. Polymers 2019;11(12):2017.
53. Fox WM, Sarkar D. Cell Surface Engineering by Chemical Reaction and Remodeling. Micro-and Nanoengineering of the Cell Surface: Elsevier; 2014:27-41.
54. Verma IM, Weitzman MD. Gene therapy: twenty-first century medicine. Annu Rev Biochem 2005;74:711-738.
55. Lee DY, Cha B-H, Jung M, Kim AS, Bull DA, Won Y-W. Cell surface engineering and application in cell delivery to heart diseases. Journal of Biological Engineering 2018;12(1):1-11.
56. O’Brien PJ, Elahipanah S, Rogozhnikov D, Yousaf MN. Bio-orthogonal mediated nucleic acid transfection of cells via cell surface engineering. ACS central science 2017;3(5):489-500.
57. Germain M, Balaguer P, Nicolas J-C, et al. Protection of mammalian cell used in biosensors by coating with a polyelectrolyte shell. Biosensors and Bioelectronics 2006;21(8):1566-1573.
58. Krol S, Del Guerra S, Grupillo M, Diaspro A, Gliozzi A, Marchetti P. Multilayer nanoencapsulation. New approach for immune protection of human pancreatic islets. Nano letters 2006;6(9):1933-1939.

59. Abbina S, Siren EM, Moon H, Kizhakkedathu JN. Surface engineering for cell-based therapies: Techniques for manipulating mammalian cell surfaces. ACS Biomaterials Science & Engineering 2017;4(11):3658-3677.
60. Fujita E, Teramura Y, Shiraga T, Yoshioka S-I, Iwatsubo T, Kawamura A, Kamimura H. Pharmacokinetics and tissue distribution of tacrolimus (FK506) after a single or repeated ocular instillation in rabbits. Journal of ocular pharmacology and therapeutics 2008;24(3):309-319.
61. Miura S, Teramura Y, Iwata H. Encapsulation of islets with ultra-thin polyion complex membrane through poly (ethylene glycol)-phospholipids anchored to cell membrane. Biomaterials 2006;27(34):5828-5835.
62. Kim MH, Woo S-K, Lee KC, et al. Longitudinal monitoring adipose-derived stem cell survival by PET imaging hexadecyl-4-124I-iodobenzoate in rat myocardial infarction model. Biochemical and biophysical research communications 2015;456(1):13-19.
63. Kim MH, Woo S-K, Kim KI, et al. Simple methods for tracking stem cells with 64Cu-labeled DOTA-hexadecyl-benzoate. ACS medicinal chemistry letters 2015;6(5):528-530.
64. Zhang Y, DaSilva JN, Hadizad T, et al. 18F-FDG cell labeling may underestimate transplanted cell homing: more accurate, efficient, and stable cell labeling with hexadecyl-4-[18F] fluorobenzoate for in vivo tracking of transplanted human progenitor cells by positron emission tomography. Cell transplantation 2012;21(9):1821-1835.
65. Ma B, Hankenson KD, Dennis JE, Caplan AI, Goldstein SA, Kilbourn MR. A simple method for stem cell labeling with fluorine 18. Nuclear medicine and biology 2005;32(7):701-705.
66. Olasz EB, Lang L, Seidel J, Green MV, Eckelman WC, Katz SI. Fluorine-18 labeled mouse bone marrow-derived dendritic cells can be detected in vivo by high resolution projection imaging. Journal of immunological methods 2002;260(1-2):137-148.
67. Tsien RY. Fluorescent probes of cell signaling. Annual review of neuroscience 1989;12(1):227-253.
68. Progatzky F, Dallman MJ, Lo Celso C. From seeing to believing: labelling strategies for in vivo cell-tracking experiments. Interface focus 2013;3(3):20130001.
69. Collot M, Kreder R, Tatarets AL, Patsenker LD, Mely Y, Klymchenko AS. Bright fluorogenic squaraines with tuned cell entry for selective imaging of plasma membrane vs. endoplasmic reticulum. Chemical Communications 2015;51(96):17136-17139.
70. Lassailly F, Griessinger E, Bonnet D. “Microenvironmental contaminations” induced by fluorescent lipophilic dyes used for noninvasive in vitro and in vivo cell tracking. Blood, The Journal of the American Society of Hematology 2010;115(26):5347-5354.
71. Loura L, Prates Ramalho J. Fluorescent membrane probes’ behavior in lipid bilayers: insights from molecular dynamics simulations. Biophysical reviews 2009;1(3):141-148.
72. Kleusch C, Hersch N, Hoffmann B, Merkel R, Csiszár A. Fluorescent lipids: functional parts of fusogenic liposomes and tools for cell membrane labeling and visualization. Molecules 2012;17(1):1055-1073.

73. Sonna LA, Fujita J, Gaffin SL, Lilly CM. Invited review: effects of heat and cold stress on mammalian gene expression. Journal of applied physiology 2002;92(4):1725-1742.
74. Thieringer HA, Jones PG, Inouye M. Cold shock and adaptation. Bioessays 1998;20(1):49-57.
75. Ting A, Pagano R. Density-dependent inhibition of cell growth is correlated with the activity of a cell surface phosphatidylinositol-specific phospholipase C. European journal of cell biology 1991;56(2):401-406.
76. Csiszár A, Hersch N, Dieluweit S, Biehl R, Merkel R, Hoffmann B. Novel fusogenic liposomes for fluorescent cell labeling and membrane modification. Bioconjugate chemistry 2010;21(3):537-543.
77. Stormont C. Acquisition of the J substance by the bovine erythrocyte. Proceedings of the National Academy of Sciences of the United States of America 1949;35(5):232.
78. Rendel J, Sorensen AN, Irwin M. Evidence for epistatic action of genes for antigenic substances in sheep. Genetics 1954;39(3):396.
79. Sneath JS, Sneath P. Transformation of the Lewis groups of human red cells. Nature 1955;176(4473):172-172.
80. Sneath JS, Sneath P. Adsorption of blood-group substances from serum on to red cells. British Medical Bulletin 1959;15(2):154-157.
81. Makela O, Makela P. Leb antigen; studies on its occurrence in red cells, plasma and saliva. Annales medicinae experimentalis et biologiae Fenniae1956:157-162.
82. Marcus DM, Cass LE. Glycosphingolipids with Lewis blood group activity: uptake by human erythrocytes. Science 1969;164(3879):553-555.
83. Renton P, Hancock JA. Uptake of A and B antigens by transfused group O erythrocytes. Vox sanguinis 1962;7(1):33-38.
84. Garretta M, Muller A, Courouce-Pauty A, Moullec J. In vitro transformation of group O red blood cells by A and B serum substances. Biomedicine/[publiee pour l'AAICIG] 1974;21(3):114-118.
85. Tilley C, Crookston M, Brown B, Wherrett J. A and B and A1Leb substances in glycosphingolipid fractions of human serum 1. Vox sanguinis 1975;28(1):25-33.
86. Callies R, Schwarzmann G, Radsak K, Siegert R, Wiegan H. Characterization of the cellular binding of exogenous gangliosides. European Journal of Biochemistry 1977;80(2):425-432.
87. Saqr H, Pearl D, Yates A. A review and predictive models of ganglioside uptake by biological membranes. Journal of neurochemistry 1993;61:395-395.
88. Schwarzmann G. Uptake and metabolism of exogenous glycosphingolipids by cultured cells. Seminars in cell & developmental biology: Elsevier; 2001:163-171.
89. Kanda S, Inoue K, Nojima S, Utsumi H, Wiegandt H. Incorporation of a ganglioside and a spin-labeled ganglioside analogue into cell and liposomal membranes. The Journal of Biochemistry 1982;91(6):2095-2098.
90. Jaferzadeh K, Sim M, Kim N, Moon I. Quantitative analysis of three-dimensional morphology and membrane dynamics of red blood cells during temperature elevation. 2019.
91. Peng Z, Li X, Pivkin IV, Dao M, Karniadakis GE, Suresh S. Lipid bilayer and cytoskeletal interactions in a red blood cell. Proceedings of the National Academy of Sciences 2013;110(33):13356-13361.

92. Filipe H. Following Amphiphilic Molecules on Their Way through Lipid Membranes: Development of a Kinetic Model of Passive Permeation through the Blood-Brain Barrier. 2014.
93. Haldar S, Chattopadhyay A. Application of NBD-labeled lipids in membrane and cell biology. Fluorescent methods to study biological membranes 2012:37-50.
94. Heerklotz H. Interactions of surfactants with lipid membranes. Quarterly reviews of biophysics 2008;41(3-4):205-264.
95. Nichols JW, Pagano RE. Kinetics of soluble lipid monomer diffusion between vesicles. Biochemistry 1981;20(10):2783-2789.
96. Liu H, Zhu Z, Kang H, Wu Y, Sefan K, Tan W. DNA-based micelles: synthesis, micellar properties and size-dependent cell permeability. Chemistry–A European Journal 2010;16(12):3791-3797.
97. Vaz WL, Almeida PF. Phase topology and percolation in multi-phase lipid bilayers: is the biological membrane a domain mosaic?: Current Opinion in Structural Biology 1993, 3: 482–488. Current Opinion in Structural Biology 1993;3(4):482-488.
98. Luxenhofer R, Sahay G, Schulz A, Alakhova D, Bronich TK, Jordan R, Kabanov AV. Structure-property relationship in cytotoxicity and cell uptake of poly (2-oxazoline) amphiphiles. Journal of Controlled Release 2011;153(1):73-82.
99. Schwarzmann G, Sandhoff K. Metabolism and intracellular transport of glycosphingolipids. Biochemistry 1990;29(49):10865-10871.
100. Honig MG, Hume RI. Fluorescent carbocyanine dyes allow living neurons of identified origin to be studied in long-term cultures. The Journal of Cell Biology 1986;103(1):171-187.
101. Gandek TB, van der Koog L, Nagelkerke A. A comparison of cellular uptake mechanisms, delivery efficacy, and intracellular fate between liposomes and extracellular vesicles. Advanced healthcare materials 2023;12(25):2300319.
102. Colin FC, Schrier SL. Spontaneous endocytosis in human neonatal and adult red blood cells: Comparison to drug-induced endocytosis and to receptor-mediated endocytosis. American journal of hematology 1991;37(1):34-40.
103. Lombardo D, Kiselev MA, Magazù S, Calandra P. Amphiphiles self-assembly: basic concepts and future perspectives of supramolecular approaches. Advances in Condensed Matter Physics 2015;2015.
104. Ruiz-Fernández A. Insertion and Expulsion Mechanism of an Amphiphile in a Membrane Mimetic. The Journal of Physical Chemistry C 2018;122(2):1192-1196.
105. Fuguet E, Ràfols C, Rosés M, Bosch E. Critical micelle concentration of surfactants in aqueous buffered and unbuffered systems. Analytica Chimica Acta 2005;548(1-2):95-100.
106. Corti M, Degiorgio V, Ghidoni R, Sonnino S, Tettamanti G. Laser-light scattering investigation of the micellar properties of gangliosides. Chemistry and physics of lipids 1980;26(3):225-238.
107. Formisano S, Johnson ML, Lee G, Aloj SM, Edelhoch H. Critical micelle concentrations of gangliosides. Biochemistry 1979;18(6):1119-1124.
108. Howard RE, Burton RM. Studies on the ganglioside micelle. Biochimica et Biophysica Acta (BBA)-Specialized Section on Lipids and Related Subjects 1964;84(4):435-440.
109. Yu D, Huang F, Xu H. Determination of critical concentrations by synchronous fluorescence spectrometry. Analytical Methods 2012;4(1):47-49.

110. Abreu MS, Estronca LM, Moreno MJ, Vaz WL. Binding of a fluorescent lipid amphiphile to albumin and its transfer to lipid bilayer membranes. Biophysical journal 2003;84(1):386-399.
111. Henry S, Tuzikov A, Bovin N. Kode Technology Illustrated Technical Manual: Kode Biotech, 2023.
112. Korchagina E, Henry S. Synthetic glycolipid-like constructs as tools for glycobiology research, diagnostics, and as potential therapeutics. Biochemistry (Moscow) 2015;80(7):857-871.
113. Simons K, Ikonen E. Functional rafts in cell membranes. nature 1997;387(6633):569-572.
114. Zalygin A, Solovyeva D, Vaskan I, et al. Structure of Supramers Formed by the Amphiphile Biotin-CMG-DOPE. ChemistryOpen 2020;9(6):641.
115. Frame T, Carroll T, Korchagina E, Bovin N, Henry S. Synthetic glycolipid modification of red blood cell membranes. Transfusion 2007;47(5):876-882.
116. Chesla S, Henry S, Eatz R, Sinor L. Solid phase syphilis test utilizing KODE technology. Transfusion: Wiley-Blackwell Publishing, Inc Commerce Place, 350 Main St, Malden 02148 …; 2010:196A-197A.
117. Poudyal A. Kode Technology Modification of Nanofibres to Capture Particulates. Auckland University of Technology; 2020.
118. Raghuraman P. Antibiofilm Function-Spacer-Lipid Coatings On Medical Surfaces. Auckland University of Technology; 2021.
119. Korchagina E, Henry S. Synthetic glycolipid-like constructs as tools for glycobiology research, diagnostics, and as potential therapeutics. Biochemistry (Moscow) 2015;80:857-871.
120. Ryzhov IM, Korchagina EY, Tuzikov AB, et al. Function-spacer-lipid constructs of Lewis and chimeric Lewis/ABH glycans. Synthesis and use in serological studies. Carbohydrate research 2016;435:83-96.
121. Williams E, Korchagina E, Frame T, Ryzhov I, Bovin N, Henry S. Glycomapping the fine specificity of monoclonal and polyclonal Lewis antibodies with type-specific Lewis kodecytes and function-spacer-lipid constructs printed on paper. Transfusion 2016;56(2):325-333.
122. Henry S. Kodecytes: Modifying the surface of red blood cells. ISBT Science Series 2020;15(3):303-309.
123. Dane MJ, van den Berg BM, Lee DH, et al. A microscopic view on the renal endothelial glycocalyx. American Journal of Physiology-Renal Physiology 2015;308(9):F956-F966.
124. Voet D, Voet JG, Pratt CW. Voet's principles of biochemistry: John Wiley & Sons, 2018.
125. Henry S, Perry H, Bovin N. Applications for kodecytes in immunohaematology. ISBT Science Series 2017.
126. Hadac EM, Federspiel MJ, Chernyy E, et al. Fluorescein and radiolabeled Function-Spacer-Lipid constructs allow for simple in vitro and in vivo bioimaging of enveloped virions. Journal of virological methods 2011;176(1-2):78-84.
127. Barr K. Bio-modification of non-biological surfaces with function-spacer-lipid constructs by methods including bioprinting. Auckland University of Technology; 2013.
128. Lautenschläger F, Paschke S, Schinkinger S, Bruel A, Beil M, Guck J. The regulatory role of cell mechanics for migration of differentiating myeloid cells. Proceedings of the National Academy of Sciences 2009;106(37):15696-15701.

129. Cone RE, Marchalonis JJ, Rolley RT. Lymphocyte membrane dynamics: metabolic release of cell surface proteins. The Journal of Experimental Medicine 1971;134(6):1373-1384.
130. Lingwood D, Simons K. Lipid rafts as a membrane-organizing principle. science 2010;327(5961):46-50.
131. Katritsis D, Kaiktsis L, Chaniotis A, Pantos J, Efstathopoulos EP, Marmarelis V. Wall shear stress: theoretical considerations and methods of measurement. Progress in cardiovascular diseases 2007;49(5):307-329.
132. Ley K. Laudanna C, Cybulsky MI, Nourshargh S. Getting to the site of inflammation: the leukocyte adhesion cascade updated Nat Rev Immunol 2007;7:678-689.
133. Rossi NA, Constantinescu I, Kainthan RK, Brooks DE, Scott MD, Kizhakkedathu JN. Red blood cell membrane grafting of multi-functional hyperbranched polyglycerols. Biomaterials 2010;31(14):4167-4178.
134. Perry H, Bovin N, Henry S. Antibody complement–mediated hemolytic studies with kodecytes reveal that human complement utilized in the classical pathway is more stable than generally accepted. Transfusion 2016;56(10):2495-2501.
135. Perry H, Bovin N, Henry S. A standardized kodecyte method to quantify ABO antibodies in undiluted plasma of patients before ABO-incompatible kidney transplantation. Transfusion 2019;59(6):2131-2140.
136. Briske-Anderson MJ, Finley JW, Newman SM. The influence of culture time and passage number on the morphological and physiological development of Caco-2 cells. Proceedings of the society for experimental biology and medicine 1997;214(3):248-257.
137. Esquenet M, Swinnen JV, Heyns W, Verhoeven G. LNCaP prostatic adenocarcinoma cells derived from low and high passage numbers display divergent responses not only to androgens but also to retinoids. The Journal of steroid biochemistry and molecular biology 1997;62(5-6):391-399.
138. Sambuy Y, De Angelis I, Ranaldi G, Scarino M, Stammati A, Zucco F. The Caco-2 cell line as a model of the intestinal barrier: influence of cell and culture-related factors on Caco-2 cell functional characteristics. Cell biology and toxicology 2005;21(1):1-26.
139. Adan A, Alizada G, Kiraz Y, Baran Y, Nalbant A. Flow cytometry: basic principles and applications. Critical reviews in biotechnology 2017;37(2):163-176.
140. der Strate Bv, Longdin R, Geerlings M, et al. Best practices in performing flow cytometry in a regulated environment: feedback from experience within the European Bioanalysis Forum. Bioanalysis 2017;9(16):1253-1264.
141. McKinnon KM. Flow cytometry: An overview. Current protocols in immunology 2018;120(1):5.1. 1-5.1. 11.
142. Woo J, Baumann A, Arguello V. Recent advancements of flow cytometry: new applications in hematology and oncology. Expert review of molecular diagnostics 2014;14(1):67-81.
143. Canellini G, Rubin O, Delobel J, Crettaz D, Lion N, Tissot J-D. Red blood cell microparticles and blood group antigens: an analysis by flow cytometry. Blood Transfusion 2012;10(Suppl 2):s39.
144. Van der Meulen F, De Bruin H, Goosen P, et al. Quantitative aspects of the destruction of red cells sensitized with IgG1 autoantibodies: an application of flow cytofluorometry. British Journal of Haematology 1980;46(1):47-56.

145. Arndt P, Garratty G. Flow cytofluorometric analysis in red blood cell immunology. Transfusion Medicine and Hemotherapy 2004;31(3):163-174.
146. Arndt PA, Kumpel BM. Blood doping in athletes—Detection of allogeneic blood transfusions by flow cytofluorometry. American journal of hematology 2008;83(8):657-667.
147. Wersto RP, Chrest FJ, Leary JF, Morris C, Stetler-Stevenson M, Gabrielson E. Doublet discrimination in DNA cell-cycle analysis. Cytometry: The Journal of the International Society for Analytical Cytology 2001;46(5):296-306.
148. Wannez A, Devalet B, Chatelain B, Chatelain C, Dogne J-M, Mullier F. Extracellular vesicles in red blood cell concentrates: an overview. Transfusion medicine reviews 2019;33(2):125-130.
149. Riccio DA, McMahon TJ. Reversing a red blood cell storage (RBCS) lesion: S-nitrosothiol replenishment in aged RBCS. Nitric Oxide 2012;27:S30.
150. Ulrich G, Ziessel R, Harriman A. The chemistry of fluorescent bodipy dyes: versatility unsurpassed. Angewandte Chemie International Edition 2008;47(7):1184-1201.
151. Wang J, Guo X, Li L, Qiu H, Zhang Z, Wang Y, Sun G. Application of the fluorescent dye BODIPY in the study of lipid dynamics of the rice blast fungus Magnaporthe oryzae. Molecules 2018;23(7):1594.
152. Boldyrev IA, Zhai X, Momsen MM, Brockman HL, Brown RE, Molotkovsky JG. New BODIPY lipid probes for fluorescence studies of membranes. Journal of lipid research 2007;48(7):1518-1532.
153. Kowada T, Maeda H, Kikuchi K. BODIPY-based probes for the fluorescence imaging of biomolecules in living cells. Chemical Society Reviews 2015;44(14):4953-4972.
154. Tario Jr JD, Humphrey K, Bantly AD, Muirhead KA, Moore JS, Wallace PK. Optimized staining and proliferation modeling methods for cell division monitoring using cell tracking dyes. JoVE (Journal of Visualized Experiments) 2012(70):e4287.
155. Caricchio R, D'Adamio L, Cohen P. Fas, ceramide and serum withdrawal induce apoptosis via a common pathway in a type II Jurkat cell line. Cell Death & Differentiation 2002;9(5):574-580.
156. Baker M. Reproducibility: Respect your cells! Nature 2016;537(7620):433-435.
157. Liu S, Yang W, Li Y, Sun C. Fetal bovine serum, an important factor affecting the reproducibility of cell experiments. Scientific Reports 2023;13(1):1942.
158. Bright FV. Bioanalytical applications of fluorescence spectroscopy. Analytical chemistry 1988;60(18):1031A-1039A.
159. Derose PC. Standard guide to fluorescence: Instrument calibration and validation: US Department of Commerce, Technology Admininstration, National Institute of …, 2007.
160. Montero MT, Hernández J, Estelrich J. Fluorescence quenching of albumin. A spectrofluorimetric experiment. Biochemical Education 1990;18(2):99-101.
161. DeRose PC. Recommendations and guidelines for standardization of fluorescence spectroscopy: US Department of Commerce, Technology Admininstration, National Institute of …, 2007.
162. Lakowicz JR. Principles of fluorescence spectroscopy: Springer, 2006.
163. Parker C, Rees W. Fluorescence spectrometry. A review. Analyst 1962;87(1031):83-111.

164. Koch CG, Duncan AI, Figueroa P, et al. Real age: red blood cell aging during storage. The Annals of Thoracic Surgery 2019;107(3):973-980.
165. Piccin A, Van Schilfgaarde M, Smith O. The importance of studying red blood cells microparticles. Blood Transfus 2015;13(2).
166. Goldmann WH. Mechanotransduction in cells 1. Cell biology international 2012;36(6):567-570.
167. Lynch EC. Peripheral blood smear. Clinical Methods: The History, Physical, and Laboratory Examinations 3rd Edition 1990.
168. Brecher G, Bessis M. Present status of spiculed red cells and their relationship to the discocyte-echinocyte transformation: a critical review. Blood 1972;40(3):333-344.
169. Bessis M. Red cell shapes. An illustrated classification and its rationale. Nouvelle revue francaise d'hematologie 1972;12(6):721-745.
170. Deuticke B. Transformation and restoration of biconcave shape of human erythrocytes induced by amphiphilic agents and changes of ionic environment. Biochimica et Biophysica Acta (BBA)-Biomembranes 1968;163(4):494-500.
171. Mustafa I, Al Marwani A, Mamdouh Nasr K, Abdulla Kano N, Hadwan T. Time dependent assessment of morphological changes: leukodepleted packed red blood cells stored in SAGM. BioMed Research International 2016;2016.
172. Möckl L, Horst AK, Kolbe K, Lindhorst TK, Bräuchle C. Microdomain Formation Controls Spatiotemporal Dynamics of Cell-Surface Glycoproteins. Chembiochem 2015;16(14):2023-2028.
173. Muzykantov VR, Smirnov MD, Klibanov AL. Avidin attachment to red blood cells via a phoshpolipid derivative of biotin provides complement-resistant immunoerythrocytes. Journal of immunological methods 1993;158(2):183-190.
174. Ferrell Jr JE, Lee KJ, Huestis WH. Membrane bilayer balance and erythrocyte shape: a quantitative assessment. Biochemistry 1985;24(12):2849-2857.
175. Isomaa B, Hägerstrand H, Paatero G. Shape transformations induced by amphiphiles in erythrocytes. Biochimica et Biophysica Acta (BBA)-Biomembranes 1987;899(1):93-103.
176. Mittal L, Aryal UK, Camarillo IG, Ferreira RM, Sundararajan R. Quantitative proteomic analysis of enhanced cellular effects of electrochemotherapy with Cisplatin in triple-negative breast cancer cells. Scientific reports 2019;9(1):13916.
177. D'Alessandro A, Liumbruno G, Grazzini G, Zolla L. Red blood cell storage: the story so far. Blood Transfusion 2010;8(2):82.
178. Obrador R, Musulin S, Hansen B. Red blood cell storage lesion. Journal of veterinary emergency and critical care 2015;25(2):187-199.
179. Zolla L, D'Alessandro A, Rinalducci S, D'Amici GM, Pupella S, Vaglio S, Grazzini G. Classic and alternative red blood cell storage strategies: seven years of "-omics" investigations. Blood Transfusion 2015;13(1):21.
180. García-Roa M, del Carmen Vicente-Ayuso M, Bobes AM, et al. Red blood cell storage time and transfusion: current practice, concerns and future perspectives. Blood Transfusion 2017;15(3):222.
181. Riley RS, Ben-Ezra JM, Goel R, Tidwell A. Reticulocytes and reticulocyte enumeration. Journal of clinical laboratory analysis 2001;15(5):267.
182. Brunskill S, Thomas S, Whitmore E, et al. What is the maximum time that a unit of red blood cells can be safely left out of controlled temperature storage? Transfusion medicine reviews 2012;26(3):209-223. e3.

183. Bosman GJCGM, Werre J, Willekens F, Novotný V. Erythrocyte ageing in vivo and in vitro: structural aspects and implications for transfusion. Transfusion Medicine 2008;18(6):335-347.
184. Roussel C, Dussiot M, Marin M, et al. Spherocytic shift of red blood cells during storage provides a quantitative whole cell–based marker of the storage lesion. Transfusion 2017;57(4):1007-1018.
185. Henry S, Komarraju S, Heathcote D, Rodionov I. Designing peptide-based FSL constructs to create Miltenberger kodecytes. ISBT Science Series 2011;6(2):306-312.
186. Wallace PK, Muirhead KA. Cell tracking 2007: a proliferation of probes and applications. Immunological investigations 2007;36(5-6):527-561.
187. Gilliver L. Novel Mechanisms for Controlled Antigen Expression (KODE™ CAE) on Erythrocyte Membranes. Auckland University of Technology; 2005.
188. Brown R, Stephenson F, Markello T, Barenholz Y, Thompson T. Properties of a specific glycolipid transfer protein from bovine brain. Chemistry and physics of lipids 1985;38(1-2):79-93.
189. Heuser E, Lipp K, Wiegandt H. Detection of sialic acid containing compounds and the behaviour of gangliosides in polyacrylamide disc electrophoresis. Analytical Biochemistry 1974;60(2):382-388.
190. Pokorny A, Almeida PF, Melo EC, Vaz WL. Kinetics of amphiphile association with two-phase lipid bilayer vesicles. Biophysical journal 2000;78(1):267-280.
191. Polat H, Eren MC, Polat M. The effect of protein BSA on the stability of lipophilic drug (docetaxel)-loaded polymeric micelles. Colloids and Surfaces A: Physicochemical and Engineering Aspects 2021;631:127712.
192. Charbonneau DM, Tajmir-Riahi H-A. Study on the interaction of cationic lipids with bovine serum albumin. The Journal of Physical Chemistry B 2010;114(2):1148-1155.
193. Mohammed A, Abdullah A. Scanning electron microscopy (SEM): A review. Proceedings of the 2018 International Conference on Hydraulics and Pneumatics—HERVEX, Băile Govora, Romania2018:7-9.
194. Minuti AE, Labusca L, Herea D-D, Stoian G, Chiriac H, Lupu N. A Simple Protocol for Sample Preparation for Scanning Electron Microscopic Imaging Allows Quick Screening of Nanomaterials Adhering to Cell Surface. International Journal of Molecular Sciences 2023;24(1):430.
195. Ferrell Jr JE, Lee KJ, Huestis WH. Lipid transfer between phosphatidylcholine vesicles and human erythrocytes: exponential decrease in rate with increasing acyl chain length. Biochemistry 1985;24(12):2857-2864.
196. Wilchek M, Bayer EA. Labeling glycoconjugates with hydrazide reagents. Methods in enzymology: Elsevier; 1987:429-442.
197. Möbius W, Herzog V, Sandhoff K, Schwarzmann G. Intracellular distribution of a biotin-labeled ganglioside, GM1, by immunoelectron microscopy after endocytosis in fibroblasts. Journal of Histochemistry & Cytochemistry 1999;47(8):1005-1014.